

University of Rousse "Angel Kanchev"

Finite Difference Methods: Theory and Applications

Proceedings of the Fifth International Conference FDM:
T&A'10, June 28 - July 2, 2010, Lozenetz, Bulgaria

M. Koleva
L. Vulkov
(Editors)

Rousse
2011

Proceedings of the Fifth International Conference **Finite Difference Method: Theory and Applications**, June 28 - July 2, 2010, Lozenetz, Bulgaria

Volume Editors:

Miglena Koleva

Lubin Vulkov

Rousse University

Faculty of Natural Science and Education

7017 Rousse, Bulgaria

E-mail: {mkoleva, lvalkov}@uni-ruse.bg

© Cover design:

Lusina Terziyan

www.lusinaterziyan.com

ISBN: 978-954-8467-44-5

© Rousse University Press
Rousse, 2011.

Preface

The papers in this book were presented at FDM: T&A'2010, the Fifth International Conference on *Finite Difference Methods: Theory and Applications*. FDM: T&A was held in Lozenetz, Bulgaria, August 26-29. An other part of talks reported at FDM:TA'2010 was published as special issue of the International Journal of Numerical Analysis and Modeling series B, V. 2 (3-4), see <http://www.math.ualberta.ca/ijnamb/AIMS.htm>

The conference continued the tradition of the previous meetings (1997 in Rousse, Bulgaria; 1998 in Minsk, Belarus; 2000 in Palanga, Lithuania and 2006 in Lozenetz, Bulgaria) as forums, where scientists from leading research groups from the "East" and "West" are provided with the opportunity to meet and exchange ideas and establish research cooperation.

The key lectures reviewed some of the advanced achievements in the field of finite difference methods and their efficient applications. The conference lectures were presented by university researchers and industry engineers including applied mathematicians, numerical analysts and computer experts.

The general theme for FDM: T&A'2010 was finite difference methods and various its applications in physics, chemistry, engineering and biology and finance. Many modern and new numerical techniques are discussed and presented in the conference, which included splitting techniques, Green's function method, multigrid methods, immersed interface method, etc.

This book issue of the journal contains contributions to the processing of the conference. All contributions have gone through a peer review.

The Sixth Conference on Finite Difference Methods: Theory and Applications will take place in 2014.

August 2011

Miglena Koleva
Lubin Vulkov

Table of Contents

Numerical investigation of the second harmonic effects in the LJJ	1
<i>P. Atanasova, [T. Boyadjiev], E. Zemlyanaya, Yu. Shukrinov</i>	
Monotone domain decomposition algorithm for solving systems of semilinear parabolic equations	9
<i>I. Boglaev</i>	
Two finite difference schemes for a conjugate fluid-body problem	22
<i>T. Chernogorova, V. Todorov</i>	
Application of VIM and HPM for the Sturm-Liouville problem	37
<i>R. Darzi, A. Neamaty</i>	
On the sharpness of Green's function estimates for a convection-diffusion problem	44
<i>S. Franz, N. Kopteva</i>	
Successive approximation for solving time-dependent problems	58
<i>J. Geiser, G. Tanoğlu</i>	
Nonisothermal oscillatory couette gas flow	68
<i>P. Gospodinov, V. Roussinov, S. Stefanov</i>	
Investigation of a proton exchange membrane fuel cell model by parameter fitting	78
<i>Á. Havasi, R. Horváth, Á. Nemes, T. Szabó</i>	
Comparison of MPI implementations memory management and data exchange for SMP-nodes clusters	88
<i>E. Karepova, E. Dementyeva, A. Malyshев</i>	
Comparison of numerical solution to a model of cell-matrix interactions and cell migration	97
<i>M. Kolev</i>	
Improved parameters for modelling with mammographic evidence of carcinoma	108
<i>M. Kolev, B. Zubik-Kowal</i>	

IV

Two-grid technique for semi-linear elliptic problems on complicated domains	119
<i>M. Koleva</i>	
A numerical method for solving parabolic equations based on the use of a multigrid method	129
<i>M. Ladonkina, O. Milyukova, V. Tishkin</i>	
Solution of BVP for hyperelastic material by means of RKPM	138
<i>V. Mošová</i>	
The solutions of fractional Sturm-Liouville problems with α - ordinary points.....	147
<i>A. Neamaty, R. Darzi</i>	
Finite-difference method for computation of the 3-D gas dynamics equations with artificial viscosity	154
<i>I. Popov, I. Fryazinov</i>	
Analogue of a cubic spline for a function with a boundary layer component	166
<i>A. Zadorin, M. Guryanova</i>	
Numerical Investigation of Time-Periodic Solitons in the Damped-Driven NLS	174
<i>E. Zemlyanaya, N. Alexeeva</i>	
Author Index	183

NUMERICAL INVESTIGATION OF THE SECOND HARMONIC EFFECTS IN THE LJJ

P. KH. ATANASOVA, T. L. BOYADJIEV, E. V. ZEMLYANAYA, AND
YU. M. SHUKRINOV

Joint Institute for Nuclear Research, Dubna 141980, Russia
poli@jinr.ru, elena@jinr.ru, shukrinv@theor.jinr.ru
<http://www.jinr.ru>

Abstract. We study the long Josephson junction (LJJ) model which takes into account the second harmonic of the Fourier expansion of Josephson current. The sign of second harmonic is important for many physical applications. The influence of the sign and value of the second harmonic on the magnetic flux distributions is investigated. At each step of numerical continuation in parameters of the model, the corresponding nonlinear boundary problem is solved on the basis of the continuous analog of Newton's method with the 4th order Numerov discretization scheme. New solutions which do not exist in the traditional model have been found. The influence of the second harmonic on stability of magnetic flux distributions for main solutions is investigated.

1 FORMULATION OF THE PROBLEM

Physical properties of magnetic flux in Josephson junctions (JJs) play important role in the modern superconducting electronics. Tunnel SIS JJs are known to be having the sinusoidal current phase relation. However, the decrease of the barrier transparency in the SIS JJs leads the deviations of the current-phase relation from the sinusoidal form [1].

We study the static magnetic flux distributions in the long JJs taking into account the second harmonic in the Fourier-decomposition of the Josephson current. This model is described by the double sine-Gordon equation (2SG) for magnetic flux distribution in the static regime [2],[3],[4]:

$$-\varphi'' + a_1 \sin \varphi + a_2 \sin 2\varphi - \gamma = 0, \quad x \in (-l; l), \quad (1)$$

with the boundary conditions in the the following form

$$\varphi'(\pm l) = h_e. \quad (2)$$

M. Koleva and L. Vulkov (Eds.), Proceedings of the Fifth Conference on Finite Difference Methods: Theory and Applications (FDM: T&A 2010) 2011, pp. 1–8.

© Rousse University Press

Here and below the prime means a derivative with respect to the coordinate x . The magnitude γ is the external current, l is the semilength of the junction, a_1 and a_2 are parameters corresponding the contribution of 1st and 2nd harmonic, respectively. h_e is external magnetic field. All the magnitudes are dimensionless.

The sign of the second harmonic depends on a physical application under study. It is important, in particular, in junctions like SNINS and SFIFS, where N is a normal metal and F is a weak metallic ferromagnet [5]. Interesting properties of long Josephson junctions with an arbitrarily strong amplitude of the second harmonic in current phase relation were considered in [6]. We investigate the existence and stability magnetic flux distributions in dependence on the second harmonic contribution in both cases of negative and positive sign.

Stability analysis of $\varphi(x, p)$ is based on numerical solution of the corresponding Sturm-Liouville problem [7, 8]:

$$-\psi'' + q(x)\psi = \lambda\psi, \quad \psi'(\pm l) = 0 \quad (3)$$

with a potential $q(x) = a_1 \cos \varphi + 2a_2 \cos 2\varphi$.

The minimal eigenvalue $\lambda_0(p) > 0$ corresponds the stable solution. In case $\lambda_0(p) < 0$ solution $\varphi(x, p)$ is unstable. The case $\lambda_0(p) = 0$ indicates the bifurcation with respect to one of parameters $p = (l, a_1, a_2, h_e, \gamma)$.

2 NUMERICAL SCHEME

For numerical solution of the boundary problem (1),(2) we apply an iteration algorithm based on the continuous analog of Newton's method (CANM) [8]. Let an initial approximation for $\varphi_0(x)$ be given. At k^{th} step ($k = 1, 2, \dots$) we calculate:

1. Iteration correction $w_k(x)$ by solving linearized boundary problem

$$-w_k'' + q_{k-1}(x)w_k = \varphi_{k-1}'' - f_{k-1}(x), \quad (4)$$

$$w_k'(-l) = -\varphi_{k-1}'(-l) + h_e, \quad (5)$$

$$w_k'(l) = -\varphi_{k-1}'(l) + h_e, \quad (6)$$

where $f(x) = a_1 \sin \varphi + a_2 \sin 2\varphi - \gamma$.

2. Next approximation

$$\varphi_k(x) = \varphi_{k-1}(x) + \tau_k w_k$$

where parameter τ_k is calculated by the Ermakov-Kalitkin formula [9].

Table 1. Values of function φ and quantities σ (7) in some points of the interval $[-l; l]$ for solution of kind Φ^1 at $2l = 10$, $\gamma = 0$, $h_e = 0$, $a_1 = 1$, $a_2 = 0$.

x	$h = 0.15625$	$h = 0.078125$	$h = 0.0390625$	$\sigma \approx$
-5.00	0.0539477770043	0.0539492562101	0.0539493470654	16.2809
-3.75	0.1018425717580	0.1018436848799	0.1018437558002	15.6954
-2.50	0.3299569440243	0.3299543520791	0.3299541941853	16.4157
-1.25	1.1169110352657	1.1169428501398	1.1169448259542	16.1022
1.25	5.1662742719134	5.1662424570391	5.1662404812249	16.1022
2.50	5.9532283631551	5.9532309551002	5.9532311129941	16.4157
3.75	6.1813427354214	6.1813416222995	6.1813415513793	15.6954
5.00	6.2292375301752	6.2292360509694	6.2292359601142	16.2809

Further in order to simplify notations the iteration indices are omitted.

We introduce the grid $M_h = \{x_i = -l + (i-1)h, i = \overline{1, N}, x_N = l, h = 2l/(N-1)\}$. Numerov's discrete approximation [10] of (4)–(6) yields the following linear algebraic system with the three-diagonal structure at $i = \overline{3, N-2}$:

$$\begin{aligned} -25w_1 + 48w_2 - 36w_3 + 16w_4 - 3w_5 &= 12h(h_e - \varphi'_1) \\ a_2 w_1 + b_2 w_2 + c_2 w_3 + d_2 w_4 + e_2 w_5 &= r_2 \\ a_i w_{i-1} + b_i w_i + c_i w_{i+1} &= r_i, \quad i = \overline{3, N-2}, \\ a_{N-1} w_N + b_{N-1} w_{N-1} + c_{N-1} w_{N-2} + d_{N-1} w_{N-3} + e_{N-1} w_{N-4} &= r_{N-1} \\ 25w_N - 48w_{N-1} + 36w_{N-2} - 16w_{N-3} + 3w_{N-4} &= 12h(h_e - \varphi'_N) \end{aligned}$$

where the coefficients are determined by the following way

$$\begin{aligned} a_2 &= 1, \quad b_2 = -2 - \frac{7h^2}{6} q_2, \quad c_2 = 1 + \frac{5h^2}{12} q_3, \quad d_2 = -\frac{h^2}{3} q_4, \quad e_2 = \frac{h^2}{12} q_5, \\ r_2 &= \frac{h^2}{12} (14f_2 - 5f_3 + 4f_4 - f_5) - \frac{h^2}{12} (14\varphi''_2 - 5\varphi''_3 + 4\varphi''_4 - \varphi''_5), \\ a_i &= 1 - \frac{h^2}{12} q_{i-1}, \quad b_i = -2 - \frac{5h^2}{6} q_i, \quad c_i = 1 - \frac{h^2}{12} q_{i+1}, \quad i = \overline{3, N-2}, \\ r_i &= \frac{h^2}{12} (f_{i+1} + 10f_i + f_{i-1}) - \frac{h^2}{12} (\varphi''_{i+1} + 10\varphi''_i + \varphi''_{i-1}), \quad i = \overline{3, N-2}, \\ a_{N-1} &= 1, \quad b_{N-1} = -2 - \frac{7h^2}{6} q_{N-1}, \quad c_{N-1} = 1 + \frac{5h^2}{12} q_{N-2}, \\ d_{N-1} &= -\frac{h^2}{3} q_{N-3}, \quad e_{N-1} = \frac{h^2}{12} q_{N-4}, \end{aligned}$$

$$\begin{aligned} r_{N-1} = & \frac{h^2}{12} (-f_{N-4} + 4f_{N-3} - 5f_{N-2} + 14f_{N-1}) - \\ & - \frac{h^2}{12} (-\varphi'' + 4\varphi''_{N-3} - 5\varphi''_{N-2} + 14\varphi''_{N-1}), \end{aligned}$$

where $\varphi_i = \varphi(x_i)$, $q_i = q(x_i)$, $f_i = f(x_i)$.

In order to test the accuracy order of the above numerical scheme we perform the calculations of (1),(2) at the sequence of uniform grids with steps h , $h/2$ and $h/4$ ($h = 0.15625$). The results for solutions of the kind Φ^1 are presented in the table 1. It is seen, the quantities σ calculated by formula

$$\sigma(x_i) = \frac{\varphi_h(x_i) - \varphi_{h/2}(x_i)}{\varphi_{h/2}(x_i) - \varphi_{h/4}(x_i)}, \quad i = 1, 2, \dots, N, \quad (7)$$

are close to 2^4 that corresponds the theoretical accuracy order $O(h^4)$ of Numerov's approximation.

The StLP (3) is approximated by the three-point finite-difference second order formulas [11]. The resulting algebraic eigenvalue problem is solved numerically with help of a standard subroutine [12].

3 NUMERICAL RESULTS AND CONCLUSIONS

Trivial solutions. In the “traditional” case $a_2 = 0$ two trivial solutions $\varphi = 0$ and $\varphi = \pi$ (denoted by M_0 and M_π respectively) are known at $\gamma = 0$ and $h_e = 0$. Accounting of the second harmonic $a_2 \sin 2\varphi$ leads to appearing two additional solutions $\varphi = \pm \arccos(-a_1/2a_2)$ (denoted as $M_{\pm ac}$). The corresponding λ_0 as functions of 2SG-equation coefficients have the form $\lambda_0[M_0] = a_1 + 2a_2$, $\lambda_0[M_\pi] = -a_1 + 2a_2$ and $\lambda_0[M_{\pm ac}] = (a_1^2 - 4a_2^2)/2a_2$. The exponential stability of these constant solutions (CS) is determined by the signs of the parameters a_1 and a_2 and by its ratio a_1/a_2 .

The full energy associated with the distribution of $\varphi(x)$ is calculated by the formula [8]

$$F(p) = \int_{-l}^l \left[\frac{1}{2} \varphi'^2 + 1 - q(x) - \gamma\varphi \right] dx - h_e \Delta\varphi.$$

The full energy behavior in dependence on a_2 for considered distributions in the junction at $h_e = 0$, $\gamma = 0$, $a_1 = 1$, $2l = 10$ is shown in Fig. 1.

Stability properties of trivial solutions have been investigated in [13].

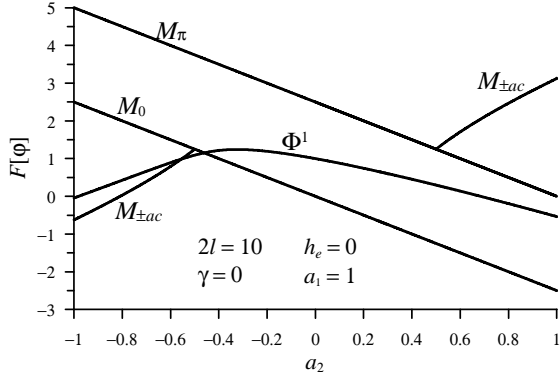


Figure 1. Full energy in dependence on $a_2 \in [-1; 1]$ at $h_e = 0$, $\gamma = 0$ and $2l = 10$ for CS and Φ^1 .

Fluxon solutions. The fluxons play an important role in the JJ physics. At small external fields h_e such distributions are fluxon Φ^1 , anti-fluxon Φ^{-1} and their bound states $\Phi^1\Phi^{-1}$ and $\Phi^{-1}\Phi^1$. As external magnetic field h_e is growing, more complicated stable fluxon and bound states appear: $\Phi^{\pm n}$ and $\Phi^{\pm n}\Phi^{\mp n}$ ($n = 1, 2, 3, \dots$).

The energy of one-fluxon distribution Φ^1 limits to unit $F(a_2 \rightarrow 0) \rightarrow 1$ which corresponds to an energy of a single fluxon Φ_∞^1 in a traditional “infinite” junction model at $a_1 = 1$, $a_2 = 0$. With change of a_2 the number of fluxons [8]

$$N(p) = \frac{1}{2l\pi} \int_{-l}^l \varphi(x) dx,$$

corresponding to the distribution Φ^1 is conserved i.e. $\partial N / \partial a_2 = 0$. Here we have $N[\Phi^1] = 1$.

Let us discuss the main features of the dependence $\lambda_0(h_e)$ for one-fluxon state Φ^1 in two intervals: $a_2 \in [0, 1]$ and $a_2 \in [-1, 0]$.

The change of the curve $\lambda_0(h_e)$ for one-fluxon state Φ^1 when the parameter a_2 increases in the interval $a_2 \in [0; 1]$ is shown in Fig. 2. When $h_e = 0$, the state Φ^1 remains unstable. With increase in a_2 , λ_0 increases monotonically and tends to zero. With increase in magnetic field this solution becomes stable. The bifurcation point moves to the left with increase of parameter in the interval $a_2 \in [0; 0.7]$. At $a_2 > 0.7$ it goes to the right again. It follows a stability interval ending at $h_{cr} \approx 2$. The second bifurcation point also moves to the left at $a_2 \in [0; 0.5]$. When a_2 is increased in $a_2 \in [0.5; 1]$, the bifurcation value h_{cr} is also increased.

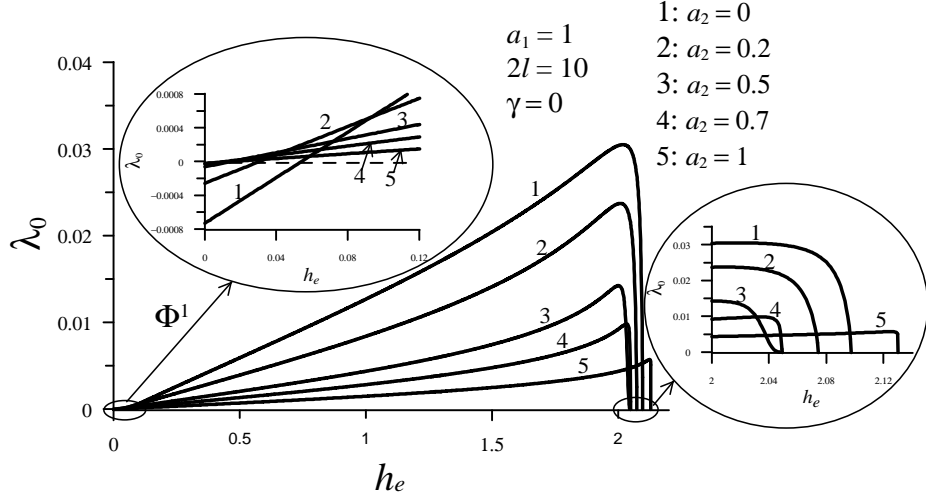


Figure 2. Dependence $\lambda_0(h_e)$ for Φ^1 at increase of $a_2 \in [0; 1]$ and $a_1 = 1$, $2l = 10$, $\gamma = 0$.

In the interval $a_2 \in [-1, 0]$ we observe the following. When a_2 increases in $(-0.5; 0]$, the curve $\lambda_0(h_e)$ for Φ^1 moves to the right (Fig. 3). At $a_2 < -0.5$ (case $a_2 = -0.7$ in Fig. 3), the curve corresponding to the stable solution Φ^1 has two separate branches that are intersected at $a_2 \approx -0.8$). Here we observe a region along h_e , where two different stable one-fluxon solutions (denoted by Φ^1 and Φ^{1*}) coexist, see Fig. 4.

Thus, we considered both positive and negative contributions of the second harmonic in 2GS equation. It is shown that its accounting leads appearing new constant solutions and changes the stability properties of the fluxon solutions. Coexisting of two stable one-fluxon solutions requires further analysis and physical interpretation.

Acknowledgements. Authors are thankfull to I.V.Puzynin and T.P. Puzynina for usefull discussions. The work of P.Kh.A. is partially supported in the frame of the Program for collaboration of JINR-Dubna and Bulgarian scientific centers “JINR – Bulgaria”. E.V.Z. was partially supported by RFFI under grant 09-01-00770-a.

References

1. A.A. Golubov, M.Yu. Kypriyanov,, E. Il'ichev, The current-phase relation in Josephson junctions. *Rev. Mod. Phys.* **76** (2004) 411–469.
2. K.K. Likharev, *Introduction in Josephson junction dynamics*, M. Nauka, GRFML (in Russian), 1985.

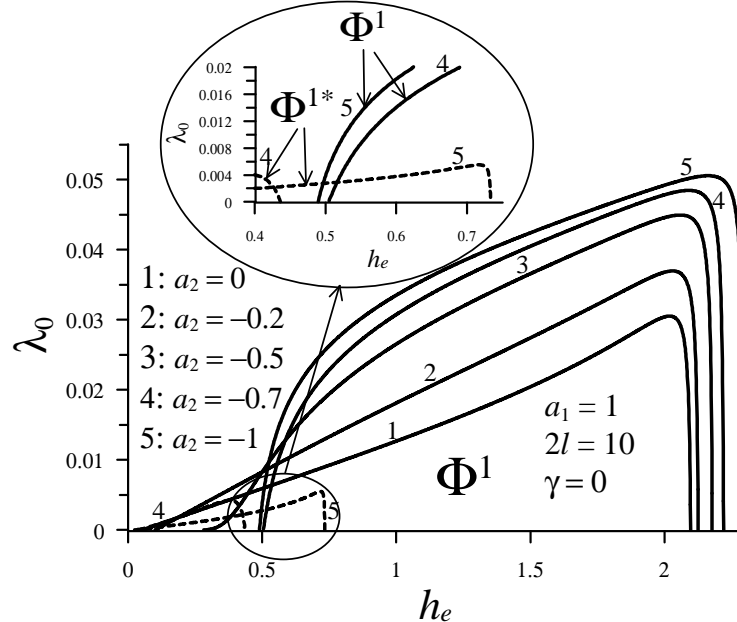


Figure 3. $\lambda_0(h_e)$ in dependence on $a_2 \in [-1; 0]$ for Φ^1 and Φ^{1*} , at $a_1 = 1$, $2l = 10$, $\gamma = 0$.

3. N. Hatakenaka, H. Takayanag, Yo. Kasai, S.Tanda, Double sine-Gordon fluxons in isolated long Josephson junction. *Physica B*. **284-288** (2000) 563-564,
4. A. Buzdin, A.E. Koshelev, Periodic alternating 0-and π -junction structures as realization of φ -Josephson junctions. *Phys. Rev. B*. **67** (2003) 220504(R)
5. V.V. Ryazanov, V.A. Oboznov, A.Yu. Rusanov, et al., Coupling of two superconductors through a ferromagnet: evidence for a pi junction. *Phys. Rev. Lett.* **36** (2001) 2427–2430.
6. E. Goldobin, D. Koelle, R.Kleiner, A. Buzdin, Josephson junctions with second harmonic in the current-phase relation: Properties of junctions. *Phys. Rev. B*. **76** (2007) 224–523.
7. Yu.S. Galpern, A.T. Filippov, Joint solution states in inhomogeneous Josephson junctions. *Sov. Phys. JETP*. **59** p. 894 (in Russian), 1984.
8. I. V. Puzynin, T. L. Boyadzhiev, S. I. Vinitskii, E. V. Zemlyanaya, T. P. Puzynina, O. Chuluunbaatar, Methods of Computational Physics for Investigation of Models of Complex Physical Systems. *Physics of Particles and Nuclei*. **38**(1) (2007) 70116.
9. V.V. Ermakov, N.N. Kalitkin, The optimal step and regularisation for Newton's method, *USSR Comp.Phys.and Math.Phys.* **21**(2), p. 235 (in Russian), 1981.
10. E.V. Zemlyanaya, I.V. Puzynin, T.P. Puzynina, PROGS2H4 – the software package for solving the boundary probem for the system of differential equations. *JINR Comm.* P11-97-414, Dubna, 18pp (in Russian), 1997.
11. N.S. Berezin, E.P. Zhidkov, *Numerical methods*, M. Nauka, GRFML (in Russian), 1960.

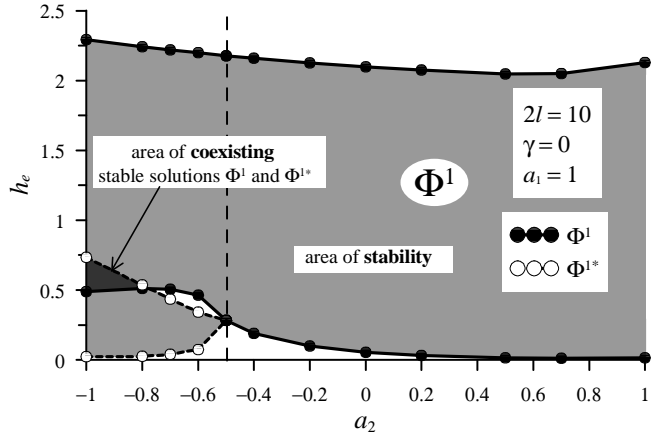


Figure 4. Bifurcation diagram of one-fluxon solutions at the plain of parameters a_2 and h_e . Here $a_1 = 1$, $2l = 10$, $\gamma = 0$.

12. TRIDIB – translation of the ALGOL procedure BISECT, Num. Math. 9, 386-393(1967) by Barth, Martin, and Wilkinson. Handbook for Auto. Comp., vol.ii – linear algebra (1971) 249-256.
13. P.Kh. Atanasova, E.V. Zemlyanaya, T.L. Boyadjiev, Yu.M. Shukrinov, Numerical modeling of long Josephson junctions in the frame of double sin-Gordon equation. JINR Preprint P11-2010-8, Dubna (2010); accepted to *Journal of Mathematical modeling*.

MONOTONE DOMAIN DECOMPOSITION ALGORITHM FOR SOLVING SYSTEMS OF SEMILINEAR PARABOLIC EQUATIONS

IGOR BOGLAEV

Institute of Fundamental Sciences, Massey University, Private Bag 11-222,
Palmerston North, New Zealand
I.Boglaev@massey.ac.nz

Abstract. For numerical solving coupled nonlinear parabolic equations, a monotone domain decomposition algorithm, which combines the monotone approach and an iterative domain decomposition method based on the Schwarz alternating, is proposed. A convergence analysis of the monotone domain decomposition algorithm is presented. An application to a gas-liquid interaction model is given.

1 INTRODUCTION

The parabolic system under consideration is given in the form

$$\partial u_i / \partial t - L_i u_i + f_i(x, t, u) = 0, \quad (x, t) \in \omega \times (0, T], \quad (1)$$

$$u_i(x, t) = g_i(x, t), \quad (x, t) \in \partial\omega \times (0, T],$$

$$u_i(x, 0) = \psi_i(x), \quad x \in \bar{\omega}, \quad i = 1, 2,$$

where $u = (u_1, u_2)$, ω is a connected bounded domain in \mathbb{R}^κ ($\kappa = 1, 2, \dots$) with boundary $\partial\omega$. $L_i u_i$, $i = 1, 2$, are given by

$$L_i u_i = \sum_{\alpha=1}^{\kappa} \frac{\partial}{\partial x_\alpha} \left(D_i(x, t) \frac{\partial u_i}{\partial x_\alpha} \right) + \sum_{\alpha=1}^{\kappa} v_{i,\alpha}(x, t) \frac{\partial u_i}{\partial x_\alpha}, \quad i = 1, 2,$$

where the coefficients of the differential operators are smooth and D_i , $i = 1, 2$, are positive in $\bar{\omega} \times [0, T]$. It is also assumed that the functions f_i , g_i , and ψ_i , $i = 1, 2$, are smooth in their respective domains.

Monotone iterative schemes for solving systems of parabolic equations were used in [1, 2]. Iterative domain decomposition algorithms based on

M. Koleva and L. Vulkov (Eds.), Proceedings of the Fifth Conference on Finite Difference Methods: Theory and Applications (FDM: T&A 2010) 2011, pp. 9–21.
© Rousse University Press 2011

Schwarz-type alternating procedures have received much attention for their potential as efficient algorithms for parallel computing. In [3, 4], for solving scalar parabolic problems, iterative algorithms which combine the monotone approach and an iterative domain decomposition method based on the Schwarz alternating procedure were proposed. In this paper, we extend the monotone domain decomposition algorithms from [3, 4] to the system of nonlinear parabolic equations (1).

The structure of the paper as follows. In Section 2, we introduce a nonlinear difference scheme for the numerical solution of (1). In Section 3, we present a monotone domain decomposition algorithm. We show that monotonic convergence is maintained under the proposed domain decomposition into nonoverlapping subdomains and associated algorithm. A convergence analysis of the monotone domain decomposition algorithm is presented. Section 4 applies the monotone domain decomposition algorithm to a gas-liquid iteration model.

2 THE NONLINEAR DIFFERENCE SCHEME

On the domains $\bar{\omega}$ and $[0, T]$, we introduce meshes $\bar{\omega}^h$ and $\bar{\omega}^\tau$, respectively. For solving (1), consider the nonlinear two-level implicit difference scheme in the canonical form [5]

$$\mathcal{L}_i U_i(p, t_k) + f_i(p, t_k, U) - \tau_k^{-1} U_i(p, t_{k-1}) = 0, \quad (p, t_k) \in \omega^h \times (\bar{\omega}^\tau \setminus \{0\}), \quad (2)$$

with the boundary and initial conditions

$$\begin{aligned} U_i(p, t_k) &= g_i(p, t_k), \quad (p, t_k) \in \partial\omega^h \times (\bar{\omega}^\tau \setminus \{0\}), \\ U_i(p, 0) &= \psi_i(p), \quad p \in \bar{\omega}^h, \quad i = 1, 2, \end{aligned}$$

where $U = (U_1, U_2)$, $\partial\omega^h$ is the boundary of $\bar{\omega}^h$ and time steps $\tau_k = t_k - t_{k-1}$, $k \geq 1$, $t_0 = 0$. The difference operators \mathcal{L}_i , $i = 1, 2$, are defined by

$$\begin{aligned} \mathcal{L}_i U_i(p, t_k) &= \mathcal{L}_i^h U_i(p, t_k) + \tau_k^{-1} U_i(p, t_k), \\ \mathcal{L}_i^h U_i(p, t_k) &= d_i(p, t_k) U_i(p, t_k) - \sum_{p' \in \sigma'_i(p)} a_i(p', t_k) U_i(p', t_k), \quad i = 1, 2, \end{aligned}$$

where $\sigma'_i(p) = \sigma_i(p) \setminus \{p\}$, $\sigma_i(p)$, $i = 1, 2$, are stencils of the scheme at an interior mesh point $p \in \omega^h$. We make the following assumptions on the coefficients of the difference operators \mathcal{L}_i^h , $i = 1, 2$:

$$d_i(p, t_k) > 0, \quad a_i(p', t_k) \geq 0, \quad p' \in \sigma'_i(p), \quad (3)$$

$$d_i(p, t_k) - \sum_{p' \in \sigma'_i(p)} a_i(p', t_k) \geq 0, \quad (p, t_k) \in \omega^h \times (\bar{\omega}^\tau \setminus \{0\}).$$

We also assume that the mesh $\bar{\omega}^h$ is connected. It means that for two interior mesh points \tilde{p} and \hat{p} , there exists a finite set of interior mesh points $\{p_1, p_2, \dots, p_s\}$ such that

$$p_1 \in \sigma'(\tilde{p}), \quad p_2 \in \sigma'(p_1), \dots, \quad p_s \in \sigma'(p_{s-1}), \quad \hat{p} \in \sigma'(p_s). \quad (4)$$

On each time level t_k , $k \geq 1$, introduce the linear problems

$$(\mathcal{L}_i + \bar{c}_i)W_i(p, t_k) = \Phi_i(p, t_k), \quad p \in \omega^h, \quad (5)$$

$$\bar{c}_i(p, t_k) \geq 0, \quad W_i(p, t_k) = g_i(p, t_k), \quad p \in \partial\omega^h, \quad i = 1, 2.$$

We formulate the maximum principle for the difference operators $\mathcal{L}_i + \bar{c}_i$, $i = 1, 2$.

Lemma 1. *Let the coefficients of the difference operators \mathcal{L}_i^h , $i = 1, 2$, satisfy (3) and the mesh $\bar{\omega}^h$ be connected. If mesh functions $W_i(p, t_k)$, $i = 1, 2$, satisfy the conditions*

$$(\mathcal{L}_i + \bar{c}_i)W_i(p, t_k) \geq 0 \ (\leq 0), \quad p \in \omega^h, \quad W_i(p, t_k) \geq 0 \ (\leq 0), \quad p \in \partial\omega^h,$$

then $W_i(p, t_k) \geq 0$ (≤ 0), $i = 1, 2$, in $\bar{\omega}^h$.

The proof of the lemma can be found in [5].

We say that the functions f_i , $i = 1, 2$, are quasi-monotone nondecreasing functions if $-\partial f_1 / \partial u_2 \geq 0$ and $-\partial f_2 / \partial u_1 \geq 0$.

In the case of the quasi-monotone nondecreasing functions, two vector mesh functions

$$\tilde{U}(p, t_k) = (\tilde{U}_1(p, t_k), \tilde{U}_2(p, t_k)), \quad \hat{U}(p, t_k) = (\hat{U}_1(p, t_k), \hat{U}_2(p, t_k)),$$

are called ordered upper and lower solutions of (2), if they satisfy the relation $\tilde{U}(p, t_k) \geq \hat{U}(p, t_k)$, $(p, t_k) \in \bar{\omega}^h \times (\bar{\omega}^\tau \setminus \{0\})$, and

$$\begin{aligned} \mathcal{L}_i \tilde{U}_i(p, t_k) + f_i(p, t_k, \tilde{U}) - \tau_k^{-1} \tilde{U}_i(p, t_{k-1}) &\geq 0, \quad (p, t_k) \in \omega^h \times (\bar{\omega}^\tau \setminus \{0\}), \\ \mathcal{L}_i \hat{U}_i(p, t_k) + f_i(p, t_k, \hat{U}) - \tau_k^{-1} \hat{U}_i(p, t_{k-1}) &\leq 0, \quad (p, t_k) \in \omega^h \times (\bar{\omega}^\tau \setminus \{0\}), \end{aligned} \quad (6)$$

$$\hat{U}_i(p, t_k) \leq g_i(p, t_k) \leq \tilde{U}_i(p, t_k), \quad p \in \partial\omega^h,$$

$$\hat{U}_i(p, 0) \leq \psi_i(p) \leq \tilde{U}_i(p, 0), \quad p \in \bar{\omega}^h, \quad i = 1, 2.$$

The ordering relation $\tilde{U} \geq \hat{U}$ is meant in the componentwise sense, that is, $\tilde{U}_i(p, t_k) \geq \hat{U}_i(p, t_k)$, $i = 1, 2$. For a given pair of ordered upper and lower solutions \hat{U} , \tilde{U} and t_k fixed, we define the sector

$$\langle \hat{U}(t_k), \tilde{U}(t_k) \rangle = \{U(p, t_k) : \hat{U}(p, t_k) \leq U(p, t_k) \leq \tilde{U}(p, t_k), p \in \bar{\omega}^h\}.$$

We assume that f_i , $i = 1, 2$, satisfy the constraints

$$\frac{\partial f_i}{\partial u_i}(p, t_k, U) \leq c_i(p, t_k), \quad \text{on } \langle \hat{U}(t_k), \tilde{U}(t_k) \rangle, \quad (7)$$

$$0 \leq -\frac{\partial f_i}{\partial u_{i'}}(p, t_k, U), \quad \text{on } \langle \hat{U}(t_k), \tilde{U}(t_k) \rangle, \quad i \neq i',$$

where $c_i(p, t_k)$, $i = 1, 2$, are nonnegative bounded functions in $\bar{\omega}^h \times \bar{\omega}^\tau$.

Remark 1 We say that f_i , $i = 1, 2$, are quasi-monotone nonincreasing functions if $-\partial f_1/\partial u_2 \leq 0$ and $-\partial f_2/\partial u_1 \leq 0$. When the functions f_i , $i = 1, 2$, are quasi-monotone nonincreasing, a transformation given by $(u_1, u_2) \rightarrow (M - u_1, u_2)$ for some constant $M > 0$ leads to a similar system where the functions are quasi-monotone nondecreasing.

We introduce the notation

$$F_i(p, t_k, U) = c_i(p, t_k)U_i(p, t_k) - f_i(p, t_k, U), \quad i = 1, 2, \quad (8)$$

and give a monotone property of F_i , $i = 1, 2$.

Lemma 2. Let U, V be any two functions in $\langle \hat{U}(t_k), \tilde{U}(t_k) \rangle$ such that $U(p, t_k) \geq V(p, t_k)$, and let (7) hold. Then

$$F_i(p, t_k, U) \geq F_i(p, t_k, V), \quad p \in \bar{\omega}^h, \quad i = 1, 2. \quad (9)$$

Proof. From (8), we have

$$\begin{aligned} F_1(p, t_k, U) - F_1(p, t_k, V) &= c_1(p, t_k)[U_1(p, t_k) - V_1(p, t_k)] - \\ &\quad [f_1(p, t_k, U_1, U_2) - f_1(p, t_k, V_1, U_2)] - \\ &\quad [f_1(p, t_k, V_1, U_2) - f_1(p, t_k, V_1, V_2)]. \end{aligned}$$

By the mean-value theorem,

$$[f_1(p, t_k, U_1, U_2) - f_1(p, t_k, V_1, U_2)] = \frac{\partial f_1}{\partial u_1}(U_1(p, t_k) - V_1(p, t_k)),$$

where the partial derivative $\partial f_1/\partial u_1$ is calculated at an intermediate point (E_1, U_2) , such that $V_1 \leq E_1 \leq U_1$, and, hence, satisfies (7). Thus, from here and the assumptions of the lemma, we conclude (9) for $i = 1$. Similarly, we can prove (9) for $i = 2$.

3 THE MONOTONE DOMAIN DECOMPOSITION ALGORITHM

We assume that ω is a rectangle

$$\bar{\omega} = \prod_{\alpha=1}^{\kappa} \bar{\omega}^{x_\alpha}, \quad \bar{\omega}^{x_\alpha} = \{0 \leq x_\alpha \leq r_\alpha\}.$$

On $\bar{\omega}^{x_\alpha}$, $\alpha = 1, \dots, \kappa$, we set up nonuniform meshes

$$\bar{\omega}^{hx_\alpha} = \{x_\alpha^{(j_\alpha)}, 0 \leq j_\alpha \leq N_\alpha; x_\alpha^{(0)} = 0, x_\alpha^{(N_\alpha)} = r_\alpha\}, \quad \alpha = 1, \dots, \kappa.$$

Thus, we can represent the mesh $\bar{\omega}^h$ in the form

$$\bar{\omega}^h = \omega^h \cup \partial\omega^h, \quad \bar{\omega}^h = \prod_{\alpha=1}^{\kappa} \bar{\omega}^{hx_\alpha}, \quad (10)$$

where ω^h and $\partial\omega^h$ are sets of interior and boundary mesh points, respectively.

By hyperplanes $x_1 = \text{const}$, we decompose the mesh $\bar{\omega}^h$ into M nonoverlapping rectangular subdomains ω_m^h , $m = 1, \dots, M$:

$$\begin{aligned} \bar{\omega}^h &= \bigcup_{m=1}^M \bar{\omega}_m^h, \quad \bar{\omega}_m^h = \bar{\omega}_m^{hx_1} \times \bar{\omega}_m^{hy}, \quad \bar{\omega}^{hy} \equiv \prod_{\alpha=2}^{\kappa} \bar{\omega}^{hx_\alpha}, \\ \bar{\omega}_m^{hx_1} &= \{r_{1,m-1} \leq x_1^{(j_1)} \leq r_{1,m}\}, \quad \omega_m^{hx_1} \cap \omega_{m+1}^{hx_1} = \emptyset, \\ r_{1,0} &= 0 < r_{1,1} < \dots < r_{1,M-1} < r_{1,M} = r_1, \quad \{r_{1,m}\}_{m=0}^M \subset \bar{\omega}^{hx_1}, \\ \bar{\omega}_m^h \cap \bar{\omega}_{m+1}^h &= \gamma_m, \quad \gamma_m = \{r_{1,m}\} \times \bar{\omega}^{hy}. \end{aligned}$$

Thus, we can write down the boundary of $\bar{\omega}_m^h$ as

$$\partial\omega_m^h = \gamma_m^0 \cup \gamma_{m-1} \cup \gamma_m, \quad \gamma_m^0 = \partial\omega^h \cap \bar{\omega}_m^h, \quad (\gamma_0 = \gamma_M = \emptyset).$$

On $\bar{\omega}^h$ we introduce $(M-1)$ interfacial subdomains $\bar{\vartheta}_m^h$, $m = 1, \dots, M-1$:

$$\bar{\vartheta}_m^h = \bar{\vartheta}_m^{hx_1} \times \bar{\omega}_m^{hy}, \quad \bar{\vartheta}_m^h \cap \bar{\vartheta}_{m+1}^h = \emptyset, \quad m = 1, \dots, M-2,$$

$$\bar{\vartheta}_m^{hx_1} = \{r_{1,m}^b \leq x_1^{(j_1)} \leq r_{1,m}^e\}, \quad r_{1,m}^b < r_{1,m} < r_{1,m}^e, \quad \{r_{1,m}^{b,e}\}_{m=1}^{M-1} \subset \omega^{hx_1},$$

where $\bar{\vartheta}_m^h$ overlaps $\bar{\omega}_m^h \cup \bar{\omega}_{m+1}^h$. The boundaries of $\bar{\vartheta}_m^h$ are denoted by

$$\begin{aligned} \partial\vartheta_m^h &= \gamma_m^c \cup \gamma_m^b \cup \gamma_m^e, \quad \gamma_m^c = \partial\omega^h \cap \bar{\vartheta}_m^h, \\ \gamma_m^b &= \{r_{1,m}^b\} \times \bar{\omega}_m^{hy}, \quad \gamma_m^e = \{r_{1,m}^e\} \times \bar{\omega}_m^{hy}. \end{aligned}$$

We assume that sizes of all the subdomains $\bar{\omega}_m^h$ and $\bar{\vartheta}_m^h$ allow to solve boundary value problems based on the difference equations from (2).

3.1 STATEMENT OF THE DOMAIN DECOMPOSITION ALGORITHM

Consider the following domain decomposition approach for solving (2). On each time level t_k , $k \geq 1$, we calculate $n_*(t_k)$ iterates $U^{(n)}(p, t_k)$, $p \in \bar{\omega}^h$, $n = 1, \dots, n_*$, as follows.

Step 1. Initialization: On the whole mesh $\bar{\omega}^h$, choose initial mesh functions $U_i^{(0)}(p, t_k)$, $p \in \bar{\omega}^h$, $i = 1, 2$.

Step 2. On subdomains $\bar{\omega}_m^h$, $m = 1, \dots, M$, compute mesh functions $U_{i,m}^{(n)}(p, t_k)$, $m = 1, \dots, M$, $i = 1, 2$, satisfying the difference schemes

$$(\mathcal{L}_i + c_i)Z_{i,m}^{(n)}(p, t_k) = -\mathcal{R}_i(p, t_k, U^{(n-1)}), \quad p \in \omega_m^h, \quad (11)$$

$$Z_{i,m}^{(1)}(p, t_k) = \begin{cases} g_i(p, t_k) - U_i^{(0)}(p, t_k), & p \in \gamma_m^0, \\ 0, & p \in \gamma_{m-1} \cup \gamma_m, \end{cases}$$

$$Z_{i,m}^{(n)}(p, t_k) = 0, \quad p \in \partial\omega_m^h, \quad n \geq 2,$$

$$U_{i,m}^{(n)}(p, t_k) = U_i^{(n-1)}(p, t_k) + Z_{i,m}^{(n)}(p, t_k), \quad p \in \bar{\omega}_m^h,$$

$$\mathcal{R}_i(p, t_k, U^{(n-1)}) = \mathcal{L}_i U_i^{(n-1)}(p, t_k) + f_i(p, t_k, U^{(n-1)}) - \tau_k^{-1} U_i(p, t_{k-1}).$$

Step 3. On the interfacial subdomains $\bar{\vartheta}_m^h$, $m = 1, \dots, M-1$, compute the difference problems

$$(\mathcal{L}_i + c_i)Y_{i,m}^{(n)}(p, t_k) = -\mathcal{R}_i(p, t_k, U^{(n-1)}), \quad p \in \vartheta_m^h, \quad (12)$$

$$Y_{i,m}^{(n)}(p, t_k) = \begin{cases} 0, & p \in \gamma_m^c, \\ Z_{i,m}^{(n)}(p, t_k), & p \in \gamma_m^b, \\ Z_{i,m+1}^{(n)}(p, t_k), & p \in \gamma_m^e, \end{cases}$$

$$V_{i,m}^{(n)}(p, t_k) = U_i^{(n-1)}(p, t_k) + Y_{i,m}^{(n)}(p, t_k), \quad p \in \bar{\vartheta}_m^h, \quad i = 1, 2.$$

Step 4. Compute the mesh functions $V_i^{(n)}(p, t_k)$, $p \in \bar{\omega}^h$, $i = 1, 2$, by piecing together the solutions on the subdomains

$$U_i^{(n)}(p, t_k) = \begin{cases} U_{i,m}^{(n)}(p, t_k), & p \in \bar{\omega}_m^h \setminus (\bar{\vartheta}_{m-1}^h \cup \bar{\vartheta}_m^h), \quad m = 1, \dots, M, \\ V_{i,m}^{(n)}(p, t_k), & p \in \bar{\vartheta}_m^h, \quad m = 1, \dots, M-1, \end{cases} \quad (13)$$

where $\bar{\vartheta}_0^h = \emptyset$ and $\bar{\vartheta}_M^h = \emptyset$.

Algorithm (11)–(13) can be carried out by parallel processing, since on each iterative step n the M problems (11) for $U_{i,m}^{(n)}(p, t_k)$, $m = 1, \dots, M$, $i = 1, 2$, and the $(M-1)$ problems (12) for $V_{i,m}^{(n)}(p, t_k)$, $m = 1, \dots, M-1$, $i = 1, 2$, can be implemented concurrently.

3.2 MONOTONE CONVERGENCE OF THE DOMAIN DECOMPOSITION ALGORITHM

In the following theorem, we prove the monotone property of the domain decomposition algorithm (11)–(13).

Theorem 1. *Assume that the coefficients of the difference operators \mathcal{L}_i , $i = 1, 2$, in (2) satisfy (3) and $f_i(p, t_k, U)$, $i = 1, 2$, satisfy (7), where \tilde{U} and \hat{U} are ordered upper and lower solutions (6) of (2). Then the sequences $\{\bar{U}^{(n)}\}$, $\{\underline{U}^{(n)}\}$ generated by (11)–(13) with $\bar{U}^{(0)} = \tilde{U}$ and $\underline{U}^{(0)} = \hat{U}$ are, respectively, ordered upper and lower solutions to (2) and converge monotonically to solutions $\bar{U}(p, t_k)$ and $\underline{U}(p, t_k)$ of (2), such that*

$$\underline{U}^{(n-1)}(p, t_k) \leq \underline{U}^{(n)}(p, t_k) \leq \bar{U}(p, t_k), \quad p \in \bar{\omega}^h, \quad (14)$$

$$\bar{U}(p, t_k) \leq \bar{U}^{(n)}(p, t_k) \leq \bar{U}^{(n-1)}(p, t_k), \quad p \in \bar{\omega}^h,$$

$$\underline{U}(p, t_k) \leq \bar{U}(p, t_k), \quad p \in \bar{\omega}^h,$$

where $k \geq 1$ and $n \geq 1$.

If $V(p, t_k)$ is any other solution in $\langle \hat{U}(t_k), \tilde{U}(t_k) \rangle$, then

$$\underline{U}(p, t_k) \leq V(p, t_k) \leq \bar{U}(p, t_k), \quad p \in \bar{\omega}^h. \quad (15)$$

Proof. Since $\bar{U}^{(0)} = \tilde{U}$ is an upper solution, then from (6) and (11) we conclude

$$(\mathcal{L}_i + c_i) \bar{Z}_{i,m}^{(1)}(p, t_1) \leq 0, \quad p \in \omega_m^h,$$

$$\bar{Z}_{i,m}^{(1)}(p, t_1) \leq 0, \quad p \in \partial\omega_m^h, \quad m = 1, \dots, M, \quad i = 1, 2.$$

By the maximum principle in Lemma 1, it follows that

$$\bar{Z}_{i,m}^{(1)}(p, t_1) \leq 0, \quad p \in \bar{\omega}_m^h, \quad m = 1, \dots, M, \quad i = 1, 2. \quad (16)$$

Similarly, from here, (12) and using the maximum principle, we have

$$\bar{Y}_{i,m}^{(1)}(p, t_1) \leq 0, \quad p \in \bar{\vartheta}_m^h, \quad m = 1, \dots, M, \quad i = 1, 2. \quad (17)$$

Similar to (16) and (17), for a lower solution $\underline{U}^{(0)} = \hat{U}$, we conclude that for $m = 1, \dots, M$, $i = 1, 2$,

$$\underline{Z}_{i,m}^{(1)}(p, t_1) \geq 0, \quad p \in \bar{\omega}_m^h, \quad \underline{Y}_{i,m}^{(1)}(p, t_1) \geq 0, \quad p \in \bar{\vartheta}_m^h.$$

We now prove that

$$\underline{U}_i^{(1)}(p, t_1) \leq \bar{U}_i^{(1)}(p, t_1), \quad p \in \bar{\omega}^h, \quad i = 1, 2. \quad (18)$$

From (11) for $m = 1, \dots, M$, $i = 1, 2$, we have

$$(\mathcal{L}_i + c_i) \bar{U}_{i,m}^{(1)}(p, t_1) = c_i \bar{U}_i^{(0)}(p, t_1) - f_i(p, t_1, \bar{U}^{(0)}) + \tau_1^{-1} U_i(p, t_0), \quad p \in \omega_m^h,$$

$$\bar{U}_{i,m}^{(1)}(p, t_1) = \begin{cases} g_i(p, t_1), & p \in \gamma_m^0, \\ \bar{U}_i^{(0)}(p, t_1), & p \in \gamma_{m-1} \cup \gamma_m, \end{cases}$$

and

$$(\mathcal{L}_i + c_i) \underline{U}_{i,m}^{(1)}(p, t_1) = c_i \underline{U}_i^{(0)}(p, t_1) - f_i(p, t_1, \underline{U}^{(0)}) + \tau_1^{-1} U_i(p, t_0), \quad p \in \omega_m^h,$$

$$\underline{U}_{i,m}^{(1)}(p, t_1) = \begin{cases} g_i(p, t_1), & p \in \gamma_m^0, \\ \underline{U}_i^{(0)}(p, t_1), & p \in \gamma_{m-1} \cup \gamma_m, \end{cases}$$

Letting $W_{i,m}^{(n)} = \bar{U}_{i,m}^{(n)} - \underline{U}_{i,m}^{(n)}$, $n \geq 1$, $m = 1, \dots, M$, $i = 1, 2$, we have

$$(\mathcal{L}_i + c_i) W_{i,m}^{(1)}(p, t_1) = F_i(p, t_1, \bar{U}^{(0)}) - F_i(p, t_1, \underline{U}^{(0)}), \quad p \in \omega_m^h,$$

$$W_{i,m}^{(1)}(p, t_1) = \begin{cases} 0, & p \in \gamma_m^0, \\ \bar{U}_i^{(0)}(p, t_1) - \underline{U}_i^{(0)}(p, t_1) \geq 0, & p \in \gamma_{m-1} \cup \gamma_m, \end{cases}$$

where F_i , $i = 1, 2$, are defined in (8). Since $\bar{U}^{(0)}(p, t_1) \geq \underline{U}^{(0)}(p, t_1)$, by Lemma 2, we conclude that the right hand sides in the difference equations are nonnegative. The positivity property in Lemma 1 implies

$$W_{i,m}^{(1)}(p, t_1) \geq 0, \quad p \in \omega_m^h, \quad m = 1, \dots, M, \quad i = 1, 2. \quad (19)$$

Similarly, denoting $X_{i,m}^{(n)} = \bar{V}_{i,m}^{(n)} - \underline{V}_{i,m}^{(n)}$, $n \geq 1$, $m = 1, \dots, M-1$, $i = 1, 2$, from (12) we get

$$(\mathcal{L}_i + c_i) X_{i,m}^{(1)}(p, t_1) = F_i(p, t_1, \bar{U}^{(0)}) - F_i(p, t_1, \underline{U}^{(0)}), \quad p \in \vartheta_m^h,$$

$$X_{i,m}^{(1)}(p, t_1) = \begin{cases} 0, & p \in \gamma_m^c, \\ W_{i,m}^{(1)}(p, t_1) \geq 0, & p \in \gamma_m^b, \\ W_{i,m+1}^{(1)}(p, t_1) \geq 0, & p \in \gamma_m^e. \end{cases}$$

Lemma 2 implies that the right hand sides of the difference equations are nonnegative. From here and (19), by Lemma 1, we conclude that

$$X_{i,m}^{(1)}(p, t_1) \geq 0, \quad p \in \bar{\vartheta}_m^h, \quad m = 1, \dots, M-1, \quad i = 1, 2.$$

From here, (19) and (13), we prove (18).

We now prove that $\bar{U}_i^{(1)}(p, t_1)$ and $\underline{U}_i^{(1)}(p, t_1)$, $i = 1, 2$, are upper and lower solutions (6), respectively. Using the mean-value theorem, from (11) we obtain for $m = 1, \dots, M$, $i = 1, 2$,

$$\mathcal{R}_i(p, t_1, \bar{U}_m^{(1)}) = - \left(c_i - \frac{\partial f_i}{\partial u_i} \right) \bar{Z}_{i,m}^{(1)}(p, t_1) + \frac{\partial f_i}{\partial u_{i'}} \bar{Z}_{i',m}^{(1)}(p, t_1), \quad p \in \omega_m^h, \quad (20)$$

where $\bar{U}_m^{(1)} = (\bar{U}_{1,m}^{(1)}, \bar{U}_{2,m}^{(1)})$, $i' \neq i$, and the partial derivatives are calculated at an intermediate point E such that $\bar{U}_i^{(1)} \leq E_i \leq \bar{U}_i^{(0)}$, $i = 1, 2$. From here and (18), it follows that the partial derivatives satisfy (7). From (7) and (16), we conclude that

$$\mathcal{R}_i(p, t_1, \bar{U}_m^{(1)}) \geq 0, \quad p \in \omega_m^h, \quad m = 1, \dots, M, \quad i = 1, 2. \quad (21)$$

Similarly, we can prove that

$$\mathcal{R}_i(p, t_1, \bar{V}_m^{(1)}) \geq 0, \quad p \in \vartheta_m^h, \quad m = 1, \dots, M-1, \quad i = 1, 2.$$

From (13), we conclude that

$$\mathcal{R}_i(p, t_1, \bar{U}^{(1)}) \geq 0, \quad p \in \omega^h \setminus \bigcup_{m=1}^{M-1} \gamma_m^{b,e}, \quad i = 1, 2.$$

From the boundary conditions for $\bar{U}_m^{(1)}$ and $\bar{V}_m^{(1)}$, it follows that $\bar{U}^{(1)}$ from (13) satisfies the boundary conditions. Thus, to prove that $\bar{U}^{(1)}$ is an upper solution of problem (2), we have to verify that the last inequality holds true on the interfacial boundaries γ_m^b , γ_m^e , $m = 1, \dots, M-1$. We check this inequality in the case of the left interfacial boundary γ_m^b , since the second case is checked in a similar way. From (11), (12), (16) and (17), we conclude that $\bar{Q}_m^{(1)}(p, t_1) = \bar{U}^{(1)}(p, t_1) - \bar{V}^{(1)}(p, t_1)$ satisfies the difference problem

$$(\mathcal{L}_i + c_i) \bar{Q}_{i,m}^{(1)}(p, t_1) = 0, \quad p \in \vartheta_m^{hb} = \omega_m^h \cap \vartheta_m^h,$$

$$\bar{Q}_{i,m}^{(1)}(p, t_1) = 0, \quad p \in \partial \vartheta_m^{hb} \setminus \gamma_m, \quad \bar{Q}_{i,m}^{(1)}(p, t_1) \geq 0, \quad p \in \gamma_m, \quad i = 1, 2.$$

In view of the maximum principle in Lemma 1,

$$\bar{Q}_{i,m}^{(1)}(p, t_1) \geq 0, \quad p \in \bar{\vartheta}_m^{hb}, \quad m = 1, \dots, M-1, \quad i = 1, 2. \quad (22)$$

From (2), (13) and taking into account that $\bar{V}_m^{(1)}(p, t_1) = \bar{U}_m^{(1)}(p, t_1)$, $p \in \gamma_m^b$, it follows that for $p \in \gamma_m^b$,

$$\begin{aligned} \mathcal{L}_i \bar{U}_i^{(1)}(p, t_1) &= d_i(p, t_1) \bar{U}_i^{(1)}(p, t_1) - \sum_{p' \in \sigma'(p)} a_i(p', t_1) \bar{U}_i^{(1)}(p', t_1) \\ &= d_i(p, t_1) \bar{U}_{i,m}^{(1)}(p, t_1) - \sum_{p' \in \sigma'_-(p)} a_i(p', t_1) \bar{U}_{i,m}^{(1)}(p', t_1) - \\ &\quad \sum_{p' \in \sigma'_+(p)} a_i(p', t_1) \bar{V}_{i,m}^{(1)}(p', t_1), \quad i = 1, 2, \end{aligned}$$

where $\sigma'_-(p)$ and $\sigma'_+(p)$ are stencil points on the left and right from p , such that $\sigma'(p) = \sigma'_-(p) \cup \sigma'_+(p)$. From here, (3) and (22), we conclude that $\mathcal{L}_i \bar{U}_i^{(1)}(p, t_1) \geq \mathcal{L}_i \bar{U}_{i,m}^{(1)}(p, t_1)$, $p \in \gamma_m^b$, and by (21),

$$\mathcal{R}_i(p, t_1, \bar{U}^{(1)}) \geq \mathcal{R}_i(p, t_1, \bar{U}_m^{(1)}) \geq 0, \quad p \in \gamma_m^b, \quad i = 1, 2.$$

Thus, $\bar{U}^{(1)}(p, t_1)$ is an upper solution. Similarly, we can prove that $\underline{U}^{(1)}(p, t_1)$ is a lower solution.

By induction on n , we can prove that $\{\bar{U}^{(n)}(p, t_1)\}$ is a monotonically decreasing sequence of upper solutions and $\{\underline{U}^{(n)}(p, t_1)\}$ is a monotonically increasing sequence of lower solutions, which satisfy (14) for t_1 .

From (14), it follows that $\lim \bar{U}^{(n)}(p, t_1) = \bar{U}(p, t_1)$, $p \in \bar{\omega}^h$ as $n \rightarrow \infty$ exists, and

$$\bar{U}(p, t_1) \leq \bar{U}^{(n)}(p, t_1), \quad p \in \bar{\omega}^h. \quad (23)$$

$$\lim_{n \rightarrow \infty} Z_{i,m}^{(n)}(p, t_1) = 0, \quad p \in \bar{\omega}_m^h, \quad \lim_{n \rightarrow \infty} Y_{i,m}^{(n)}(p, t_1) = 0, \quad p \in \bar{\vartheta}_m^h.$$

From here, (11) and (12), we conclude that

$$\lim_{n \rightarrow \infty} \mathcal{R}_i(p, t_1, \bar{U}^{(n)}) = 0, \quad p \in \omega^h, \quad i = 1, 2.$$

It means that $\bar{U}(p, t_1)$ solves (2) at t_1 . By the assumption of the theorem that $\tilde{U}(p, t_2)$ is an upper solution and from (23), it follows that $\tilde{U}(p, t_2)$ is an upper solution with respect to $\bar{U}(p, t_1)$. Using a similar argument, we can prove that the following limit

$$\lim_{n \rightarrow \infty} \bar{U}^{(n)}(p, t_2) = \bar{U}(p, t_2), \quad p \in \bar{\omega}^h, \quad (24)$$

exists and solves (2) at t_2 , where according (14), $\{\bar{U}^{(n)}(p, t_2)\}$ is a sequence of upper solutions with respect to $\bar{U}(p, t_1)$.

By induction on k , $k \geq 1$, we can prove that

$$\bar{U}(p, t_k) = \lim_{n \rightarrow \infty} \bar{U}^{(n)}(p, t_k), \quad p \in \bar{\omega}^h, \quad k \geq 1,$$

is a solution of the nonlinear difference scheme (2). Similarly, we can prove that the mesh function $\underline{U}(p, t_k)$ defined by

$$\underline{U}(p, t_k) = \lim_{n \rightarrow \infty} \underline{U}^{(n)}(p, t_k), \quad p \in \bar{\omega}^h, \quad k \geq 1, \quad (25)$$

is a solution of the nonlinear difference scheme (2).

If $V(p, t_k)$ is any other solution of (2) in $\langle \hat{U}(t_k), \tilde{U}(t_k) \rangle$, then we consider $\hat{U}(p, t_k)$ and $V(p, t_k)$ as ordered upper and lower solutions. Since the sequence $\{\underline{U}^{(n)}(p, t_k)\} = V(p, t_k)$ consists of the single element $V(p, t_k)$ for all n , relation (14) implies that

$$V(p, t_k) \leq \bar{U}(p, t_k), \quad p \in \bar{\omega}^h, \quad k \geq 1.$$

We now consider $V(p, t_k)$ and $\hat{U}(p, t_k)$ as ordered upper and lower solutions. Since the sequence $\{\bar{U}^{(n)}(p, t_k)\} = V(p, t_k)$ consists of the single element $V(p, t_k)$ for all n , relation (14) implies that

$$\underline{U}(p, t_k) \leq V(p, t_k), \quad p \in \bar{\omega}^h, \quad k \geq 1.$$

Thus, we prove (15) and the theorem.

4 THE GAS-LIQUID INTERACTION MODEL

The gas-liquid interaction model is governed by (1) with $L_i v_i = D_i \Delta v_i$, $f_i = \varsigma_i v_1 v_2$, $i = 1, 2$, where $v_1(x, t)$ and $v_2(x, t)$ the concentrations of the dissolved gas and the reactant, $D_i > 0$, $i = 1, 2$, are the diffusion coefficients, and ς_1 is the rate constant, $\varsigma_2 = k_1 \varsigma_1$ (see [6] for details). By choosing a suitable positive constant $K_1 > 0$ and letting $u_1 = K_1 - v_1 \geq 0$, $u_2 = v_2$, the system (1) is reduced to

$$\partial u_i / \partial t - D_i \Delta u_i + f_i(u_1, u_2) = 0, \quad (x, t) \in \omega \times (0, T], \quad i = 1, 2, \quad (26)$$

$$u_1(x, t) = g_1^*(x) \geq 0, \quad u_2(x, t) = g_2(x) \geq 0, \quad (x, t) \in \partial\omega \times (0, T],$$

$$u_1(x, 0) = \psi_1^*(x) \geq 0, \quad u_2(x, 0) = \psi_2(p), \quad x \in \bar{\omega},$$

$$f_1(u_1, u_2) = -\varsigma_1(K_1 - u_1)u_2, \quad f_2(u_1, u_2) = \varsigma_2(K_1 - u_1)u_2,$$

where $g_1^* = K_1 - g_1$, $\psi_1^* = K_1 - \psi_1$, $g_1 \geq 0$ on $\partial\omega$ and $\psi_1 \geq 0$ on $\bar{\omega}^h$. Based on physical considerations, the boundary and initial data are

assumed nonnegative in their respective domains. It is clear that f_1 and f_2 are quasi-monotone nondecreasing in the rectangle $S_K = [0, K_1] \times [0, K_2]$ for any positive constant K_2 .

The nonlinear difference scheme (2) is reduced to

$$\mathcal{L}_i U_i(p) + f_i(U_1, U_2) - \tau_k^{-1} U_i(p, t_{k-1}) = 0, \quad (p, t_k) \in \omega^h \times (\bar{\omega}^\tau \setminus \{0\}), \quad (27)$$

$$U_1(p, t_k) = g_1^*(p), \quad U_2(p, t_k) = g_2(p) \quad p \in \partial\omega^h \times (\bar{\omega}^\tau \setminus \{0\}),$$

$$U_1(p, 0) = \psi_1^*(p), \quad U_2(p, 0) = \psi_2(p), \quad p \in \bar{\omega}^h, \quad i = 1, 2,$$

where f_i , $i = 1, 2$, are defined in (26) and \mathcal{L}_i^h is an approximation of $D_i \Delta$ on a mesh $\bar{\omega}^h$. We assume that the coefficients of the difference operators \mathcal{L}_i^h , $i = 1, 2$, satisfy (3) and constant K_1 satisfies the inequality

$$K_1 \geq \max_{p \in \bar{\omega}^h} [\max(g_1(p), \psi_1(p))].$$

Consider the mesh functions

$$\tilde{U}(p, t_k) = (K_1, \bar{U}_2(p, t_k)), \quad \hat{U}(p, t_k) = (\underline{U}_1(p, t_k), 0), \quad (28)$$

where \bar{U}_2 solves the linear problem

$$\mathcal{L}_2 \bar{U}_2(p, t_k) = \tau_k^{-1} \bar{U}_2(p, t_{k-1}), \quad (p, t_k) \in \omega^h \times (\bar{\omega}^\tau \setminus \{0\}), \quad (29)$$

$$\bar{U}_2(p, t_k) = g_2(p), \quad p \in \partial\omega^h \times (\bar{\omega}^\tau \setminus \{0\}), \quad \bar{U}_2(p, 0) = \psi_2(p), \quad p \in \bar{\omega}^h,$$

and \underline{U}_1 solves the linear problem

$$\mathcal{L}_1 \underline{U}_1(p, t_k) = \tau_k^{-1} \underline{U}_1(p, t_{k-1}), \quad (p, t_k) \in \omega^h \times (\bar{\omega}^\tau \setminus \{0\}), \quad (30)$$

$$\underline{U}_1(p, t_k) = g_1^*(p), \quad p \in \partial\omega^h \times (\bar{\omega}^\tau \setminus \{0\}), \quad \underline{U}_1(p, 0) = \psi_1^*(p), \quad p \in \bar{\omega}^h.$$

Since $\psi_2 \geq 0$ and $g_2 \geq 0$, by the maximum principle in Lemma 1 we conclude that $\bar{U}_2(p, t_1) \geq 0$, $p \in \bar{\omega}^h$. Now by induction on k , we prove that

$$\bar{U}_2(p, t_k) \geq 0, \quad p \in \bar{\omega}^h, \quad k \geq 1.$$

Similarly, we can prove that

$$\underline{U}_1(p, t_k) \geq 0, \quad p \in \bar{\omega}^h, \quad k \geq 1.$$

From (29), (30), it follows that \tilde{U} and \hat{U} from (28) satisfy (6). Since $\bar{U}_2 \geq 0$, then for proving that these mesh functions are ordered upper

and lower solutions of (2), we only need to check that $K_1 \geq \underline{U}_1$. From (30), it follows that the function $W = K_1 - \underline{U}_1$ satisfies the problem

$$\mathcal{L}_1 W(p, t_k) \geq \tau_k^{-1} W(p, t_{k-1}), \quad (p, t_k) \in \omega^h \times (\bar{\omega}^\tau \setminus \{0\}),$$

$$W(p, t_k) \geq 0, \quad p \in \partial\omega^h \times (\bar{\omega}^\tau \setminus \{0\}), \quad W(p, 0) \geq 0, \quad p \in \bar{\omega}^h.$$

Since $W(p, 0) \geq 0$ on $\bar{\omega}^h$ and $W(p, t_1) \geq 0$ on $\partial\omega^h$, by the maximum principle in Lemma 1, we conclude that $W(p, t_1) \geq 0$ on $\bar{\omega}^h$. Now by induction on k , we prove that $W(p, t_k) \geq 0$ on $\bar{\omega}^h$. Thus, we prove that the functions from (28) are ordered upper and lower solutions to (27).

From (26), we conclude that in $\langle \hat{U}, \tilde{U} \rangle$

$$\frac{\partial f_1}{\partial u_1}(p, t_k, U) \leq \varsigma_1 U_2(p, t_k) \leq \varsigma_1 \bar{U}_2(p, t_k), \quad p \in \bar{\omega}^h, \quad k \geq 1,$$

$$\frac{\partial f_2}{\partial u_2}(p, t_k, U) \leq \varsigma_2(K_1 - U_1(p, t_k)) \leq \varsigma_2 K_1, \quad p \in \bar{\omega}^h, \quad k \geq 1,$$

and the assumptions in (7) hold true with

$$c_1(p, t_k) = \varsigma_1 \bar{U}_2(p, t_k), \quad c_2(p, t_k) = \varsigma_2 K_1.$$

References

1. C.V. Pao, Numerical methods for coupled systems of nonlinear parabolic boundary value problems, *J. Math. Anal. Appl.* **151** (1990) 581–608.
2. C.V. Pao, Numerical analysis of coupled systems of nonlinear parabolic equations, *SIAM J. Numer. Anal.* **36** (1999) 393–416 .
3. I. Boglaev, Monotone algorithms for solving nonlinear monotone difference schemes of parabolic type in the canonical form, *Numer. Math.* **14** (2006) 247–266.
4. I. Boglaev, Domain decomposition for a parabolic convection-diffusion problem, *Numer. Methods Partial Diff. Eqs.* **22** (2006) 1361–1378 .
5. A. Samarskii, *The Theory of Difference Schemes*, Marcel Dekker, New York-Basel, 2001.
6. P.V. Danckwerts, *Gas-Liquid Reactions*, McGraw-Hill, New York, 1970.

TWO FINITE DIFFERENCE SCHEMES FOR A CONJUGATE FLUID-BODY PROBLEM

T. CHERNOGOROVA AND V. TODOROV

Sofia University, Faculty of Mathematics and Informatics
`{chernogorova, venelintodorov}@fmi.uni-sofia.bg`

Abstract In this paper we study numerically a model problem for a heat transfer between a fluid and a solid. For this model we construct two difference schemes - explicit and explicit-implicit. The schemes are first order accurate in the space and time grid size. The monotonicity and the stability of the schemes are studied. Richardson extrapolation to improve the accuracy of the schemes is used. Some results from computational experiments are also presented.

1 INTRODUCTION

The heat-mass transfer is an area that has many interesting scientific and engineering applications. From scientific point of view it is interesting to mathematically derive and study for stability, convergence, etc. the appropriate numerical approximations of various differential model problems.

When the solution is known to be smooth outside the interface and the grid points lie on the interface, it is easy to obtain highly accurate finite-difference discretizations. But when the interface is curve-linear or moving (which is a natural situation for the problem considered below) the well-known procedures become invalid. Several strategies have been proposed to tackle this issue [1, 3].

A large class of problems in nature and technology involves an inherently unsteady and coupled interaction between fluid and rigid bodies. The well-posedness of the differential problems that describe a fluid-body interaction studies in many papers, starting from [2].

In the recent year many numerical techniques are developed for interface problems, see for example [1, 3, 4].

The outline of the paper is the following. In the next section the formulation of the problem is introduced. In Section 3 an explicit difference scheme is studied, while in Section 4 - an semi-explicit difference scheme.

M. Koleva and L. Vulkov (Eds.), Proceedings of the Fifth Conference on Finite Difference Methods: Theory and Applications (FDM: T&A 2010) 2011, pp. 22–36.
© Rousse University Press 2011

Effective algorithms for solution of the linear algebraic systems of equations are proposed. Numerical experiments combined with Richardson extrapolation are discussed in Section 5.

2 THE DIFFERENTIAL PROBLEM

The particular application in [4] is a micro scale satellite cold gas propulsion system with heat sources that can be used for controlling the flow rate, see Fig.1 in [4]. This engineering system is described by the hyperbolic-parabolic system [4] :

$$\mathbf{w}_t + \mathbf{A}\mathbf{w}_x = \varepsilon\mathbf{B}\mathbf{w}_{xx}, \quad -1 \leq x \leq 0, \quad 0 \leq t \leq t_0, \quad (1)$$

$$T_t = kT_{xx}, \quad 0 \leq x \leq 1, \quad 0 \leq t \leq t_0, \quad (2)$$

where

$$\mathbf{w} = \begin{bmatrix} \rho \\ u \\ J \end{bmatrix}, \quad \mathbf{A} = \begin{pmatrix} a & b & 0 \\ b & a & c \\ 0 & c & a \end{pmatrix}, \quad \mathbf{B} = \begin{pmatrix} 0 & 0 & 0 \\ 0 & \alpha & 0 \\ 0 & 0 & \beta \end{pmatrix}. \quad (3)$$

Here ρ is density of the gas, u is the velocity of the gas, and J the temperature of the gas, while with T is denoted the temperature of the canal wall (the rigid body). We will assume that a, b, c, α and β are positive numbers.

Let us rewrite the system (1) - (3) in the scalar form. We have

1) for $-1 < x < 0$ -

$$\frac{\partial \rho}{\partial t} + a \frac{\partial \rho}{\partial x} + b \frac{\partial u}{\partial x} = 0, \quad (4)$$

$$\frac{\partial u}{\partial t} + b \frac{\partial \rho}{\partial x} + a \frac{\partial u}{\partial x} + c \frac{\partial J}{\partial x} = \varepsilon \alpha \frac{\partial^2 u}{\partial x^2}, \quad (5)$$

$$\frac{\partial J}{\partial t} + c \frac{\partial u}{\partial x} + a \frac{\partial J}{\partial x} = \varepsilon \beta \frac{\partial^2 J}{\partial x^2}; \quad (6)$$

2) for $0 < x < 1$ -

$$\frac{\partial T}{\partial t} = k \frac{\partial^2 T}{\partial x^2}. \quad (7)$$

We will solve (4) - (7) at additional conditions for conjugation on the interface $x = 0$:

$$J(0-0, t) = T(0+0, t), \quad \beta \varepsilon \frac{\partial J}{\partial x}(0-0, t) = k \frac{\partial T}{\partial x}(0+0, t); \quad (8)$$

and boundary conditions

1) for $x = -1$ -

$$\frac{1}{d}(-c\rho(-1, t) + bJ(-1, t)) = g_1(t), \quad d = \sqrt{b^2 + c^2}, \quad (9)$$

$$\frac{1}{\sqrt{2}d}(b\rho(-1, t) + du(-1, t) + cJ(-1, t)) = g_2(t), \quad (10)$$

$$\alpha d \frac{\partial u}{\partial x}(-1, t) - \beta c \frac{\partial J}{\partial x}(-1, t) = g_3(t); \quad (11)$$

2) for $x = 0$ -

$$u(0, t) = u_{0,s}(t); \quad (12)$$

3) for $x = 1$ -

$$T(1, t) = T_{0,r}(t). \quad (13)$$

and initial conditions

$$\rho|_{t=0} = \rho_c(x), \quad u|_{t=0} = u_c(x), \quad J|_{t=0} = J_c(x), \quad T|_{t=0} = T_c(x). \quad (14)$$

To derive difference schemes, we will reformulate the boundary conditions at $x = -1$. From (9) we express the function ρ and get

$$\rho(-1, t) = \frac{b}{c}J(-1, t) - \frac{d}{c}g_1(t). \quad (15)$$

Then placing (15) in (10) we obtain

$$dJ(-1, t) + cu(-1, t) = \sqrt{2}cg_2(t) + bg_1(t). \quad (16)$$

3 EXPLICIT DIFFERENCE SCHEME

For problem (4) - (8), (11) - (16) we construct an explicit difference scheme for all equations on the following two uniform meshes in the intervals $[-1, 0]$ and $[0, 1]$ and uniform mesh in the interval $[0, t_0]$:

$$\bar{\omega}_{hl} = \{x_i = -1 + (i - 1)h, \quad i = 1, 2, \dots, M + 1, \quad h = 1/M\},$$

$$\bar{\omega}_{hd} = \{x_i = (i - 1)h, \quad i = 1, 2, \dots, N + 1, \quad h = 1/N\},$$

$$\bar{\omega}_\tau = \{t_j = (j - 1)\tau, \quad j = 1, 2, \dots, j_0 + 1, \quad \tau = t_0/j_0\}.$$

The difference scheme is the following:

for $i = 2, 3, \dots, M + 1$ -

$$\frac{\hat{\rho}_i - \rho_i}{\tau} + a \frac{\rho_i - \rho_{i-1}}{h} + b \frac{u_i - u_{i-1}}{h} = 0; \quad (17)$$

for $i = 2, 3, \dots, M$ -

$$\frac{\hat{u}_i - u_i}{\tau} + b \frac{\rho_i - \rho_{i-1}}{h} + a \frac{u_i - u_{i-1}}{h} + c \frac{J_i - J_{i-1}}{h} = \varepsilon \alpha \frac{u_{i+1} - 2u_i + u_{i-1}}{h^2}, \quad (18)$$

$$\frac{\hat{J}_i - J_i}{\tau} + c \frac{u_i - u_{i-1}}{h} + a \frac{J_i - J_{i-1}}{h} = \varepsilon \beta \frac{J_{i+1} - 2J_i + J_{i-1}}{h^2}; \quad (19)$$

for $i = 2, 3, \dots, N$ -

$$\frac{\hat{T}_i - T_i}{\tau} = k \frac{T_{i+1} - 2T_i + T_{i-1}}{h^2}; \quad (20)$$

for boundary conditions and conjugation conditions -

$$\hat{\rho}_1 = \frac{b}{c} \hat{J}_1 - \frac{d}{c} g_1(t_{j+1}), \quad (21)$$

$$d\hat{J}_1 + c\hat{u}_1 = \sqrt{2}cg_2(t_{j+1}) + bg_1(t_{j+1}), \quad (22)$$

$$\alpha d \frac{\hat{u}_2 - \hat{u}_1}{h} - \beta c \frac{\hat{J}_2 - \hat{J}_1}{h} = g_3(t_{j+1}), \quad (23)$$

$$\hat{u}_{M+1} = u_{0,s}(t_{j+1}), \quad (24)$$

$$\hat{T}_{N+1} = T_{0,r}(t_{j+1}), \quad (25)$$

$$\hat{J}_{M+1} = \hat{T}_1, \quad \beta \varepsilon \frac{\hat{J}_{M+1} - \hat{J}_M}{h} = k \frac{\hat{T}_2 - \hat{T}_1}{h}. \quad (26)$$

The local error of approximation of the differential scheme (17) - (26) is $O(\tau + h)$.

We briefly describe the ALGORITHM for realization of the explicit scheme. We let $\gamma = \frac{\tau}{h^2}$ и $\delta = \frac{\tau}{h}$. Then the formulas for the computation of approximate solution are as follows:

1. From (17)

$$\hat{\rho}_i = \rho_i - a\delta(\rho_i - \rho_{i-1}) - b\delta(u_i - u_{i-1}), \quad i = 2, 3, \dots, M + 1;$$

2. From (18) and (24)

$$\hat{u}_i = \left(1 - \frac{a\tau}{h} - \frac{2\varepsilon\alpha\tau}{h^2}\right) u_i + \frac{\varepsilon\alpha\tau}{h^2} u_{i+1} + \left(\frac{a\tau}{h} + \frac{\varepsilon\alpha\tau}{h^2}\right) u_{i-1} -$$

$$b\tau \frac{\rho_i - \rho_{i-1}}{h} - c\tau \frac{J_i - J_{i-1}}{h}, \quad i = 2, 3, \dots, M, \quad \hat{u}_{M+1} = u_{0,s}(t_{j+1});$$

3. From (19)

$$\hat{J}_i = \left(1 - \frac{a\tau}{h} - \frac{2\varepsilon\beta\tau}{h^2}\right) J_i + \left(\frac{a\tau}{h} + \frac{\varepsilon\beta\tau}{h^2}\right) J_{i-1} + \frac{\varepsilon\beta\tau}{h^2} J_{i+1} - c\tau \frac{u_i - u_{i-1}}{h},$$

$$i = 2, 3, \dots, M;$$

4. From (22), (23) we obtain

$$d\hat{J}_1 + c\hat{u}_1 = \sqrt{2}cg_2(t_{j+1}) + bg_1(t_{j+1}),$$

$$\beta c\hat{J}_1 - \alpha d\hat{u}_1 = hg_3(t_{j+1}) + \beta c\hat{J}_2 - \alpha d\hat{u}_2.$$

Let us introduce the notations

$$F_1 = \sqrt{2}cg_2(t_{j+1}) + bg_1(t_{j+1}),$$

$$F_2 = hg_3(t_{j+1}) + \beta c\hat{J}_2 - \alpha d\hat{u}_2.$$

Then from the system

$$\begin{cases} d\hat{J}_1 + c\hat{u}_1 = F_1 \\ \beta c\hat{J}_1 - \alpha d\hat{u}_1 = F_2 \end{cases}$$

we get

$$\hat{J}_1 = \frac{\Delta_1}{\Delta}, \quad \hat{u}_1 = \frac{\Delta_2}{\Delta},$$

where

$$\Delta = -\alpha d^2 - \beta c^2, \quad \Delta_1 = -\alpha dF_1 - cF_2, \quad \Delta_2 = -\beta cF_1 + dF_2.$$

Now for the function ρ we have

$$\hat{\rho}_1 = \frac{b}{c}\hat{J}_1 - \frac{d}{c}g_1(t_{j+1}).$$

5. From (20) and (25)

$$\hat{T}_i = \left(1 - \frac{2k\tau}{h^2}\right) T_i + \frac{k\tau}{h^2} T_{i+1} + \frac{k\tau}{h^2} T_{i-1}, \quad i = 2, 3, \dots, N,$$

$$\hat{T}_{N+1} = T_{0,r}(t_{j+1});$$

6. Formula (26) implies

$$\hat{J}_{M+1} = \hat{T}_1, \quad \beta\varepsilon (\hat{J}_{M+1} - \hat{J}_M) = k (\hat{T}_2 - \hat{T}_1), \quad \beta\varepsilon (\hat{T}_1 - \hat{J}_M) = k (\hat{T}_2 - \hat{T}_1),$$

and we find

$$\hat{J}_{M+1} = \hat{T}_1 = \frac{k\hat{T}_2 + \beta\varepsilon\hat{J}_M}{\beta\varepsilon + k}.$$

This completes the *Algorithm*.

We will investigate the monotonicity and stability of the difference scheme using the discrete maximum principle [5].

Theorem 1. *Let*

$$\delta = \frac{\tau}{h} < \frac{1}{a} \text{ and } \gamma = \frac{\tau}{h^2} < \min \left\{ \frac{1}{2k}, \frac{1}{ah + 2\alpha\varepsilon}, \frac{1}{ah + 2\beta\varepsilon} \right\}. \quad (27)$$

Then the difference scheme (17) - (26) is monotone and stable in the discrete maximal norm.

Outline of the proof. *Writing the discrete equations for the density ρ in canonical form, we find the condition that provide monotonicity and stability [5]: $\delta < \frac{1}{a}$ namely the left part of (27).*

Again, writing the discrete equations for the velocity u in canonical form we get

$$h > \frac{2\varepsilon\alpha\delta}{1 - a\delta}.$$

However $\delta < 1/a$ implies $1 - a\delta > 0$ and it follows from above that

$$\frac{\tau}{h^2} < \frac{1}{ah + 2\alpha\varepsilon}. \quad (28)$$

In a similar way, for \hat{J} and \hat{T} , we arrive to the conditions:

$$\frac{\tau}{h^2} < \frac{1}{ah + 2\beta\varepsilon}, \quad \frac{\tau}{h^2} < \frac{1}{2k}. \quad (29)$$

4 EXPLICIT-IMPLICIT DIFFERENCE SCHEME

For the problem (4) - (8) and (11) - (16) we will construct a new difference scheme. For the equation (4) it will be explicit and for (5) - (8) - purely implicit [6]. We will call this scheme *explicit-implicit*. On the new time level we will obtain a complicated system of equations for which we propose an effective algorithm.

The difference scheme looks as follows:
for $i = 2, 3, \dots, M+1$ -

$$\frac{\hat{\rho}_i - \rho_i}{\tau} + a \frac{\rho_i - \rho_{i-1}}{h} + b \frac{\hat{u}_i - \hat{u}_{i-1}}{h} = 0; \quad (30)$$

for $i = 2, 3, \dots, M$ -

$$\frac{\hat{u}_i - u_i}{\tau} + b \frac{\rho_i - \rho_{i-1}}{h} + a \frac{\hat{u}_i - \hat{u}_{i-1}}{h} + c \frac{\hat{J}_i - \hat{J}_{i-1}}{h} = \varepsilon \alpha \frac{\hat{u}_{i+1} - 2\hat{u}_i + \hat{u}_{i-1}}{h^2}, \quad (31)$$

$$\frac{\hat{J}_i - J_i}{\tau} + c \frac{\hat{u}_i - \hat{u}_{i-1}}{h} + a \frac{\hat{J}_i - \hat{J}_{i-1}}{h} = \varepsilon \beta \frac{\hat{J}_{i+1} - 2\hat{J}_i + \hat{J}_{i-1}}{h^2}; \quad (32)$$

for $i = 2, 3, \dots, N$ -

$$\frac{\hat{T}_i - T_i}{\tau} = k \frac{\hat{T}_{i+1} - 2\hat{T}_i + \hat{T}_{i-1}}{h^2}; \quad (33)$$

boundary conditions and conditions of conjugation -

$$\hat{\rho}_1 = \frac{b}{c} \hat{J}_1 - \frac{d}{c} g_1(t_{j+1}), \quad (34)$$

$$d\hat{J}_1 + c\hat{u}_1 = \sqrt{2}cg_2(t_{j+1}) + bg_1(t_{j+1}), \quad (35)$$

$$\alpha d \frac{\hat{u}_2 - \hat{u}_1}{h} - \beta c \frac{\hat{J}_2 - \hat{J}_1}{h} = g_3(t_{j+1}), \quad (36)$$

$$\hat{u}_{M+1} = u_{0,s}(t_{j+1}), \quad (37)$$

$$\hat{T}_{N+1} = T_{0,r}(t_{j+1}), \quad (38)$$

$$\hat{J}_{M+1} = \hat{T}_1, \quad \beta \varepsilon \frac{\hat{J}_{M+1} - \hat{J}_M}{h} = k \frac{\hat{T}_2 - \hat{T}_1}{h}. \quad (39)$$

The local error of approximation of the difference scheme (30) - (39) is $O(\tau + h)$.

Suppose that on the j -th level the numerical solution is already obtained. Then the algorithm for solution of the difference system consist in the following steps.

We perform forward stage of the matrix Thomas' algorithm [7] for the system of equations (31), (32), (35) and (36). The goal is to obtain a relation between \hat{J}_{M+1} and \hat{J}_M and then to use $\hat{J}_{M+1} = \hat{T}_1$ in the second relation of the conjugation condition (39). There in (39) participate only \hat{T}_2 and \hat{T}_1 . Therefore we obtain a boundary condition at the left end for \hat{T} .

We perform right Thomas' algorithm for \hat{T} - equation (33) with boundary conditions (38) and the modified (39). As a result we obtain the values of \hat{T} and from here we find \hat{T}_1 .

We perform back stage of the Thomas' algorithm for the system of equations (31), (32), (35) and (36). Let introduce vector $\hat{\mathbf{Y}} = \begin{pmatrix} \hat{u}_i \\ \hat{J}_i \end{pmatrix}$, $i = 1, 2, \dots, M+1$ and use the fact that $\hat{J}_{M+1} = \hat{T}_1$ and $\hat{u}_{M+1} = u_{0,s}(t_{j+1})$. As a result we obtain $\hat{\mathbf{Y}}$. Finally, we solve the equation (30) for density ρ .

Now we will describe the ALGORITHM in details. We write the boundary equations (35), (36) and equations (31) and (32), as well as the conjugation conditions (39), in the matrix form

$$\begin{pmatrix} \alpha d - \beta c \\ 0 \end{pmatrix} \begin{pmatrix} \hat{u}_2 \\ \hat{J}_2 \end{pmatrix} - \begin{pmatrix} \alpha d - \beta c \\ -c - d \end{pmatrix} \begin{pmatrix} \hat{u}_1 \\ \hat{J}_1 \end{pmatrix} = - \begin{pmatrix} -hg_3(t_{j+1}) \\ -\sqrt{2}cg_2(t_{j+1}) - bg_1(t_{j+1}) \end{pmatrix}, \quad (40)$$

$i = 2, 3, \dots, M$:

$$\begin{aligned} & \begin{pmatrix} \varepsilon\alpha\gamma & 0 \\ 0 & \varepsilon\beta\gamma \end{pmatrix} \begin{pmatrix} \hat{u}_{i+1} \\ \hat{J}_{i+1} \end{pmatrix} - \begin{pmatrix} 2\varepsilon\alpha\gamma + a\delta + 1 & c\delta \\ c\delta & 2\varepsilon\beta\gamma + a\delta + 1 \end{pmatrix} \begin{pmatrix} \hat{u}_i \\ \hat{J}_i \end{pmatrix} + \\ & + \begin{pmatrix} \varepsilon\alpha\gamma + a\delta & c\delta \\ c\delta & \varepsilon\beta\gamma + a\delta \end{pmatrix} \begin{pmatrix} \hat{u}_{i-1} \\ \hat{J}_{i-1} \end{pmatrix} = - \begin{pmatrix} u_i - b\delta(\rho_i - \rho_{i-1}) \\ J_i \end{pmatrix}, \quad (41) \end{aligned}$$

$$- \begin{pmatrix} 1 & 0 \\ 0 & 0 \end{pmatrix} \begin{pmatrix} \hat{u}_{M+1} \\ \hat{J}_{M+1} \end{pmatrix} + \begin{pmatrix} 0 & 0 \\ 0 & -\varepsilon\beta\hat{T}_1 \end{pmatrix} \begin{pmatrix} \hat{u}_M \\ \hat{J}_M \end{pmatrix} = - \begin{pmatrix} u_{0,s}(t_{j+1}) \\ \varepsilon\beta\hat{T}_1 - k(\hat{T}_2 - \hat{T}_1) \end{pmatrix}. \quad (42)$$

We introduce the matrices

$$\begin{aligned} \mathbf{A}_1 &= \begin{pmatrix} \alpha d - \beta c \\ 0 \end{pmatrix}, \quad \mathbf{B}_1 = \begin{pmatrix} \alpha d - \beta c \\ -c - d \end{pmatrix}, \quad \mathbf{F}_1 = \begin{pmatrix} -hg_3(t_{j+1}) \\ -\sqrt{2}cg_2(t_{j+1}) - bg_1(t_{j+1}) \end{pmatrix}, \\ \mathbf{A}_i &= \begin{pmatrix} \varepsilon\alpha\gamma & 0 \\ 0 & \varepsilon\beta\gamma \end{pmatrix}, \quad \mathbf{B}_i = \begin{pmatrix} 2\varepsilon\alpha\gamma + a\delta + 1 & c\delta \\ c\delta & 2\varepsilon\beta\gamma + a\delta + 1 \end{pmatrix}, \\ \mathbf{C}_i &= \begin{pmatrix} \varepsilon\alpha\gamma + a\delta & c\delta \\ c\delta & \varepsilon\beta\gamma + a\delta \end{pmatrix}, \quad \mathbf{F}_i = \begin{pmatrix} u_i - b\delta(\rho_i - \rho_{i-1}) \\ J_i \end{pmatrix}, \\ i &= 2, 3, \dots, M, \end{aligned}$$

$$\mathbf{B}_{M+1} = \begin{pmatrix} 1 & 0 \\ 0 & 0 \end{pmatrix}, \quad \mathbf{C}_{M+1} = \begin{pmatrix} 0 & 0 \\ 0 & -\varepsilon\beta\hat{T}_1 \end{pmatrix}, \quad \mathbf{F}_{M+1} = \begin{pmatrix} 0 \\ \varepsilon\beta\hat{T}_1 - k(\hat{T}_1 - \hat{T}_0) \end{pmatrix}.$$

The system (40) - (42) is a particular case of the problem [7]: find the vectors \mathbf{Y}_i , $i = 1, 2, \dots, M+1$, that satisfy the system

$$\begin{cases} \mathbf{A}_1 \mathbf{Y}_2 - \mathbf{B}_1 \mathbf{Y}_1 = -\mathbf{F}_1, \\ \mathbf{A}_i \mathbf{Y}_{i+1} - \mathbf{B}_i \mathbf{Y}_i + \mathbf{C}_i \mathbf{Y}_{i-1} = -\mathbf{F}_i, \quad 2 \leq i \leq M, \\ -\mathbf{B}_{M+1} \mathbf{Y}_{M+1} + \mathbf{C}_{M+1} \mathbf{Y}_M = -\mathbf{F}_{M+1}, \end{cases} \quad (43)$$

where $\mathbf{A}_i, \mathbf{B}_i, \mathbf{C}_i$, $i = 1, 2, \dots, M$ are square matrices. The solution of the problem (43) is given by [7]:

$$\begin{aligned} \mathbf{X}_2 &= \mathbf{B}_1^{-1} \mathbf{A}_1, \quad \mathbf{X}_{i+1} = (\mathbf{B}_i - \mathbf{C}_i \mathbf{X}_i)^{-1} \mathbf{A}_i, \quad i = 2, 3, \dots, M, \\ \mathbf{Z}_2 &= \mathbf{B}_1^{-1} \mathbf{F}_1, \quad \mathbf{Z}_{i+1} = (\mathbf{B}_i - \mathbf{C}_i \mathbf{X}_i)^{-1} (\mathbf{C}_i \mathbf{Z}_i + \mathbf{F}_i), \quad i = 2, 3, \dots, M+1, \\ \mathbf{Y}_{M+1} &= \mathbf{Z}_{M+2}, \quad \mathbf{Y}_i = \mathbf{X}_{i+1} \mathbf{Y}_{i+1} + \mathbf{Z}_{i+1}, \quad i = M, M-1, \dots, 1. \end{aligned}$$

In our case, using these formulas, we are ready to find relation between \hat{J}_{M+1} and \hat{J}_M in the form

$$\hat{\mathbf{Y}}_M = \mathbf{X}_{M+1} \hat{\mathbf{Y}}_{M+1} + \mathbf{Z}_{M+1}.$$

More in details

$$\begin{pmatrix} \hat{u}_M \\ \hat{J}_M \end{pmatrix} = \begin{pmatrix} X_{M+1}^{11} & X_{M+1}^{12} \\ X_{M+1}^{21} & X_{M+1}^{22} \end{pmatrix} \begin{pmatrix} \hat{u}_{M+1} \\ \hat{J}_{M+1} \end{pmatrix} + \begin{pmatrix} Z_{M+1}^1 \\ Z_{M+1}^2 \end{pmatrix}.$$

We consider only the second equation

$$\hat{J}_M = X_{M+1}^{21} \hat{u}_{M+1} + X_{M+1}^{22} \hat{J}_{M+1} + Z_{M+1}^2.$$

From (39) $\hat{J}_{M+1} = \hat{T}_1$. Hence

$$\hat{J}_M = X_{M+1}^{21} \hat{u}_{M+1} + X_{M+1}^{22} \hat{T}_1 + Z_{M+1}^2.$$

Let us replace in (39) \hat{J}_{M+1} и \hat{J}_M and use that $\hat{u}_{M+1} = u_{0,s}(t_{j+1})$. So, we obtain consequently

$$\begin{aligned} \beta\varepsilon \left[\hat{T}_1 - \left(X_{M+1}^{21} \hat{u}_{M+1} + X_{M+1}^{22} \hat{T}_1 + Z_{M+1}^2 \right) \right] &= k \left(\hat{T}_2 - \hat{T}_1 \right), \\ k \hat{T}_2 - (k + \beta\varepsilon - \beta\varepsilon X_{M+1}^{22}) \hat{T}_1 &= \\ &= -\beta\varepsilon (Z_{M+1}^2 + X_{M+1}^{21} u_{0,s}(t_{j+1})). \end{aligned} \quad (44)$$

For \hat{T} we have the system of equations

$$\begin{aligned} - (k + \beta\varepsilon - \beta\varepsilon X_{M+1}^{22}) \hat{T}_1 + k\hat{T}_2 &= -\beta\varepsilon (Z_{M+1}^2 + X_M^{21}u_{0,s}(t_{j+1})), \\ k\gamma\hat{T}_{i-1} - (2k\gamma + 1)\hat{T}_i + k\gamma\hat{T}_{i+1} &= -T_i, \quad 2 \leq i \leq N, \\ \hat{T}_{N+1} &= T_{0,r}(t_{j+1}). \end{aligned} \quad (45)$$

We solve (45) by right Thomas' algorithm [5], [7] where

$$\begin{aligned} C_1 &= k + \beta\varepsilon - \beta\varepsilon X_{M+1}^{22}, \quad B_1 = k, \quad F_1 = \beta\varepsilon (Z_{M+1}^2 + X_M^{21}u_{0,s}(t_{j+1})) \\ A_i &= k\gamma, \quad C_i = (2k\gamma + 1), \quad B_i = k\gamma, \\ F_i &= T_i, \quad i = 2, 3, \dots, N, \\ A_{N+1} &= 0, \quad C_{N+1} = 1, \quad F_{N+1} = T_{0,r}(t_{j+1}). \end{aligned}$$

The last formulas show that for system (45) the conditions for correctness and stability of Thomas' algorithm are fulfilled [5], [7].

Now we turn back to \hat{J} and perform back stage of the matrix Thomas' algorithm, using that

$$\mathbf{Y}_{M+1} = \begin{pmatrix} u_{0,s}(t_{j+1}) \\ \hat{T}_1 \end{pmatrix}.$$

Finally, we solve the problem for density

$$\hat{\rho}_1 = \frac{b}{c}\hat{J}_1 - \frac{d}{c}g_1(t_{j+1}),$$

$$\hat{\rho}_i = \rho_i - a\delta(\rho_i - \rho_{i-1}) - b\delta(\hat{u}_i - \hat{u}_{i-1}), \quad i = 2, 3, \dots, M+1.$$

The algorithm is completed.

We will investigate for monotonicity and stability in discrete maximum norm the explicit-implicit scheme using the discrete maximum principle. Writing the discrete equation for the density ρ in canonical form, we find the condition

$$\delta = \frac{\tau}{h} < \frac{1}{a}, \quad (46)$$

that provides monotonicity and stability. One can check that the scheme for the velocity u and for the two temperatures J and T is unconditionally monotone and stable in discrete maximum norm.

Summarizing all above, we have the assertion

Theorem 2. *If condition (46) is fulfilled, then the difference scheme (30) - (39) is monotone and stable in the discrete maximal norm and the Algorithm is correct and stable.*

5 NUMERICAL EXPERIMENTS

Numerical experiments were performed in order to examine the rate of convergence of the constructed scheme. We use the functions [4]

$$\begin{aligned}\rho(x, t) &= \cos(2\pi x - t) + \sin(2\pi x - t), \\ u(x, t) &= x + \cos(2\pi x - t), \\ J(x, t) &= \frac{1}{\varepsilon} \sin(2\pi x) e^{-mt}, \\ T(x, t) &= \frac{1}{k} \sin(2\pi x) e^{-mt},\end{aligned}$$

as analytical solution of the problem under consideration. Then inserting them in the equation (1) and (2) we obtain a modified system of equations with additional forcing function. The used data are the following:

$$m = 0.1, a = 0.5, b = \frac{1}{\sqrt{\eta}}, c = \sqrt{\frac{\eta - 1}{\eta}}, \eta = 1.4, \varepsilon = 1, \alpha = \beta = 1, k = 1.$$

Relative discrete maximum norm of the error is calculated by the formula

$$\|z_{h\tau}\|_C \equiv ER \equiv \|U_{h\tau} - Y_{h\tau}\|_C = \frac{\max_{(x_i, t_j) \in \bar{\omega}_{h\tau}} |U_i^j - Y_i^j|}{\max_{(x_i, t_j) \in \bar{\omega}_{h\tau}} |U_i^j|},$$

where U is the exact solution and Y is the approximate solution.

The rate of convergence (RC) is calculated using double mesh principle

$$RC = \ln \left(\frac{ER^K}{ER^{2K}} \right) / \ln 2.$$

In the Table 1 and Table 2 we have presented the results obtained by the explicit-implicit scheme. The results obtained by the explicit scheme are similar, but the condition (28) and the first of (29) are very strong and that leads to very small time step in the explicit scheme. It can be seen from the tables, that the accuracy is not very good and the rate of convergence is of first order with respect to the space step h .

We have performed numerical experiments with time step $\tau = h^2$. The results obtained with time step $\tau = h$ are more accurate.

We have used Richardson extrapolation to accelerate the accuracy and the convergence rate of the explicit-implicit scheme on two and three inserted meshes. Obtained results are presented in the Tables 3 - 6. In

Table1. Explicit-implicit scheme, $\tau = h$

$M = N = j_0$	C-norm of the error for ρ	RC	C-norm of the error for u	RC
10	9.142 E-1	-	6.489 E-1	-
20	4.978 E-1	0.88	3.194 E-1	1.02
40	2.648 E-1	0.91	1.576 E-1	1.02
80	1.367 E-1	0.96	7.862 E-2	1.01
160	6.980 E-2	0.96	3.927 E-2	1.00
320	3.557 E-2	0.97	1.962 E-2	1.00
640	1.807 E-2	0.98	9.808 E-3	1.00

Table2. Explicit-implicit scheme, $\tau = h$

$M = N = j_0$	C-norm of the error for J	RC	C-norm of the error for T	RC
10	5.470 E-1	-	2.747 E-1	-
20	2.563 E-1	1.10	1.244 E-2	1.14
40	1.274 E-1	1.01	6.037 E-2	1.04
80	6.357 E-2	1.01	2.968 E-2	1.02
160	3.175 E-2	1.00	1.471 E-2	1.01
320	1.587 E-2	1.00	7.322 E-3	1.01
640	7.931 E-3	1.00	3.653 E-3	1.00

Table3. Explicit-implicit scheme, $\tau = h$, two inserted meshes

$M = N = j_0$	C-norm of the error for ρ	RC	C-norm of the error for u	RC
10	1.273 E-1	-	2.392 E-2	-
20	4.346 E-2	1.55	7.260 E-3	1.72
40	1.497 E-2	1.54	2.136 E-3	1.77
80	5.083 E-3	1.56	5.910 E-4	1.85
160	1.787 E-3	1.51	1.568 E-4	1.91

Table4. Explicit-implicit scheme, $\tau = h$, two inserted meshes

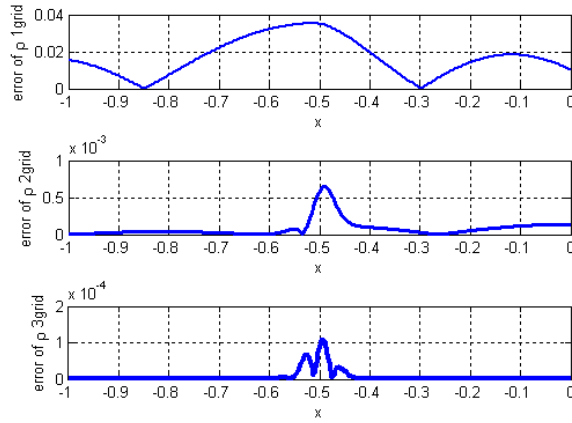
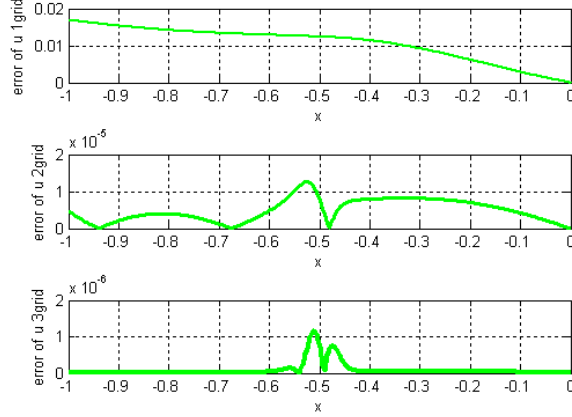
$M = N = j_0$	C-norm of the error for J	RC	C-norm of the error for T	RC
10	2.017 E-2	-	2.624 E-2	-
20	4.607 E-3	2.31	6.470 E-3	2.02
40	1.407 E-3	1.71	1.667 E-3	1.96
80	4.318 E-4	1.70	4.230 E-4	1.98
160	1.291 E-4	1.74	1.066 E-4	1.97

Table5. Explicit-implicit scheme, $\tau = h$, three inserted meshes

$M = N = j_0$	C-norm of the error for ρ	RC	C-norm of the error for u	RC
10	1.497 E-2	-	4.675 E-3	-
20	5.158 E-3	1.54	1.100 E-3	2.09
40	1.982 E-3	1.38	2.374 E-4	2.21
80	7.815 E-4	1.34	5.286 E-5	2.17
160	3.115 E-4	1.33	1.348 E-5	1.97

Table6. Explicit-implicit scheme, $\tau = h$, three inserted meshes

$M = N = j_0$	C -norm of the error for J	RC	C -norm of the error for T	RC
10	3.652 E-3	-	1.013 E-3	-
20	8.321 E-4	2.13	2.020 E-4	2.32
40	1.829 E-4	2.19	3.497 E-5	2.52
80	4.143 E-5	2.14	6.136 E-6	2.51
160	1.073 E-5	1.95	9.561 E-7	2.68

**Figure1.** $z = \rho_{num}(x, 1) - \rho_{ex}(x, 1)$ **Figure2.** $z = u_{num}(x, 1) - u_{ex}(x, 1)$

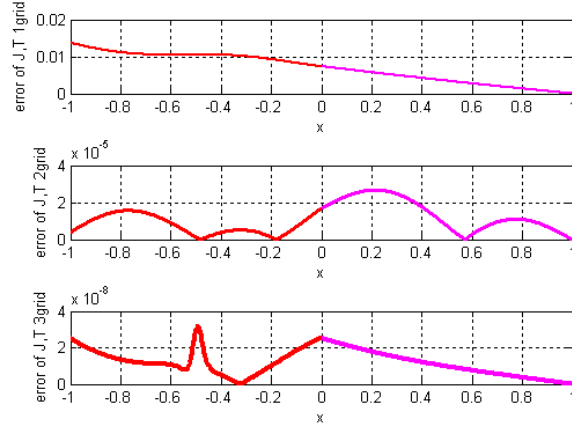


Figure3. $z = J_{num}(x, 1) - J_{ex}(x, 1), x \in [-1, 0], z = T_{num}(x, 1) - T_{ex}(x, 1), x \in [0, 1]$

the first column the numbers of the subinterval of the most coarse mesh are given. It can be seen from these tables that the accuracy on two and particularly on three meshes is much higher than on one.

In Fig. 1 we have represented the error for the function ρ , in Fig. 2 - for the u and in Fig. 3 - the error for the functions J and T at the last moment $t = t_0 = 1$ on two and three meshes. From these figures it can be seen that the error of the numerical solutions on two and particularly on three meshes is much smaller than on one.

6 SUMMARY AND CONCLUSIONS

A hyperbolic-parabolic system of equations is coupled with heat equation in one space dimension. Two difference schemes are studied for monotonicity and stability in the maximal discrete norm. Effective algorithms for realization of the schemes are proposed. Richardson extrapolation to increase the accuracy of the computation is discussed.

Some open questions remain, for example the theoretical validation of the Richardson extrapolation; the computational and theoretical study of boundary and interior layers when the specific heat coefficients are small that corresponds to real physical situations.

It is also interesting to be considered the problem with non-stationary interface, i. e. a moving body as all as two and three dimensional problems.

Acknowledgment: The first author is supported by the Sofia University Foundation under Grant No 154/2011.

References

1. D. Kim, H. Choi, Immersed boundary method for flow around an arbitrary moving body, *J. of Comp. Phys.* **212** (2006), 662-680.
2. O. A. Ladyzhenskaya, *Mathematical Questions of Dynamics of Incompressible Fluid*, Moscow, Nauka (1970) (in Russian).
3. Z. Li. K. Ito, *The Immersed Interface Method*, SIAM, Philadelphia, 2006.
4. J. Lindström, J. Nordström, A stable and high-order accurate conjugate heat transfer problem, *J. of Comp. Phys.* **229** (2010) 5440-5456.
5. A. A. Samarskii, *Theory of Finite Difference Schemes*, New York, Marcel Decker, (2003).
6. A. A. Samarskii, A. V. Gulin, *Stability of the Difference Schemes*, Moscow, Nauka, (1973) (in Russian).
7. A. A. Samarskii, E. S. Nikolaev, *Methods for Solving the Difference Equations*, Moscow, Nauka, (1978) (in Russian).
8. A. M. Miheev, U. M. Miheeva, *Fundamentals of Heat-Transfer*, M: Energyia (1977) (in Russian).

APPLICATION OF VIM AND HPM FOR THE STURM-LIOUVILLE PROBLEM

R. DARZI¹ AND A. NEAMATY²

¹ Islamic Azad University Neka Branch, Neka, Iran
R.Darzi@umz.ac.ir

² Department of Mathematics, University of Mazandaran, Babolsar, Iran
Namaty@umz.ac.ir

Abstract. In this paper, we applied the Variational iteration method and the Homotopy perturbation method to solve linear Sturm-Liouville eigenvalue and boundary value problems. The main advantage of these methods is the flexibility to give approximate and exact solutions to both linear and nonlinear problems without linearization or discretization. The results show that both methods are simple and effective.

1 INTRODUCTION

The variational iteration method (VIM)[1,7] and homotopy perturbation method (HPM)[2,3,5] proposed by He, are powerful analytical methods for various kinds of linear and nonlinear problems. For example, the variational iteration method has been applied to autonomous ordinary differential equation [6]. Also homotopy perturbation method was successfully applied to Volterra's integro-differential equation [4] and boundary value problem. In this paper we exert these methods for linear Sturm-Liouville eigenvalue and boundary value problems (BVP). A linear Sturm-Liouville operator has the form

$$\ell y(t) : Ly(t) = \lambda r(t)y(t),$$

where

$$L = -\frac{d}{dt}[p(t)\frac{d}{dt}] + q(t)$$

and $t \in I = [a, b]$. Associated with the differential equation (1) are the separated homogeneous boundary conditions:

$$\alpha_1 y(a) + \beta_1 y'(a) = 0,$$

M. Koleva and L. Vulkov (Eds.), Proceedings of the Fifth Conference on Finite Difference Methods: Theory and Applications (FDM: T&A 2010) 2011, pp. 37–43.
© Rousse University Press 2011

$$\alpha_2 y(b) + \beta_2 y'(b) = 0,$$

where $\alpha_1, \alpha_2, \beta_1$ and β_2 are arbitrary constants. We will assume that $p(t), p'(t), q(t)$ and $r(t)$ are continuous for simplicity.

2 HE'S VARIATIONAL ITERATION METHOD AND HOMOTOPY PERTURBATION METHOD

To illustrate the basic concept of He's variational iteration method, we consider the following nonlinear differential equation:

$$L(u) + N(u) = g(t), \quad (1)$$

where L is a linear operator, N is a nonlinear operator and $g(t)$ is a nonhomogeneous term. Ji. Haun. He has modified the general Lagrange multiplier method into an iteration method, which is called correction functional, in the following way

$$u_{n+1}(t) = u_n(t) + \int_0^t \mu [Lu_n(r) + N\tilde{u}_n(r) - g(r)] dr,$$

where μ is a general Lagrange multiplier, which can be identified optimally via the variational theory. The subscript n denotes the n th approximation, \tilde{u}_n is considered as a restricted variation i.e., $\delta\tilde{u}_n = 0$. Employing the restricted variation in above equation makes it easy to compute the Lagrange multiplier. It is shown that this method is very effective and easy and can solve a large class of nonlinear problems. For linear problems its exact solution can be obtained only one iteration, because μ can be exactly identified.

To solve Eq.(1), by means of homotopy perturbation method, we choose linear operator

$$L(y) = -\frac{d}{dt} [p(t) \frac{dy}{dt}],$$

with the property $L(c_1) = 0$, where c_1 is constant of integration, and suggests that we define a nonlinear operator as

$$N(y) = (q(t) - \lambda r(t))y(t).$$

Also $g(t)$ is known analytic function representing the nonhomogeneous term. Therefore, Eq.(1) can be rewritten as follows $L(y) + N(y) - g(t) = 0$. By the homotopy perturbation technique proposed by He [2], we can construct a homotopy

$$Y(t, p) : [-l, l] \times [0, 1] \longrightarrow R,$$

$$\begin{aligned} H(Y, p) &= (1 - p)[\frac{d}{dt}(p(t)\frac{d}{dt}Y(t)) - \frac{d}{dt}(p(t)y'_0(t))] \\ &\quad + p[\frac{d}{dt}(p(t)\frac{d}{dt}Y(t)) - \{q(t) - \lambda r(t)\}Y(t) + g(t)] = 0. \end{aligned} \quad (2)$$

One may now try to obtain a solution of equation in the form

$$Y(t) = Y_0(t) + pY_1(t) + p^2Y_2(t) + \dots,$$

where the $Y_i(t)$ for $i = 0, 1, 2, \dots$ are functions yet to be determined. The substituting $Y(t)$ into (2) and collecting terms of the same powers of p yields: Collecting terms of the same powers of p yields:

$$\begin{aligned} p^0 : \frac{d}{dt}[p(t)\frac{d}{dt}Y_0(t)] - \frac{d}{dt}[p(t)\frac{d}{dt}y_0(t)] &= 0, \\ p^1 : \frac{d}{dt}[p(t)\frac{d}{dt}Y_1(t)] + \frac{d}{dt}[p(t)\frac{d}{dt}y_0(t)] - \{q(t) - \lambda r(t)\}Y_0(t) - g(t) &= 0, \\ p^2 : \frac{d}{dt}[p(t)\frac{d}{dt}Y_2(t)] - \{q(t) - \lambda r(t)\}Y_1(t) &= 0, \\ \vdots & \\ \vdots & \\ p^n : \frac{d}{dt}[p(t)\frac{d}{dt}Y_n(t)] - \{q(t) - \lambda r(t)\}Y_{n-1}(t) &= 0. \end{aligned}$$

The initial approximation $Y_0(t)$ or $y_0(t)$ can be freely chosen.

Example 1 Consider the Sturm-Liouville equation

$$-y''(t) + \lambda y(t) = 0,$$

with initial approximation $y_0(t, \lambda) = A + Bt$, where A and B are constants. To solve this equation using the VIM, we have correction functional

$$y_{n+1}(t, \lambda) = y_n(t, \lambda) + \int_0^t \mu[-y_n''(r, \lambda) + \lambda y_n(r, \lambda)]dr, \quad (3)$$

where $\mu = \mu(r, t; \lambda)$ is Lagrange multiplier. Making the above correction functional stationary, we can obtain the following stationary conditions:

$$\begin{aligned} \mu''(r, t; \lambda) - \lambda \mu(r, t; \lambda) &= 0, \\ 1 - \mu'(r, t; \lambda)|_{r=t} &= 0, \\ \mu(r, t; \lambda)|_{r=t} &= 0. \end{aligned}$$

The Lagrange multiplier can, therefore, be identified as:

$$\mu(r, t; \lambda) = \frac{1}{\sqrt{\lambda}} \left(\frac{e^{\sqrt{\lambda}(r-t)} - e^{-\sqrt{\lambda}(r-t)}}{2} \right) = \sinh(\sqrt{\lambda}(r-t)).$$

Substituting μ into correction functional, we have the following iteration formula

$$y_{n+1}(t, \lambda) = y_n(t, \lambda) + \int_0^t \sinh(\sqrt{\lambda}(r-t))[-y_n''(r, \lambda) + y_n(r, \lambda)]dr.$$

Using this iteration formula and initial approximation, for $n \geq 1$, we obtain:

$$y_n(t, \lambda) = A \cosh(\sqrt{\lambda}t) + \frac{B}{\sqrt{\lambda}} \sinh(\sqrt{\lambda}t),$$

which means that the exact solution of equation, is

$$y(t, \lambda) = A \cosh(\sqrt{\lambda}t) + \frac{B}{\sqrt{\lambda}} \sinh(\sqrt{\lambda}t).$$

In order to solve Ex.1 using the HPM, according to (2) we can readily construct a homotopy which satisfies

$$H(Y, p) = (1-p)[\frac{d^2}{dt^2}Y(t) - \frac{d^2}{dt^2}y_0(t)] + p[\frac{d^2}{dt^2}Y(t) - \lambda Y(t)] = 0, \quad p \in [0, 1]$$

We Consider $Y(t)$ as

$$Y(t) = Y(t, \lambda) = Y_0(t, \lambda) + pY_1(t, \lambda) + p^2Y_2(t, \lambda) + \dots$$

Substituting $Y(t)$ into Eq.(4), collecting terms of the same power and using initial approximation we have the following set of linear equations

$$\begin{aligned} p^0 : \frac{d^2}{dt^2}[Y_0(t, \lambda)] &= 0, \\ p^1 : \frac{d^2}{dt^2}[Y_1(t, \lambda)] - \frac{d^2}{dt^2}[y_0(t, \lambda)] - \lambda Y_0(t, \lambda) &= 0, \\ p^2 : \frac{d^2}{dt^2}[Y_2(t, \lambda)] - \lambda Y_1(t, \lambda) &= 0, \\ &\vdots \\ &\vdots \\ p^n : \frac{d^2}{dt^2}[Y_n(t, \lambda)] - \lambda Y_{n-1}(t, \lambda) &= 0. \end{aligned}$$

Solving the above equations, we have

$$Y_0(t, \lambda) = A + Bt, \quad Y_1(t, \lambda) = A(1 + \frac{(\sqrt{\lambda}t)^2}{2!}) + \frac{B}{\sqrt{\lambda}}(\sqrt{\lambda}t + \sqrt{\lambda}\frac{(\sqrt{\lambda}t)^3}{3!}), \quad \dots$$

$$Y_n(t, \lambda) = A(1 + \frac{(\sqrt{\lambda}t)^2}{2!} + \dots + \frac{(\sqrt{\lambda}t)^{2n}}{(2n)!}) + \frac{B}{\sqrt{\lambda}}(\sqrt{\lambda}t + \sqrt{\lambda}\frac{(\sqrt{\lambda}t)^3}{3!} + \dots + \frac{(\sqrt{\lambda}t)^{2n+1}}{(2n+1)!}).$$

Continuing, in this manner we can obtain

$$Y(t, \lambda) = A \cosh(\sqrt{\lambda}t) + \frac{B}{\sqrt{\lambda}} \sinh(\sqrt{\lambda}t),$$

which is exactly the same as that obtained by VIM.

Example 2. As another example, we consider Sturm-Liouville problem

$$-y''(t) + (t - \lambda)y(t) = 0, \quad t \geq 0, \quad (5)$$

with initial conditions $y(0) = A$ and $y'(0) = B$, where A and B are constants. To solve Eq.(5) by means of variational method, we construct a correction functional

$$y_{n+1}(t, \lambda) = y_n(t, \lambda) + \int_0^t \mu[-y_n''(r, \lambda) + r\tilde{y}_n(r, \lambda) - \lambda y_n(r, \lambda)]dr,$$

where $\mu = \mu(r, t; \lambda)$ is the Lagrange multiplier and \tilde{y}_n denotes restricted variation, that is $\delta\tilde{y}_n = 0$. Then, we have

$$\delta y_{n+1}(t, \lambda) = \delta y_n(t, \lambda) + \delta \int_0^t \mu[-y_n''(r, \lambda) + r\tilde{y}_n(r, \lambda) - \lambda y_n(r, \lambda)]dr.$$

Calculus of variations and integration by parts give the stationary conditions

$$\begin{aligned} \mu''(r, t; \lambda) + \lambda\mu(r, t; \lambda) &= 0, \\ 1 + \mu'(r, t; \lambda)|_{r=t} &= 0, \\ \mu(r, t; \lambda)|_{r=t} &= 0. \end{aligned}$$

for which the Lagrange multiplier μ should satisfy. The Lagrange multiplier can, therefore, be identified as

$$\mu(r, t; \lambda) = -\frac{1}{\sqrt{\lambda}} \sin(\sqrt{\lambda}(r - t)).$$

Substituting μ into correction functional results in the following iteration formula:

$$y_{n+1}(t, \lambda) = y_n(t, \lambda) - \int_0^t \frac{1}{\sqrt{\lambda}} \sin(\sqrt{\lambda}(r-t))[-y_n''(r, \lambda) + r\tilde{y}_n(r, \lambda) - \lambda y_n(r, \lambda)]dr.$$

According to initial conditions, it is natural to choose initial approximation $y_0(t, \lambda) = A + Bt$. Using the above variational formula, we can obtain the following result:

$$y_1(t, \lambda) = A \cos(\sqrt{\lambda}t) + \frac{A}{\lambda^{\frac{3}{2}}} \left(\frac{(\sqrt{\lambda}t)^3}{3!} - \frac{(\sqrt{\lambda}t)^5}{5!} + \dots \right) + \frac{B}{\sqrt{\lambda}} \sin(\sqrt{\lambda}t) + \frac{2B}{\lambda^2} \left(\frac{(\sqrt{\lambda}t)^4}{4!} - \frac{(\sqrt{\lambda}t)^6}{6!} + \dots \right), \quad \dots$$

In order to solve Eq.(5) using HPM, after applying HPM and rearranging

based on powers of p -terms, we have

$$\begin{aligned} p^0 : \frac{d^2}{dt^2}[Y_0(t, \lambda)] - \frac{d^2}{dt^2}[y_0(t, \lambda)] &= 0, \\ p^1 : \frac{d^2}{dt^2}[Y_1(t, \lambda)] - \frac{d^2}{dt^2}[y_0(t, \lambda)] + (-t + \lambda)Y_0(t, \lambda) &= 0, \\ p^2 : \frac{d^2}{dt^2}[Y_2(t, \lambda)] + (-t + \lambda)Y_1(t, \lambda) &= 0, \dots \end{aligned}$$

Solving the above equations, we get:

$$\begin{aligned} Y_1(t, \lambda) &= A\left(1 - \frac{(\sqrt{\lambda}t)^2}{2!}\right) + \frac{A}{\lambda^{\frac{3}{2}}}\left(\frac{(\sqrt{\lambda}t)^3}{3!}\right) + \frac{B}{\sqrt{\lambda}}\left(\sqrt{\lambda}t - \frac{(\sqrt{\lambda}t)^3}{3!}\right) + \frac{2B}{\lambda^2}\left(\frac{(\sqrt{\lambda}t)^4}{4!}\right), \\ Y_2(t, \lambda) &\simeq A\left(1 - \frac{(\sqrt{\lambda}t)^2}{2!} + \frac{(\sqrt{\lambda}t)^4}{4!}\right) + \frac{A}{\lambda^{\frac{3}{2}}}\left(\frac{(\sqrt{\lambda}t)^3}{3!} - \frac{(\sqrt{\lambda}t)^5}{5!}\right) + \frac{B}{\sqrt{\lambda}}\left(\sqrt{\lambda}t - \frac{(\sqrt{\lambda}t)^3}{3!} + \frac{(\sqrt{\lambda}t)^5}{5!}\right) + \frac{2B}{\lambda^2}\left(\frac{(\sqrt{\lambda}t)^4}{4!} - \frac{(\sqrt{\lambda}t)^6}{6!}\right), \quad \dots \end{aligned}$$

Example 3. Finally, we consider eigenvalue Sturm-Liouville problem

$$-y''(t) - \lambda y(t) = 0, \quad t \in (-l, l), \quad l > 0, \quad (6)$$

along with the Dirichlet boundary conditions $y(-l) = 0$ and $y(l) = 0$. To solve Eq.(6) by means of variational method, we construct a correction functional for (6) reads as

$$y_{n+1}(t, \lambda) = y_n(t, \lambda) + \int_0^t \mu[-y_n''(r, \lambda) - \lambda y_n(r, \lambda)]dr,$$

where $\mu = \mu(r, t; \lambda)$ is Lagrange multiplier. Following the discussion presented in the previous example, we obtain the following iteration formula

$$y_{n+1}(t, \lambda) = y_n(t, \lambda) - \int_0^t \frac{1}{\sqrt{\lambda}} \sin(\sqrt{\lambda}(r-t))[-y_n''(r, \lambda) - \lambda y_n(r, \lambda)]dr.$$

Let us begin with an initial approximation $y_0(t, \lambda) = A + Bt$, where A and B are constants to be determined. Substituting the proposed initial iterate $y_0(t, \lambda)$ in (7) gives

$$y_n(t, \lambda) = A \cos(\sqrt{\lambda}t) + \frac{B}{\sqrt{\lambda}} \sin(\sqrt{\lambda}t), \quad n \geq 1.$$

So, we can derive that

$$y(t, \lambda) = A \cos(\sqrt{\lambda}t) + \frac{B}{\sqrt{\lambda}} \sin(\sqrt{\lambda}t),$$

is the exact solution of Eq.(6).

In order to solve Eq.(6) using HPM, similar to previous examples, after

applying HPM, we obtain

$$Y(t, \lambda) = A \cos(\sqrt{\lambda}t) + \frac{B}{\sqrt{\lambda}} \sin(\sqrt{\lambda}t), \quad (7)$$

which is exactly the same as that obtained by VIM. Now, we use the Dirichlet boundary condition to obtain eigenvalue and eigenfunctions of (6). Imposing the boundary conditions in (7) yields two infinite sequences of eigenvalues λ_m as

$$\lambda_m = \left(\frac{(2m-1)\pi}{2l} \right)^2, \quad \lambda_m = \left(\frac{m\pi}{l} \right)^2, \quad m = 1, 2, \dots$$

Thus, corresponding linearly nontrivial solutions are

$$u_m(t) = A \cos \left(\frac{(2m-1)\pi}{2l} t \right), \quad v_m(t) = B \frac{l}{m\pi} \sin \left(\frac{m\pi}{l} t \right), \quad m = 1, 2, \dots$$

Since $u_m(t)$ and $v_m(t)$ are of class $C(I, \mathbb{R})$, that is are continuous real valued functions of $t \in (-l, l)$, using the definition of inner product on $C(I, \mathbb{R})$, and the norm induced by inner product, we get the normalization constants as

$$A = \frac{1}{\sqrt{l}}, \quad B = \frac{m\pi}{\sqrt{l^3}}.$$

Consequently, we obtain

$$\tilde{u}_m(t) = \frac{1}{\sqrt{l}} \cos \left(\frac{(2m-1)\pi}{2l} t \right), \quad \tilde{v}_m(t) = \frac{1}{\sqrt{l}} \sin \left(\frac{m\pi}{l} t \right), \quad m = 1, 2, \dots,$$

where, $\tilde{u}_m(t)$ and $\tilde{v}_m(t)$ are normalised eigenfunctions, i.e.

$$\tilde{u}_m(t) = \frac{u_m(t)}{\| u_m \|_2}, \quad \tilde{v}_m(t) = \frac{v_m(t)}{\| v_m \|_2}.$$

References

1. J.H. He, Variational iteration method - a kind of nonlinear analytic technique: Some examples, *Int. J. Nonlinear Mech* **34** (1999) 699-708.
2. J.H. He, A new approach to nonlinear partial differential equations, *Commun. Nonlinear Sci. Numer. Simul* **2** (1997) 230-235.
3. J.H. He, Homotopy perturbation technique:A new nonlinear analytical technique, *Appl. Math. Comput* **135** (2003) 73-79.
4. M.E. Shahed, Application of He's homotopy perturbation method to Volterra's integro-differential equation, *Int. J. Nonlinear Mech* **34** (1999) 699-708.
5. J. H. He, Homotopy perturbation technique, *Comput. Method Appl. Mech. Eng* **178** (1999) 257-262.
6. J.H. He, Variational iteration method for autonomous ordinary differential system, *Appl. Mech. Comput* **114** (2000) 115-123.
7. S. Momani, S. Abuasad, Application of He's Variational iteration method to Helmholtz equation, *Chaos, Solitons Fractals* **27** (2006) 1119-1123.

ON THE SHARPNESS OF GREEN'S FUNCTION ESTIMATES FOR A CONVECTION-DIFFUSION PROBLEM

SEBASTIAN FRANZ AND NATALIA KOPTEVA

Department of Mathematics and Statistics, University of Limerick, Limerick, Ireland,
`{sebastian.franz,natalia.kopteva}@ul.ie`

Abstract. Linear singularly perturbed convection-diffusion problems with characteristic layers are considered in three dimensions. We demonstrate the sharpness of our recently obtained upper bounds for the associated Green's function and its derivatives in the L_1 norm. For this, in this paper we establish the corresponding lower bounds. Both upper and lower bounds explicitly show any dependence on the singular perturbation parameter.

1 INTRODUCTION

Consider the convection-diffusion problem in the domain $\Omega = (0, 1)^3$:

$$\mathcal{L}_{\mathbf{x}} u(\mathbf{x}) = -\varepsilon \Delta_{\mathbf{x}} u(\mathbf{x}) - 2\alpha \partial_{x_1} u(\mathbf{x}) = f(\mathbf{x}) \quad \text{for } \mathbf{x} \in \Omega, \quad (1a)$$

$$u(\mathbf{x}) = 0 \quad \text{for } \mathbf{x} \in \partial\Omega. \quad (1b)$$

Here $\varepsilon \in (0, 1]$ is a small positive parameter, while α is a positive constant. Then (1) is a singularly perturbed convection-dominated problem, whose solutions typically exhibit sharp characteristic boundary and interior layers.

This article addresses the sharpness of our recently published obtained upper bounds for the associated Green's function and its derivatives in the L_1 norm. Our interest in considering the Green's function of problem is motivated by the numerical analysis of this computationally challenging problem. More specifically, these estimates will be used in the forthcoming paper [4] to derive robust a posteriori error bounds for computed solutions of this problem using finite-difference methods. (This approach is related to recent articles [10, 2], which address the numerical solution of singularly perturbed equations of reaction-diffusion type.) In a more

M. Koleva and L. Vulkov (Eds.), Proceedings of the Fifth Conference on Finite Difference Methods: Theory and Applications (FDM: T&A 2010) 2011, pp. 44–57.
© Rousse University Press 2011

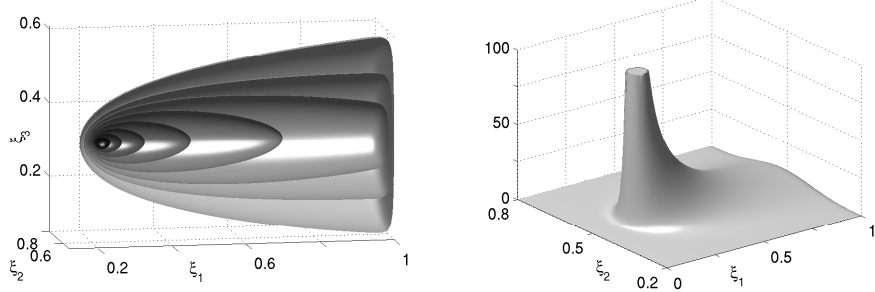


Figure 1. Anisotropy of the Green's function $G(\mathbf{x}; \boldsymbol{\xi})$ associated with (1) for $\varepsilon = 0.01$ and $\mathbf{x} = (\frac{1}{5}, \frac{1}{2}, \frac{1}{3})$. Left: isosurfaces at values of 1, 4, 8, 16, 32, 64, 128, and 256. Right: a two-dimensional graph for fixed $\xi_3 = x_3$.

general numerical-analysis context, we note that sharp estimates for continuous Green's functions (or their generalised versions) frequently play a crucial role in a priori and a posteriori error analyses [3, 8, 11].

For each fixed $\mathbf{x} \in \Omega$, the Green's function G associated with (1) satisfies

$$\mathcal{L}_\xi^* G(\mathbf{x}; \boldsymbol{\xi}) := -\varepsilon \Delta_\xi G(\mathbf{x}; \boldsymbol{\xi}) + 2\alpha \partial_{\xi_1} G(\mathbf{x}; \boldsymbol{\xi}) = \delta(\mathbf{x} - \boldsymbol{\xi}) \quad \text{for } \boldsymbol{\xi} \in \Omega, \quad (2a)$$

$$G(\mathbf{x}; \boldsymbol{\xi}) = 0 \quad \text{for } \boldsymbol{\xi} \in \partial\Omega. \quad (2b)$$

Here \mathcal{L}_ξ^* is the adjoint differential operator to \mathcal{L}_x , and $\delta(\cdot)$ is the three-dimensional Dirac δ -distribution.

Note that the Green's function for a singularly perturbed self-adjoint reaction-diffusion operator $-\varepsilon \Delta_x + \alpha$ is almost radially symmetric and exponentially decaying away from the singular point [2]. By contrast, the Green's function for our convection-diffusion problem (1) exhibits a strong anisotropic structure, which is demonstrated by Figure 1.

In [5, 6] we have obtained certain upper bounds for the Green's function associated with a variable-coefficient version of (1), which we now cite.

Theorem 1 ([5, 6]). *Let $\varepsilon \in (0, 1]$. The Green's function G associated with (1) on the unit cube $\Omega = (0, 1)^3$ satisfies, for all $\mathbf{x} \in \Omega$, the following upper bounds:*

$$\|\partial_{\xi_1} G(\mathbf{x}; \cdot)\|_{1;\Omega} \leq C(1 + |\ln \varepsilon|), \quad (3a)$$

$$\|\partial_{\xi_k} G(\mathbf{x}; \cdot)\|_{1;\Omega} \leq C\varepsilon^{-1/2}, \quad k = 2, 3. \quad (3b)$$

Furthermore, for any ball $B(\mathbf{x}', \rho)$ of radius ρ centred at any $\mathbf{x}' \in \Omega$, we have

$$\|G(\mathbf{x}; \cdot)\|_{1,1;\Omega \cap B(\mathbf{x}', \rho)} \leq C\rho/\varepsilon, \quad (3c)$$

while for any ball $B(\mathbf{x}, \rho)$ of radius ρ centred at $\mathbf{x} \in \Omega$, we have

$$\|\partial_{\xi_1}^2 G(\mathbf{x}; \cdot)\|_{1;\Omega \setminus B(\mathbf{x}, \rho)} \leq C\varepsilon^{-1} \ln(2 + \varepsilon/\rho), \quad (3d)$$

$$\|\partial_{\xi_k}^2 G(\mathbf{x}; \cdot)\|_{1;\Omega \setminus B(\mathbf{x}, \rho)} \leq C\varepsilon^{-1}(|\ln \varepsilon| + \ln(2 + \varepsilon/\rho)), \quad k = 2, 3. \quad (3e)$$

Remark 2. Theorem 1 is given in [5, 6] for a more general variable-coefficient operator $-\varepsilon \Delta_{\mathbf{x}} - a(\mathbf{x}) \partial_{x_1} + b(\mathbf{x})$ with sufficiently smooth coefficients that satisfy $a(\mathbf{x}) \geq 2\alpha > 0$, $b(\mathbf{x}) \geq 0$ and $b(\mathbf{x}) + \partial_{x_1} a(\mathbf{x}) \geq 0$ for all $\mathbf{x} \in \bar{\Omega}$.

The purpose of this paper is to show the sharpness of the bounds of Theorem 1 up to a constant ε -independent multiplier in the following sense.

Theorem 3. Let $\varepsilon \in (0, c_0]$ for some sufficiently small positive c_0 . The Green's function G associated with the constant-coefficient problem (1) in the unit cube $\Omega = (0, 1)^3$ satisfies, for all $\mathbf{x} \in [\frac{1}{4}, \frac{3}{4}]^3$, the following lower bounds:

$$\|\partial_{\xi_1} G(\mathbf{x}; \cdot)\|_{1;\Omega} \geq c |\ln \varepsilon|, \quad (4a)$$

$$\|\partial_{\xi_k} G(\mathbf{x}; \cdot)\|_{1;\Omega} \geq c \varepsilon^{-1/2}, \quad k = 2, 3. \quad (4b)$$

Furthermore, for any ball $B(\mathbf{x}; \rho)$ of radius $\rho \leq \frac{1}{8}$, we have

$$\|G(\mathbf{x}; \cdot)\|_{1,1;\Omega \cap B(\mathbf{x}, \rho)} \geq \begin{cases} c\rho/\varepsilon, & \text{if } \rho \leq 2\varepsilon, \\ c(\rho/\varepsilon)^{1/2}, & \text{otherwise,} \end{cases} \quad (4c)$$

$$\|\partial_{\xi_1}^2 G(\mathbf{x}; \cdot)\|_{1;\Omega \setminus B(\mathbf{x}, \rho)} \geq c\varepsilon^{-1} \ln(2 + \varepsilon/\rho), \quad \text{if } \rho \leq c_1\varepsilon, \quad (4d)$$

$$\|\partial_{\xi_k}^2 G(\mathbf{x}; \cdot)\|_{1;\Omega \setminus B(\mathbf{x}, \rho)} \geq c\varepsilon^{-1} (\ln(2 + \varepsilon/\rho) + |\ln \varepsilon|), \quad \text{if } \rho \leq \frac{1}{8}, \quad (4e)$$

where $k = 2, 3$, and c_1 is a sufficiently small positive constant.

Remark 4. The restriction $\mathbf{x} \in [\frac{1}{4}, \frac{3}{4}]^3$ is somewhat arbitrary and can be replaced by $\mathbf{x} \in [\theta, 1 - \theta]^3$ with any ε -independent constant $\theta \in (0, \frac{1}{2})$ (then $\rho \leq \frac{1}{2}\theta$ is imposed instead of $\rho \leq \frac{1}{8}$).

The paper is structured as follows. Sharp lower bounds for the fundamental solution in \mathbb{R}^3 are derived in Section 2. The next Section 3 is

devoted to the proof of Theorem 3 in a simpler setting, for the domain $(0, 1) \times \mathbb{R}^2$. Sections 4 and 5 briefly describe an extension of the analysis of Section 2 to the domain $\Omega = (0, 1)^3$ and to convection-reaction-diffusion problems. Finally, in Section 6, we give an outlook for problems in n dimensions.

Notation. Throughout the paper, C denotes a generic positive constant, typically sufficiently large, while c denotes a sufficiently small generic positive constant; they take different values in different formulas, but are independent of the singular perturbation parameter ε . The usual Sobolev spaces $W^{m,p}(D)$ and $L_p(D)$ on any measurable set $D \subset \mathbb{R}^3$ are used; the $L_p(D)$ norm is denoted by $\|\cdot\|_{p,D}$, while the $W^{m,p}(D)$ norm is denoted by $\|\cdot\|_{m,p,D}$. By $\mathbf{x} = (x_1, x_2, x_3)$ we denote an element of \mathbb{R}^3 . For an open ball in \mathbb{R}^3 , we employ the notation $B(\mathbf{x}', \rho) = \{\mathbf{x} \in \mathbb{R}^3 : \sum_{k=1}^3 (x_k - x'_k)^2 < \rho^2\}$. The notation $\partial_{x_1} f$, $\partial_{x_1}^2 f$ and $\Delta_{\mathbf{x}}$ is used for the first- and second-order partial derivatives of a function f in variable x_1 , and the Laplacian in variable \mathbf{x} , respectively.

2 THE FUNDAMENTAL SOLUTION

In this section we investigate the fundamental solution g that solves a similar problem to (2) but posed in the domain \mathbb{R}^3 :

$$\mathcal{L}_{\xi}^* g(\mathbf{x}; \xi) = -\varepsilon \Delta_{\xi} g(\mathbf{x}; \xi) + 2\alpha \partial_{\xi_1} g(\mathbf{x}; \xi) = \delta(\mathbf{x} - \xi) \quad \text{for } \xi \in \mathbb{R}^3. \quad (5)$$

Using [2, 9] (see also [5, 6]), a calculation shows that the fundamental solution g is explicitly represented by

$$g = g(\mathbf{x}; \xi) = \frac{1}{4\pi\varepsilon^2} \frac{e^{\alpha(\hat{\xi}_{1,[x_1]} - \hat{r}_{[x_1]})}}{\hat{r}_{[x_1]}} \quad (6)$$

with the scaled variables $\hat{\xi}_{1,[x_1]} = \frac{\xi_1 - x_1}{\varepsilon}$, $\hat{\xi}_2 = \frac{\xi_2 - x_2}{\varepsilon}$, $\hat{\xi}_3 = \frac{\xi_3 - x_3}{\varepsilon}$ and the scaled distance between \mathbf{x} and ξ denoted by $\hat{r}_{[x_1]} = \sqrt{\hat{\xi}_{1,[x_1]}^2 + \hat{\xi}_2^2 + \hat{\xi}_3^2}$. We use the subindex $[x_1]$ in $\hat{\xi}_{1,[x_1]}$ and $\hat{r}_{[x_1]}$ to highlight their dependence on x_1 as in many places x_1 will take different values; but when there is no ambiguity, we shall simply write $\hat{\xi}_1$ and \hat{r} .

Next, we evaluate derivatives of g of order one and two:

$$\partial_{\xi_1} g = \frac{e^{\alpha(\hat{\xi}_1 - \hat{r})}}{4\pi\varepsilon^3} \hat{r}^{-2} \left[\alpha(\hat{r} - \hat{\xi}_1) - \frac{\hat{\xi}_1}{\hat{r}} \right], \quad (7a)$$

$$\partial_{\xi_k} g = -\frac{e^{\alpha(\hat{\xi}_1 - \hat{r})}}{4\pi\varepsilon^3} (\alpha\hat{r} + 1) \frac{\hat{\xi}_k}{\hat{r}^3}, \quad k = 2, 3, \quad (7b)$$

$$\partial_{\xi_1}^2 g = \frac{e^{\alpha(\hat{\xi}_1 - \hat{r})}}{4\pi\varepsilon^4} \hat{r}^{-3} \left[\alpha^2(\hat{r} - \hat{\xi}_1)^2 - \alpha(\hat{r} - \hat{\xi}_1) \left(1 + 3\frac{\hat{\xi}_1}{\hat{r}} \right) + \frac{3\hat{\xi}_1^2 - \hat{r}^2}{\hat{r}^2} \right], \quad (7c)$$

$$\partial_{\xi_k}^2 g = \frac{e^{\alpha(\hat{\xi}_1 - \hat{r})}}{4\pi\varepsilon^4} \hat{r}^{-3} \left[\alpha^2 \hat{\xi}_k^2 + (\alpha\hat{r} + 1) \frac{3\hat{\xi}_k^2 - \hat{r}^2}{\hat{r}^2} \right], \quad k = 2, 3. \quad (7d)$$

Lemma 5. *Let $\Omega_* := (0, 1) \times \mathbb{R}^2$, $\varepsilon \in (0, c_0]$ for some sufficiently small constant c_0 , and $0 < \alpha \leq C$. Then the function g of (6) satisfies, for any $\mathbf{x} \in [2\varepsilon, \frac{3}{4}] \times \mathbb{R}^2$, the following bounds*

$$\|\partial_{\xi_1} g(\mathbf{x}; \cdot)\|_{1; \Omega_*} \geq c |\ln \varepsilon|, \quad (8a)$$

$$\|\partial_{\xi_k} g(\mathbf{x}; \cdot)\|_{1; \Omega_*} \geq c \varepsilon^{-1/2}, \quad k = 2, 3. \quad (8b)$$

Furthermore, for any ball $B(\mathbf{x}; \rho)$ of radius $\rho \leq \frac{1}{8}$, we have

$$\|g(\mathbf{x}; \cdot)\|_{1,1; \Omega_* \cap B(\mathbf{x}; \rho)} \geq \begin{cases} c\rho/\varepsilon, & \text{if } \rho \leq 2\varepsilon, \\ c(\rho/\varepsilon)^{1/2}, & \text{otherwise,} \end{cases} \quad (8c)$$

$$\|\partial_{\xi_1}^2 g(\mathbf{x}; \cdot)\|_{1; \Omega_* \setminus B(\mathbf{x}; \rho)} \geq c \varepsilon^{-1} \ln(2 + \varepsilon/\rho), \quad \text{if } \rho \leq c_1 \varepsilon, \quad (8d)$$

$$\|\partial_{\xi_k}^2 g(\mathbf{x}; \cdot)\|_{1; \Omega_* \setminus B(\mathbf{x}; \rho)} \geq c \varepsilon^{-1} (\ln(2 + \varepsilon/\rho) + |\ln \varepsilon|), \quad \text{if } \rho \leq \frac{1}{8}, \quad (8e)$$

where $k = 2, 3$, and c_1 is a sufficiently small positive constant.

Remark 6. The statement of the above Lemma 5 is almost identical with the statement of Theorem 3 with G replaced by g and Ω_* replaced by Ω .

Proof. Throughout the proof, x_1 is fixed, so we employ the notation $\hat{\xi}_1 := \hat{\xi}_{1,[x_1]}$ and $\hat{\boldsymbol{\xi}} := (\hat{\xi}_1, \hat{\xi}_2, \hat{\xi}_3)$. First, we rewrite all integrals that appear in (8) in variable $\hat{\boldsymbol{\xi}} \in \hat{\Omega}_* := (-\frac{x_1}{\varepsilon}, \frac{1-x_1}{\varepsilon}) \times \mathbb{R}^2$ using $d\hat{\boldsymbol{\xi}} = \varepsilon^3 d\boldsymbol{\xi}$. Now it suffices to prove the desired lower bounds on any sub-domain of $\hat{\Omega}_*$. In particular, we employ the non-overlapping sub-domains $\hat{\Omega}_1$ and $\hat{\Omega}_2$ of $\hat{\Omega}_*$:

$$\hat{\Omega}_1 := B(\mathbf{0}, 1) \cap \left\{ \hat{\xi}_1^2 \geq \hat{\xi}_2^2 + \hat{\xi}_3^2 \right\}, \quad \hat{\Omega}_2 := \left\{ \max\{1, \sqrt{\hat{\xi}_2^2 + \hat{\xi}_3^2}\} \leq \hat{\xi}_1 \leq \frac{1}{4}\varepsilon^{-1} \right\}$$

(but other sub-domains of $B(\mathbf{0}, 1)$ similar to $\widehat{\Omega}_1$ will be considered as well). The notation $[v]^+ := \max\{v, 0\}$ will be used for any function v .

(i) The bounds (8a), (8b) will be obtained using $\widehat{\Omega}_2$. Note that for $\widehat{\boldsymbol{\xi}} \in \widehat{\Omega}_2$ one has $\widehat{\xi}_1 \leq \widehat{r} \leq \sqrt{2}\widehat{\xi}_1$. Introduce the new variables $\psi_k := \widehat{\xi}_k / \sqrt{2\widehat{\xi}_1}$ for $k = 2, 3$, so

$$d\widehat{\xi}_2 d\widehat{\xi}_3 = 2\widehat{\xi}_1 d\psi_2 d\psi_3, \quad \Omega_\Psi = \left\{ \psi_2^2 + \psi_3^2 \leq \frac{1}{2}\widehat{\xi}_1 \right\}, \quad \frac{\widehat{r} - \widehat{\xi}_1}{\psi_2^2 + \psi_3^2} \in [c_2, 1],$$

where $c_2 := 2(1 + \sqrt{2})^{-1}$, and we used $\widehat{r} - \widehat{\xi}_1 = (\widehat{\xi}_2^2 + \widehat{\xi}_3^2)/(\widehat{\xi}_1 + \widehat{r})$ to get the final relation above.

Now a calculation using (7a) yields the first desired bound (8a) as follows:

$$\begin{aligned} \|\partial_{\xi_1} g\|_{1,\Omega_*} &\geq c \iiint_{\widehat{\Omega}_2} e^{\alpha(\widehat{\xi}_1 - \widehat{r})} \widehat{\xi}_1^{-2} \left[\alpha(\widehat{r} - \widehat{\xi}_1) - \frac{\widehat{\xi}_1}{\widehat{r}} \right]^+ d\widehat{\boldsymbol{\xi}} \\ &\geq c \int_1^{\frac{1}{4}\varepsilon^{-1}} \widehat{\xi}_1^{-1} d\widehat{\xi}_1 \iint_{\Omega_\Psi} e^{-\alpha(\psi_2^2 + \psi_3^2)} \left[\alpha c_2(\psi_2^2 + \psi_3^2) - 1 \right]^+ d\psi_2 d\psi_3 \\ &\geq c |\ln \varepsilon|. \end{aligned}$$

A similar calculation using (7b) with $k = 2, 3$ yields (8b); indeed,

$$\begin{aligned} \|\partial_{\xi_k} g\|_{1,\Omega_*} &\geq c \iiint_{\widehat{\Omega}_2} e^{\alpha(\widehat{\xi}_1 - \widehat{r})} (\alpha\widehat{r} + 1) \widehat{\xi}_1^{-3} |\widehat{\xi}_k| d\widehat{\boldsymbol{\xi}} \\ &\geq c \int_1^{\frac{1}{4}\varepsilon^{-1}} d\widehat{\xi}_1 (\alpha\widehat{\xi}_1 + 1) \widehat{\xi}_1^{-3/2} \iint_{\Omega_\Psi} e^{-\alpha(\psi_2^2 + \psi_3^2)} |\psi_k| d\psi_2 d\psi_3 \geq c \varepsilon^{-1/2}. \end{aligned}$$

(ii) To show (8c) for $\rho \leq 2\varepsilon$, we note that $\|g\|_{1,1;B(\mathbf{x},\rho)} \geq \|\partial_{\xi_2} g\|_{1;B(\mathbf{x},\rho)}$ so set $\widehat{\rho} := \rho/\varepsilon$ and consider the sub-domain $\widehat{\Omega}_3 := B(\mathbf{0}, \widehat{\rho}) \cap \{\widehat{\xi}_2^2 \geq \widehat{\xi}_1^2 + \widehat{\xi}_3^2\}$. Note that in this sub-domain, $e^{\alpha(\widehat{\xi}_1 - \widehat{r})} \geq c$ and $\widehat{\xi}_2 \geq \widehat{r}/\sqrt{2}$ so (7b) yields

$$\|\partial_{\xi_2} g\|_{1,\Omega_* \cap B(\mathbf{x},\rho)} \geq c \iiint_{\widehat{\Omega}_3} \widehat{r}^{-2} d\widehat{\boldsymbol{\xi}} \geq c \int_0^{\widehat{\rho}} d\widehat{r} \geq c \widehat{\rho} = c \rho/\varepsilon,$$

which immediately implies (8c) for $\rho \leq 2\varepsilon$.

Next, for $\rho \in [2\epsilon, \frac{1}{8}]$ consider $\partial_{\xi_2} g$ in the sub-domain $\widehat{\Omega}_2 \cap B(\mathbf{0}, \widehat{\rho})$. Imitating the calculation in part (i), one gets

$$\begin{aligned} \|\partial_{\xi_2} g\|_{1, \Omega_* \cap B(\mathbf{x}, \rho)} &\geq c \iiint_{\widehat{\Omega}_2 \cap B(\mathbf{0}, \widehat{\rho})} e^{\alpha(\widehat{\xi}_1 - \widehat{r})} (\alpha \widehat{r} + 1) \widehat{\xi}_1^{-3} |\widehat{\xi}_2| d\widehat{\boldsymbol{\xi}} \\ &\geq c \int_1^{\widehat{\rho}} d\widehat{\xi}_1 (\alpha \widehat{\xi}_1 + 1) \widehat{\xi}_1^{-3/2} \iint_{\Omega_\Psi} e^{-\alpha(\psi_2^2 + \psi_3^2)} |\psi_2| d\psi_2 d\psi_3 \\ &\geq c \widehat{\rho}^{-1/2}, \end{aligned}$$

which completes the proof of (8c) for $\rho \leq \frac{1}{8}$.

(iii) To obtain (8d), we use the sub-domain $\widehat{\Omega}_1 \setminus B(\mathbf{0}, \widehat{\rho})$, where $\widehat{\rho} := \rho/\epsilon$. Note that for $\widehat{\boldsymbol{\xi}} \in \widehat{\Omega}_1$ one has $e^{\alpha(\widehat{\xi}_1 - \widehat{r})} \geq c$ and $\frac{3\widehat{\xi}_1^2 - \widehat{r}^2}{\widehat{r}^2} \geq 1$. So using (7c), one gets

$$\begin{aligned} \|\partial_{\xi_1}^2 g\|_{1, \Omega_* \setminus B(\mathbf{x}, \rho)} &\geq c \epsilon^{-1} \iiint_{\widehat{\Omega}_1 \setminus B(\mathbf{0}, \widehat{\rho})} \widehat{r}^{-3} [0 - 4\alpha \widehat{r} + 1]^+ d\widehat{\boldsymbol{\xi}} \\ &\geq c \epsilon^{-1} \int_{\widehat{\rho}}^{\min\{1, \frac{1}{8\alpha}\}} \widehat{r}^{-1} d\widehat{r} \geq c \epsilon^{-1} \ln(2 + \rho/\epsilon). \end{aligned}$$

So we have shown (8d) for $\rho \leq c_1 \epsilon$ with $c_1 := \frac{1}{2} \min\{1, \frac{1}{8\alpha}\}$.

(iv) In a similar manner as in part (iii), using (7d), one can show that $\|\partial_{\xi_k}^2 g\|_{1, \Omega \setminus B(\mathbf{x}, \rho)} \geq c \epsilon^{-1} \ln(2 + \rho/\epsilon)$ for $k = 2, 3$ and $\rho \leq \frac{1}{2} \epsilon$. Note that now we use the sub-domain $B(\mathbf{0}, 1) \cap \{\widehat{\xi}_k^2 \geq \widehat{\xi}_1^2 + \widehat{\xi}_j^2\}$ instead of $\widehat{\Omega}_1$, with $j = 3$ for $k = 2$ and $j = 2$ for $k = 3$.

Consequently, to obtain (8e) for any $\rho \leq \frac{1}{8}$, it remains to show that $\|\partial_{\xi_k}^2 g\|_{1, \Omega_* \setminus B(\mathbf{x}, \rho)} \geq c \epsilon^{-1} |\ln \epsilon|$. For this, consider (7d) in $\widehat{\Omega}_2 \setminus B(\mathbf{0}, \widehat{\rho})$. Combining the observations made in part (i) with $\alpha \widehat{r} + 1 \leq (\alpha\sqrt{2} + 1) \widehat{\xi}_1$ and $\frac{3\widehat{\xi}_k^2 - \widehat{r}^2}{\widehat{r}^2} \geq -1$, yields

$$\begin{aligned} \|\partial_{\xi_k}^2 g\|_{1, \Omega_* \setminus B(\mathbf{x}, \rho)} &\geq c \epsilon^{-1} \iiint_{\widehat{\Omega}_2 \setminus B(\mathbf{0}, \widehat{\rho})} e^{\alpha(\widehat{\xi}_1 - \widehat{r})} \widehat{\xi}_1^{-3} [2\alpha^2 \widehat{\xi}_1 \psi_k^2 - (\alpha\sqrt{2} + 1) \widehat{\xi}_1]^+ d\widehat{\boldsymbol{\xi}} \\ &\geq c \int_{\max\{1, \widehat{\rho}\}}^{\frac{1}{4}\epsilon^{-1}} \widehat{\xi}_1^{-1} d\widehat{\xi}_1 \iint_{\Omega_\Psi} e^{-\alpha(\psi_2^2 + \psi_3^2)} [2\alpha^2 \psi_k^2 - (\alpha\sqrt{2} + 1)]^+ d\psi_2 d\psi_3 \\ &\geq c \epsilon^{-1} |\ln \epsilon|. \end{aligned}$$

Here we also used $\widehat{\rho} \leq \frac{1}{8} \epsilon^{-1}$. So we have proved the final desired assertion (8e). \square

3 APPROXIMATION OF THE GREEN'S FUNCTION AND PROOF OF THEOREM 3 FOR THE DOMAIN $\Omega_* = (0, 1) \times \mathbb{R}^2$

To approximate the Green's function, we use the fundamental solution g of Section 2 and the cut-off function ω , defined by

$$\omega(t) \in C^2(0, 1), \quad \omega(t) = 0 \text{ for } t \leq \frac{1}{6}, \quad \omega(t) = 1 \text{ for } t \geq \frac{1}{3}, \quad (9)$$

so $\omega'(x) = 0$ for $x = 0, 1$. Then we set

$$\bar{G}(\mathbf{x}; \boldsymbol{\xi}) = \frac{e^{\alpha\hat{\xi}_{1,[x_1]}}}{4\pi\varepsilon^2} \left\{ \left[\frac{e^{-\alpha\hat{r}_{[x_1]}}}{\hat{r}_{[x_1]}} - \frac{e^{-\alpha\hat{r}_{[-x_1]}}}{\hat{r}_{[-x_1]}} \right] - \left[\frac{e^{-\alpha\hat{r}_{[2-x_1]}}}{\hat{r}_{[2-x_1]}} - \frac{e^{-\alpha\hat{r}_{[2+x_1]}}}{\hat{r}_{[2+x_1]}} \right] \omega(\xi_1) \right\},$$

which approximates the Green's function G associated with the domain $\Omega_* = (0, 1) \times \mathbb{R}^2$; in particular, it satisfies the boundary condition $\bar{G}|_{\partial\Omega_*} = \bar{G}|_{\xi_1=0,1} = 0$. Using the notations

$$g_{[d]} := g(d, x_2, x_3; \boldsymbol{\xi}), \quad \lambda^\pm := e^{2\alpha(1 \pm x_1)/\varepsilon}, \quad p := e^{-2\alpha x_1/\varepsilon},$$

we can rewrite the definition of \bar{G} as

$$\bar{G}(\mathbf{x}; \boldsymbol{\xi}) = [g_{[x_1]} - p g_{[-x_1]}] - [\lambda^- g_{[2-x_1]} - p \lambda^+ g_{[2+x_1]}] \omega(\xi_1). \quad (10)$$

We now present a version of [5, Lemma 4.2], which gives certain upper bounds for g that involve a weight function λ of type λ^\pm .

Lemma 7. *Let $\mathbf{x} \in [1 + \varepsilon, 3] \times \mathbb{R}^2$. Then for the function g of (6) and the weight $\lambda := e^{2\alpha(x_1-1)/\varepsilon}$ one has the following bounds*

$$\|(\lambda g)(\mathbf{x}; \cdot)\|_{1,\Omega_*} \leq C\varepsilon, \quad (11a)$$

$$\|(\lambda \partial_{\xi_k} g)(\mathbf{x}; \cdot)\|_{1,\Omega_*} \leq C, \quad k = 1, 2, 3, \quad (11b)$$

$$\|(\lambda \partial_{\xi_k}^2 g)(\mathbf{x}; \cdot)\|_{1,\Omega_*} \leq C\varepsilon^{-1}, \quad k = 1, 2, 3, \quad (11c)$$

while for any ball $B(\mathbf{x}'; \rho)$ of radius $\rho \leq \frac{1}{8}$ centred at $\mathbf{x}' \in [0, \frac{3}{4}] \times \mathbb{R}^2$, one has

$$\|(\lambda g)(\mathbf{x}; \cdot)\|_{1,1;\Omega_* \cap B(\mathbf{x}'; \rho)} \leq C \min\{\rho/\varepsilon, (\rho/\varepsilon)^{1/2}\} e^{-\frac{1}{8}\alpha/\varepsilon}. \quad (11d)$$

Proof. The bounds (11a), (11b) appear in [5, Lemma 4.2]. The estimate (11c) is slightly sharper compared to the similar bound in [5, Lemma 4.2]; the latter is for the domain $\Omega_* \setminus B(\mathbf{x}, \rho)$ and involves the logarithmic term $\ln(2 + \varepsilon/\rho)$ as it is valid for $x_1 \in [1, 3]$. In the above Lemma 7 we make a

stronger assumption that $x_1 \in [1 + \varepsilon, 3]$, under which $\Omega_* \setminus B(\mathbf{x}, \varepsilon) = \Omega_*$ and the logarithmic term becomes $\ln 3$ so can be dropped.

To obtain the final desired bound (11d), note that $x_1 \geq 1 + \varepsilon$ implies that $\widehat{r} > 1$ in Ω_* so (6), (7a) and (7b) yield $\lambda(|g| + |\partial_{\xi_k} g|) \leq C\varepsilon^{-3}\lambda e^{\alpha(\widehat{\xi}_1 - \widehat{r})}$ for $k = 1, 2, 3$. Here $\widehat{\xi}_1 - \widehat{r} = -(|\widehat{\xi}_1| + \widehat{r}) \geq -2|\widehat{\xi}_1|$ so $\lambda e^{\alpha(\widehat{\xi}_1 - \widehat{r})} \leq e^{2\alpha[(x_1 - 1)/\varepsilon - |\widehat{\xi}_1|]}$. Note also that in $B(\mathbf{x}'; \rho)$ we have $\xi_1 \leq 1 - \frac{1}{8}$ so $|\widehat{\xi}_1| = \frac{x_1 - \xi_1}{\varepsilon} \geq \frac{x_1 - 1}{\varepsilon} + \frac{1}{8}\varepsilon^{-1}$. Consequently, $\lambda(|g| + |\partial_{\xi_k} g|) \leq C\varepsilon^{-3}\lambda e^{-\frac{1}{4}\alpha/\varepsilon}$, so $\|(\lambda g)(\mathbf{x}; \cdot)\|_{1,1; \Omega_* \cap B(\mathbf{x}'; \rho)} \leq C(\rho/\varepsilon)^3 e^{-\frac{1}{4}\alpha/\varepsilon}$. Combining this with $(\rho/\varepsilon)^3 \leq C(\rho/\varepsilon)^p e^{\frac{1}{8}\alpha/\varepsilon}$ for $p = 1, \frac{1}{2}$ yields (11d). \square

Lemma 8. *Let $\Omega_* := (0, 1) \times \mathbb{R}^2$, $\varepsilon \in (0, c_0]$ for some sufficiently small constant c_0 , and $0 < \alpha \leq C$. Then the function \bar{G} of (10) satisfies, for any $\mathbf{x} \in [1/4, 3/4] \times \mathbb{R}^2$, all the bounds (8) of Lemma 5 with g replaced by \bar{G} .*

Proof. Let D be any of the first- or second-order differential operators that appear in (8). Now for any $\Omega'_* \subset \Omega_*$, the representation (10) yields

$$\begin{aligned} \|D\bar{G}(\mathbf{x}; \cdot)\|_{1, \Omega'_*} &= \|Dg_{[x_1]} - p Dg_{[-x_1]} - \lambda^- Dg_{[2-x_1]} + p \lambda^+ Dg_{[2+x_1]}\|_{1, \Omega'_*} \\ &\geq \|Dg_{[x_1]}\|_{1, \Omega'_*} - p \|Dg_{[-x_1]}\|_{1, \Omega'_*} - \|\lambda^- Dg_{[2-x_1]}\|_{1, \Omega'_*} \\ &\quad - p \|\lambda^+ Dg_{[2+x_1]}\|_{1, \Omega'_*}. \end{aligned} \quad (12)$$

For the first term that involves $g_{[x_1]}$, we use the corresponding lower bound from Lemma 5 so it remains to show that this bound will dominate the remaining three terms. For the second term we note that $g_{[-x_1]}$ satisfies the upper bounds of type (3) with Ω replaced by Ω_* [5]. Now, as $x_1 \geq \frac{1}{4}$ implies that $p \leq e^{-\frac{1}{2}\alpha/\varepsilon}$, the second term will be dominated by the first term if ε is sufficiently small (i.e. if the constant c_0 is sufficiently small).

To estimate the terms that involve $\lambda^\pm g_{[2\pm x_1]}$ in (12), we use the bounds (11) of Lemma 7. In particular, by (8d), (11c),

$$\begin{aligned} \frac{1}{3} \|\partial_{\xi_1}^2 g(\mathbf{x}; \cdot)\|_{1, \Omega_* \setminus B(\mathbf{x}; \rho)} - \|\lambda^\pm \partial_{\xi_1}^2 g_{[2\pm x_1]}\|_{1, \Omega_* \setminus B(\mathbf{x}; \rho)} \\ \geq \varepsilon^{-1} [c \ln(2 + \varepsilon/\rho) - C] \\ \geq c \varepsilon^{-1} \ln(2 + \varepsilon/\rho) \end{aligned}$$

for $\rho \leq c_1 \varepsilon$ if c_1 is sufficiently small, so we get a version of (8d) for \bar{G} . Similarly, by (8e), (11c), for $k = 2, 3$ one gets

$$\begin{aligned} \frac{1}{3} \|\partial_{\xi_k}^2 g(\mathbf{x}; \cdot)\|_{1, \Omega_* \setminus B(\mathbf{x}; \rho)} - \|\lambda^\pm \partial_{\xi_k}^2 g_{[2\pm x_1]}\|_{1, \Omega_* \setminus B(\mathbf{x}; \rho)} \\ \geq \varepsilon^{-1} [c \ln(2 + \varepsilon/\rho) + c |\ln \varepsilon| - C] \\ \geq c \varepsilon^{-1} (\ln(2 + \varepsilon/\rho) + |\ln \varepsilon|) \end{aligned}$$

provided that ε is sufficiently small. This yields a version of (8e) for \bar{G} . Finally, (11d) implies that

$$\begin{aligned} \|(\lambda^\pm g_{[2\pm x_1]})(\mathbf{x}; \cdot)\|_{1,1;\Omega_* \cap B(\mathbf{x}; \rho)} &\leq C \min\{\rho/\varepsilon, (\rho/\varepsilon)^{1/2}\} e^{-\frac{1}{8}\alpha/\varepsilon} \\ &\leq \frac{1}{3}c \min\{\rho/\varepsilon, (\rho/\varepsilon)^{1/2}\} \end{aligned}$$

for any arbitrarily small c provided that ε is sufficiently small. This observation yields a version of (8c) for \bar{G} . \square

Proof of Theorem 3 for the domain $\Omega_ = (0, 1) \times \mathbb{R}^2$.* As, by Lemma 8, the approximation \bar{G} satisfies the bounds that we need to prove for G , it suffices to estimate the function $v = \bar{G} - G$, which satisfies the differential equation

$$\mathcal{L}_\xi^* v(\mathbf{x}; \xi) = -\varepsilon \Delta_\xi v(\mathbf{x}; \xi) + 2\alpha \partial_{\xi_1} v(\mathbf{x}; \xi) = \phi(\mathbf{x}; \xi) \quad \text{for } \xi \in \Omega_*, \quad (13)$$

and the boundary condition $v(\mathbf{x}; \xi)|_{\xi \in \partial\Omega_*} = 0$. Here for the right-hand side ϕ , it was shown in [5, Lemma 5.1] that

$$\|\phi(\mathbf{x}; \cdot)\|_{1;\Omega_*} \leq C e^{-c_3 \alpha/\varepsilon} \quad (14)$$

for some constant c_3 . In view of (13), the function v can be represented using the Green's function G as

$$v(\mathbf{x}; \xi) = \iiint_{\Omega_*} G(\mathbf{s}; \xi) \phi(\mathbf{x}; \mathbf{s}) d\mathbf{s}.$$

So applying $\partial_{\xi_k}^p$ to this representation with $p = 0, 1, 2$, $k = 1, 2, 3$, for any sub-domain $\Omega'_* \subset \Omega_*$, one gets

$$\begin{aligned} \|\partial_{\xi_k}^p v(\mathbf{x}; \cdot)\|_{1;\Omega'_*} &\leq \left(\max_{\mathbf{s} \in \Omega'_*} \|\partial_{\xi_k}^p G(\mathbf{s}; \cdot)\|_{1,\Omega'_*} \right) \cdot \|\phi(\mathbf{x}; \cdot)\|_{1,\Omega_*} \\ &\leq C e^{-c_3 \alpha/\varepsilon} \cdot \max_{\mathbf{s} \in \Omega'_*} \|\partial_{\xi_k}^p G(\mathbf{s}; \cdot)\|_{1,\Omega_*}, \end{aligned}$$

where we also used (14). We shall use the above estimate with $\Omega'_* := \Omega_*$ for $p = 0, 1$ and $\Omega'_* := \Omega_* \setminus B(\mathbf{x}, \rho)$ for $p = 2$. As the bounds (3) of Theorem 1 remain valid for the domain Ω_* and also $\|G(\mathbf{x}; \cdot)\|_{1,\Omega_*} \leq C$ [5, 6], one now concludes that

$$\begin{aligned} \|\partial_{\xi_k}^2 v(\mathbf{x}; \cdot)\|_{1;\Omega_* \setminus B(\mathbf{x}, \rho)} &\leq C e^{-c_3 \alpha/\varepsilon} \cdot \varepsilon^{-1} (\ln(2 + \varepsilon/\rho) + |\ln \varepsilon|) \\ &\leq c' \varepsilon^{-1} \ln(2 + \varepsilon/\rho) \quad \text{for } k = 1, 2, 3, \end{aligned} \quad (15a)$$

where c' is arbitrarily small provided that ε is sufficiently small. Similarly

$$\|v(\mathbf{x}; \cdot)\|_{1,1;\Omega_*} \leq C e^{-c_3 \alpha/\varepsilon} \cdot \varepsilon^{-1/2} \leq c' \varepsilon, \quad (15b)$$

which also implies

$$\|v(\mathbf{x}; \cdot)\|_{1,1;\Omega_* \cap B(\mathbf{x}, \rho)} \leq c' \min\{\rho/\varepsilon, (\rho/\varepsilon)^{1/2}\}. \quad (15c)$$

As c' in the bounds (15) can be made arbitrarily small, combining them with Lemma 8 yields the desired bounds of Theorem 3 for the domain $\Omega_* = (0, 1) \times \mathbb{R}^2$. \square

4 PROOF OF THEOREM 3 FOR THE DOMAIN $\Omega = (0, 1)^3$

The proof of Theorem 3 for the domain $\Omega = (0, 1)^3$ is very similar to the above proof for the domain $\Omega_* = (0, 1) \times \mathbb{R}^2$ presented in Section 3. The only difference is that instead of the approximation \bar{G} for the domain $(0, 1) \times \mathbb{R}^2$ we now use the approximation $\bar{\bar{G}}$ defined by

$$\begin{aligned} \bar{\bar{G}}(\mathbf{x}; \boldsymbol{\xi}) &:= \bar{G}(\mathbf{x}; \boldsymbol{\xi}) - \omega_0(\xi_2) \bar{G}(\mathbf{x}; \xi_1, -\xi_2, \xi_3) - \omega_1(\xi_2) \bar{G}(\mathbf{x}; \xi_1, 2 - \xi_2, \xi_3), \\ \bar{\bar{\bar{G}}}(\mathbf{x}; \boldsymbol{\xi}) &:= \bar{\bar{G}}(\mathbf{x}; \boldsymbol{\xi}) - \omega_0(\xi_3) \bar{\bar{G}}(\mathbf{x}; \xi_1, \xi_2, -\xi_3) - \omega_1(\xi_3) \bar{\bar{G}}(\mathbf{x}; \xi_1, \xi_2, 2 - \xi_3). \end{aligned}$$

Here $\omega_0(t) := \omega(1-t)$ and $\omega_1(t) := \omega(t)$ with ω defined in (9), so that $\omega_k(k) = 1$ and $\omega_k(1-k) = 0$ for $k = 0, 1$. This approximation was constructed employing the method of images; an inclusion of cut-off functions ensures that it vanishes on $\partial\Omega$.

All the properties of \bar{G} given in Section 3 remain valid for this new approximation $\bar{\bar{G}}$ with Ω_* replaced by Ω provided that $\mathbf{x} \in [\frac{1}{4}, \frac{3}{4}]^3$. We leave out the details and only note that the application of the method of images in the ξ_2 - and ξ_3 -directions is relatively straightforward as an inspection of (6) shows that in these directions, the fundamental solution g is symmetric and exponentially decaying away from the singular point. \square

5 THE CONVECTION-REACTION-DIFFUSION CASE

We now slightly generalize (1) by including a reaction term with a constant coefficient $\beta \geq 0$:

$$\tilde{\mathcal{L}}_{\mathbf{x}} u(\mathbf{x}) = -\varepsilon \Delta_{\mathbf{x}} u(\mathbf{x}) - 2\alpha \partial_{x_1} u(\mathbf{x}) + \beta u(\mathbf{x}) = f(\mathbf{x}) \quad \text{for } \mathbf{x} \in \Omega \quad (16a)$$

$$u(\mathbf{x}) = 0 \quad \text{for } \mathbf{x} \in \partial\Omega. \quad (16b)$$

Now the fundamental solution g in \mathbb{R}^3 satisfies, for each fixed $\mathbf{x} \in \mathbb{R}^3$ the following version of (5) with the adjoint operator $\tilde{\mathcal{L}}_{\xi}^*$:

$$\tilde{\mathcal{L}}_{\xi}^* g(\mathbf{x}; \xi) = -\varepsilon \Delta_{\xi} g(\mathbf{x}; \xi) + 2\alpha \partial_{\xi_1} g(\mathbf{x}; \xi) + \beta g(\mathbf{x}; \xi) = \delta(\mathbf{x} - \xi) \quad \text{for } \xi \in \mathbb{R}^3.$$

Again imitating a calculation of [2, 9], one gets a version of (6):

$$g(\mathbf{x}; \xi) = \frac{1}{4\pi\varepsilon^2} \frac{e^{\alpha\hat{\xi}_{1,[x_1]} - \gamma\hat{r}_{[x_1]}}}{\hat{r}_{[x_1]}}, \quad \text{where } \gamma := \sqrt{\alpha^2 + \varepsilon\beta}.$$

In view of $\gamma = \alpha + \frac{\beta}{2\alpha}\varepsilon + \mathcal{O}(\varepsilon^2)$, an inspection of the proof of Theorem 3 shows that the lower bounds (4) remain valid for the convection-reaction-diffusion problem (16).

6 OUTLOOK FOR PROBLEMS IN n DIMENSIONS

It was shown in [7] that the upper bounds of Theorem 1 remain valid for a two-dimensional variable-coefficient version of (1). Note that the fundamental solution $g_{\mathbb{R}^2}$ that solves (5) in \mathbb{R}^2 , and also its derivatives involve the modified Bessel functions of second kind of order zero $K_0(\cdot)$ and order one $K_1(\cdot)$. This fundamental solution is given by

$$g_{\mathbb{R}^2}(\mathbf{x}; \xi) = \frac{1}{2\pi\varepsilon} e^{\alpha\hat{\xi}_1} K_0(\alpha\hat{r})$$

with the notations \mathbf{x} , ξ , and \hat{r} appropriately adapted. Using this explicit representation, one can imitate the proof of Theorem 3 and get similar lower bounds for the two-dimensional case. A certain difficulty lies in having to deal with the Bessel functions, for which one can simply employ asymptotic expansions [1, 12]:

$$\begin{aligned} K_0(z) &= \left(\frac{\pi}{2z}\right)^{1/2} e^{-z} \left(1 + \mathcal{O}(z^{-1})\right) && \text{for } |z| \gg 1, \\ K_1(z) &= K_0(z) \left(1 + \frac{1}{2z} + \mathcal{O}(z^{-2})\right) && \text{for } |z| \gg 1, \\ K_0(z) &= -\ln z + \mathcal{O}(1), \quad K_1(z) = \frac{1}{z} + \mathcal{O}(1) && \text{for } |z| \ll 1. \end{aligned}$$

In this manner one gets the following result.

Theorem 9. *The Green's function associated with problem (1) in the unit-square domain $\Omega := (0, 1)^2$, satisfies a two-dimensional version of Theorem 3.*

Finally, let us take a look at the problem (1) in the n -dimensional domain $\Omega := (0, 1)^n$ of an arbitrary dimension $n \geq 2$. The corresponding fundamental solution $g_{\mathbb{R}^n}$ is given by

$$g_{\mathbb{R}^n}(\mathbf{x}; \boldsymbol{\xi}) = \frac{1}{(2\pi)^{n/2} \varepsilon^{n-1}} \left(\frac{\alpha}{\hat{r}} \right)^{n/2-1} e^{\alpha \hat{\xi}_1} K_{n/2-1}(\alpha \hat{r})$$

with the modified Bessel functions $K_{n/2-1}(\cdot)$ of second kind of (half-)integer order $n/2-1$, and the notations \mathbf{x} , $\boldsymbol{\xi}$, and \hat{r} appropriately adapted. Using asymptotic expansions of these Bessel functions [1, 12], one can again get a version of Theorem 3.

ACKNOWLEDGEMENTS

This work has been supported by Science Foundation Ireland under the Research Frontiers Programme 2008; Grant 08/RFP/MTH1536. The second author was also supported by the Bulgarian Foundation for Science; project DID 02/37-2009.

References

1. M. Abramowitz and I. A. Stegun. *Handbook of Mathematical Functions with Formulas, Graphs and Mathematical Tables*. Applied Mathematics Series. National Bureau of Standards, Washington, D.C., 1964.
2. N.M. Chadha and N. Kopteva. Maximum norm a posteriori error estimate for a 3d singularly perturbed semilinear reaction-diffusion problem. doi: 10.1007/s10444-010-9163-2 (published online 1 June 2010), 2010.
3. K. Eriksson. An adaptive finite element method with efficient maximum norm error control for elliptic problems. *Math. Models Methods Appl. Sci.*, **4**:313–329, 1994.
4. S. Franz and N. Kopteva. A posteriori error estimation for a convection-diffusion problem with characteristic layers. in preparation, 2011.
5. S. Franz and N. Kopteva. Full Analysis of Green's function estimates for a convection-diffusion problem with characteristic boundary layers in 3d. Technical report, University of Limerick, 2011.
6. S. Franz and N. Kopteva. Green's Function Estimates for a Convection-Diffusion Problem in Three Dimensions. in preparation, 2011.
7. S. Franz and N. Kopteva. Green's function estimates for a singularly perturbed convection-diffusion problem. submitted, 2011.
8. J. Guzmán, D. Leykekhman, J. Rossmann, and A. H. Schatz. Hölder estimates for Green's functions on convex polyhedral domains and their applications to finite element methods. *Numer. Math.*, **112**:221–243, 2009.
9. R. B. Kellogg and S. Shih. Asymptotic analysis of a singular perturbation problem. *SIAM Journal on Mathematical Analysis*, **18**(5):1467–1510, 1987.
10. N. Kopteva. Maximum norm a posteriori error estimate for a 2d singularly perturbed reaction-diffusion problem. *SIAM J. Numer. Anal.*, **46**:1602–1618, 2008.

11. R. H. Nochetto. Pointwise a posteriori error estimates for elliptic problems on highly graded meshes. *Math. Comp.*, **64**:1–22, 1995.
12. F.W.J. Olver, D.W. Lozier, R. F. Boisvert, and C.W. Clark. *NIST Handbook of Mathematical Functions*. Cambridge University Press, Cambridge, 2010.

SUCCESSIVE APPROXIMATION FOR SOLVING TIME-DEPENDENT PROBLEMS

JÜRGEN GEISER¹ AND GAMZE TANOĞLU²

¹ Humboldt Universität zu Berlin, D- Berlin, Germany,
geiser@mathematik.hu-berlin.de

² Izmir Institute of Technology, Gulbahce Campus, Urla, Izmir, 35430, Turkey
gamzetaoglu@iyte.edu.tr

Abstract. Methods for time-dependent equations are a challenging and important topic. While the Magnus expansion has been intensely studied and widely applied for solving explicitly time-dependent problems, we propose an alternative method that is based on successive approximation methods. We take into account the temporally inhomogeneous equation (method of Tanabe and Sobolevski). Due to its exponential character, Magnus expansion is rather difficult to derive practical algorithms beyond the sixth-order. In this work, we show that the recently derived ideas of the successive approximation method in a splitting method. In Examples we can beat standard magnus expansion schemes.

1 INTRODUCTION

In this paper we concentrate on solving linear evolution equations, such as the time-dependent differential equation,

$$\partial_t u = A(t)u, \quad u(0) = u_0, \quad (1)$$

where A can be an unbounded and time-dependent operator. For solving Hamiltonian problems, it is often the case that $A(t) = T + V(t)$, where only the potential operator $V(t)$ is time-dependent. Our main focus will be to consider and contrast higher order algorithms derived from the Magnus expansion with those from Successive Approximation method. The higher order Magnus algorithms have been well studied by Blanes *et al.*, see their recent comprehensive review[3]. Successive Approximation methods can be applied to a iterative splitting method tested in [7] and [8].

M. Koleva and L. Vulkov (Eds.), Proceedings of the Fifth Conference on Finite Difference Methods: Theory and Applications (FDM: T&A 2010) 2011, pp. 58–67.
© Rousse University Press 2011

The Magnus expansion[1, 3] is an attractive and widely applied method of solving explicitly time-dependent problems. However, it requires computing time-integrals and nested commutators to higher orders. Successive approximation is based on recursive integral formulations in which an iterative method is enforce the time dependency.

The paper is outlined as follows: In Section 2, we present the successive approximation method and its application. In Section 3, we present the error analysis for the proposed splitting scheme. The numerical results are presented in Section 4.

In Section 5, we briefly summarize our results.

2 SPLITTING METHOD BASED ON SUCCESSIVE APPROXIMATION

For solving explicit time-dependent problems, one can also directly implement successive approximation method, instead of deriving an extention to the timedependent term, see [2].

The problem is given as in equation (1), we rewrite:

$$\frac{\partial u}{\partial t} = A(a)u(t) + (A(t) - A(a))u(t) \quad (2)$$

The abstract integral is given as, by the so called Duhamel Principle:

$$u(t) = \exp((t-a)A(a))u_0 + \int_a^t \exp((t-s)A(a))(A(s) - A(a))u(s) ds. \quad (3)$$

With successive approximation we obtain:

$$u_1(t) = \exp((t-a)A(a))u_0, \quad (4)$$

...

$$\begin{aligned} u_{n+1}(t) &= \exp((t-a)A(a))u_0 \\ &\quad + \int_a^t \exp((t-s)A(a))(A(s) - A(a))u_n(s) ds, \end{aligned} \quad (5)$$

and formally we have:

$$u(t) = \exp((t-a)A(a))u_0 + \int_a^t \exp((t-s)A(a))R(s,a)u_0 ds, \quad (6)$$

where the recursive operators are given as:

$$R(t,s) = \sum_{m=1}^{\infty} R_m(t,s), \quad (7)$$

$$R_1(t) = \begin{cases} (A(t) - A(s)) \exp((t-s)A(a)) ds, & s < t \\ 0, & s \geq t \end{cases}, \quad (8)$$

$$R_m(t) = \int_s^t R_1(t, \sigma) R_{m-1}(\sigma, t) d\sigma. \quad (9)$$

2.1 ALGORITHM FOR SUCCESSIVE APPROXIMATION

In this section, we will construct a new numerical algorithm in order to use successive approximation as a computational tool. To illustrate how this task can be accomplished, define a solution, for one time step, h , in the interval $[t_n, t_n + h]$, is given by

$$u(t_n + h) = e^{hA_a} u(t_n) + \int_{t_n}^{t_n+h} e^{(t_n+h-s)A_a} (A(s) - A_a) u(s) ds, \quad (10)$$

where $A_a = A(a)$ is $n \times n$ constant matrix. Successive approximation steps then can be read as

$$u_1(t_n + h) = e^{hA_a} u(t_n), \quad (11)$$

$$u_2(t_n + h) = e^{hA_a} u(t_n) + \int_{t_n}^{t_n+h} e^{(t_n+h-s)A_a} (A(s) - A_a) u_1(s) ds \quad (12)$$

$$\dots \quad (13)$$

$$u_k(t_n + h) = e^{hA_a} u(t_n) + \int_{t_n}^{t_n+h} e^{(t_n+h-s)A_a} (A(s) - A_a) u_{k-1}(s) ds. \quad (14)$$

After approximating the integrals in each iterations by quadrature formulas, we rewrite the solutions as

$$u_k(t_n + h) = e^{hA_a} u(t_n) + \sum_{j=1}^s w_j F(c_j^*), \quad k = 2, \dots, m \quad (15)$$

where $F(s) = e^{(t_n+h-s)A_a}$, w_j are weights and $c_j^* \in [t_n, t_n + h]$ are nodes.

We simply use the trapezoidal rule for approximating the integrals, we then have following iterative solving scheme,

$$\begin{aligned} u_k(t_n + h) &= e^{hA_a} \left(I + \frac{h}{2} (A(t_n) - A_a) \right) u(t_n) \\ &\quad + \frac{h}{2} (A(t_n + h) - A_a) u_{k-1}(t_n + h), \end{aligned} \quad (16)$$

for $k = 2, \dots, m$. Here $u(t_0) = u_0$ (initial condition), $u(t_n) = u_k(t_{n-1} + h)$, $n = 1, \dots, N$ and $N = \frac{b-a}{h}$. The algorithm will continue until the following condition is fulfilled,

$$|u_k - u_{k-1}| \leq err, \quad (17)$$

where err is a tolerance for the accuracy of the iterative scheme, e.g. $err = 10^{-6}$. It can be easily seen in Equation (16), the scheme involves only one approximation of exponential of a constant matrix.

3 ERROR ANALYSIS

We study the consistency of the iterative scheme given as:

$$\frac{\partial u_i(t)}{\partial t} = Au_i(t) + B(t)u_{i-1}(t), \quad (18)$$

with $u_i(t_n) = u^n$

$$\frac{\partial u_{i+1}(t)}{\partial t} = Au_i(t) + B(t)u_{i+1}(t), \quad (19)$$

with $u_{i+1}(t_n) = u^n$,

where u^n is the known split approximation at the time-level $t = t_n$. The initialization is given as $u_0(t_n) = u^n$ and the starting solution is given as $u_{-1} = 0.0$.

We assume the perturbation theory given in [4] and we apply the variation of constants to time-dependent operators, see [10].

Theorem 1. *Let us consider the abstract Cauchy problem in a Banach space \mathbf{X}*

$$\begin{aligned} \partial_t u(t) &= Au(t) + B(t)u(t), \quad 0 < t \leq T \text{ and } x \in \Omega, \\ u(0) &= u_0, \quad t \in [0, T], \end{aligned} \quad (20)$$

where $A, B(t) : D(\mathbf{X}) \rightarrow \mathbf{X}$ are given linear bounded operators which are generators of the C_0 -semigroup and $u_0 \in \mathbf{X}$ is a given element.

Further, we assume the estimations of the bounded time-dependent operator, see [4]:

$$\|B(t) \exp(At)x\| \leq \beta \|x\|, \quad (21)$$

$$\tau_n = (t^{n+1} - t^n).$$

The error of the first time-step is of accuracy $\mathcal{O}(\tau_n^m)$, where $\tau_n = t^{n+1} - t^n$ and we have equidistant time-steps, with $n = 1, \dots, N$. Then the iteration process (18)–(19) for $i = 1, 3, \dots, 2m + 1$ is consistent with the order of the consistency $\mathcal{O}(\tau_n^{2m+1})$.

Proof. For $i = 1$, we have:

$$u_1(t^{n+1}) = \exp(A\tau_n)u(t^n),$$

and the solution is given as

$$\begin{aligned} u(t^{n+1}) &= \exp(A\tau_n)u(t^n) \\ &+ \int_{t^n}^{t^{n+1}} \exp(A(t^{n+1}-s))B(s)\exp(sA + \int_0^s B(\tilde{s})d\tilde{s})u(t^n) ds, \end{aligned}$$

We obtain:

$$\begin{aligned} \|e_1\| &\leq \left\| \exp\left(A\tau + \int_{t^n}^{t^{n+1}} B(s)ds\right)u(t^n) - u_1 \right\| \\ &= \left\| \int_{t^n}^{t^{n+1}} \exp(A(t^{n+1}-s))B(s)\exp(sA + \int_0^s B(\tilde{s})d\tilde{s})u(t^n) ds \right\| \\ &\leq C\tau\|B(\xi)\|\|u(t^n)\| \end{aligned}$$

where $\xi \in [t^n, t^{n+1}]$ and the exp functions can be estimated by C .

The same argumentation is used for $i = 2$:

$$\begin{aligned} \|e_2\| &\leq \\ &= \int_{t^n}^{t^{n+1}} \left\| \exp\left(\int_0^{t^{n+1}-s} B(\tilde{s})d\tilde{s}\right)A \right\| \\ &\quad \int_{t^n}^s \left\| \exp(A(s-\rho))B(s)\exp((\rho-t^n)(A+B))u(t^n) d\rho \right\| ds \\ &= \tilde{C}\tau^2\|A\|\|B(\xi)\|\|u(t^n)\| \end{aligned}$$

where $\xi \in [t^n, t^{n+1}]$

Based on the bounded operators we can apply the recursive argument.

For the odd iterations: $i = 2m + 1$, with $m = 0, 1, 2, \dots$, we obtain for u_i and u :

$$\begin{aligned} \|e_i\| &\leq \int_0^{\tau_n} \left\| \exp(As)B(s) \right\| \\ &\quad \int_0^{\tau_n-s} \left\| \exp\left(\int_0^{\tau_n-s} B(\tilde{s})d\tilde{s}\right)A \right\| \int_0^{\tau_n-s_1-s_2} \exp(s_3A)B(s_3) \dots \\ &\quad \int_0^{\tau_n-\sum_{j=1}^i s_j} \exp(As_{i+1})B(s_{i+1})\exp((\tau_n - \sum_{j=1}^i s_j)(A \\ &\quad + \int_0^{(\tau_n-\sum_{j=1}^i s_j)} B(\tilde{s})d\tilde{s}))u(0) ds_{i+1} \dots ds_1. \end{aligned}$$

By shifting $0 \rightarrow t^n$ and $\tau_n \rightarrow t^{n+1}$, we obtain our result:

$$\|e_i\| \leq \tilde{C} \|A\|^{m+1} \|B(\xi)\|^m \tau_n^{2m+1} \|u(t^n)\|,$$

where $\xi \in [t^n, t^{n+1}]$ and \tilde{C} is a non-timedependent constant.

The same proof idea can be applied to the even iterative scheme, see also [6].

Numerical results related to this algorithm is presented in the next section.

4 NUMERICAL EXAMPLE

We consider the radial Schrödinger equation, see [9]:

$$\frac{\partial^2 u}{\partial r^2} = f(r, E)u(r) \quad (22)$$

where

$$f(r, E) = 2V(r) - 2E + \frac{l(l+1)}{r^2}$$

The equation (22) can be transformed as a harmonic oscillator with a time dependent spring constant after relabeling $r \rightarrow t$ and $u(r) \rightarrow q(t)$ and defining

$$k(t, E) = -f(t, E).$$

By redefining the variables as $u(t) = q(t)$ and $\dot{u}(t) = p(t)$, and $u(t) = (q(t), p(t))$, the Equation (22) can be put into the system of equation as

$$\dot{u}(t) = A(t)u(t)$$

and Hamiltonian of the system is written by

$$H = \frac{1}{2}p^2 + \frac{1}{2}k(t, E)q^2.$$

For specific example, the ground state of hydrogen atom can be modeled as Schrodinger equation with the parameters $l = 0, E = -1/2, V(t) = -1/(t - a)$, a is arbitrary constant. Now the time dependent oscillator corresponds to

$$A(t) = \begin{pmatrix} 0 & 1 \\ f(t) & 0 \end{pmatrix} = \begin{pmatrix} 0 & 1 \\ 0 & 0 \end{pmatrix} + \begin{pmatrix} 0 & 0 \\ f(t) & 0 \end{pmatrix} \equiv T + V(t),$$

with

$$f(t) = \left(1 - \frac{2}{t-a}\right).$$

The exact solution for this model with the initial conditions $q(0) = -a, p(0) = 1 + a, a = -0.001$ is

$$q(t) = (t - a)e^{-t}.$$

The comparison of exact and approximation of the hydrogen ground state wave function by various scheme are exhibited in Figure 1 for $T=15, 20$ and $h=0.0002$ and $T=15, h=0.0001$, respectively.

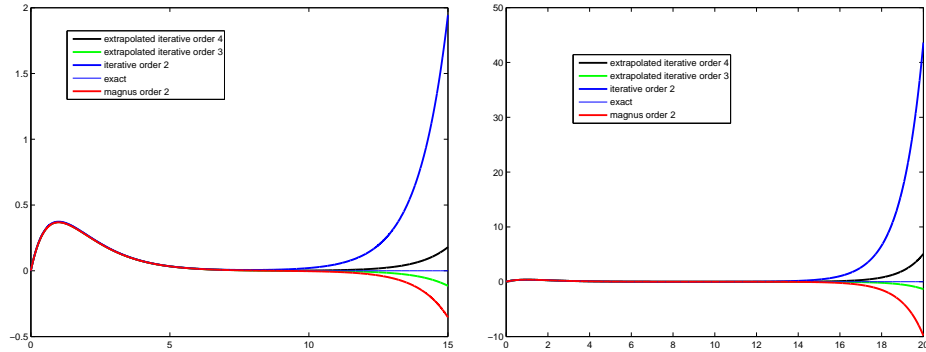


Figure 1. Comparison of exact and approximation of the hydrogen ground state wave function for various schemes (Left Figure:shorter time scale, Right Figure: longer time scale).

Remark 2. In Figure (1), the comparisons of the standard Runge-Kutta order 2, magnus order 3 and iterative method of orders 2,3 with exact solution are exhibited. As can be seen in this figure, standard method does not work for the long time.

Finally, we compare the third order time dependent iterative scheme with third order Crouch-Grossman given as

$$\begin{aligned} A_1 &= A(t_n, y_n); \\ A_2 &= A\left(t_n + \frac{3}{4}h, \exp\left(\frac{3}{4}hA_1\right)y_n\right); \\ A_3 &= A\left(t_n + \frac{3}{4}h, \exp\left(\frac{1}{108}hA_2\right)\exp\left(\frac{119}{216}hA_1\right)y_n\right); \end{aligned}$$

$$y_{n+1} = \exp\left(\frac{13}{51}hA_3\right) \exp\left(-\frac{2}{3}hA_2\right) \exp\left(\frac{24}{17}hA_1\right) y_n$$

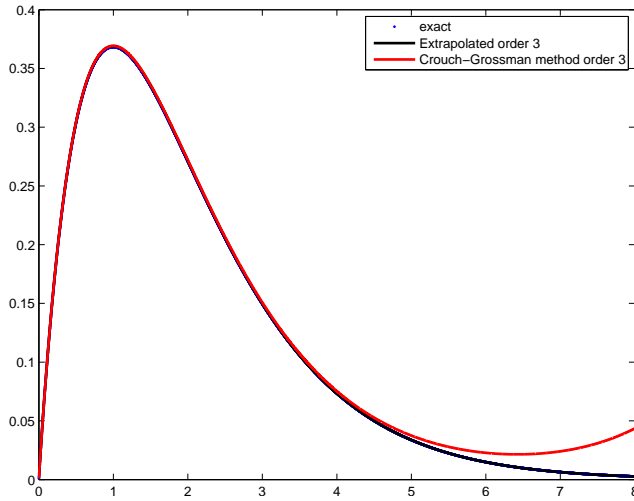


Figure 2. Comparison of exact and approximation of the hydrogen ground state wave function for various schemes for small time step $h=0.0002$.

Table 1. Comparison of errors for $h = 0.001$ on $[0, 5]$ interval with various methods

	err_{L_∞}	err_{L_1}
* Iterative order 2	0.0039	0.0106
Runge-Kutta order 2	0.0198	0.0579
* Extrapolated iterative order 3	0.0012	0.0033
Crouch-Grossman method order 3	0.0038	0.0113

Remark 3. The numerical results show that our higher order treatment gives a better long time behavior than the standard Magnus expansion. We can achieve higher order results and reduce computational time. The implementation of the approximation methods are more simpler. Cheap numerical integration schemes can beat the delicate timeintensive computation of commutators which are used in Magnus expansions.

Table 2. Comparison of errors for $h = 0.002$ on $[0, 5]$ interval with various methods

	err_{L_∞}	err_{L_1}
* Iterative order 2	0.0086	0.0230
Runge-Kutta order 2	0.0396	0.1141
* Extrapolated iterative order 3	0.0023	0.0064
Crouch-Grossman method order 3	0.0075	0.0223

Table 3. Comparison of errors for $h = 0.001$ on $[0, 6]$ interval with various method

	err_{L_∞}	err_{L_1}
* Iterative order 2	0.0039	0.0109
Runge-Kutta order 2	0.0417	0.1090
* Extrapolated iterative order 3	0.0012	0.0034
Crouch-Grossman method order 3	0.0079	0.0210

5 CONCLUSIONS AND DISCUSSIONS

In this work, we have presented application to successive approximations that are related to iterative splitting schemes. We presented iterative splitting methods of higher accuracy as known standard schemes. In the error analysis we discuss the benefit of the proofs which can be extended to time-dependent cases. By the numerical approximation and choice of the time-dependent operator we have seen benefits in their computational time. Higher order results can also be achieved with at least 2 or 3 iterative steps, which beat standard 3rd and 4th order methods.

References

1. S. Blanes, P.C. Moan, Fourth- and sixth-order commutator free Magnus integrators for linear and nonlinear dynamical systems, *Appl. Numer. Math.* **56** (2006) 1519-1537.
2. S. Blanes, P.C. Moan, Splitting Methods for Non-autonomous Hamiltonian Equations, *J. of Comp. Phys.* **170**(2001) 205-230.
3. S. Blanes, F. Casas, J.A. Oteo, J. Ros, The Magnus expansion and some of its applications, arXiv.org:0810.5488 (2008).
4. K.-J. Engel, R. Nagel, *One-Parameter Semigroups for Linear Evolution Equations*, Springer, New York, 2000.
5. E. Forest, R. D. Ruth, *4th-order symplectic integration*. *Physica D* **43**(105) (1990).
6. J. Geiser, Higher order splitting methods for differential equations: Theory and applications of a fourth order method. Numerical Mathematics: Theory, Methods and Applications, *Global Science Press*, Hong Kong, China, accepted, April 2008.
7. J. Geiser, Consistency of Iterative Operator-Splitting Method: Theory and Applications, *NMPDE*, published online, 2009,
<http://www3.interscience.wiley.com/journal/107630294/issue>. 2008.

Table 4. Comparison of errors for $h = 0.001$ on $[0, 8]$ interval with various method

	err_{L_∞}	err_{L_1}
* Iterative order 2	0.0039	0.0122
Runge-Kutta order 2	0.2156	0.4923
* Extrapolated iterative order 3	0.0012	0.0035
Crouch-Grossman method order 3	0.0409	0.0937

8. J. Geiser, Iterative operator-splitting methods for nonlinear differential equations and applications, *NMPDE*, accepted November 2009.
9. J. Geiser, S. Chin, Multi-product expansion, Suzuki's method and the Magnus integrator for solving time-dependent problems, Preprint 2009-4, Humboldt University of Berlin, Department of Mathematics, Germany, 2009, submitted to IMA.
10. A. Pazy, *Semigroups of Linear Operators and Applications to Partial Differential Equations*, Appl. Math. Sci. **44**, Springer, Berlin, 1983.

NONISOTHERMAL OSCILLATORY COUETTE GAS FLOW

PETER GOSPODINOV, VLADIMIR ROUSSINOV, and STEFAN STEFANOV

Institute of Mechanics, Bulgarian Academy of Sciences,
Acad. G. Bonchev Str., bl. 4, 1113 Sofia, Bulgaria,
{png,vladimir,stefanov}@imbm.bas.bg

Abstract. The oscillatory Couette flow between a stationary inner cylinder and an oscillating outer cylinder is numerically investigated. The continuous model is based on the Navier-Stokes equations for compressible fluid, completed with the equations of continuity and energy transport. Two types of velocity boundary conditions for the outer cylinder are used – harmonic oscillations and stepwise oscillations. Results for the two types of boundary conditions in the energy transfer equation for the inner cylinder wall are also considered. The first one corresponds to a constant wall temperature and the second one – to an adiabatically isolated inner cylinder. Thus, the capabilities of the model and the numerical solution are extended to some important practical cases. Calculated results for density, velocity, pressure and temperature distribution are presented. Circular frequencies in some interesting cases are analyzed.

1 INTRODUCTION

The study of Couette flow is an important part of MEMS modeling. As a fundamental problem of rarefied gas dynamics, it has been investigated by Cercignani et al. [1]. Neitzel [2] studied the finite-amplitude stability of a viscous incompressible fluid in the space between a pair of concentric cylinders, treating oscillatory shear-driven gas flows in transition and free-molecular-flow regimes. Analytical results valid for slip flow and an early transition regime were found using a recently proposed rigorous second-order slip model with no adjustable coefficients [6]. Manela et al, [9] considered the linear temporal stability of a Couette flow of a Maxwell gas using the Navier-Stokes equations. Park et al.[5] presented a thorough study of oscillatory Couette flows between two parallel smooth walls, using DSMC solutions. The non-planar effects in an oscillatory cylindrical gas flow are studied in [10], where a continuum viscous flow model and

M. Koleva and L. Vulkov (Eds.), Proceedings of the Fifth Conference on Finite Difference Methods: Theory and Applications (FDM: T&A 2010) 2011, pp. 68–77.
© Rousse University Press 2011

the direct simulation Monte Carlo method were used to predict the velocity and shear stress profiles within the whole range of Knudsen number. The linear temporal stability was analyzed in [8, 11] using DSMC. A steady state one-dimensional flow, examined on the basis of a nonlinear BGK model with Maxwell diffusive boundary conditions, was presented by Midaniis et al. [12]. The compressible Taylor-Couette flow between concentric cylinders, has been computed using a DSMC method and a pseudo-spectral/finite difference method in [7]. The cylindrical Couette flow of a rarefied gas between two cylinders in the generalized setup in which the inner cylinder not only rotates but also slides along its axis, The analysis is based on the numerical solution of the S-model kinetic equation [13]. Microscale gas flows between two rotating coaxial circular cylinders of infinite length with different temperatures are investigated by Taheri et al. [14], where Navier-Stokes-Fourier (NSF) and regularized 13-moment equations in their linear form are used to independently analyze velocity and temperature fields in shear-driven rotary flows, i.e., cylindrical Couette flows. A set of second-order boundary conditions for velocity slip and temperature jump are derived for the NSF system.

In the present paper we investigate numerically the continuum model of nonisothermal Couette gas flow in slip regime by a numerical solution of the continuum Navier-Stokes equations for compressible flow.

2 CONTINUOUS MODEL AND NUMERICAL SIMULATION

We study a rarefied gas flow between two coaxial cylinders (one dimensional, axis-symmetrical problem). The inner cylinder has radius R_1 , wall temperature T_1 and peripheral velocity v_1 , the outer - R_2 , T_2 and v_2 respectively.

The continuous model is based on the Navier-Stokes equations for compressible fluid, completed with the equations of continuity and energy transport. The governing equations, when neglecting the gravity, are written as follows:

$$\frac{\partial \rho}{\partial t} + \operatorname{div}(\rho V) = 0, \quad (1)$$

$$\rho \left(\frac{\partial u}{\partial t} + u \frac{\partial u}{\partial r} - \frac{v^2}{r} \right) = -\frac{\partial P}{\partial r} - \frac{1}{r} \frac{\partial}{\partial r} (r \tau_{rr}) + \frac{\tau_{\varphi\varphi}}{r}, \quad (2)$$

$$\rho \left(\frac{\partial v}{\partial t} + u \frac{\partial v}{\partial r} + \frac{uv}{r} \right) = -\frac{1}{r^2} \frac{\partial}{\partial r} (r^2 \tau_{r\varphi}), \quad (3)$$

$$\rho c_P \frac{DT}{Dt} = \operatorname{div}(\lambda \operatorname{grad} T) - P \operatorname{div} V + \mu \Phi, \quad (4)$$

$$P = \rho R T, \quad (5)$$

where V is the velocity vector, u and v are the velocity components along axis r and φ . A rather standard notation is used in Eqs. (1)-(2): P is the pressure, ρ is the density and T is the temperature. ρ , P , T , $u, v = f(r, t)$. $\tau_{i,j}$ are the stress tensor components and Φ is the dissipation function [4]. For a perfect monatomic gas, the viscosity and the heat transfer coefficient read as [3]:

$$\mu = \mu(T) = C_\mu \rho_0 l_0 V_0 \sqrt{T}, \quad C_\mu = \frac{5}{16} \sqrt{\pi} \quad (6)$$

$$\lambda = \lambda(T) = C_\lambda \rho_0 l_0 V_0 \sqrt{T}, \quad C_\lambda = \frac{15}{32} \sqrt{\pi} \quad (7)$$

The above written equations are normalized by using the following scales: for density, $\rho_0 = mn_0$ (m – is the molecular mass, n_0 -the average number density), for velocity $V_0 = \sqrt{2RT_0}$ - R is the gas constant, for length - the distance between the cylinders $L = R_2 - R_1$, for time $t_0 = L/V_0$, for temperature T_0 - the wall temperature of both cylinders i.e. $T_i = T_0$, $i = 1, 2$. The Knudsen number is $\text{Kn} = l_0/L$, where the mean free path is l_0 and $\gamma = c_P/c_V = 5/3$ (c_P and c_V are the heat capacities at constant pressure and constant volume respectively). In this way in the dimensionless model the characteristic number Kn and the constants C_μ and C_λ take part. After the scaling, the same symbols for the dimensionless ρ , P , T , u, v and R_i, T_i , $i = 1, 2$ are used.

For the problem (1)-(5) first-order slip boundary conditions are imposed at both walls, which can be written directly in dimensionless form as follows [3, ?]:

$$v \mp 1.1466 \text{Kn} \left(\frac{\partial v}{\partial r} - \frac{v}{r} \right) = \bar{V}_i(t), \quad (8)$$

$$u = 0, \quad (9)$$

$$T \pm 2.1904 \text{Kn} \frac{\partial T}{\partial r} = \bar{T}_i, \quad (10)$$

at $r = R_i$,

Two types velocity boundary conditions for the outer cylinder are used, when the inner cylinder is at rest (i.e. $V_1 = 0$).

– harmonic oscillations:

$$\bar{V}_2 = V_2 + \Delta V_2 \sin(\bar{\omega}t), \quad (11)$$

where the dimensionless circular frequency $\bar{\omega}$ is scaled to $(L/V_0)^{-1}$.

-stepwise oscillations

$$\bar{V}_2 = \begin{cases} V_2 + \Delta V_2, & 0 + 2k\pi \leq \bar{\omega}t \leq 2k\pi + \pi \\ V_2 - \Delta V_2, & 2k\pi + \pi \leq \bar{\omega}t \leq (2k+1)\pi \end{cases}, \quad (12)$$

where $k = 1, 2, 3, \dots$, t_{PER} is the dimensionless period of the oscillations:

$$t_{PER} = 2\pi/\bar{\omega}. \quad (13)$$

In (11)-(13) V_2 is the dimensionless mean wall velocity and ΔV_2 - hers amplitude.

In the boundary velocity condition (12) are included the cases of suddenly started" and "suddenly stopped" outer cylinder.

Let introduce the Stokes number [5, 10]:

$\beta = \sqrt{\frac{\omega L^2}{\nu}}$, where ν is the kinematic viscosity and ω – the dimensional circular frequency. Then using Eq.(6) the following relation between dimensionless frequency $\bar{\omega}$ and Stokes number β can be written.

$$\bar{\omega} = C_\mu \text{Kn} \beta^2. \quad (14)$$

The equations of transfer (1)-(5), together with the boundary conditions (8)-(12) and zero initial distributions for u , v and T , formulate the initial non-steady boundary-value problem. A second order of approximation, implicit difference scheme to solve numerically the formulated problem is used [15]. Starting from the inner cylinder wall M grid knots are introduced along the coordinate r . Thus, the difference value problem, for a given time t , is reduced to the solution of 4 linearized systems of M algebraic equations. The obtained algebraic system has a diagonal and weakly filled matrix. An appropriate optimized sparse linear system solver from IMSL Fortran library is applied for solution of the algebraic system. Due to the problem non-linearity, additionally an internal iteration process is used.

3 NUMERICAL RESULTS

The results presented in this section are computed for $R_1 = 1$, $R_2 = 2$ and $\text{Kn}=0.1$. This value of Knudsen number is close to the upper limit for the slip-flow regime [5, 6].

On Fig-1-3 are presented density, tangential velocity and gas temperature depending on dimensionless coordinate r and dimensionless time t . With a) are denoted the results obtained for harmonic outer cylinder oscillations according to (11), with b) – results for stepwise outer cylinder

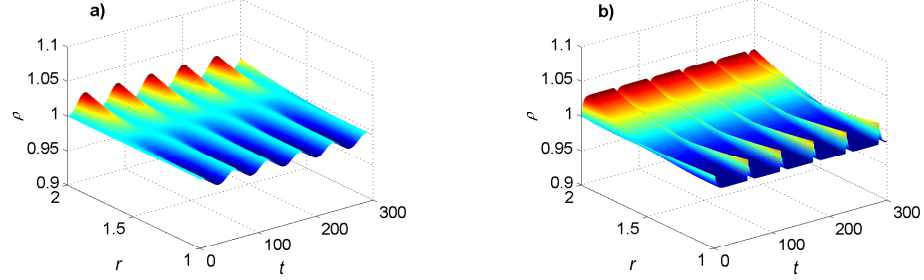


Figure 1. Density variation in (r, t) coordinates – comparison between harmonic and stepwise outer cylinder oscillating, $\text{Kn} = 0.1$, $V_1 = 0$, $V_2 = 0$, $\Delta V_2 = 0.3$ and $\beta = 1$.

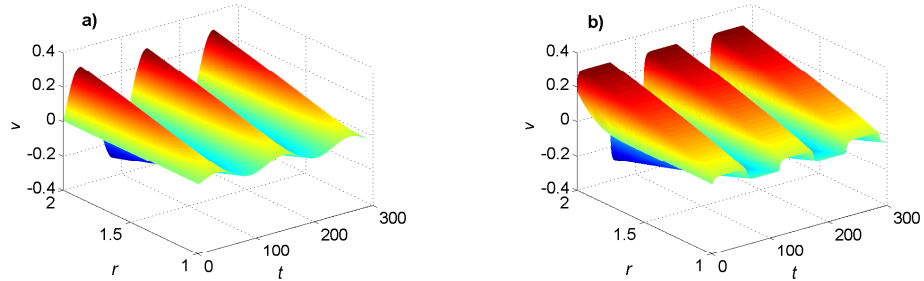


Figure 2. Velocity variation in (r, t) coordinates – comparison between harmonic and stepwise outer cylinder oscillating. $\text{Kn} = 0.1$, $V_1 = 0$, $V_2 = 0$, $\Delta V_2 = 0.3$ and $\beta = 1$.

oscillations according to (12). In both cases $V_2 = 0$, $\Delta V_2 = 0.3$, $r = R_2$, $\bar{\omega} = 0.0554$ and $\beta = 1$. As shown on the above mentioned figures, the stepwise oscillations generate more kinetic energy. This yields more significant gas heating and significant oscillations of gas density. Fig. 4, Fig. 5 and Fig. 6 show the variation in time of gas velocity, temperature and pressure at the wall of the outer cylinder. Regardless of the oscillation type, the basic circular frequency of temperature variation is twice larger than the velocity frequency –Fig.4 and Fig.5. Consider a period when wall velocity changes its sign. Then, two positive impulses are introduced into gas enthalpy, being proportional to the square of wall velocity. The impulses generated under outer cylinder stepwise oscillations have larger values. Hence, temperature field variation is more considerable and its frequency analysis proves the occurrence of additional frequencies which are divisible by (Fig.5b).

Consider real MEMS. Then, to realize boundary condition (10) at the inner cylinder wall proves more difficult than the realization of a condition

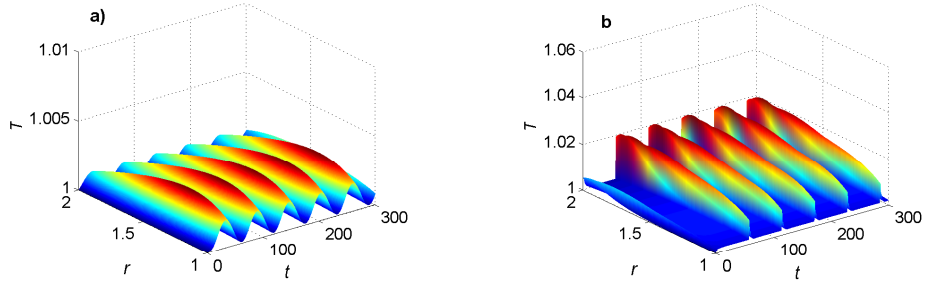


Figure 3. Temperature distribution in (r, t) coordinates – comparison between harmonic and stepwise outer cylinder oscillating. $\text{Kn} = 0.1$, $V_1 = 0$, $V_2 = 0$, $\Delta V_2 = 0.3$ and $\beta = 1$.

of an adiabatically isolated cylinder, i.e.

$$\frac{\partial T}{\partial r} = 0, \quad r = R_1 \quad (15)$$

The tangential velocity boundary condition (12) allows investigating the cases of suddenly started or suddenly stopped, rotating outer cylinder. The results in Fig.7, Fig. 8 and Fig.9 are found for $V_2 = 0.15$, $\Delta V_2 = 0.15$, $\beta = 2$. Two types of boundary conditions (10) and (15) at the wall of the inner cylinder are used to derive the energy equation. They are denoted by a) and b), respectively.

Fig.7 a) and b) shows gas velocity profile at the wall of the outer cylinder. Within the range of dimensionless time $8 \leq t \leq t_{per}$, velocity profile can be taken as illustrating the variation of gas velocity at the wall of the outer cylinder, which rotates with constant velocity and is suddenly stopped at moment $t = t_{per}/2$, and for $t_{per}/2 \leq t \leq t_{per}$, the outer cylinder is suddenly started. ($t_{per} = 28.36$)

Fig.8 plots the distribution of gas temperature at the wall of the inner cylinder, while Fig.9 - gas temperature as a function of coordinates r and t . (Once again note that a) in Fig.7, 8 and Fig. 9 denotes the results for constant temperature of the inner cylinder, and b) – those for an adiabatically isolated cylinder.) Considering an adiabatically isolated wall, the mean value of gas temperature is significantly larger and it varies within wider ranges..

4 CONCLUSIONS

The proposed continual model allows the study of oscillatory Couette flows under different conditions. The possibility of prescribing two types

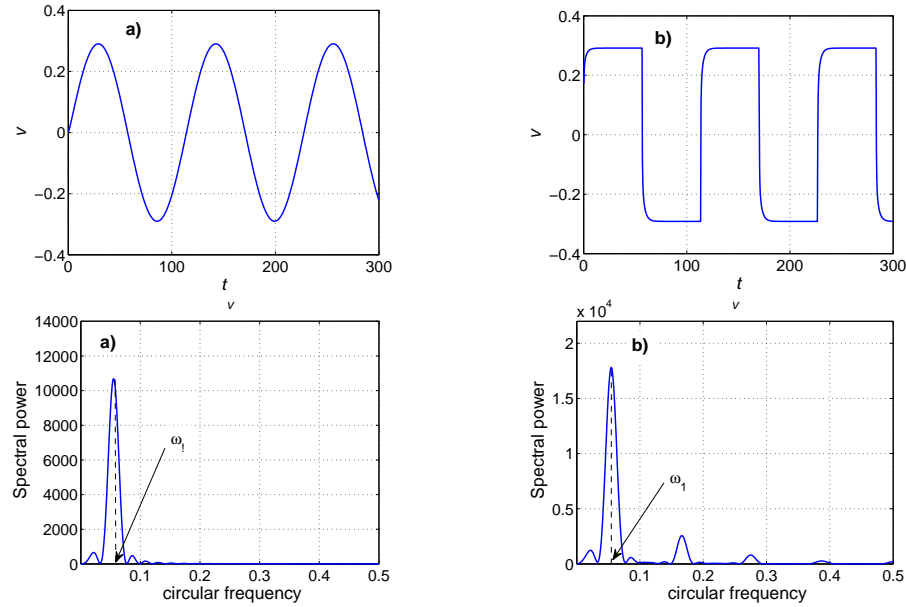


Figure 4. Gas velocity at the outer cylinder wall and frequency analysis at $r = R_2$ – comparison between harmonic and stepwise outer cylinder oscillating, a) $\omega_1 = 0.0554$ (forced frequency), b) $\omega_1 = 0.0554$

of oscillation of the outer cylinder, as well as two types of conditions of energy transfer at the wall of the inner cylinder enables one to analyze a number of interesting cases for a known Knudsen number. We will further compare our results to those found using DSMC in order to specify the limits of applicability (validity) of the continual model.

ACKNOWLEDGMENTS

The research leading to these results has received funding from the European Community's Seventh Framework Programme FP7/2007-2013 under grant agreement ITN GASMEMS - No 215504 and from the NSF of Bulgaria under Grant No DID 02/20-2009

References

1. C. Cercignani, F. Sernagiotto, Cylindrical Couette Flow of a Rarefied Gas, *Physics of Fluids* **10**(1200), 1967.
2. G. P. Neitzel Stability of circular Couette flow with variable inner cylinder speed, *Journal of Fluid Mechanics* **123** (1982) 43-57.

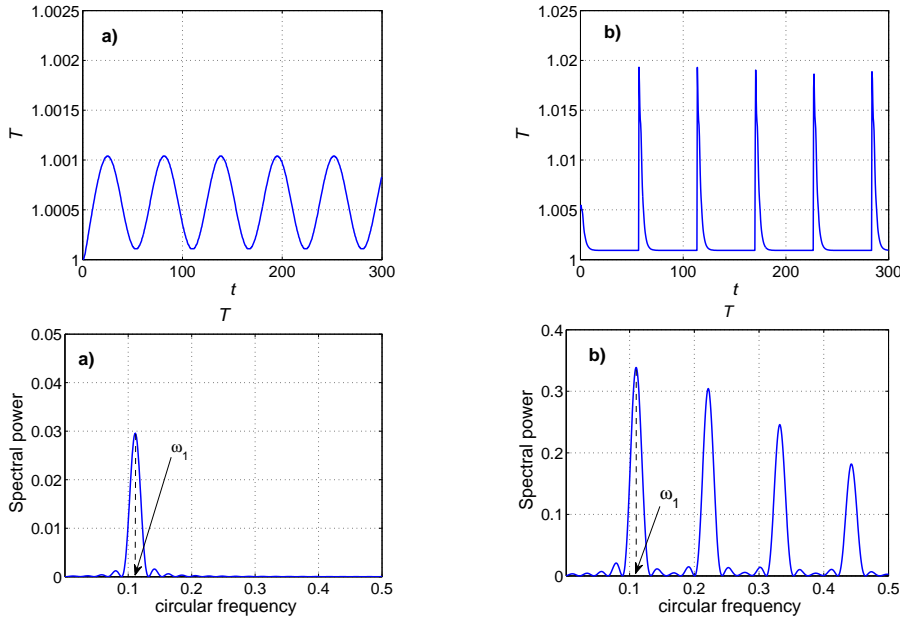


Figure 5. Gas temperature at the outer cylinder wall and frequency analysis at $r = R_2$ – comparison between harmonic and stepwise outer cylinder oscillating, a) $\omega_1 = 0.1108$, b) $\omega_1 = 0.1108$

3. S. Stefanov, P. Gospodinov and C. Cercignani, Monte Carlo Simulation and Navier-Stokes finite difference calculation of unsteady-state rarefied gas flows, *Physics of Fluids* **10**(1) (1998) 289-300.
4. R. B. Bird, W. E. Stewart and E. N. Lightfoot, "Transport Phenomena", 2nd edition, John Wiley, New York, 2002
5. J.H. Park, P. Bahukudumbi and A. Beskok, "Rarefaction effects on shear driven oscillatory gas flows: A DSMC study in the entire Knudsen regime," *Phys. Fluids* **16** (2004) 317.
6. N. G. Hadjiconstantinou, Oscillatory shear-driven gas flows in the transition and free-molecular-flow regimes *Phys. Fluids* **17** (2005) 100611.
7. B. Larignon, K. Marr, D. B. Goldstein D.B., Monte Carlo and Navier-Stokes Simulations of Compressible, Taylor-Couette Flow. *J. Thermophys* **20**(4) (2006) 544-551.
8. H. Yoshida, K. Aoki, Linear stability of the cylindrical Couette flow of a rarefied gas, *Phys. Rev. E* **73** (2006) 021201.
9. A. Manela, I. Frankel, On the compressible Taylor–Couette problem, *J. Fluid Mech.* **588** (2007) 59–74.
10. D. R. Emerson, Xiao-Jun Gu, S. K. Stefanov, S. Yuhong, R. W. Barber, Nonplanar oscillatory shear flow: From the continuum to the free-molecular regime, *Phys. Fluids* **19** (2007) 107105.
11. M. Malik, J. Dey, M. Alam, Linear stability, transient energy growth, and the role of viscosity stratification in compressible plane Couette flow, *Phys. Rev. E* **77**

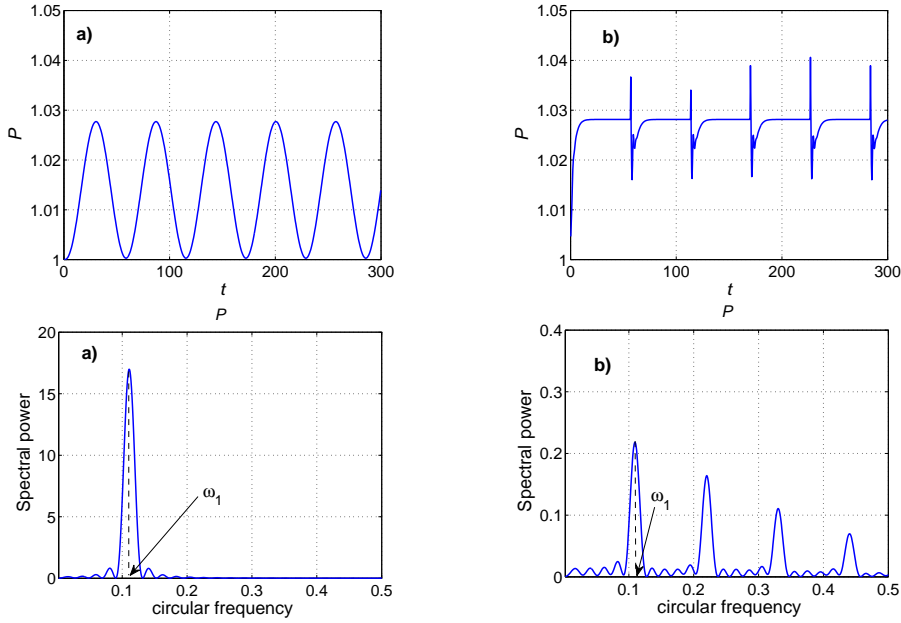


Figure 6. Pressure variation at the outer cylinder wall and frequency analysis at $r = R_2$ – comparison between harmonic and stepwise outer cylinder oscillating, a) $\omega_1 = 0.1108$, b) $\omega_1 = 0.1108$

(2008) 036322.

12. S. Midaniis, D. Valougeorgis, Couette flow with heat transfer in the whole range of the Knudsen number, *Proc. Of the Sixth Int. ASME Conf. of Nanochannels, Microchannels and Minichannels*, ICNMM2008, June 23-25, Darmstadt, Germany (2008) 1-8.
13. E. M. Shakhov, V. A. Titarev, Numerical study of the generalized cylindrical Couette flow of rarefied gas, *European Journal of Mechanics B/Fluids*, **28** (2009) 152–169.
14. P. Taheri, H. Struchtrup, Effects of rarefaction in microflows between coaxial cylinders, *Phys. Rev. E* **80** (2009) 066317.
15. P. Gospodinov, D. Dankov, V. Roussinov, S. Stefanov, Modeling of cylindrical Couette flow of rarefied gas. The case of rotating outer cylinder, *First Conference of the Euro-American Consortium for Promoting the Application of Mathematics in Technical and Natural Sciences*, Sozopol, Bulgaria, AIP Conf. Proc. **1186** (2009) 200-205.

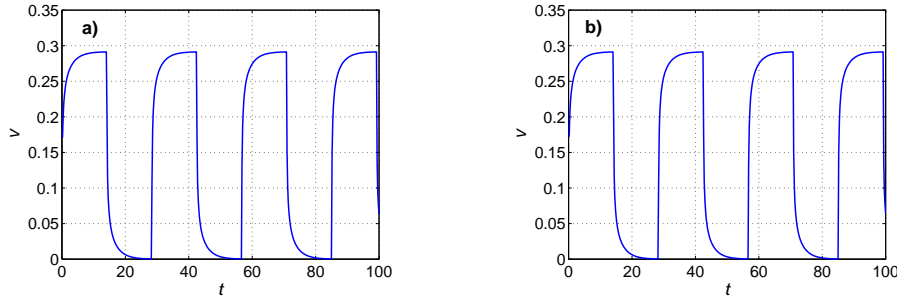


Figure 7. Gas velocity distribution at the outer cylinder wall $r = R_2$ for stepwise oscillations of the outer cylinder - a) constant wall temperature, b) adiabatically isolated inner cylinder

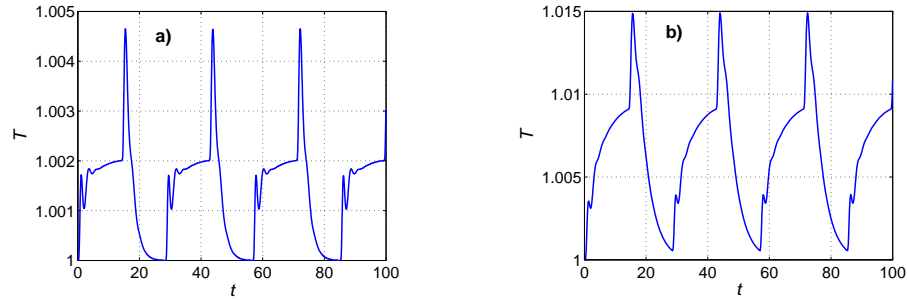


Figure 8. Gas temperature variation at the inner cylinder wall (stepwise oscillations of the outer cylinder) , $r = R_1$ - a) constant wall temperature b) adiabatically isolated inner cylinder

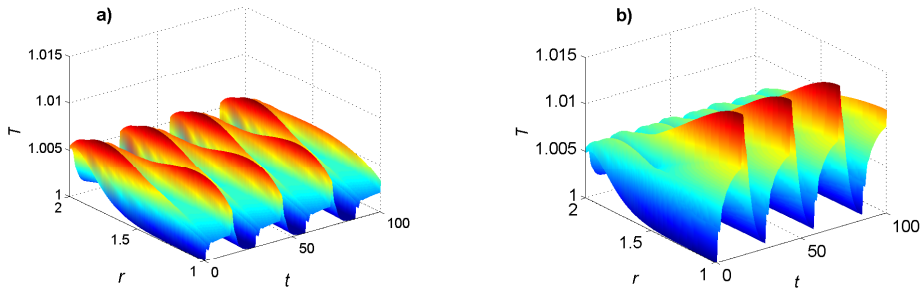


Figure 9. Gas temperature variations in (r,t) coordinates – stepwise oscillations of the outer cylinder, a) inner cylinder with constant wall temperature b) adiabatic isolated inner cylinder $\text{Kn} = 0.1$, $V_2 = 0.15$, $\Delta V_2 = 0.15$, $\beta = 2$

INVESTIGATION OF A PROTON EXCHANGE MEMBRANE FUEL CELL MODEL BY PARAMETER FITTING

ÁGNES HAVASI¹, RÓBERT HORVÁTH², ÁKOS NEMES¹, AND TAMÁS SZABÓ¹

¹ Eötvös Loránd University, Pázmány P. s. 1, H-1117 Budapest, Hungary

² Budapest University of Technology and Economics, Egry J. u. 1, H-1111, Budapest, Hungary

Abstract. The functioning and the achievable power of a proton exchange membrane fuel cell (PEMFC) are determined by several parameters simultaneously. Part of these cannot be measured directly, and can only be calculated from approximate formulas. In our model of a PEMFC cathode these parameters include the effective conductivity of the solution phase, the exchange current density of the cathode and the limiting current of the cathode. Our aim is to study the real values of these parameters and their behavior as a function of the cell conditions. To this aim the unknown parameters are determined by fitting the model results to measurements.

For the solution of the parameter fitting problem we use the minimization method of Levenberg and Marquardt, which is a combination of the well-known Newton and steepest descent methods. During the measurements, the current density is measured as a function of the cell potential. We investigate the behavior of the obtained parameters as a function of temperature, pressure and Nafion content.

1 INTRODUCTION

A fuel cell is an electrochemical conversion device [8, 9]. It produces electricity from fuel (e.g., hydrogen) on the negative electrode and an oxidant (e.g., oxygen) on the positive electrode, which react in the presence of an electrolyte (e.g., Nafion). In the archetypal hydrogen-oxygen proton exchange membrane fuel cell (PEMFC), the electrolyte is a proton-conducting, electrically insulating polymer membrane. The electrons and protons of the hydrogen are separated in a catalytic reaction, and the electrons are forced to travel through a circuit, hence producing electrical power.

M. Koleva and L. Vulkov (Eds.), Proceedings of the Fifth Conference on Finite Difference Methods: Theory and Applications (FDM: T&A 2010) 2011, pp. 78–87.
© Rousse University Press 2011

It is desirable to construct fuel cells with as high as possible achievable power. To this aim it is important that we are able to model the fuel cell for different compositions of the Membrane-Electrode Assembly (MEA). In this paper we present a simplified PEMFC model [3] with an emphasis on the positive electrode (cathode) where the major losses take place. This model is based on the numerical solution of equations that describe the physics and chemistry of the cathode processes.

The model equations contain several material parameters, some of which can be measured directly, while another part of them cannot be measured after assembling the MEA. In our model there are three unknown parameters, namely, the effective conductivity of the solution phase, the exchange current density of the cathode and the limiting current of the cathode. There exist formulas for the calculation of these parameters, however, they are rather crude, and they do not describe their dependence on the cell conditions. Our aim is to investigate the real values of the above parameters and their behavior against temperature, pressure and Nafion content. To this aim we set the three parameters in such a way that the numerical solution, obtained by our model, is as close to the measurements as possible. For the solution of this problem we use the Levenberg–Marquardt method, which is a clever combination of the well-known Newton and steepest descent methods.

The structure of the paper is as follows. In Section 2 the PEMFC model and the parameters used in the model are introduced. Then we present the parameter estimation problem, and introduce the Levenberg–Marquardt method for its solution. Finally, the results of the parameter fittings are discussed and the dependence of the studied parameters on temperature, pressure and Nafion content is investigated.

2 THE PEMFC MODEL

The fuel cell model applied is based on Litster's potential summation algorithm [6] and Kulikovsky's diffusion kinetic approximation [4] and the Weber membrane conductivity model [10]. Additionally, the double layer capacity is taken into account to simulate the time-dependent (transient) curves as well. The cell potential according to Litster can be calculated from the equation

$$E_{\text{cell}}(t) = E_{\text{OC}}(t) - V^*(t) - \eta^a(t) - \frac{W_{\text{mem}}}{\kappa_{\text{mem}}} I(t), \quad (1)$$

where E_{OC} is the open circuit potential, V^* is the potential loss at the cathode, W_{mem} is the thickness of the membrane, κ_{mem} is the membrane

conductivity and η^a is the potential loss at the anode, which is the solution of the equation

$$I(t) = i_0^a \left[\exp \left(\frac{\alpha_a^a F}{RT} \eta^a \right) - \exp \left(-\frac{\alpha_c^a F}{RT} \eta^a \right) \right]. \quad (2)$$

(The description and the units of the parameters used in the model are given in Table 1.) Our aim is to calculate the cell potential as a function of the load current. The potential loss at the cathode is $V^*(t) = \phi_1(t, L) - \phi_2(t, 0)$. If we choose $\phi_2(t, 0) = 0$, then by definition of the overpotential we obtain

$$V^*(t) = \phi_1(t, L) = \eta(t, L) + \phi_2(t, L), \quad (3)$$

where

$$\phi_2(t, L) = \phi_2(t, 0) + \int_0^L \left(-\frac{\sigma_{\text{eff}}}{\kappa_{\text{eff}} + \sigma_{\text{eff}}} \partial_s \eta(t, s) + \frac{1}{\kappa_{\text{eff}} + \sigma_{\text{eff}}} I(t) \right) ds. \quad (4)$$

Here the overpotential η of the cathode is computed from the solution $u(t, x)$ of the basic cathode equation

$$\begin{aligned} \partial_t u(t, x) &= \partial_x S(x) \frac{1}{aC_{\text{dl}}} (-I(t) \frac{1}{K} + \sigma_{\text{eff}} \partial_x u(t, x)) \\ &\quad + \frac{S(x)}{aC_{\text{dl}}} \partial_x (\sigma_{\text{eff}} \partial_x u(t, x)) - \frac{i_0}{C_{\text{dl}} K} g(u(t, x)). \end{aligned} \quad (5)$$

The function u is related to η by the transformation $u(t, x) = \eta(t, x)/K$ with $K = RT/(\alpha F)$, and usually depends on space and time. The notation $S(x)$ stands for the expression $S(x) = \kappa_{\text{eff}}/(\kappa_{\text{eff}} + \sigma_{\text{eff}})$. Equation (5) is supplemented with an initial condition

$$u(0, x) = 0, \quad x \in (0, L) \quad (6)$$

where L is the thickness of the cathode, and the Neumann type boundary condition

$$\partial_x u(t, L) = \frac{1}{\sigma_{\text{eff}}(L) K} I(t), \quad t \in (0, T). \quad (7)$$

The function g on the right-hand side of (5) describes the kinetics of the oxygen reduction reaction. In our case diffusion kinetics was used, where

$$g(u(t, x)) = \frac{j_D \exp(u(t, x))}{i_0 \exp(u(t, x)) + j_D} - \frac{j_D \exp(-u(t, x))}{i_0 \exp(-u(t, x)) + j_D}. \quad (8)$$

The above initial-boundary value problem is solved numerically, by using an implicit-explicit Euler method. The method is explicit in the source

Table 1. The parameters in the PEMFC model.

Symbol	Description	Unit
$a(x)$	Specific interfacial area	cm^{-1}
$C_{\text{dl}}(x)$	Double-layer capacitance	F/cm^2
$E_{\text{cell}}(t)$	Cell potential	V
E_{OC}	Open circuit potential	V
F	Faraday constant (96487)	C/mol
$I(t)$	Total cell current density	A/cm^2
$i_0(x)$	Exchange current density at the cathode	A/cm^2
i_0^a	Exchange current density at the anode	A/cm^2
$j_D(x)$	Limiting current at the cathode	A/cm^2
L	Thickness of the cathode	cm
R	Universal gas constant (8.3144)	J/molK
T	Cell temperature	K
$V^*(t)$	Potential loss at the cathode	V
W_{mem}	Membrane thickness	cm
α	Transfer coefficient in the cathode	
α_a^a	Anodic transfer coefficient at the anode	
α_c^a	Cathodic transfer coefficient at the anode	
$\eta(t, x)$	Overpotential at the cathode	V
$\eta^a(t)$	Overpotential at the anode	V
$\phi_1(t, x)$	Solid phase potential	V
$\phi_2(t, x)$	Solution phase potential	V
$\kappa_{\text{eff}}(x)$	Effective solution phase conductivity	S/cm
$\sigma_{\text{eff}}(x)$	Effective solid phase conductivity	S/cm
κ_{mem}	Membrane conductivity	S/cm

term, so iterations for solving nonlinear problems can be avoided. At the same time, the spatial derivative is approximated using an implicit scheme, which maintains the stability of the time stepping. This approach provides a good balance between accuracy and relatively low computational costs. The method was enhanced with Richardson extrapolation to accelerate the convergence. The Newton–Raphson method is used for solving Eq. (2) of the anode [1].

3 THE PARAMETER ESTIMATION PROBLEM

In the PEMFC model, introduced in the previous section, little is known about the following parameters:

- κ_{eff} - the effective conductivity of the solution phase;
- j_D - the limiting current at the cathode, involved by the function g on the right-hand side of (5) in case of diffusion kinetics (see (8));
- i_0 - the exchange current density of the cathode.

In [3], the following values, calculated on the base of [4] and [6], are given: $\kappa_{\text{eff}} = 0.0202 \text{ Scm}^{-1}$, $j_D = 1.05 \text{ Acm}^{-2}$ and $i_0 = 7.22 \cdot 10^{-8} \text{ Acm}^{-2}$. These values can only be considered as rough estimations, since they have been calculated from simplified formulas and for given cell conditions. The dependence of these parameters on the cell conditions (such as temperature, pressure and Nafion content) are not given by these formulas. Our aim is to specify the same parameters in another way, where measurements, taken under different conditions and our numerical model are applied together. We consider the stationary case, i.e., we assume that the quantities in the equation do not depend on time. During the measurements, the cell potential E_{cell} , derived from the unknown function u , is measured for different constant values of the current density I . The three parameters are to be set such that the $E_{\text{cell}} - I$ curve calculated by the model best fits the measured $E_{\text{cell}} - I$ curve.

The mathematical formulation of the problem is as follows. Let us introduce the following notations:

- $w := [\kappa_{\text{eff}}, j_D, i_0]^T$ - the column vector of the three parameters to be estimated,
- M : the number of measurements,
- I_i : the current density in the i th measurement, $i = 1, 2, \dots, M$,
- $E_{\text{cell},i}^*$: the cell potential measured at the constant current density I_i ,
- $E_{\text{cell}}(I_i : w)$ - the cell potential calculated by the model with parameter vector w for current density I_i ,
- $r_i(w) := E_{\text{cell}}(I_i : w) - E_{\text{cell},i}^*$ - the i th remainder,
- $r(w) := [r_1(w), r_2(w), \dots, r_M(w)]^T$.

Our aim is to minimize the scalar function

$$f : \mathbb{R}^3 \rightarrow \mathbb{R}, \quad f(w) = \frac{1}{2} r^T(w) r(w) \quad (9)$$

which is called objective function, and measures the distance between the measurements and model results. So, the task is to find a minimum point of a multi-variable scalar function. This is a nonlinear optimization problem, for which the application of the Levenberg–Marquardt (LM) method is advocated in [2] for a PMEFC cathode model.

The Levenberg–Marquardt method can be generally applied to minimization problems where a local minimum point of a function $f : \mathbb{R}^n \rightarrow \mathbb{R}$ is to be found. For the objective function f , the following properties are required:

- There exists a point w^* and a positive constant δ such that $f(w^*) \leq f(w)$ for all $w \in B_\delta(w^*)$, where $B_\delta(w^*)$ denotes the open ball with radius δ centered at w^* ,
- f is sufficiently smooth,
- $\nabla f(w^*) = 0$,
- the Hessian matrix $\nabla^2 f(w^*)$ is strictly positive definite.

The Newton method is known to converge quickly to the solution of a nonlinear equation when the initial iterate is close to the minimum point. The steepest descent method shows slower convergence in the vicinity of the solution than Newton's method, however, from a distant initial iterate it can get quickly to the vicinity of the solution. The Levenberg–Marquardt method [5, 7], introducing a weighting coefficient, combines the Newton method and the steepest descent method as applied to the solution of the equation $\nabla f = 0$.

Denote by w_c the current estimation to w^* , and by w_+ the estimation obtained in the next iteration step. Let the weighting coefficient, the so-called Levenberg-Marquardt parameter, be denoted by λ . Then the LM method iterates as follows:

1. We choose a stating estimation w_c and an initial value of λ , say, $\lambda := 100$.
2. We calculate the next estimation w_+ from the formula

$$w_+ = w_c - (\nabla^2 f(w_c) + \lambda \text{diag}(\nabla^2 f(w_c)))^{-1} \nabla f(w_c). \quad (10)$$

3. If $f(w_+) \geq f(w_c)$, then we keep w_c and increase λ , e.g., by multiplying it by 10 (closer to the steepest descent method).
If $f(w_+) < f(w_c)$, then we accept the new iteration w_+ , and decrease λ , e.g., divide it by 10 (closer to the Newton method).
4. We check a stopping condition (is $\|\nabla f(w_+)\|$ or/and $\|w_+ - w_c\|$ sufficiently small). If it is fulfilled, we stop the procedure and if it is not, we go back to step 2 with $w_c = w_+$.

Now we apply the LM method in the PEMFC model. Taking into account the special form of the objective function (9), in our case the gradient vector $\nabla f(w)$ and the Hessian matrix $\nabla^2 f(w)$ can be given as follows. Denote by J the Jacobian matrix

$$J(w) = \left[\frac{\partial r_i(w)}{\partial w_j} \right]_{M \times 3}$$

of f at w . The gradient vector and the Hessian matrix can be expressed in terms of J as

$$\nabla f(w) = J^T(w)r(w) \in \mathbb{R}^3,$$

and

$$\nabla^2 f(w) = J^T(w)J(w) + \sum_{i=1}^M r_i(w)\nabla^2 r_i(w) \in \mathbb{R}^{3 \times 3}.$$

In the latter expression we omit the sum on the right-hand side, and use the approximate equality $\nabla^2 f(w) \approx J^T(w)J(w)$. Then the application of the LM method yields the iteration

$$w_+ = w_c - (J^T(w_c)J(w_c) + \lambda \text{diag}(J^T(w_c)J(w_c))^{-1}J^T(w_c)r(w_c)).$$

Here the computation of the Jacobian matrix J is crucial. In the literature [2] two basic approaches are recommended:

1. Finite difference method

The elements of J are approximated by some finite difference method, e.g., by the forward differences:

$$J_{ij} = \frac{r_i(\dots, w_{cj} + \Delta w_j, \dots) - r_i(\dots, w_{cj}, \dots)}{\Delta w_j}, \quad i = 1, \dots, M, \quad j = 1, 2, 3,$$

where Δw_j is a small increment in the current value of the j th parameter. This method is easy to apply, however, it only gives approximate elements due to the truncation error. The smaller the increment, the smaller the truncation error, however, with a decrease of Δw_j the rounding error increases.

2. Sensitivity approach

Differential equations are derived for the derivatives in J , which are then solved numerically. In principle, this method should give more exact results, however, it is rather complicated to implement. Moreover, in [2] the application of forward differences proved to be competitive with the sensitivity approach.

In the present phase of the experiments we decided to apply the first approach, i.e., approximating the elements of J by forward differences. Note that computing each element of J in this manner requires a further model run (with the modified parameters). Therefore this method is rather time-consuming.

4 PARAMETER ESTIMATION RESULTS

In the numerical experiments the current density was studied as a function of the cell potential. The measurements were done at three temperatures ($40\text{ }^{\circ}\text{C}$, $60\text{ }^{\circ}\text{C}$ and $80\text{ }^{\circ}\text{C}$) and two pressures (1 bar and 2 bar). We studied catalysts with different Nafion contents (14, 30 and 50%) in the fuel cell. The parameters κ_{eff} , j_D and i_0 were fitted to the measurements by using the Levenberg–Marquardt method. The starting values for the iteration were those obtained by manual fitting. For comparison we also show the numerical solution obtained by manual fitting.

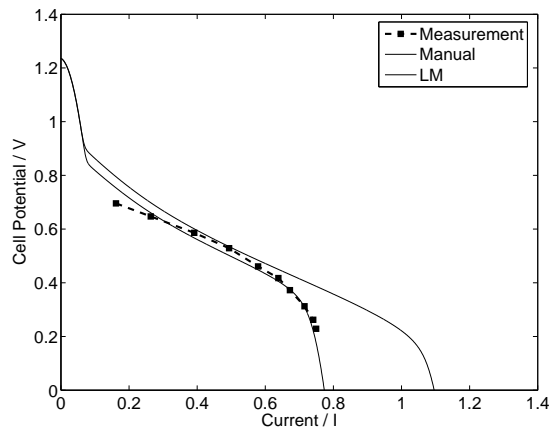


Figure 1. Cell potential versus current density obtained by parameter estimation (“LM”) and by manual fitting (“Manual”) in comparison with measurements ($80\text{ }^{\circ}\text{C}$, 1 bar, 50% Nafion content).

In Fig. 1 a typical example from the results of the fittings is given ($80\text{ }^{\circ}\text{C}$, 1 bar pressure, 50% Nafion content). The curves show the cell potential versus the current density. One can see clearly that the LM curve is much closer to the measurements than the curve obtained by manual fitting.

Since the improved parameter values gave satisfactory results in comparison with the measurements, our model is applicable for studying the dependence of the investigated parameter values on the pressure, temperature and Nafion content. Tables 2 and 3 show the results obtained for the pressures of 1 bar and 2 bar, in both cases for different temperatures and Nafion contents.

The values of all the three parameters are smallest for 30% of Nafion content.

The effective conductivity κ_{eff} is expected to be of the magnitude of $10^{-2} - 10^{-3}$. As one can see, the obtained values are in this range in most of the cases. It should be independent of pressure, however, the obtained dependence is negligible. It is promising that the trend of the changes of κ_{eff} are in accordance with the results of the manual fitting, not given here.

The values of the exchange current density J_D are everywhere in the expected interval. The manual fitting gave somewhat better results only on low pressure. For higher pressure j_D is bigger, and at 2 bar it clearly increases with temperature.

The most problematic parameter during manual fitting was the limiting current i_0 . The formula used in the numerical model is not able to describe reliably the temperature dependence of this quantity. The results obtained by parameter estimation is of the expected behavior and magnitude. Since the temperature dependence is an exponential function, therefore it seems correct that it increases more rapidly for higher temperatures. The comparison of the two tables shows that it also increases with pressure.

Table 2. The parameter values κ_{eff} [Scm^{-1}], J_D [Acm^{-1}] and i_0 [Acm^{-1}] obtained by parameter estimation for different temperatures T [$^{\circ}\text{C}$] and Nafion contents at 1 bar.

T	14% Nafion content			30% Nafion content			50% Nafion content		
	κ_{eff}	J_D	i_0	κ_{eff}	J_D	i_0	κ_{eff}	J_D	i_0
40	4.76E-3	5.12E-3	9.07E-12	3.57E-3	3.21E-3	6.13E-13	5.97E-3	5.15E-3	2.95E-11
60	4.92E+1	5.82E-3	6.65E-11	3.57E-3	4.11E-3	6.04E-12	1.98E-2	4.78E-3	3.89E-10
80	1.15E-2	4.76E-3	2.56E-8	6.88E-3	3.89E-3	2.99E-10	8.93E-2	4.60E-3	6.71E-9

Table 3. The parameter values κ_{eff} [Scm^{-1}], J_D [Acm^{-1}] and i_0 [Acm^{-1}] obtained by parameter estimation for different temperatures T [$^{\circ}\text{C}$] and Nafion contents at 2 bar.

T	14% Nafion content			30% Nafion content			50% Nafion content		
	κ_{eff}	J_D	i_0	κ_{eff}	J_D	i_0	κ_{eff}	J_D	i_0
40	6.79E-3	6.63E-3	3.93E-11	3.57E-3	3.86E-3	4.72E-12	9.63E-2	5.42E-3	3.93E-11
60	9.00E-2	7.69E-3	6.51E-10	3.71E-3	4.56E-3	6.19E-11	7.23E-1	6.43E-3	2.46E-9
80	7.94E-3	7.93E-3	1.14E-7	2.33E-3	6.06E-3	7.37E-8	5.94E-1	6.58E-3	2.01E-7

5 CONCLUSION

We used the Levenberg–Marquardt method in the model of a PEMFC cathode to obtain improved values of three critical parameters and study their behavior in different functioning conditions. These parameters included the effective conductivity of the solution phase, the exchange current density of the cathode and the limiting current of the cathode. The results of the parameter estimation were in most cases better than those obtained by manual fitting, and they were in good agreement with the expected magnitudes and the tendencies obtained by manual fitting.

Acknowledgements. The Financial support of the National Office of Research and Technology (OMFB-00121-00123/2008) is acknowledged. This work is connected to the scientific program of the "Development of quality-oriented and harmonized R+D+I strategy and functional model at BME" project. This project is supported by the New Hungary Development Plan (Project ID: TÁMOP-4.2.1/B-09/1/KMR-2010-0002). Furthermore, the European Union and the European Social Fund have provided financial support to the project under the grant agreement no. TÁMOP 4.2.1./B-09/1/KMR-2010-0003.

References

1. I. Faragó, F. Izsák, T. Szabó, Á. Kriston, A heterogeneous PEMFC model (to be submitted).
2. Q. Guo, V. A. Sethuraman, R. E. White, Parameter estimates for a PEMFC cathode, *Journal of Electrochemical Society* **151**(7) (2004) A983-A993.
3. Á. Kriston, Gy. Inzelt, I. Faragó, T. Szabó, Simulation of the transient behavior of fuel cells by using operator splitting techniques for real-time applications, *Computers and Chemical Engineering* **34** (2010) 339-348, doi:10.1016/j.compchemeng.2009.11.006
4. A. A. Kulikovsky, The voltage-current curve of a polymer electrolyte fuel cell: 'exact' and fitting equations, *Electrochemistry Communications* **4** (2002) 845-852.
5. K. Levenberg, A Method for the solution of certain non-linear problems in least squares, *The Quarterly of Applied Mathematics* **2** (1944) 164-168.
6. S. Litster, N. Djilali, Performance analysis of microstructured fuel cells for portable devices, *Electrochimica Acta* **52**(11) (2007) 3849-3862.
7. D. Marquardt, An algorithm for least-squares estimation of nonlinear parameters, *SIM Journal on Applied Mathematics* **II** (1963) 431-441.
8. J. T. Pukrushpan, A. G. Stefanopoulou, H. Peng, Control of Fuel Cell Power Systems, *Principles, Modeling, Analysis and Feedback Design*, Springer, p. 161, 2004.
9. V. R. Subramanian, S. Devan, R. E. White, An approximate solution for a pseudo-capacitor, *Journal of Power Sources* **135** (2004) 361-367.
10. A. Z. Weber, J. Newman, Transport in Polymer-Electrolyte Membranes, *Journal of the Electrochemical Society* **151** (2004) A311.

COMPARISON OF MPI IMPLEMENTATIONS MEMORY MANAGEMENT AND DATA EXCHANGE FOR SMP-NODES CLUSTERS

EVGENIYA D. KAREPOVA¹, EKATERINA V. DEMENTYEVA², AND
ANDREY V. MALYSHEV³

¹ Institute of Computational Modeling SB RAS, Akademgorodok, Krasnoyarsk,
Russia, jane@icm.krasn.ru

² Institute of Mathematics of Siberian Federal University, Krasnoyarsk, Russia,
jane@icm.krasn.ru

³ Institute of Computational Modeling SB RAS, Akademgorodok, Krasnoyarsk,
Russia, amal@icm.krasn.ru

Abstract. In this paper some problems of the effective use of cluster systems are considered as an example, paralleling an implementation of the finite element method for the numerical solution of an initial boundary value problem for the shallow water equations [1, 3, 2] is used.

When developing parallel software for this problem, we faced some difficulties caused by lack of information of efficiency of a certain method for the solution of particular problem. In this context, we have performed a study whose results are related not only to the problem itself but to a greater extent to tools for its solution. In particular, we compared efficiency of two popular implementation of the MPI standard and studied the behavior of our software when using various ways of memory allocation. Besides, we found some interesting effects which arise when measuring and estimating costs of data exchanges between computational processes.

1 PARALLEL IMPLEMENTATION

Basing on explicitly parallelizing with respect to data, we can subdivide an original computational domain into several partially overlapping sub-domains. In each subdomain calculation are performed independently of each other in the framework of a Jacobi iteration step. After each Jacobi iteration step, data adjustment in overlapping is required. There exist at least two versions of decomposition of a computational domain.

M. Koleva and L. Vulkov (Eds.), Proceedings of the Fifth Conference on Finite Difference Methods: Theory and Applications (FDM: T&A 2010) 2011, pp. 88–96.
© Rousse University Press 2011

1. *Decomposition with shadow lines.* An original domain includes mutually overlapping subdomains, width of the overlapping is defined by the stencil of a discrete scheme. Residual at the boundary points of the subdomain of the i -th process is calculated in the subdomains of neighbouring processes. Taking into account the seven-point stencil and consistent triangulation, in this case the overlapping of subdomains consisting of two layers of computational nodes will suffice. The algorithm for the calculation of residual requires to store seven coefficients of a stiffness matrix, three values of the vector of a solution at actual and previous iteration steps, and the value of a right-hand side at each boundary point of a subdomain. Hence, information storage redundancy for p processes is $56(p - 1)N_{bnd}*\text{SizeOfDouble}$ byte. Here N_{bnd} is the number of points on a cut, **SizeOfDouble** is the number of bytes for storage of a double precision variable.
2. *Decomposition without shadow lines.* An original domain is subdivided into subdomains which intersect each other only in boundaries of a cut. For each boundary point of a subdomain, residual is partially calculated only over the triangles lying in this subdomain. When exchanging data after each Jacobi iteration step, additional summation for the values of residual at boundary points of a subdomain is required.

The second way of decomposition is more efficient with respect to memory and simple in coding, however, it assumes additional arithmetic operations at each Jacobi iteration step. The number of points on a cut is small in comparison with the total number of computational points in a subdomain, hence, the time required for additional summation is insignificant, besides, it does not depend on the number of processes being used. In numerical experiments the time required for additional summation is less by three orders than that for exchange of values on a cut one point in width. Thus, the decomposition without shadow lines looks more attractive for our aims. Its advantage is obvious for unstructured grids where boundaries of subdomains are not successive sets of points.

The parallel program is implemented in the C language with the use of functions of the MPI library.

In the context of the data distribution scheme, all processes perform the same calculations but over different subdomains. The exchange structure is homogeneous except the first and the last processes. After each Jacobi iteration step, a process exchange data with all its neighbours, the

number of neighbours is defined by decomposition and does not depend on the number of processes involved in calculations.

For the numerical study of acceleration of the parallel algorithm, we consider the following model problem. Let Ω be a "square" on a sphere: $\Omega = [0, \pi/18] \times [\pi/2, \pi/2 + \pi/18]$. The boundaries of Ω are assumed to be "solid".

In the computational domain an 801×801 uniform square grid with corresponding consistent triangulation is constructed. In the numerical test 1000 time step were performed.

In Fig. 1 a version of decomposition of a computational domain into "squares" for 8 processes is shown. A numerical solution for this subdivision of a grid is presented in Fig. 2.

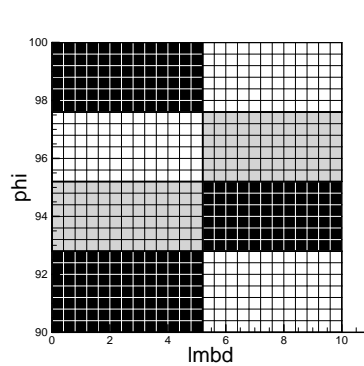


Figure 1. Decomposition of a domain into "squares"

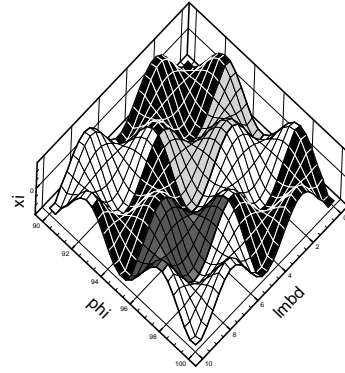


Figure 2. Results of a numerical test with 8 processes

2 COMPARISON OF TWO MPI IMPLEMENTATIONS AND OF MEMORY MANAGEMENT STRATEGIES

Memory management strategy was analyzed with the cluster system of ICM SB RUS (in-hose assembly, 48 computational nodes, 96 cores, Gigabit Ethernet interconnect, 1 Gb RAM per a node, performance for the LINPACK test is 300 GFlops). Of course, results of this comparison, which is performed for a specific problem with a specific supercomputer, may not be generalized immediately to the case of arbitrary architecture of a cluster and software. However, they are rather interesting.

In this paper, performance of two popular MPI implementation (well-known MPICH2 v.1.2.1p1 and OpenMPI v.1.4.1 being a "heritor" of the LAM package) is compared.

Two modification (with static and dynamic – *calloc - free* – memory allocation for main arrays and buffers) of the problem were tested. We immediately notice that the version with static allocation does not show considerable advantage of any package. The difference in running time and in time of data exchanges for all tested configurations turns out to be too small to be taken into account.

Conversely, the version with dynamic memory allocation shows dependence on a package being used and on its settings. In the strict sense, the studies show that the differences in the behavior of the problem are related to distinctions in dynamic memory management rather than to features of implementation of MPI functions in both packages.

In particular, in the OpenMPI package the *ptmalloc* memory manager is used for dynamic memory allocation. It is applied for fragmentation control as well as for improving performance of an application due to acceleration of operation of the *malloc/free* procedure. A setting managing an allocation/disposal memory strategy is called *mpi_leave_pinned* and on default this setting is on. In MPICH2 package there is no such a setting, however, there is a possibility to manage the strategy which is used by the *glibc* system library when processing a memory allocation request by the call of the *mallopt()* function with corresponding arguments.

In Fig. 3, graphs of dependence of execution time of a program on the number of nodes for different strategies of memory management are shown. The best results in running time and agreement with the theoretical estimates [2], which are expressed in smoothness of a curve, are shown by the version of the program managing static memory.

The second result in running time and agreement with theory is shown by the "dynamic allocation + *mallopt*" strategy (the MPICH2 package) where memory is dynamically allocated but the command not to use the *mmap* mechanism (memory pages mapping) for memory allocation is given to the system library. In condition where an application uses OS Linux resources in the exclusive usage mode (allocates large memory space one time when starting and deallocate it only at the end of work), memory fragmentation is not a typical problem and it is likely that the rate of management of memory allocated from a heap turns out to be higher. The authors do not insist upon this hypothesis but still have no another one.

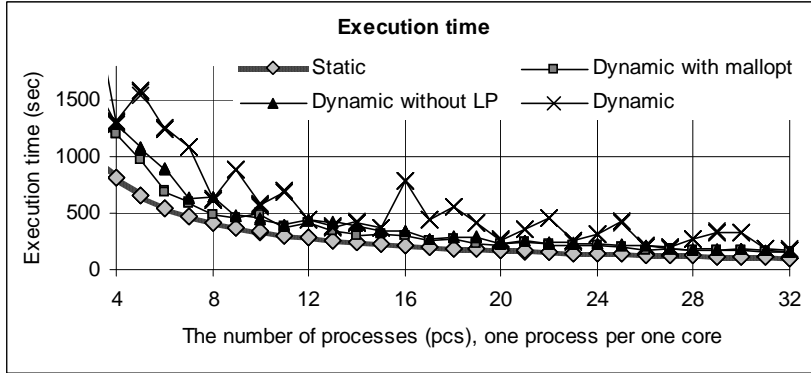


Figure 3. Graphs of dependence of execution time on the number of nodes being used for different memory management strategies

Mpi_leave_pinned being off in the OpenMPI package gives the third curve in Fig. 3.

For all types of dynamic memory allocation, the graphs of efficiency have approximately the same form (up to localization of peaks) and are similar to the graph in Fig. 4.

Thus, the study shows that dynamic memory allocation without correction of strategy provides the worst results in rate as well as in smoothness of the time expense curve. We notice that the results for both packages coincide with high degree of accuracy.

3 ON MEASUREMENT OF DATA EXCHANGE TIME FOR SMP-NODE CLUSTER

Many problems, including the testing one, use the block parallelizing with respect to data domain. This approaches in the need for regular intermediate data exchanges along cut lines of a domain between nodes processing adjacent domains [2]. In addition, it is not unusual that it is impossible to proceed calculations on a certain node (or implementation of this function is too complicated) until such an exchange is completed. In other words, the chain "calculations – exchange – calculations – exchange – ..." in essence is of sequential nature inside each node. In these conditions, the exchange operation is a local barrier that breaks calculations until data of all neighbors are received. The last statement is valid for any exchange strategy (nonblocking as well as blocking one). The latter strategy may

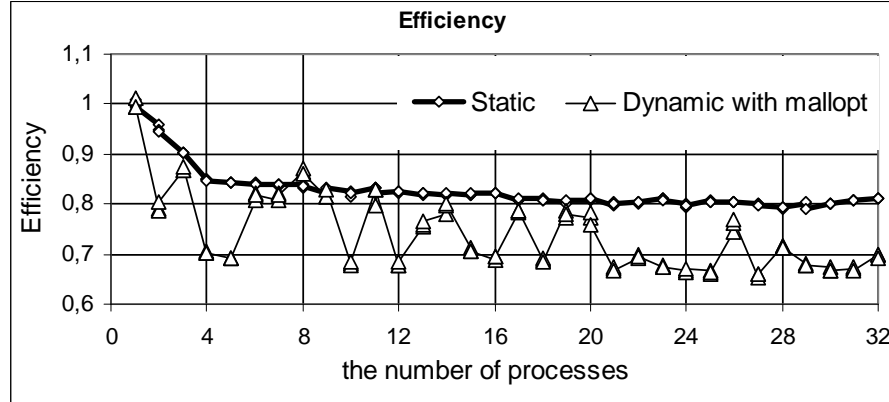


Figure 4. Graphs of dependence of execution time on the number of nodes being used for different memory management strategies

help to "parallelize" an exchange among several neighbors but one fails to combine exchanges and calculations.

If cuts of computational domain are performed by a linear scheme, then from the theoretical point of view the total time of data transfer may not depend on the number of processes [2]. Usually in this case, in attempting to measure communication time for data exchange, one proceeds as shown in Listing 1 for nonblocking version (Fig. 5). Points 3 and 4 may be called in a loop or in fact may be blocking calls, in this case this is of little importance. Further the values of time t are summed up and used for estimates of time or rate data exchanges.

```
t0=MPI_Wtime();
// p.1. -- call data receive functions
// p.2. -- call data send functions
// p.3. -- test of availability of receiving data
// p.4. -- test of disposal of sending data
t1=MPI_Wtime();
t=t1-t0;
```

Figure 5. Listing 1

However, sometimes results of such measurements are far from reality due to the "barrier" nature of send-receive functions. If by some reason a

neighbor is not ready to data transfer, then the time waiting its readiness is taken into account in the value t being measured.

If measurements are performed with a cluster consisting of the same one-processor one-core host and data are uniformly distributed, then these errors are small and are not of systematic nature. Something other may be observed when a problem is calculated with an SMP-node cluster where each host has some number (m) of computational nodes (cores) [2]. This experiment was performed with the SKIF Cyberia cluster (283 two-processors two-cores computational hosts) of Tomsk State University and with the HP computational complex (on the base of a cluster consisting of 64 eight-cores computational hosts) of Novosibirsk State University. In both cases dependence of $\sum t$ on the number of computational nodes is of typical saw-tooth form with a period equal to the number of cores per hosts (Fig. 6). Besides, maxima are achieved at the points $p = m * i + 1$, $i = 1, 2, \dots$. This is related to the fact that a process, which is performed alone on a host, always completes calculations somewhat faster than those taking several cores of one host. This difference takes the maximal value, for example, when on one host m processes are performed and on other host only one process is performed. Conversely, minimum is achieved when all hosts are uniformly loaded, i.e., the number p of processes is a multiple of m .

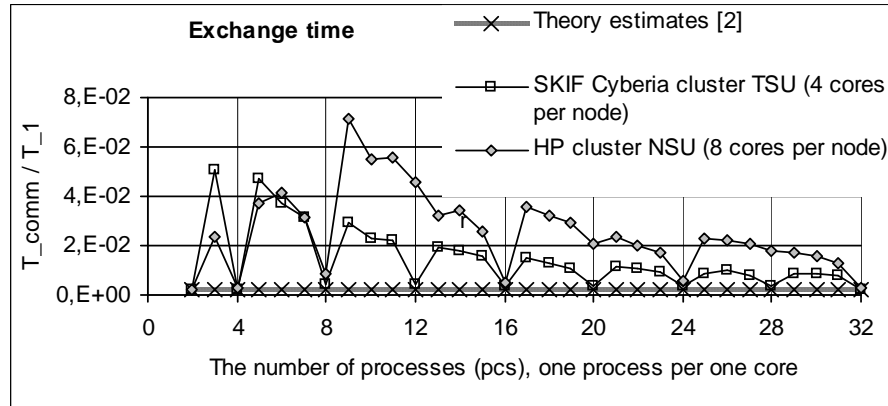


Figure 6. Graphs of dependence of exchange time on the number of computational processes (one process per core) for SMP-node clusters of different architecture

Hence, the procedure of time measurement have to be modified to exclude waiting time from measurements. For example, with the help of *MPI_BARRIER()* exchanging hosts can be synchronized with each other and only after this time is fixed and exchange is performed. A thinner technique is in individual time measurement for each nonblocking call, synchronization before each blocking call, or hand-held control of simultaneous transfer considering topology of a data decomposition.

In Fig. 7, graphs of communication time for the problem are shown.

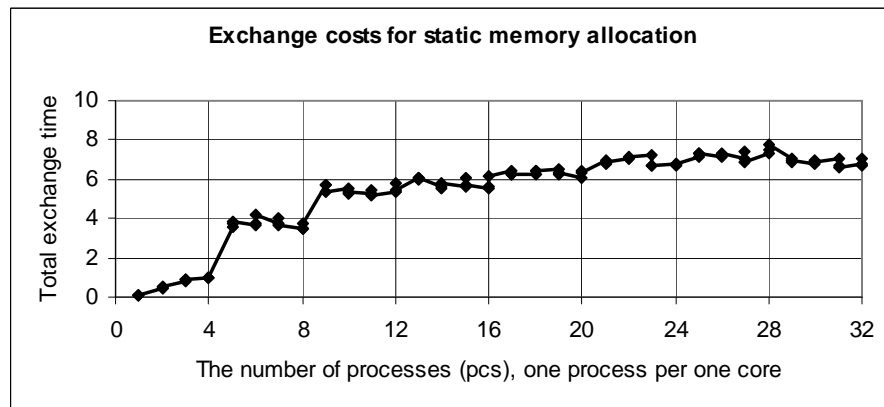


Figure 7. Graph of dependence of exchange time with synchronization on the number of computational processes (one process per core) for SMP-node two-cores two-processors per host cluster architecture

Exchange time differs only slightly for all strategies, therefore only one graph is that at the point $p = 4$ it has an expected jump due to putting into operation a network of data transfer for exchanges between processors 3 and 4 which are found to be different hosts. Further we observe a less evident but also explicable jump at the point $p = 8$ where the host carrying processes 4 – 7 begins to exchange with two external neighbors (the third and eighth ones) over the same network. Then the number of external neighbors no longer increases, and we see slight smooth increase of exchange time on the graph. The last fact is related to the need to perform exchanges of the total value of discrete uniform norm, and cost of this procedure depends on the number of processes although this dependence is weak.

This research was supported by Integrational Projects 26 and 89 of Siberian Branch of Russian Academy of Science and Federal Special-Purpose Programme GK 02.740.11.0621.

References

1. V.I. Agoshkov, Inverse problems of the mathematical theory of tides: boundary-function problem, *Russ. J. Numer. Anal. Math. Modelling* **20**(1) (2005) 1–18.
2. E.D. Karepova, Shaidurov V.V. Parallel implementation of FEM for the initial boundary value problem, *Computational Technologies* **14**(6) (2009) 45-57. (In Russian)
3. L.P. Kamenshchikov, E.D. Karepova, V.V. Shaidurov, Simulation of surface waves in basins by the finite element method, *Russ. J. Numer. Anal. Math. Modelling* **21**(4) (2006) 305 - 320.

COMPARISON OF NUMERICAL SOLUTIONS TO A MODEL OF CELL-MATRIX INTERACTIONS AND CELL MIGRATION

MIKHAIL KOLEV

University of Warmia and Mazury, Słoneczna 54, 10-710 Olsztyn, Poland

Abstract. The model equations describe interactions between tumor cells and microenvironmental factors such as extracellular matrix and matrix degradative enzymes. An important property of the solution to the modelling PDE system is its nonnegativity (a continuous maximum principle).

We have proposed a numerical scheme for the approximation of the modelling system of PDE by a system of nonlinear ODEs.

We examine the proposed numerical integration method with respect to its ability to maintain the nonnegativity of the solution as well as to satisfy the discrete analog of some conservation and evolution laws satisfied by the PDE system solution.

Numerical experiments are provided to demonstrate the behavior of the model.

1 INTRODUCTION

During the last decade, there has been a significant increase in the computation of differential equation models from mathematical biology and medicine. This help for understanding of biological process, for the verification of hypothesis about the underlying biology and also for the application of such models to patient specific data in medicine [2]. The complexity of the model equations nearly always necessitates the application of efficient numerical methods. Despite the modest accuracy requirements it remains important to resolve certain qualitative solution properties correctly. One such property is the nonnegativity of density (concentration) values participating in the model equations. Moreover, the developed numerical method should represent correctly conservation

M. Koleva and L. Vulkov (Eds.), Proceedings of the Fifth Conference on Finite Difference Methods: Theory and Applications (FDM: T&A 2010) 2011, pp. 97–107.
© Rousse University Press 2011

(or evolution) laws satisfied by the solutions that are direct consequence from the basic PDE system.

The paper is organized as follows. In Section 2 the parabolic system studied herein is briefly described. In Section 3 we perform space discretization of the modeled system by the use of finite elements. In Section 4 numerical experiments are discussed. Finally in Section 5 we give some conclusions.

2 THE MATHEMATICAL MODEL

The present paper is devoted to mathematical and numerical analysis of the following model of cancer invasion:

$$\begin{aligned} \frac{\partial n}{\partial t} &= d_n \frac{\partial^2 n}{\partial x^2} - \gamma \frac{\partial}{\partial x} \left(n \frac{\partial f}{\partial x} \right), \\ \frac{\partial f}{\partial t} &= -\eta m f, \\ \frac{\partial m}{\partial t} &= d_m \frac{\partial^2 m}{\partial x^2} + \alpha n - \beta m. \end{aligned} \quad (1)$$

The unknown functions $n(x, t)$, $f = f(x, t)$ $m = m(x, t)$ depend on the space variable x belonging to the scaled domain $\overline{\Omega} = [0, 1]$ of tissue, and time t . The system (1) describes interactions between cancer cells (their density is denoted by the function n), extracellular matrix (ECM) (its density is denoted by the function f), and matrix degradative enzymes (MDEs) (their concentration is denoted by the function m).

This system is a part of a more general model of cancer invasion proposed by Anderson *et al.*[1] and developed later in a series of papers (see for example [4–6]). Various modifications of the model have been numerically investigated in [8] and applied to experimental data for prostate cancer growth in [9].

The system (1) will be solved numerically at the boundary conditions

$$\frac{\partial n}{\partial x}(0, t) = \frac{\gamma}{d_n} n(0, t) \frac{\partial f}{\partial x}(0, t), \quad \frac{\partial m}{\partial x}(0, t) = 0, \quad (2)$$

$$n(1, t) = 0, \quad m(1, t) = 0, \quad (3)$$

or the zero-flux boundary condition

$$\frac{\partial n}{\partial x}(1, t) = \frac{\gamma}{d_n} n(1, t) \frac{\partial f}{\partial x}(1, t), \quad \frac{\partial m}{\partial x}(1, t) = 0; \quad (4)$$

and initial conditions

$$n(x, 0) = n_0(x), \quad f(x, 0) = f_0(x), \quad m(x, 0) = m_0(x). \quad (5)$$

We assume that $n_0(x), f_0(x), m_0(x) \geq 0, \neq 0$.

It is known (cf: [8,9]) that the problems (1), (2), (4), (5) and (1), (3), (4), (5) at sufficient smoothness of the input data admit a unique classical solution (n, f, m) globally in time. On the other hand, by integration of the corresponding differential equation and taking into account the boundary and initial conditions, one obtains

$$n(x, t), \quad f(x, t), \quad m(x, t) \geq 0, \quad \not\equiv 0 \quad (x, t) \in \overline{Q}_T \equiv [0, 1] \times [0, T)$$

(conservation of non-negativity)

Also, for problem (1), (2), (4), (5) we obtain

$$\int_0^1 n(x, t) dx = \int_0^1 n_0(x) dx \equiv n_0, \quad t \in [0, \infty), \quad (6)$$

(conservation of total cancer cell density)

$$\int_0^1 m(x, t) dx = \left(m_0 - \frac{\alpha n_0}{\beta} \right) e^{-\beta t} + \frac{\alpha n_0}{\beta}, \quad m_0 = \int_0^1 m_0(x) dx, \quad (7)$$

(evolution of total MDEs concentration);

$$\int_0^1 \ln f(x, t) dx = -\frac{\eta}{\beta} \left[\alpha n_0 t + \left(m_0 - \frac{\alpha n_0}{\beta} \right) (1 - e^{-\beta t}) \right] \quad (8)$$

(evolution the logarithmic total ECM density).

3 SPACE DISCRETIZATION

Let $V = H^1(\Omega)$ be the usual Sobolev space. Multiplying both sides of each equations of the system (1) by a function $v \in V$ and integrating on Ω , after integrating by parts and taking the boundary conditions (2) into account, we obtain the following variational formulation of (1), (2), (4), (5):

$$\frac{\partial}{\partial t} \int_0^1 n v dx = -d_n \int_0^1 \frac{\partial n}{\partial x} \frac{dv}{dx} dx + \gamma \int_0^1 n \frac{\partial f}{\partial x} \frac{dv}{dx} dx, \quad (9)$$

$$\frac{\partial}{\partial t} \int_0^1 f v dx = -\eta \int_0^1 m f v dx, \quad (10)$$

$$\frac{\partial}{\partial t} \int_0^1 m v dx = -d_m \int_0^1 \frac{\partial m}{\partial x} \frac{dv}{dx} dx + \alpha \int_0^1 n v dx - \beta \int_0^1 m v dx \quad (11)$$

$\forall v \in V$ and initial conditions (5).

Let us introduce the uniform mesh on Ω , $x_i = (i-1)h$, $\Omega_i = (x_i, x_{i+1})$, $i = 1, \dots, N+1$.

The space V is approximated by the subspace of functions defined from Ω in R which are polynomials of first degree on each Ω_i , $v(x) = \sum_{i=1}^{N+1} v_i S_i(x)$, where the functions S_i , which form a basis of V_h , are defined by

$$S_1 = \begin{cases} (x_2 - x)/h, & x \in \Omega_1, \\ 0, & x \in \Omega \setminus \Omega_1; \end{cases} \quad S_{N+1} = \begin{cases} (x - x_N)/h, & x \in \Omega_N, \\ 0, & x \in \Omega \setminus \Omega_N; \end{cases}$$

$$S_i = \begin{cases} (x - x_{i-1})/h, & x \in \Omega_{i-1}, \\ (x_{i+1} - x)/h, & x \in \Omega_i, \\ 0, & x \in \Omega \setminus (\Omega_i \cup \Omega_{i-1}), \end{cases} \quad i = 2, \dots, N.$$

We will seek the approximated (FEM) solution

$$n_h(x, t) = \sum_{i=1}^{N+1} n_i(t) S_i(x),$$

$$f_h(x, t) = \sum_{i=1}^{N+1} f_i(t) S_i(x), \quad (12)$$

$$m_h(x, t) = \sum_{i=1}^{N+1} m_i(t) S_i(x).$$

In the case of Dirichlet boundary conditions (3) we take $n_{N+1}(t) = f_{N+1}(t) = m_{N+1}(t) \equiv 0$.

Substituting these approximations in equations (9)-(11) and taking successively $v(x) = S_i(x)$, $i = 1, \dots, N+1$, we obtain the following ODEs system:

$$2n'_1 + n'_2 = \frac{6d_n}{h^2} (n_2 - n_1) + \frac{3\gamma}{h^2} (n_1 f_1 - n_1 f_2 + n_2 f_1 - n_2 f_2),$$

$$\begin{aligned}
n'_{i-1} + 4n'_i + n'_{i+1} &= \frac{6d_n}{h^2}(n_{i-1} - 2n_i + n_{i+1}) + \frac{3\gamma}{h^2}(-n_{i-1}f_{i-1} + n_{i-1}f_i \\
&\quad - n_if_{i-1} + 2n_if_i - n_if_{i+1} + n_{i+1}f_i - n_{i+1}f_{i+1}), \quad i = 2, \dots, N, \\
n'_N + 2n'_{N+1} &= \frac{6d_n}{h^2}(n_N - n_{N+1}) \\
&\quad + \frac{3\gamma}{h^2}(-n_Nf_N + n_Nf_{N+1} - n_{N+1}f_N + n_{N+1}f_{N+1}); \\
2f'_1 + f'_2 &= -\frac{\eta}{2}(3f_1m_1 + f_1m_2 + f_2m_1 + f_2m_2), \quad (13) \\
f'_{i-1} + 4f'_i + f'_{i+1} &= -\frac{\eta}{2}(f_{i-1}m_{i-1} + f_{i-1}m_i + f_im_{i-1} \\
&\quad + 6f_im_i + f_im_{i+1} + f_{i+1}m_i + f_{i+1}m_{i+1}), \quad i = 2, \dots, N, \\
f'_N + 2f'_{N+1} &= -\frac{\eta}{2}(f_Nm_N + f_Nm_{N+1} + f_{N+1}m_N + 3f_{N+1}m_{N+1}); \\
2m'_1 + m'_2 &= \frac{6d_m}{h^2}(m_2 - m_1) + \alpha(2n_1 + n_2) - \beta(2m_1 + m_2), \\
m'_{i-1} + 4m'_i + m'_{i+1} &= \frac{6d_m}{h^2}(m_{i-1} - 2m_i + m_{i+1}) \\
&\quad + \alpha(n_{i-1} + 4n_i + n_{i+1}) - \beta(m_{i-1} + 4m_i + m_{i+1}) \quad i = 2, \dots, N, \\
m'_N + 2m'_{N+1} &= \frac{6d_m}{h^2}(m_N - m_{N+1}) + \alpha(n_N + 2n_{N+1}) - \beta(m_N + 2m_{N+1}).
\end{aligned}$$

The obtained system (13) is a semi-discrete version of the model (1). It is composed of $3N + 3$ ordinary differential equations. Its numerical solution is discussed in the next Section. It gives the approximate solutions (12) to the model (1).

4 NUMERICAL EXPERIMENTS

The semi-discrete system of ODE (13) has to be closed by appropriate initial conditions (5). Following [4], we assume that the initial tumor is centered at $x = 0$, the initial MDE concentration is proportional to the initial tumor cell density with 1/2 as the constant of the proportionality, and the MDE has already degraded the ECM, thus we consider the same initial conditions as in [4], which are presented in Fig. 1 and are defined as follows:

$$n(x, 0) = \exp\left(\frac{-x^2}{\varepsilon}\right), \quad f(x, 0) = 1 - 0.5n(x, 0), \quad m(x, 0) = 0.5n(x, 0),$$

for $x \in [0, 1]$.

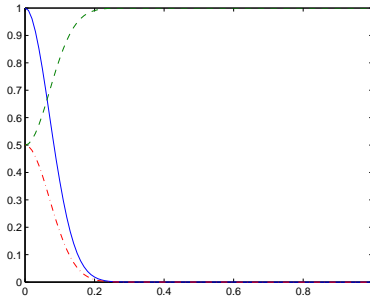


Figure 1. The initial distribution of cancer cell density (solid), ECM density (dashed), and MDE concentration (dashdot).

4.1 POSITIVITY OF THE SOLUTIONS

In the first part of our numerical experiments we compare several algorithms for solving the approximate semi-discrete model with respect to their capability to reproduce the positivity of the continuous solution of the model (1), (2), (4), (5).

The approximate semi-discrete initial value problem has been solved by using the codes `ode23`, `ode45`, `ode113`, `ode15s` and `ode23s` from the Matlab ODE suite [13] with $RelTol = 10^{-3}$ and $AbsTol = 10^{-6}$.

`ode23` is a one-step solver, which uses an explicit Runge-Kutta (2,3) pair of Bogacki and Shampine [3].

`ode45` is also a one-step solver. It uses an explicit Runge-Kutta (4,5) formula, the Dormand-Prince pair [7].

`ode113` is a multistep solver based on Adams-Bashforth-Moulton formulas [12].

`ode15s` is also a multistep solver. It uses numerical differentiation formulas [13, 14].

`ode23s` is a one-step solver based on a modified Rosenbrock formula of order 2 [13].

The numerical experiments show that the nonstiff solvers `ode23`, `ode45` and `ode113` are not able to maintain the required positivity of the approximate solutions. On the other side, the stiff solvers `ode15s` and `ode23s` reproduce the nonnegativity of the solutions at sufficiently dense mesh on Ω (i.e. $N = 80$ grid-points).

4.2 THE ROLE OF HAPTOTAXIS FOR THE MIGRATION OF CANCER CELLS

Here we present the approximations (12) to the model (1) for tumor cells, ECM, and MDE. The results of our numerical experiments are obtained by the use of `ode15s` solver. Some important illustrations are presented in Figures 2-5.

We use the parameter values $\alpha = 0.1$, $\beta = 0.5$, $\eta = 10$, $\varepsilon = 0.01$, $d_m = 0.001$, $d_n = 0.001$, $N = 80$ and different values of γ specified in the captions of the figures.

The different values of γ allow us to compare two possible mechanisms of cancer migration and invasion, namely the diffusion (random motility) described by the term $d_n \Delta^2 n$ and the haptotaxis described by $-\gamma \Delta \cdot (n \Delta f)$ of the model (1). For high values of parameter γ more important is the haptotactic migration of tumor cells. Such situation is presented in Figs. 2-3, where γ was set to 0.03.

For lower values of parameter γ more important is the random motility of tumor cells. Such situation is presented in Figs. 4-5, where γ was set to 0.005.

The numerical results show that in the case with higher haptotactic coefficient γ (presented in Figures 2 and 3) clusters of cancer cells are created at the leading edge of the tumor as a result of the haptotactic migration. As time increases, the tumor invade deeply into the tissue. In the case of lower haptotactic coefficient γ (presented in Figures 4 and 5) the moving cluster is not so high and is not able to invade very deep into the tissue during the time interval.

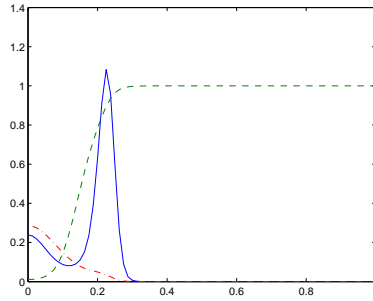


Figure 2. Cancer cell migration and interactions between the cancer and the surrounding tissue: cancer cell density (solid), ECM density (dashed), and MDE concentration (dashdot). Solutions to (1), (2), (4), (5) with the parameter value $\gamma = 0.03$ at time $t = 1$.

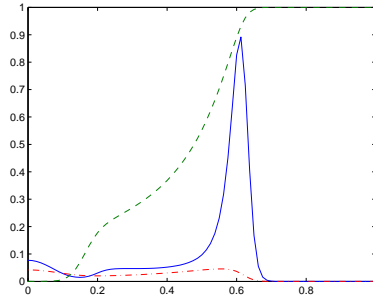


Figure 3. Solutions to (1), (2), (4), (5) with the parameter value $\gamma = 0.03$ at time $t = 5$.

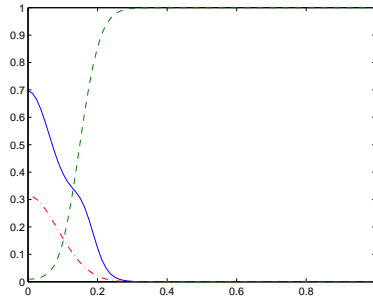


Figure 4. Solutions to (1), (2), (4), (5) with the parameter values $\gamma = 0.005$ at time $t = 1$.

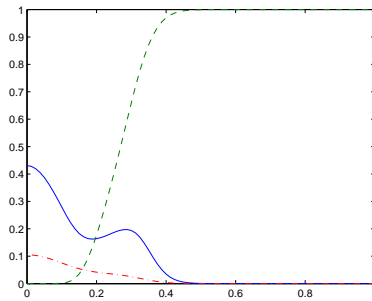


Figure 5. Solutions to (1), (2), (4), (5) with the parameter values $\gamma = 0.005$ at time $t = 5$.

These two cases illustrate the possible migration mechanisms of cancer invasion through tissue. Their knowledge can be useful for choice of treatment in the respective real situations.

4.3 COMPARISON BETWEEN TWO STIFF SOLVERS WITH RESPECT TO CONSERVATION LAWS

In order to check the accuracy of the proposed semi-discrete approximation, we have applied and compared the stiff solvers `ode15s` and `ode23s` to the corresponding initial value problem with $N = 80$. Then we have calculated the differences between the left-hand and right-hand sides for the conservation and evolution properties given in Eqs. 6 - 8. For Eqs. 6 and 7 it is of the order $10^{-6} - 10^{-12}$ and for the property given in Eq. 8 is of the order 10^{-2} . The corresponding errors are presented in Table 1 and Table 2 for the four cases illustrated in Figs. 2-5. There is no significant difference between the both stiff solvers with respect to the errors and the time of the solution.

The obtained results confirm the high accuracy of the proposed approximation scheme.

Table 1. Differences between theoretical and calculated values for Eqs. 6 - 8 for `ode15s`.

Figure i	Error for Eq. 6	Error for Eq. 7	Error for Eq. 8
2	$1.96 * 10^{-6}$	$1.99 * 10^{-7}$	-0.0567
3	$2.26 * 10^{-7}$	$2.85 * 10^{-8}$	-0.0601
4	$-4.91 * 10^{-12}$	$2.71 * 10^{-7}$	-0.0570
5	$1.08 * 10^{-12}$	$6.68 * 10^{-9}$	-0.0605

Table 2. Differences between theoretical and calculated values for Eqs. 6 - 8 for `ode23s`.

Figure i	Error for Eq. 6	Error for Eq. 7	Error for Eq. 8
2	$1.97 * 10^{-6}$	$-6.11 * 10^{-8}$	-0.0569
3	$2.79 * 10^{-7}$	$-2.99 * 10^{-8}$	-0.0602
4	$-8.80 * 10^{-12}$	$-3.23 * 10^{-7}$	-0.0575
5	$1.86 * 10^{-12}$	$-7.31 * 10^{-7}$	-0.0645

5 CONCLUSIONS

In this work, we have proposed a numerical scheme for the solution to a model of tumor invasion. We have compared several algorithms and showed that only those able to solve stiff systems of ODEs preserve the nonnegativity of the solutions. Two stiff ODE solvers have been compared with respect to the conservation properties of the solution. The model evaluation proves the high accuracy of the numerical method. In future work we plan to address the development of the numerical method for more complicated mathematical models. Also, discrete maximum principle and convergence of the FEM approximations will be theoretically studied.

References

1. A.R.A. Anderson, M.A.I. Chaplain, E.L. Newman, R.i.C. Steele, A.M. Thompson, Mathematical modelling of tumour invasion and metastasis, *Journal of Theoretical Medicine* **2** (2000) 129-154.
2. N. Bellomo, N.K. Li, P.K. Maini, On the foundations of cancer modeling, selected topics, speculations and perspectives. *Mathematical Models in Applied Sciences* **18** (2008) 593-646.
3. P. Bogacki, L.F. Shampine, A 3(2) pair of Runge-Kutta formulas, *Applied Mathematical Letters* **2** (1989) 1-9.
4. M.A.I. Chaplain, A.R.A. Anderson, Mathematical modelling of tissue invasion. *Cancer modelling and simulation*, Chapman & Hall/CRC, pp. 269-297, 2003.
5. M.A.I. Chaplain, G. Lolas, Mathematical modelling of cancer cell invasion of tissue: The role of the urokinase plasminogen activation system, *Mathematical Models and Methods in Applied Sciences* **15** (2005) 1685-1734.
6. M.A.I. Chaplain, G. Lolas, Mathematical modelling of cancer invasion of tissue: dynamic heterogeneity, *Networks and Heterogeneous Media* **1**(3) 399-439 (2006).
7. J.R. Dormand, P.J. Prince, A family of embedded Runge-Kutta formulae, *Journal of Computational and Applied Mathematics* **6** (1980) 19-26.
8. M. Kolev, B. Zubik-Kowal, Numerical solutions for a model of tissue invasion and migration of tumour cells, *Computational and Mathematical Methods in Medicine* **2011** (2011) 16 pages, Article ID 452320, doi:10.1155/2011/452320.
9. M. Kolev, B. Zubik-Kowal, Numerical versus experimental data for prostate tumour growth, *Journal of Biological Systems* **19**(1) (2011) 1-14.

10. G. Litcanu, C. Morales-Rodrigo, Asymptotic behavior of global solutions to a model of cell invasion, *Mathematical Models and Methods in Applied Sciences* **20**(9) (2010) 1721-1758.
11. C. Morales-Rodrigo, Local existence and uniqueness of regular solutions in a model of tissue invasion by solid tumor, *Mathematical and Computer Modelling* **47** (2008) 604-613.
12. L.F. Shampine, M.K. Gordon, *Computer Solution of Ordinary Differential Equations*, W.H. Freeman, (1975).
13. L.F. Shampine, M.W. Reichelt, The Matlab ODE suite, *SIAM Journal on Scientific Computing* **18** (1997) 1-22.
14. L.F. Shampine, M.W. Reichelt, J.A. Kierzenka, Solving Index-1 DAEs in Matlab and Simulink, *SIAM Review* **41** (1999) 538-552.

IMPROVED PARAMETERS FOR MODELLING WITH MAMMOGRAPHIC EVIDENCE OF CARCINOMA

MIKHAIL KOLEV¹ AND BARBARA ZUBIK-KOWAL²

¹ Faculty of Mathematics and Computer Science, University of Warmia and Mazury,
Słoneczna 54, 10-710 Olsztyn, Poland

² Department of Mathematics, Boise State University, 1910 University Drive, Boise,
Idaho 83725, USA

Abstract. We present a mathematical model of cellular immune response to breast cancer. The model is formulated within the framework of the kinetic theory for active particles and is a nonlinear system of partial integro-differential equations of Boltzmann type. The model is a generalization of a kinetic model describing cellular immune response to cancer. We apply clinical data on breast cancer development and show that the generalized model fits the data better than the previous model.

1 INTRODUCTION

The applications of mathematical and computational methods in life sciences is a challenging and promising area of research. It requires a close collaboration between mathematicians, biologists and clinicians. An important possible advantage of such interdisciplinary collaboration may be the successful complementation of traditional experimental biological methods by mathematical modelling approaches. This can lead to a deeper understanding of the mechanisms of biological processes and to reduction of the amount of costly experiments needed for the design of therapeutical strategies [12].

The power and limitations of the mathematical modelling approach to biological phenomena are considered by leading biologists and documented in several recent papers, among others in Asquith and Bangham [6], May [32], Antia et al. [2], etc. One of the most important difficulty for mathematical description and analysis of living entities follows from the fact that living matter in contrast to inert matter cannot be simply

M. Koleva and L. Vulkov (Eds.), Proceedings of the Fifth Conference on Finite Difference Methods: Theory and Applications (FDM: T&A 2010) 2011, pp. 108–118.

© Rousse University Press 2011

modelled by the rules of classical mechanics. It is governed by different laws and is characterized by specific features such as reproduction, competition, cell cycle, self-organization, ability to communicate with other entities and concomitant notion of function or purpose. An additional complication is the fact that cells contain millions copies of thousands of different components, each with very specific features and interactions. Furthermore, the properties of living matter depend on gene expression and resulting phenotypic characteristics, which can be changed due to random gene mutations and may alter the environment, which in turn affects the evolutionary selection. The proper modelling of these dynamic genetic and evolutionary components is a particular challenge for applied mathematicians.

One of the mathematical modelling approaches that describes some of the most significant properties of living matter is *the kinetic theory of active particles*. It has been developed during the last two decades for modelling the evolution of large systems constituted by interacting individuals or entities, called *active particles*, which are able to perform specific functions, called *activities*, typical of the living matter. The interactions between the particles may change their activities according to complex rules which attempt to model typical behaviors of the studied living system, and in particular the ability of developing strategies taking into account the behaviors of the surrounding individuals [20].

One of the first papers introducing the methods of kinetic theory for active particles is that by Jäger and Segel [27], devoted to modelling the social behavior of colonies of insects. The theory has been developed, by using diverse methods, with references to various fields of applied and life sciences, such as complex biological systems [13, 17, 18], psychological interactions [9, 21], politics and social sciences [19, 20, 30, 31], traffic flow [22, 23], population dynamics [5] etc. Mathematical structures concerning the kinetic theory of active particles are proposed in the paper by Arlotti et al. [3] and in the book by Arlotti et al. [4]. The book by Bellomo [7] presents recent development and applications of this theory. A broad bibliography can be found in the recent review papers by Bellomo and Delitala [20] and Bellomo et al. [8].

The paper includes five sections. Clinical data and observations as well as the mathematical description of the kinetic model are provided in Section 2. Numerical methods for solving the model equations are described in Section 3. In Section 4, we present results of numerical experiments with the model and correlations between numerical and *in vivo* experimental data. They are compared with the results of the numerical

experiments of Drucis et al. [24]. Finally, Section 5 includes concluding remarks.

2 MATHEMATICAL MODEL

The mathematical modelling of cancer onset and development is an actively developing area of research during the last decades. A vast bibliography can be found, among others, in the review papers [12, 20], special issues of mathematical journals [14–16], and collection of surveys devoted to cancer modelling [1, 10, 33]. Recent models of breast tumor development are presented and analysed, e.g., in [25, 26].

In this paper we present a mathematical model describing cellular immune response to breast cancer formulated within the framework of the kinetic theory for active particles. The model is a generalization of the kinetic model proposed in Kolev [28]. We apply the oncological data provided in Drucis et al. [24] where are presented mammographic data on carcinoma for five different cases, which are denoted by: Mk, Sm, Bi, MI, and Kw. Measurements of the diameters of their carcinomas have been performed in different instants of time. The results of the mammographic examinations for these cases are presented in Table 1 as well as in Figure 1 by \triangleleft , \diamond , x , \circ , and $*$, see [24] for more detail. Moreover, we extend the model from [28] to improve its ability to fit the clinical data.

Patient Code	Sm	Bi	Mk	MI	Kw
Year of Birth	1920	1924	1933	1930	
Dates Measurement 1	29.06.99 16mm	15.05.00 40mm	20.10.89 10mm	17.07.00 17mm	2002 0mm
Dates Measurement 2	10.05.02 25mm	09.10.01 40mm	27.05.91 15mm	30.08.00 14mm	12.03.07 12mm
Dates Measurement 3	23.05.05 30mm	25.11.02 49mm	06.06.94 15mm	26.10.01 9mm	07.07.08 25mm
Dates Measurement 4		19.08.04 50mm	05.06.96 25mm	06.11.02 8mm	
Dates Measurement 5			22.08.97 28mm		

Table 1. Data on mammographic examinations of five patients with breast cancer.

The model describes the interactions between the cellular immunity and cancer [29]. The interactions between six main populations, each denoted by subscript i , are taken into account in our model.

The population of cancer cells (CCs) is denoted by subscript $i = 1$. Further, the population of the helper T cells (Th cells) is denoted by the subscript $i = 2$, the population of the cytotoxic T lymphocytes (CTLs) is denoted by the subscript $i = 3$, the population of the antigen presenting cells (APCs) is denoted by the subscript $i = 4$, the population of the antigen-loaded APCs ([Ag-APC]) is denoted by the subscript $i = 5$, and the population of the host environment cells (HE) is denoted by the subscript $i = 6$.

As in [28], the distribution density of the i -th population with activation state $u \in [0, 1]$ at time $t \geq 0$ is denoted by

$$f_i(t, u), \quad f_i : [0, \infty) \times [0, 1] \rightarrow R_+, \quad i = 1, \dots, 6.$$

Furthermore, the functions

$$n_i(t) = \int_0^1 f_i(t, u) du, \quad n_i : [0, \infty) \rightarrow R_+, \quad i = 1, \dots, 6, \quad (1)$$

denote the concentration of the i -th population of cells at time $t \geq 0$.

In the present model, the meaning of the state of activity of the interacting populations is as follows.

The state of activity of a given CC denotes the probability of recognition of this CC by APCs. The higher the activation state of a tumor cell, the higher the possibility of the immune system to kill the CC.

The population of T helper cells participates in the cellular immunity through secretion of cytokines. The secreted cytokines influence the function of a variety of immunological cells, e.g. the proliferation and the activation of APCs, T cells etc. [29]. In this model, the activation state of a given Th cell denotes the normalized quantity of cytokines produced by the helper T cell after its activation due to interaction with antigen-loaded APC. Therefore, the activity of T helper cells is proportional to their ability to improve the functioning of the immunological cells.

Activated CTLs participate in the destruction of tumor cells e.g. through release of cytotoxins. Here, the activation state of a given CTL denotes the probability of killing of a recognized CC after its interaction with the given CTL.

The activation states of the populations denoted by $i \in \{1, 2, 3\}$ are allowed all possible values $u \in [0, 1]$.

As a simplification of the biological reality, for the populations denoted by $i \in \{4, 5, 6\}$ we assume that their distribution functions are independent of the state of activity u and therefore

$$f_i(t, u) = n_i(t), \quad \forall u \in [0, 1], \quad t \geq 0, \quad i = 4, 5, 6.$$

Furthermore, the distribution function f_6 of the HE is assumed to be constant in time.

The generalized model describing the interactions between the cellular immunity and cancer includes linear source terms for the populations $i \in \{1, 2, 3, 5\}$, that are not considered in [28], which model the age-dependence of breast cancer and possible influx of immune cells. It is the following nonlinear system of partial integro-differential equations:

$$\begin{aligned} \frac{\partial f_1}{\partial t}(t, u) &= p_{16}^{(1)} J_1(t) + t_{16}^{(1)} \left(2uJ_1(t) - u^2 f_1(t, u) \right) \\ &\quad - d_{12} F_{1,2}(t, u) - d_{13} F_{1,3}(t, u) + a_1 t + b_1, \end{aligned} \quad (2)$$

$$\begin{aligned} \frac{\partial f_2}{\partial t}(t, u) &= p_{16}^{(2)}(1-u) + p_{25}^{(2)} G(t, u) - d_{21} F_{2,1}(t, u) - d_{26} f_2(t, u) \\ &\quad + t_{25}^{(2)} n_5(t) H_2(t, u) + a_2 t + b_2, \end{aligned} \quad (3)$$

$$\begin{aligned} \frac{\partial f_3}{\partial t}(t, u) &= p_{16}^{(3)}(1-u) + p_{25}^{(3)} G(t, u) - d_{31} F_{3,1}(t, u) \\ &\quad + t_{23}^{(3)} J_2(t) H_3(t, u) - d_{36} f_3(t, u) + a_3 t + b_3, \end{aligned} \quad (4)$$

$$\frac{d}{dt} n_4(t) = p_{16}^{(4)} + p_{25}^{(4)} n_5(t) I_2(t) - b_{14}^{(5)} n_4(t) I_1(t) - d_{46} n_4(t), \quad (5)$$

and

$$\frac{d}{dt} n_5(t) = b_{14}^{(5)} n_4(t) I_1(t) - d_{51} n_5(t) J_1(t) - d_{56} n_5(t) + a_5 t + b_5. \quad (6)$$

Here,

$$\begin{aligned} F_{j,k}(t, u) &= f_j(t, u) \int_0^1 v f_k(t, v) dv, \quad I_j(t) = \int_0^1 v f_j(t, v) dv, \\ G(t, u) &= (1-u) n_5(t) \int_0^1 v f_2(t, v) dv, \quad J_j(t) = \int_0^1 f_j(t, v) dv, \\ H_j(t, u) &= 2 \int_0^u (u-v) f_j(t, v) dv - (1-u)^2 f_j(t, u). \end{aligned}$$

System (2)-(6) is supplemented by the initial conditions:

$$\begin{aligned} f_j(t_0, u) &= f_j^{(0)}(u), \quad j = 1, 2, 3, \quad u \in [0, 1], \\ n_k(t_0) &= n_k^{(0)}, \quad k = 4, 5. \end{aligned} \quad (7)$$

Equation (2) describes the temporary evolution of the population of cancer cells. The meaning of the parameters and corresponding terms is the following.

$p_{16}^{(1)}$ - characterizes the generation of new tumor cells;

$t_{16}^{(1)}$ - characterizes the steady progress of the cancer cells towards decreasing their activation states;

d_{12} - characterizes the destruction of cancer cells due to the activity of Th cells;

d_{13} - characterizes the destruction of cancer cells due to the response of CTLs;

a_1, b_1 - characterize linear production of cancer cells.

Equations (3) and (4) describe the temporary evolution of the populations of Th cells and CTLs and the meaning of their parameters is the following:

$p_{16}^{(2)}$ - characterizes the generation of new Th cells by HE;

$p_{16}^{(3)}$ - characterizes the production of new CTLs by HE;

$p_{25}^{(2)}$ - characterizes the generation of new Th cells due to the interactions between Th cells and antigen-loaded APCs;

$p_{25}^{(3)}$ - characterizes the production of new CTLs due to the interactions between Th cells and antigen-loaded APCs;

$t_{25}^{(2)}$ - characterizes the steady progress of the Th cells towards increasing their activation states due to the interactions between Th cells and antigen-loaded APCs;

$t_{23}^{(3)}$ - characterizes the steady progress of the CTLs towards increasing their activation states due to the interactions between Th cells and CTLs;

d_{21} - characterizes the destruction of Th cells due to their interactions with cancer cells;

d_{31} - characterizes the destruction of CTLs due to their interactions with cancer cells;

d_{26} - characterizes the natural death of Th cells;

d_{36} - characterizes the natural death of CTLs;

a_2, b_2 - characterize the possible (linear) inlet of Th cells;

a_3, b_3 - characterize the possible (linear) inlet of CTLs cells.

Equation (5) describes the dynamics of the population $i = 4$ of APCs.

The meaning of the parameters used in this equation is the following:

$p_{16}^{(4)}$ - characterizes the constant production of new APCs by HE;

$p_{25}^{(4)}$ - characterizes the generation of new APCs due to the interactions between Th cells and antigen-loaded APCs;

$b_{14}^{(5)}$ - characterizes the appearance of new antigen-loaded APCs due to the interactions between APCs and CCs;

d_{46} - characterizes the natural death of APCs.

Equation (6) describes the dynamics of the population $i = 5$ of antigen-loaded APCs. The meaning of the parameters used in this equation is the following:

d_{51} - characterizes the destruction of antigen-loaded APCs due to their interactions with cancer cells;

d_{56} - characterizes the natural death of antigen-loaded APCs;

a_5, b_5 - characterize the possible (linear) inlet of antigen-loaded APCs.

In the next section, we solve the system (2)-(6) supplemented by the initial conditions chosen according to the clinical data presented in Table 1 and Figure 1, where the initial value is represented by the first grid-point denoted by the first $\triangleleft, \diamond, x, \circ,$ and $*$ for the each patient code Mk, Sm, Bi, MI, and Kw, respectively.

3 APPROXIMATE SOLUTION OF THE MODEL

The goal of this section is to construct a numerical solution to the concentrations of individuals $n_i(t)$, $i = 1, \dots, 5$, at any time variable $t > 0$. The concentrations $n_1(t)$, $n_2(t)$, and $n_3(t)$ will be computed from (1) by the use of the functions $f_1(t, u)$, $f_2(t, u)$, and $f_3(t, u)$. First, we perform a discretization of the system (2)-(6) with respect to the activation variable $u \in [0, 1]$ by introducing the uniform grid-points

$$u_i = i\Delta u, \quad i = 0, \dots, N,$$

where N is a positive integer and $\Delta u = 1/N$. Then, instead of the functions $f_1(t, u)$, $f_2(t, u)$, and $f_3(t, u)$ in (2)-(6) we consider their approximations $f_{1,i}(t)$, $f_{2,i}(t)$, and $f_{3,i}(t)$ defined in such a way that

$$f_j(t, u_i) \approx f_{j,i}(t), \quad j = 1, 2, 3, \tag{8}$$

for each grid-point $u_i \in [0, 1]$ with $i = 0, \dots, N$. Thus, we replace the continuous variable u by the discrete activation state variables u_i . The integrals in (2)-(6) for the approximations (8) are computed by the use of quadrature formulae:

$$\begin{aligned}
\int_0^1 f_j(t, v) dv &\approx Q_0^N [f_j(t, v)], \quad j = 1, 2, \\
\int_0^1 v f_j(t, v) dv &\approx Q_0^N [v f_j(t, v)], \quad j = 1, 2, 3, \\
\int_{u_i}^1 f_1(t, v) dv &\approx Q_i^N [f_1(t, v)], \\
\int_0^{u_i} (u_i - v) f_j(t, v) dv &\approx Q_0^i [(u_i - v) f_j(t, v)], \quad j = 2, 3.
\end{aligned} \tag{9}$$

The approximations in (9) represent arbitrary quadratures. In Section 4 the integrals (9) are approximated by the composite trapezoidal rule.

The performed discretization of the model equations (2)-(6) with respect to the variable $u \in [0, 1]$ yields a system of ordinary integro-differential equations. The corresponding initial value problem is solved in the next section by a time stepping method.

4 SIMULATIONS AND COMPARISON OF NUMERICAL DATA WITH MAMMOGRAPHIC EVIDENCE OF CARCINOMA

The system (2)-(6) discretized in u and t is supplemented with initial conditions corresponding to the clinical observations presented in Section 2. Namely, the distribution function of the cancer cell $f_1^{(0)}(u_i)$ are chosen according to the mammographic measurements presented in the third row of Table 1. The initial value problem is solved separately for each of the clinical cases: Mk, Sm, Bi, MI, and Kw, by using the code `ode15s` from the Matlab ODE suite [34] with $RelTol = 10^{-2}$ and $AbsTol = 10^{-6}$. The numerical solutions are computed iteratively for different sets of the parameters $p_{16}^{(1)}, t_{16}^{(1)}$, etc... and are used to minimize the sums of squared errors (differences between the numerical and clinical data (mammographical measurements) for each patient listed it Table 1).

The concentration of the cancer cells is computed by the use of the obtained approximations $f_{1,i}(t)$, for $i = 0, 1, 2, \dots, N$

$$n_1(t) \approx Q_0^N [f_1(t, v)].$$

In Figure 1, we present these approximations for each of the cases Mk, Sm, Bi, MI, and Kw, and compare them with their mammographical data. The data from Table 1 are indicated by \triangleleft , \diamond , x , \circ , and $*$ for Mk, Sm, Bi, MI, and Kw, respectively. The numerical solutions of the model are presented by the solid lines. For comparison, the dashed lines present the corresponding solutions of the model [28].

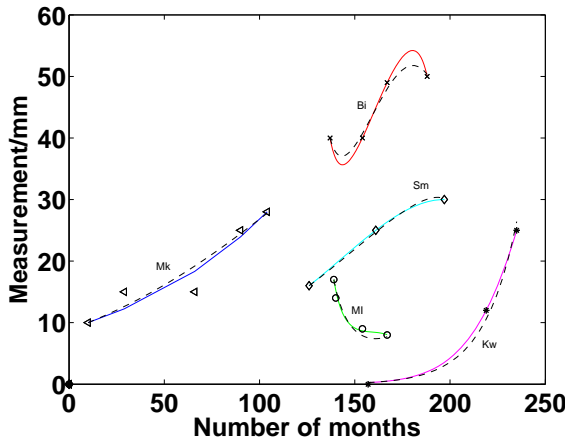


Figure 1. Mammographic (grid-points) versus numerical (solid) data.

5 CONCLUDING REMARKS AND FUTURE DIRECTIONS

The comparison between the numerical solutions of the generalized model proposed in this paper and the model presented in [28] shows that the extended model fits the clinical data recorded for five patients with carcinoma better than the model [28]. The dependence of the breast cancer development on the age of the patients may be one of possible reasons for this improvement.

Our future work will address the development of the mathematical models in order to describe and investigate drug and chemotherapy treatment of cancer disease.

References

1. J.A. Adam and N. Bellomo N, editors, *A survey of models on tumor immune systems dynamics*, Birkhäuser, 1997.
2. R. Antia, V.V. Ganusov, R. Ahmed, The role of models in understanding CD8+ T-cell memory, *Nature Reviews Immunology* **5** (2005) 101-111.
3. L. Arlotti, N. Bellomo, E. De Angelis, Generalized kinetic (Boltzmann) models: Mathematical structures and applications, *Mathematical Models and Methods in Applied Sciences* **12** (2002) 567-591.
4. L. Arlotti, N. Bellomo, E. De Angelis, M. Lachowicz, *Generalized Kinetic Models in Applied Sciences*, World Sci., 2003.
5. L. Arlotti, N. Bellomo, K. Latrach, From the Jäger and Segel model to kinetic population dynamics: Nonlinear evolution problems and applications, *Mathematical and Computer Modelling* **30** (1999) 15-40.

6. B. Asquith, Ch.R.M. Bangham, An introduction to lymphocyte and viral dynamics: the power and limitations of mathematical analysis, *Proceedings of the Royal Society B: Biological Sciences* **270** (2003) 1651-1657.
7. N. Bellomo, *Modelling complex living systems a kinetic theory and stochastic game approach*, Birkhäuser, 2008.
8. N. Bellomo, C. Bianca, M. Delitala, Complexity analysis and mathematical tools towards the modelling of living systems, *Physics of Life Reviews* **6** (2009) 144-175.
9. N. Bellomo, B. Carbonaro, On the complexity of multiple interactions with additional reasoning about Kate, Jules and Jim, *Mathematical and Computer Modelling* **47** (1-2) (2008) 168-177.
10. N. Bellomo, M.A.J. Chaplain, E. De Angelis, editors, *Selected topics on cancer modeling. Genesis. Evolution. Immune competition. Therapy*, Birkhäuser, 2008.
11. N. Bellomo, M. Delitala, From the mathematical kinetic, and stochastic game theory to modelling mutations, onset, progression and immune competition of cancer cells, *Physics of Life Reviews* **5** (2008) 183-206.
12. N. Bellomo, N.K. Li, P.K. Maini, On the foundations of cancer modeling, selected topics, speculations and perspectives, *Mathematical Models in Applied Sciences* **18** (2003) 593-646.
13. N. Bellomo, G. Forni, Complex multicellular systems and immune competition: New paradigms looking for a mathematical theory, *Current Topics in Developmental Biology* **81** (2008) 485-502.
14. N. Bellomo, P. Maini, Preface. Cancer Modelling (II), *Mathematical Models and Methods in Applied Sciences* **16** (7b), (2006) iii-vii (special issue).
15. N. Bellomo, P. Maini, Preface. Challenging mathematical problems on cancer modelling, *Mathematical Models and Methods in Applied Sciences* **17** (2007) 1641-1645 (special issue).
16. N. Bellomo, B. Sleeman, Preface. Multiscale Cancer Modelling, *Computational and Mathematical Methods in Medicine* **20** (2-3) (2006) 67-70 (special issue).
17. A. Bellouquid, M. Delitala, Mathematical methods and tools of kinetic theory towards modelling complex biological systems, *Mathematical Models and Methods in Applied Sciences* **15** (2005) 1639-1666.
18. A. Bellouquid, M. Delitala, *Modelling complex biological systems a kinetic theory approach*, Birkhäuser, 2006.
19. M.L. Bertotti, M. Delitala, From discrete kinetic theory and stochastic game theory to modelling complex systems in applied sciences, *Mathematical Models and Methods in Applied Sciences* **14** (2004) 1061-1084.
20. M.L. Bertotti, M. Delitala, Conservation laws and asymptotic behavior of a model of social dynamics, *Nonlinear Analyses: Real World Applications* **9** (2008) 183196.
21. B. Carbonaro, C. Giordano, A second step towards mathematical models in psychology: A stochastic description of human feelings, *Mathematical and Computer Modelling* **41** (2005) 587-614.
22. V. Coscia, M. Delitala, P. Frasca, On the mathematical theory of vehicular traffic flow models II. Discrete velocity kinetic models, *International Journal of Nonlinear Mechanics* **42** (2007) 411-421.
23. M. Delitala, A. Tosin. Mathematical modelling of vehicular traffic: A discrete kinetic theory approach, *Mathematical Models and Methods in Applied Sciences* **17** (2007) 901-932.
24. K. Druikis, M. Kolev, W. Majda, B. Zubik-Kowal. Nonlinear modeling with mammographic evidence of carcinoma, *Nonlinear Analysis: Real World Applications* **11** (5) (2010) 4326-4334.

25. H. Enderling, A.R.A. Anderson, M.A.J. Chaplain, A.J. Munro, J.S. Vaidya, Mathematical modelling of radiotherapy strategies for early breast cancer, *Journal of Theoretical Biology* **241** (1) (2006), 158-171.
26. H. Enderling, M.A.J. Chaplain, A.R.A. Anderson, J.S. Vaidya, A mathematical model of breast cancer development, local treatment and recurrence, *Journal of Theoretical Biology* **246** (2007) 245-259.
27. E. Jäger, L. Segel, On the distribution of dominance in populations of social organisms, *SIAM Journal of Applied Mathematics* **52** (5) (1992) 1442-1468.
28. M. Kolev, A mathematical model of cellular immune response to leukemia, *Mathematical and Computer Modelling* **41** (2005) 1071-1081.
29. J. Kuby, *Immunology*, W.H. Freeman, 1997.
30. M. Lo Schiavo, The modelling of political dynamics by generalized kinetic (Boltzmann) models, *Mathematical and Computer Modelling* **37** (2003) 261-281.
31. M. Lo Schiavo, A dynamical model of electoral competition, *Mathematical and Computer Modelling* **43** (2006) 1288-1309.
32. R.M. May, Uses and abuses of mathematics in biology, *Science* **303** (2004) 790-793.
33. L. Preziosi, *Modeling cancer growth*, CRC Press. Chapman Hall, 2003.
34. L.F. Shampine, M.W. Reichelt, The Matlab ODE suite, *SIAM Journal on Scientific Computing* **18** (1997) 1-22.

TWO-GRID TECHNIQUE FOR SEMI-LINEAR ELLIPTIC PROBLEMS ON COMPLICATED DOMAINS

MIGLENA N. KOLEVA

FNSE, Rousse University, 8 Stidentska St., 7017 Rousse, Bulgaria,
`mkoleva@uni-ruse.bg`

Abstract. In this paper we apply the two-grid method for solving semi-linear elliptic problems on general domains with different boundary conditions (Dirichlet, Neumann, Robin), imposed on parts of the boundary. The algorithm is based on the finite element discretization on two (or more) subspaces V_{h_k} , $\dim V_{h_k} << \dim V_{h_{k+1}}$, $k = 0, 1, \dots$. Numerical results are discussed. It is shown, that the optimal accuracy is reached for $h_{k+1} = h_k^{2^k}$. Moreover, the coarse space V_{h_0} can be extremely coarse and the algorithm still achieve asymptotically optimal approximation.

1 INTRODUCTION

Let $\Omega \in \mathbb{R}^d$, $d = 1, 2, 3$ be a bounded Lipschits domain with polygonal/-hedral boundary $\partial\Omega = \bigcup_i \partial\Omega_i$, $\partial\Omega_i \cap \partial\Omega_j = \emptyset$, $i \neq j$, where $i, j = 1, \dots, I$ ($I > 0$ is integer) and $\bar{\Omega} = \Omega \cup \partial\Omega$. We consider the following semi-linear elliptic model problem

$$\begin{aligned} -\nabla \cdot (\kappa \nabla u) + au &= f(\mathbf{x}, u) \quad \text{in } \Omega, \quad \mathbf{x} \in \Omega, \\ b_i u + e_i \kappa \frac{\partial u}{\partial n} &= c_i \quad \text{on } \partial\Omega_i, \end{aligned} \tag{1}$$

where $\kappa(\mathbf{x})$, $a(\mathbf{x})$, $b_i(\mathbf{x})$, $c_i(\mathbf{x})$ and $f(\cdot)$ are given functions: $\kappa(\mathbf{x}) \geq \kappa_0 > 0$, $a(\mathbf{x}) \geq 0$, $b_i(\mathbf{x}) \geq 0$ in Ω , $e_i = \{0, 1\}$, f is sufficiently smooth and n is the unit outward normal vector to the boundary, i.e. $\frac{\partial u}{\partial n} = \nabla u \cdot n$.

The model (1) is well known in mathematical physics as heat conductivity problem, see [9, 11]. Dirichlet boundary condition ($b_i = 1$, $e_i = 0$) represents the given temperature, Neumann boundary condition ($b_i = 0$,

M. Koleva and L. Vulkov (Eds.), Proceedings of the Fifth Conference on Finite Difference Methods: Theory and Applications (FDM: T&A 2010) 2011, pp. 119–128.

© Rousse University Press 2011

$e_i = 1$) describes the heat flow and Robin's boundary condition ($b_i \neq 0$, $e_i = 1$) sets the heat transfer by the Newton's law.

In this paper we develop a fast numerical finite element algorithm for solving the model problem (1), based on the two-grid technique. The two-grid method was first introduced by Axelsson [1] and J. Xu [12, 13], independently of each other, as a discretization method for non-symmetric indefinite and non-linear problems. The basic idea of the two-grid method is to solve a complicated problem (non-linear, non-symmetric indefinite, etc.) on a coarse grid (with mesh size H) and then solve easier problem (SPD, linear, etc.) on the fine grid (with mesh size h and $h \ll H$) as correction.

In recent years there has been significant research and development related to the two-grid approach. A multi-grid method based on composite finite elements for a linear elliptic Neumann problem on complicated domain is presented in [10]. Another two-grid modifications for elliptic problems are also available in the literature: for example, two-grid finite volume element method [2], two-grid decoupling method for transmission problems [5–7], etc. Estimates for the rate of convergence of the two-grid method for problems defined on complicated domains are not known to the author.

The algorithm presented in this work is an extension of the two-grid idea of J. Xu [12, 13] and our previous work [8].

The rest of the paper is organized as follows. The next section is devoted to the finite element discretization and linearization. The main two-grid or multi-grid algorithm is presented in Section 3. In Section 4 we discuss numerical results. Finally, we give some concluding remarks.

2 FINITE ELEMENT SOLUTION

Let $W_p^m(\Omega)$ be the standard Sobolev space with a norm $\|\cdot\|_{m,p}$, given by $\|v\|_{m,p}^p = \sum_{|\alpha| \leq m} \|D^\alpha v\|_{L^p(\Omega)}^p$. For $p = 2$, we denote $H^m(\Omega) = W_2^m(\Omega)$ and $\|\cdot\|_m = \|\cdot\|_{m,2}$, $\|\cdot\| = \|\cdot\|_{0,2}$.

Let the equation (1) has at least one solution $u \in H^2(\Omega)$ and the linearized operator $\nabla \cdot (\kappa \nabla) - a + f'(u)$ is nonsingular.

We assume that Ω is partitioned by a quasi-uniform triangulation $\mathcal{T}_h = \{\tau_s\}$, where τ_s are triangles of size $h \in (0, 1)$, $h = \max\{\text{diam}(\tau_s), \tau_s \in \mathcal{T}_h\}$ and $\bar{\Omega} = \bigcup_s \bar{\tau}_s$. Further we will refer h as a mesh size.

For a given triangulation \mathcal{T}_h a finite element space $V_h \subset H^1(\Omega)$ is defined by

$$V_h = \{v \in C(\bar{\Omega}) : v|_\tau \in V_\tau^r \quad \forall \tau \in \mathcal{T}_h, v|_{\partial\Omega_D} = 0\},$$

where $\partial\Omega_D$ is those parts of $\partial\Omega$, where Dirichlet boundary conditions are imposed and V_τ^r is the space of polynomial of degree not greater than the positive integer r .

It is well-known [3] that V_h satisfies the following approximation property $\inf_{w \in V_h} \{\|v - w\|_{0,q} + h\|v - w\|_{1,q}\} \leq h^{m-2/p+2/q}|v|_{m,p}$, for all $v \in W_p^m(\Omega) \cap H^1(\Omega)$, $2 \leq m \leq r+1$ and $1 \leq p \leq q \leq \infty$.

The standard finite element discretization of (1) is to find $u_h \in V_h$ such that

$$\begin{aligned} & \int_{\Omega} [\kappa \nabla u_h \nabla w + a u_h w] d\mathbf{x} + \sum_{i=1}^I e_i \int_{\partial\Omega_i} [b_i u_h - c_i] w d\xi \\ & = \int_{\Omega} f(\mathbf{x}, u_h) w d\mathbf{x} \quad \forall w \in V_h. \end{aligned} \quad (2)$$

Next, applying Newton's quazilinearization, from (2) we obtain the following iterative process: for given initial guess $u_h^{(0)}$ we seek a sequence of solutions $u_h^{(l)}$, $l = 1, 2, \dots$

$$\begin{aligned} & \int_{\Omega} [\kappa \nabla u_h^{(l)} \nabla w + a u_h^{(l)} w] d\mathbf{x} + \sum_{i=1}^I e_i \int_{\partial\Omega_i} [b_i u_h^{(l)} - c_i] w d\xi \\ & = \int_{\Omega} [f(\mathbf{x}, u_h^{(l-1)}) + f'_u(\mathbf{x}, u_h^{(l-1)})(u_h^{(l)} - u_h^{(l-1)})] w d\mathbf{x} \quad \forall w \in V_h. \end{aligned} \quad (3)$$

3 NUMERICAL ALGORITHM

Let divide the domain Ω into $K+1$ families of triangles $\mathcal{T}_{h_k} = \{\tau_{s_k}\}$, $k = 0, 1, \dots, K$, $h_k = \max\{\text{diam}(\tau_{s_k})\}$, $\tau_{s_k} \in \mathcal{T}_{h_k}$ and $\bar{\Omega} = \bigcup_{s_k} \bar{\tau}_{s_k}$. Analogically to V_h , we define finite element spaces $V_{h_k} \in H^1(\Omega)$, of different scales with $h_k \ll h_{k+1}$. The first space V_{h_0} (corresponding to the triangulation \mathcal{T}_{h_0}) we call *coarse* and denote by V_H , $H = h_0$. For $k > 0$ we call V_{h_k} *fine* space.

Algorithm

1. ($k = 0$) Find $u_H \in V_H$ from (2), using iteration process (3) and set $u_{h_0} := u_H$;
2. For each $k = 1, 2, \dots, K$ perform *only one* iteration (3) with $u_{h_k}^{(l-1)} := u_{h_{k-1}}$ and find $u_{h_k} \in V_{h_k}$.

Actually at each step of the **Algorithm** we perform *one and the same type* iterations - (3), but on different meshes. At first stage we solve nonlinear problem on the coarse mesh, using iteration process (3), while at each next step $k = 1, 2, \dots, K$ we perform *only one* iteration (3) on the fine mesh with step size h_k .

In order to start iteration procedure at $k = 0$ for initial guess we can chose $u_H^{(0)} = 0$, or otherwise to obtain $u_H^{(0)}$ as a solution of an appropriate linear problem (as is done in the numerical examples in the last section).

It can be proven (cf. [10, 12, 13]) that for the solution $u_h \in V_h$ of (2), obtained at k -th step of the **Algorithm**, the following estimates hold:

$$\|u_h - u_h^k\|_1 = \mathcal{O}(H^{r2^k}), \quad \|u_h - u_h^k\| = \mathcal{O}(H^{(r+1)2^k}), \quad (4)$$

i.e.

$$\|u - u_h^k\|_1 = \mathcal{O}(h^r + H^{r2^k}), \quad \|u - u_h^k\| = \mathcal{O}(h^{r+1} + H^{(r+1)2^k}), \quad h = h_K. \quad (5)$$

Therefore the *optimal choice* of the fine mesh step size at k -th step of the **Algorithm** is $h_k = H^{2^k}$, i.e. $h_k = h_{k-1}^2$, $k = 1, 2, \dots, K$.

Remark 1. The **Algorithm** above can be performed in two-grid manner. The first step ($k = 0$) is the same. Then we perform K iterations (3) on one and the same fine mesh \mathcal{T}_h with size $h = H^{2^K}$. Estimates (4), (5) are still true and the algorithm is cheaper (in the sense of computational time) than the standard method ($k = 0$, $H = \sqrt[2^K]{h}$), but more expensive than the presented approach to refine the mesh at each $k = 0, 1, \dots, K$. For that reason we will not discuss it here.

4 NUMERICAL TESTS

In this section we test the efficiency of the proposed **Algorithm** for the model problem (1) in the case $\Omega \in \mathbb{R}^2$ with different geometry of the domain and two type boundary conditions ($i = 2$) - Dirichlet boundary conditions on $\partial\Omega_1 = \partial\Omega_D$ and Robin's boundary conditions on $\partial\Omega_2 = \partial\Omega_R$, see Figures 1, 3, 5.

Mesh generation \mathcal{T}_{h_k} is based on the Delaunay-Voronoi algorithm - inner vertices are determined by the density of points on the boundary, denoted by N_D^k on $\partial\Omega_D$ and N_R^k on $\partial\Omega_R$, n_t^k refers is the number of triangles in \mathcal{T}_h and n_v^k to the number of vertices. The validation of (4), (5) is verified for continuous piecewise linear (P1) and continuous piecewise quadratic (P2) elements.

We take $\kappa(x_1, x_2) = e^{x_1+x_2}$, $a(x_1, x_2) = 2x_1^2 + x_2^2$, $b_1 = 1$, $b_2 = x_1^2 + x_2^2 + 1$, $e_1 = 0$, $e_2 = 1$, $f(x_1, x_2, u) = -u^\lambda + g(x_1, x_2)$, $\lambda = 2$ and $g(x_1, x_2)$, $c_1(x_1, x_2)$, $c_2(x_1, x_2)$ are determined such that $u(x_1, x_2) = \cos(x_1 + x_2) + 2$ is the exact solution of the test problem. We give error in H^1 norm (E_1) and L_2 -norm (E) and convergence rate (CR_1 and CR , respectively), computed using well known double mesh principle.

The initial guess is obtained as a solution of the linear problem $\lambda = 1$. The iterations of the nonlinear solver continue until the maximal difference between two subsequent iterations is less than 10^{-12} . The number of iterations is denoted by $iter$. The CPU time is also given. For $k > 0$, according to (4), (5), the fine mesh step sizes are chosen such that $h_k \lesssim h_{k-1}^2$. For all computations we use **Freefem++** [4]. To solve the generated linear systems of equations we use the implemented in **Freefem++** LU solver.

Example 1. (*Rosetta domain*) Let for $0 \leq t \leq 2\pi$, $\partial\Omega$ is defined by

$$x = [\rho_0 + \rho_1 \sin(\sigma t)] \cos(t) + \bar{x}_1, \quad y = [\rho_0 + \rho_1 \sin(\sigma t)] \sin(t) + \bar{x}_2,$$

where $\bar{x}_1 = \bar{x}_2 = 0.02\sqrt{5}$, $\rho_0 = 0.6$ and first we take $\rho_1 = 0.1$ and $\sigma = 3$, see Figure 1. Results from computations with one grid procedure in V_H with P2 elements are given in Table 1. The efficiency (convergence rate and CPU time) of the Algorithm for $k = 1, 2$ is illustrated in Tables 2, 5, $N^k = N_R^k = N_D^k$. It is clear that for P2 elements (i.e. $r = 2$) convergence rate in L_2 and H^1 norm, respectively is

CR	CR₁	k
$\mathcal{O}(H^3)$,	$\mathcal{O}(H^2)$,	$k = 0$,
$\mathcal{O}(H^6) = \mathcal{O}(h_1^3 + H^6)$,	$\mathcal{O}(H^4) = \mathcal{O}(h_1^2 + H^4)$,	$k = 1$,
$\mathcal{O}(H^{12}) = \mathcal{O}(h_2^3 + h_1^6 + H^{12})$,	$\mathcal{O}(H^8) = \mathcal{O}(h_2^2 + h_1^4 + H^8)$	$k = 2$.

In Tables 1, 2 we show how, *saving a computational time*, one and the same accuracy can be achieved with multi-grid procedure, see the lines which are boldfaced and underlined. Instead of solving the nonlinear problem on the mesh with size h , we solve the nonlinear problem on the mesh with size \sqrt{h} and perform only one iteration on the mesh with size h , or alternatively we solve the nonlinear problem on the mesh with size $\sqrt[4]{h}$, then we perform only one iteration on the mesh with size \sqrt{h} and one iteration on the mesh with size h and analogically for $k > 2$. This approach reduce the computational time significantly. On Figure 2, we plot numerical solution obtained by the Algorithm for $k = 2$ with $N^0 = 4$, $N^1 = 8$ and $N^2 = 32$.

Table 1. One grid procedure ($k = 0$) with P2 elements: number of grid nodes on the boundary, number of elements and vertices, error and convergence rate in H^1 and L_2 norms, number of iterations and CPU time for $\rho_1 = 0.1$ and $\sigma = 3$, Example 1

N_D^0	N_R^0	H	n_t^0	n_v^0	E	CR	E_1	CR_1	$iter$	CPU
4	4	0.720	10	10	4.6328e-4		7.5362e-3		4	0.187
8	8	0.361	50	34	7.4775e-5	2.6313	2.2155e-3	1.7662	4	0.203
16	16	0.201	212	123	1.0033e-5	2.8978	6.1155e-4	1.8571	4	0.281
32	32	0.099	848	457	1.1808e-6	3.0869	1.4786e-4	2.0482	4	0.671
64	64	0.053	3404	1767	1.5669e-7	2.9138	3.8125e-5	1.9555	4	2.652
<u>128</u>	<u>128</u>	0.028	13622	6940	<u>2.0729e-8</u>	2.9182	<u>9.7819e-6</u>	<u>1.9625</u>	4	<u>19.843</u>

Table 2. Algorithm for $k = 1, 2$ with P2 elements: number of grid nodes on the boundary, error and convergence rate in H^1 and L_2 norms and CPU time for $\rho_1 = 0.1$ and $\sigma = 3$, Example 1

N^0	N^1	$k = 1$				$k = 2$				
		E	CR	E_1	CR_1	CPU	N^2	E	E_1	CPU
4	8	2.5126e-5		2.2160e-3		0.218	32	4.734e-7	1.479e-4	0.323
8	32	4.791e-7	5.713	1.479e-4	3.906	0.344				
<u>16</u>	<u>128</u>	<u>6.509e-9</u>	<u>6.184</u>	<u>9.782e-6</u>	<u>3.918</u>	<u>3.869</u>				

We repeat the same computations with P1 elements for $\rho_1 = 0.2$ and $\sigma = 5$, see Figure 3. The results are listed in Tables 3, 4, 5. The convergence rate is closed enough to those, predicted by the theory, i.e.

CR	CR₁	k
$\mathcal{O}(H^2),$	$\mathcal{O}(H),$	$k = 0,$
$\mathcal{O}(H^4) = \mathcal{O}(h_1^2 + H^4),$	$\mathcal{O}(H^2) = \mathcal{O}(h_1 + H^2),$	$k = 1,$
$\mathcal{O}(H^8) = \mathcal{O}(h_2^2 + h_1^4 + H^8),$	$\mathcal{O}(H^4) = \mathcal{O}(h_2 + h_1^2 + H^4)$	$k = 2.$

Table 3. One grid procedure ($k = 0$) with P1 elements: number of grid nodes on the boundary, number of elements and vertices, error and convergence rate in H^1 and L_2 discrete norms, number of iterations and CPU time for $\rho_1 = 0.2$ and $\sigma = 5$, Example 1

N_D^0	N_R^0	H	n_t^0	n_v^0	E	CR	E_1	CR_1	$iter$	CPU
4	4	0.748	8	9	2.7269e-2		2.2711e-1		4	0.187
8	8	0.455	28	23	1.0268e-2	1.4091	1.5227e-1	0.5768	4	0.203
16	16	0.277	116	75	2.9134e-3	1.8171	7.9690e-2	0.9341	4	0.234
32	32	0.115	610	338	9.7748e-4	1.5755	4.2555e-2	0.9051	4	0.405
64	64	0.084	2974	1552	2.5200e-4	1.9557	2.1371e-2	0.9937	4	1.326
<u>128</u>	<u>128</u>	<u>0.048</u>	<u>12390</u>	<u>6324</u>	<u>6.4845e-5</u>	<u>1.9583</u>	<u>1.0817e-2</u>	<u>0.9824</u>	4	<u>5.257</u>

Again, the comparable results (see Tables 3, 4) are boldfaced and underlined. On Figure 4 we show numerical solution obtained by the Algorithm for $k = 1$ with $N^0 = 4$, $N^1 = 8$ and $N^2 = 32$.

Table 4. Algorithm for $k = 1, 2$ with P1 elements: number of grid nodes on the boundary, error and convergence rate in H^1 and L_2 norms and CPU time for $\rho_1 = 0.2$ and $\sigma = 5$, Example 1

$k = 1$						$k = 2$				
N^0	N^1	E	CR	E_1	CR_1	CPU	N^2	E	E_1	CPU
4	8	5.081e-3		1.527e-1		0.187	32	5.249e-4	4.255e-2	0.231
8	32	5.249e-4	3.275	4.256e-2	1.843	0.237				
<u>16</u>	<u>128</u>	<u>3.980e-5</u>	<u>3.7210</u>	<u>1.082e-2</u>	<u>1.9761</u>	<u>0.999</u>				

Table 5. Algorithm for $k = 2$ with P1 elements for $\rho_1 = 0.2$ and $\sigma = 5$ and P2 elements for $\rho_1 = 0.1$ and $\sigma = 3$: number of grid nodes on the boundary, error and convergence rate in H^1 and L_2 norms, Example 1

$N^0(H)$	$N^1(h_1)$	$N^2(h_2)$	E	CR	E_1	CR_1
P2 elements, $\rho_1 = 0.1, \sigma = 3$						
3 (0.866)	6 (0.473)	12 (0.255)	1.1590e-5		1.2346e-3	
6 (0.473)	24 (0.134)	192 (0.019)	1.8372e-9	12.623	4.4434e-6	8.118
P1 elements, $\rho_1 = 0.2, \sigma = 5$						
3 (0.755)	6 (0.537)	12 (0.311)	3.8224e-3		1.0141e-1	
6 (0.537)	24 (0.195)	192 (0.033)	1.7327e-5	7.7853	7.1969e-3	3.8167

Example 2. (*Triangle domain*) The domain is triangle with vertices $A(0, 0)$, $B(0, 5)$, $C(3, 6)$, see Figure 5. With N_R^k we denote the number of grid nodes at each boundary AB and BC , i.e. on the boundary $AB \cup BC$ we have $2N_R^k$ grid nodes.

Finite difference algorithm on adaptive mesh for semi-linear elliptic equation on triangle domain with zero Dirichlet boundary conditions is developed in [9]. Tests with standard finite element method ($k = 0$) show that the solution does not converge: in Table 6 we list the results with P2 elements. A similar situation is for P1 elements. Nevertheless, the two-grid procedure works well both for P1 and P2 elements, see Tables 7, 8. In fact, each step k of the Algorithm provides a good enough initial solution for the next stage $k + 1$. Now estimates (4), (5) still hold, but we need to perform $K + 1$ steps in order to obtain the same accuracy (and convergence) as for K steps. On Figure 6 we plot numerical solution computed with the Algorithm for $k = 1$ with $N^0 = 16$ and $N^1 = 64$.

Table 6. One grid procedure ($k = 0$) with P2 elements: number of grid nodes on the boundary, number of elements and vertices, error and CPU time, Example 2

N_D^0	N_R^0	H	n_t^0	n_ν^0	E	E_1	CPU
16	16	0.587	248	149	1.8451e-3	3.6849e-2	0.156
32	32	0.307	984	541	6.0103e-4	9.2516e-3	0.374
64	64	0.152	3836	2015	5.6715e-4	2.7876e-3	1.357
128	128	0.087	15198	7792	5.6684e-4	1.6198e-3	8.206
256	256	0.046	61042	30906	5.6685e-4	1.5134e-3	83.506

Table 7. Algorithm for $k = 2$ with P1 elements: error and convergence rate in L_2 and H^1 norm and CPU time, Example 2

N^0	N^1	E	CR	E_1	CR_1	CPU
16	64	2.8892e-3		1.3971e-1		0.312
32	128	7.4338e-4	1.9585	7.0989e-2	0.9768	1.014
64	256	1.8504e-4	2.0063	3.5307e-2	1.0076	4.976

Table 8. Algorithm for $k = 2$ with P2 elements: error and convergence rate in L_2 and H^1 norm and CPU time, Example 2

N^0	N^1	E	CR	E_1	CR_1	CPU
16	64	7.0406e-6		2.3455e-4		0.624
32	128	9.2949e-7	2.9212	5.9642e-4	1.9755	3.775
64	256	1.1673e-7	2.9933	1.4963e-4	1.9950	40.294

5 CONCLUSIONS

In this work we presented an efficient two-grid based algorithm for solving semi-linear elliptic problems. The fundamental idea is that one can solve non-linear equation by applying Newton-like iterations on a (cheap) coarse grid, then execute *only one* (expensive) grid iteration at each next fine mesh \mathcal{T}_{h_k} , $k = 1, 2, \dots, K$. It is shown, that the first (coarse) mesh can be extremely coarse and still maintain a good accuracy approximation as long as the mesh size satisfy $H = \mathcal{O}(\sqrt[2^k]{h_k})$ or $H = \mathcal{O}(\sqrt[2^K]{h})$ if we apply the algorithm on two meshes \mathcal{T}_H and \mathcal{T}_h (i.e. h is fixed for all $k = 1, 2, \dots, K$). The main advantage of the two (multi)-grid procedure is in saving computational time.

Acknowledgements. This research is supported by the Bulgarian National Fund of Science under Project DID 02/37-2009.

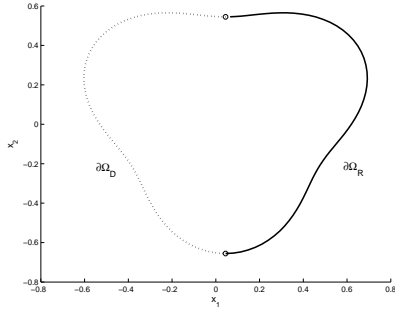


Figure 1. Rosetta domain Ω , $\rho_0 = 0.6$, $\rho_1 = 0.1$ and $\sigma = 3$, Example 1

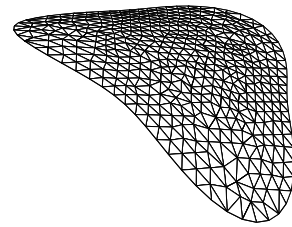


Figure 2. Numerical solution, Algorithm for $k = 2$, P2 elements, $N^0 = 4$, $N^1 = 8$, $N^2 = 32$, Example 1

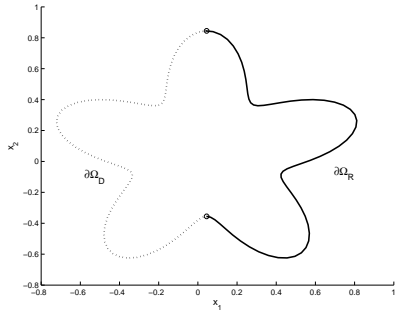


Figure 3. Rosetta domain Ω , $\rho_0 = 0.6$, $\rho_1 = 0.2$ and $\sigma = 5$, Example 1

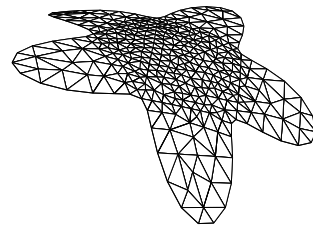


Figure 4. Numerical solution, Algorithm for $k = 2$, P1 elements, $N^0 = 4$, $N^1 = 8$, $N^2 = 32$, Example 1

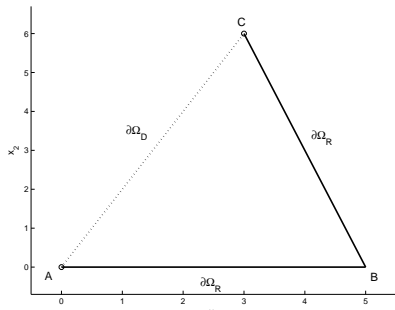


Figure 5. Triangle domain, Example 2

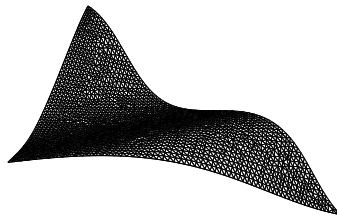


Figure 6. Numerical solution, Algorithm for $k = 1$, P2 elements, $N^0 = 16$, $N^1 = 64$, Example 2

References

1. O. Axelsson, On mesh independence and Newton methods, *Appl. Math.* **38**(4-5) (1993) 249 – 265.
2. C. Bi, V. Ginting, Two-grid finite volume element method for linear and nonlinear elliptic problems, *Numer. Math.* **1089**(2) (2007) 177–198.
3. P. Ciarlet, *The Finite Element Method for Elliptic Problems*, North-Holland, NY, 1978.
4. J. Hecht, Freefem, Third Edition, Version 3.5 (www.freefem.org/ff++).
5. B. Jovanovic, M. Koleva, L. Vulkov, Application of the two-grid method to a heat radiation problem, *AIP CP* **1186** (2009) 352–360.
6. B. Jovanovic, M. Koleva, L. Vulkov, Convergence of a FEM and two-grid algorithms for elliptic problems on disjoint domains, *J. of Comp. and Appl. Math.* **235**(3) (2011) 364–374
7. M. Koleva, L. Vulkov, Two-grid decoupling method for elliptic problems on disjoint domains, *Lect. Notes in Comp. Sci.* **5910** (2010) 787–795.
8. M. Koleva, L. Vulkov, Two-grid quasilinearization approach to ODEs with applications to model problems in physics and mechanics, *Comput. Phys. Commun.* **181**(3) (2010) 663–670.
9. G.I. Marchuk, V.V. Shaidurov, Improving the Accuracy of the Finite Difference Schemes Solutions, Nauka, Moskow, 1979 (in Russian).
10. S. Nicaise, S.A. Sauter, Efficient numerical solution of Neumann problems on complicated domains, *Calcolo* **43**(2) (2006) 95–120.
11. A.A. Samarskii, B.V. Andreev, *Difference Methods for Elliptic Equations*, Nauka, Moskow, 1976 (in Russian).
12. J. Xu, A novel two-grid method for semilinear elliptic equations, *SIAM J. Sci. Comput.* **15** (1994) 231-237.
13. J. Xu, Two-grid discretization techniques for linear and nonlinear PDEs, *SIAM J. Numer. Anal.* **33** (1996) 1759-1777.

A NUMERICAL METHOD FOR SOLVING PARABOLIC EQUATIONS BASED ON THE USE OF A MULTIGRID METHOD

MARINA E. LADONKINA, OLGA YU. MILYUKOVA, AND VLADIMIR F.
TISHKIN

Institute for Mathematical Modeling, Russ. Ac. Sci. 4A Miusskaya square,
125047, Moscow, Russia,
olgamilyukova@mail.ru

Abstract. A numerical method is proposed for solving parabolic equations, based on the use of a multigrid method. Theoretical and numerical analysis is performed of the stability and accuracy of the method as applied to model initial-boundary value problems for the heat equation, and the conservative property of the scheme is demonstrated. The method reduces computational complexity as compared to implicit and explicit schemes. A parallelization of the method is proposed.

1 INTRODUCTION

Numerical simulations of various problems in mathematical physics must take into account diffusion processes, which are modeled by parabolic equations. In certain cases, the use of both explicit and implicit finite difference schemes for approximating parabolic equations drastically increases the computing time. The application of the classical multigrid [1,2] may also entail high computational costs. Therefore, new methods should be developed for parabolic equations.

2 ALGORITHM

As an example, we construct and analyze an algorithm for solving initial-boundary value problems for the heat equation:

$$\begin{aligned} \rho C_v \frac{\partial u}{\partial t} &= \operatorname{div}(\kappa \operatorname{grad} u) + f, \quad (\vec{x}, t) \in G, \\ u(\vec{x}, t) &= g(\vec{x}, t) \quad \text{if } \vec{x} \in \gamma, u(\vec{x}, 0) = T_0(\vec{x}), \end{aligned} \tag{1}$$

M. Koleva and L. Vulkov (Eds.), Proceedings of the Fifth Conference on Finite Difference Methods: Theory and Applications (FDM: T&A 2010) 2011, pp. 129–137.

© Rousse University Press 2011

where C_v is specific heat at constant volume, ρ is density, κ is thermal conductivity, u is the temperature at point $\vec{x} = (x, y)$ or $\vec{x} = (x, y, z)$ at time t , $G = \{0 < x < l_1, 0 < y < l_2, 0 < t \leq T\}$ or $G = \{0 < x < l_1, 0 < y < l_2, 0 < z < l_3, 0 < t \leq T\}$, γ is the computational domain boundary, f is the heat source density, and $g(\vec{x})$ and $T_0(\vec{x})$ are given functions. To approximate problem (1), we use a fully implicit scheme with constant mesh sizes h_x , h_y , and h_z along the x , y , and z directions, respectively, and time step τ . The scheme is a system of linear algebraic equations in the unknown solution values at the $(n + 1)$ th time level: $A_h u^{n+1} = f_h$.

As applied to this problem, the new method differs from the classical multigrid in that only one iteration of the multigrid V-cycle is performed, while any number of smoothing iterations may be performed on each grid. Thus, the calculation of the solution at each time level can be represented as the V-cycle in Fig. 1, which is performed only once. The mesh sizes of the k th-level grid are $h_{x,k} = 2^{k-1}h_x$, $h_{y,k} = 2^{k-1}h_y$, $h_{z,k} = 2^{k-1}h_z$. We use L grids, assuming that

$$L < k_0,$$

where k_0 is maximum k for which $\max(h_{x,k}^2, h_{y,k}^2, h_{z,k}^2) \leq \tau$, (2)

$$h_{x,L}^2 = o(\tau), \quad h_{y,L}^2 = o(\tau), \quad h_{z,L}^2 = o(\tau).$$

The algorithm is performed at each time level as follows. At each smoothing step, any number of Jacobi iterations may be performed: $\Delta_{h_k}^{s+1} = \Delta_{h_k}^s - \sigma D_{h_k}^{-1}(A_{h_k} \Delta_{h_k}^s - F_{h_k})$, where $F_{h_1} = C_v \rho / \tau + f$, $\Delta_{h_1}^0 = u^n$, $F_{h_k} = R_{h_k}$, $\Delta_{h_k}^0 = 0$ ($1 < k < L$), and σ is a weight factor. Hereinafter, index h_k denotes grid functions and matrices defined on the k th-level grid. The thermal conductivity in the matrix A_{h_k} is $\bar{\kappa}$, instead of κ in A_h . Formulas for calculating $\bar{\kappa}$ on each grid in 2D problems were given in [3]. The matrix D_{h_k} is the diagonal part of the matrix A_{h_k} . The resulting grid function is denoted by u_h^{sm} or $\Delta_{h_k}^{sm}$ ($1 < k < L$). Then, a residual is calculated as $r_{h_1} = A_h u_h^{sm} - F_{h_1}$ or $r_{h_k} = A_{h_k} \Delta_{h_k}^{sm} - F_{h_k}$, where $2 < k < L$. In Fig. 1, each smoothing and residual calculation step is represented by \otimes . The restriction of a residual to the next coarser grid, represented by \searrow in Fig. 1, is calculated in a 2D problem as

$$(R_{h_{k+1}})_{lp} = r_{2i,2j}/4 + 9/64(r_{2i+1,2j} + r_{2i-1,2j} + r_{2i,2j+1} + r_{2i,2j-1}) + 81/(32^2)(r_{2i+1,2j+1} + r_{2i-1,2j-1} + r_{2i-1,2j+1} + r_{2i+1,2j-1}) - 9/(32^2)(r_{2i+3,2j+1} + r_{2i+3,2j-1} + r_{2i-3,2j+1} + r_{2i-3,2j-1} + r_{2i+1,2j+3} + r_{2i+1,2j-3} + r_{2i-1,2j+3} + r_{2i-1,2j-3})/(32^2) - (r_{2i+3,2j+3} + r_{2i+3,2j-3} + r_{2i-3,2j+3} + r_{2i-3,2j-3})/(32^2) - (r_{2i+3,2j} + r_{2i-3,2j} + r_{2i,2j+3} + r_{2i,2j-3})/64+, \quad l = i, p = j.$$
(3)

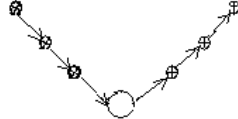


Figure 1: Structure of a multigrid cycle.

On the right-hand side of (3), index h_k is omitted. The coarse grid correction equation $A_{h_L} \Delta_{h_L} = R_{h_L}$ is solved by a direct or iterative method, as represented by \bigcirc in Fig. 1. The correction is interpolated to the next finer grid, as represented by \nearrow in Fig. 1. In the 2D problem, this is done by using the formulas

$$\tilde{\Delta}_{ij} = \begin{cases} \Delta_{lp}, & i = 2l, j = 2p, \\ \frac{9}{16}(\Delta_{lp} + \Delta_{l+1,p}) - \frac{1}{16}(\Delta_{l-1,p} + \Delta_{l+2,p}), & i = 2l + 1, j = 2p, \\ \frac{9}{16}(\Delta_{lp} + \Delta_{l,p+1}) - \frac{1}{16}(\Delta_{l,p-1} + \Delta_{l,p+2}), & i = 2l, j = 2p + 1, \\ 81(\Delta_{lp} + \Delta_{l+1,p} + \Delta_{l,p+1} + \Delta_{l+1,p+1})/256 + \\ (\Delta_{l-1,p-1} + \Delta_{l-1,p+2} + \Delta_{l+2,p+2} + \Delta_{l+2,p-1})/256 - \\ -9(\Delta_{l-1,p} + \Delta_{l-1,p+1} + \Delta_{l,p+2} + \Delta_{l+1,p+2} + \Delta_{l+2,p+1} + \\ +\Delta_{l+2,p} + \Delta_{l+1,p-1} + \Delta_{l,p-1})/256, & i = 2l + 1, j = 2p + 1. \end{cases} \quad (4)$$

On the left- and right-hand sides of (4), indices h_k and h_{k+1} are omitted, respectively. Second-order interpolation does not provide the required accuracy of solution. Analogous formulas are used to calculate $R_{h_{k+1}}$ and $\tilde{\Delta}_{h_k}$ in 3D problems. The calculations of the k th-level correction and the solution u^{n+1} , represented by \oplus in Fig. 1, are performed by the formulas $\Delta_{h_k} = \Delta_{h_k}^{sm} - \tilde{\Delta}_{h_k}$ ($1 < k < L$), $u^{n+1} = u_h^{sm} - \tilde{\Delta}_{h_1}$.

Under the conditions

$$N_x = N_y = N, \quad h_x = h_y = h, \quad \tau = h^\beta, \quad 0 < \beta < 2, \quad (5)$$

it can be shown that the computational complexity of a simple iterative solution of the equation $A_{h_L} \Delta_{h_L} = R_{h_L}$ in 2D problem (1) is $o(N^2)$ if $L > 0.25(2 - \beta) \log_2 N + 1$, which is lower than the complexity $O(N^2)$ of the rest of the algorithm. It is obvious that the proposed method reduces the computational cost at each time level, as compared to the implicit scheme used on the fine grid.

It can be shown that the computational complexity of the method, with a single smoothing iteration performed on each grid, is higher by a factor of 4.0 to 4.5 than that of an explicit finite difference solution when L is sufficiently large. At the same time, numerical and theoretical analysis for model problems shows that the method provides the accuracy and stability of the fully implicit scheme on the fine grid. This makes it

possible to significantly increase the time step, as compared to the explicit finite difference scheme, and reduce the computational cost.

3 STABILITY, ACCURACY, AND CONSERVATIVE PROPERTY: THEORETICAL ANALYSIS

We analyze the method with $L = 2$ as applied to the one-dimensional model problem (Problem 1)

$$\begin{aligned} \frac{\partial u}{\partial t} &= \frac{\partial^2 u}{\partial x^2}, & 0 < x < 1, \quad 0 < t \leq T, \\ u(x, 0) &= T_0(x), \quad u(0, t) = u(1, t) = 0, \end{aligned} \quad (6)$$

where T_0 has the appropriate number of bounded derivatives. The norm $\|\cdot\|_1$ a vector is defined as the square root of the sum of its components squared in the basis of eigenvectors of the multigrid operator defined above. It was proved in [3] that the algorithm is absolutely stable with respect to initial conditions in this norm and in the L_2 norm when $L = 2$ and $\sigma = 0.5$: $\|u^{n+1}\|_1 \leq \|u^n\|_1$, $\|u^{n+1}\|_{L_2} \leq \bar{c}\|u^0\|_{L_2}$, where $\bar{c} = \text{const}$ is independent of h, τ, n .

Denote by u^T the exact solution to the parabolic problem and let u^{im} be the fully implicit solution on the fine grid. The following theorem [3] estimates the accuracy of the solution to problem (6).

Theorem 1. *Let the fourth derivatives of the initial condition function are bounded in the L_2 norm and $\tau = h^\beta$, where $0 < \beta < 2$. Then, for any n , the solution u^n to problem (6) at the n th time level obtained with $L = 2$ using a single smoothing iteration with $\sigma = 0.5$ satisfies the estimates $\|u^n - (u^{im})^n\|_{L_2} \leq ch^2$ and $\|u^n - u^T\|_{L_2} = O(\tau + h^2)$.*

We examine the accuracy of the new method with $L \geq 2$ grids for the two-dimensional model problem (Problem 2)

$$\begin{aligned} \frac{\partial u}{\partial t} &= \frac{\partial^2 u}{\partial x^2} + \frac{\partial^2 u}{\partial y^2}, & 0 < x < 1, \quad 0 < y < 1, \quad 0 < t \leq T, \\ u(x, y, 0) &= T_0(x, y), \quad u(x, y, t) = 0 \text{ at } (x, y) \in \gamma. \end{aligned} \quad (7)$$

Theorem 2. *Let the conditions (5) be satisfied. Assume that $\|\Lambda_h u^0\|_{L_2}$, $\|(\Lambda_h u^0)_{\bar{x}\bar{x}}\|_{L_2}$, $\|(\Lambda_h u^0)_{\bar{y}\bar{y}}\|_{L_2}$ are bounded, where Λ_h is the difference operator approximating $\frac{\partial^2 u}{\partial x^2} + \frac{\partial^2 u}{\partial y^2}$ on the grid with stepsize h . Let $\|M^n\| \leq$*

c_1 , where M is the operator of the transition to the next time-layer, corresponding to the proposed method with L grids and single smoothing iteration with $\sigma = 0.5$ on each grid, $c_1 = \text{const}$ independent of n, h, τ , and L satisfies conditions (2). Then for any n it holds: $\|u^n - (u^{im})^n\|_{L_2} = o(\tau)$, $\|u^n - u^T\|_{L_2} = O(\tau + h^2)$.

Note that, if conditions (5) and (2), then $L < k_0 = [0.5(2-\beta) \log_2 N + 1]$, where $[a]$ is the integral part of a .

Note that the condition of the uniform by n boundedness of $\|M^n\|$ is equivalent to the condition of the stability of the proposed method in L_2 norm. In the general case the proof of the stability is not finalized yet due to technical complications. However, the stability of the proposed method was observed in the numerical testing of many different test problems.

To demonstrate the conservative property of the scheme of the method with $L = 2$, we have analyzed problem (7), assuming that certain grid functions are bounded in the C norm, as specified in [3], for any n . For one-dimensional problem (6), it has been proved that analogous conditions are satisfied under certain requirements for smoothness of the initial conditions. It was shown in [3] that $\sum_{i=i_1}^{i_2} \sum_{j=j_1}^{j_2} (u_{ij}^{n+1} - u_{ij}^n)h^2 = \tilde{Q}_{i_2}^1 - \tilde{Q}_{i_1-1}^1 + \tilde{Q}_{j_2}^2 - \tilde{Q}_{j_1-1}^2$, where $\tilde{Q}_i^1 = \sum_{j=j_1}^{j_2} \tau h[(u_{i+1,j} - u_{i,j})/h + O(h^2/\tau)]$, $\tilde{Q}_j^2 = \sum_{i=i_1}^{i_2} \tau h[(u_{i,j+1} - u_{i,j})/h + O(h^2/\tau)]$, $1 \leq i_1 < i_2 \leq N-1$, $1 \leq j_1 < j_2 \leq N-1$. As $h^2/\tau \rightarrow 0$, the brackets in the expressions for \tilde{Q}_i^1 and \tilde{Q}_j^2 can be interpreted as an order $O(h + h^2/\tau)$ accurate approximation of $-\vec{W}$, where $\vec{W} = -\text{grad } u$ is proportional to heat flux. Therefore, the scheme is conservative for $L = 2$.

4 PARALLELIZATION OF THE ALGORITHM

Since our method has been developed for solving parabolic equations on detailed spatial grids, a parallelization of the algorithm is required. A survey of multigrid parallelization was presented in [4]. Our approach to parallelization is based on domain decomposition without overlap. A rectangular computational domain is decomposed into rectangular subdomains containing approximately equal numbers of grid points, with even number of points in each subgrid along each direction.

After each smoothing iteration performed in a subdomain, the corresponding processor stores the values of the desired grid functions at the grid points inside the subdomain and at their nearest neighbors in other subdomains. Each processor computes the residuals r_{h_k} at the corresponding subgrid points. Then, the data transfer required before the

restriction to the next coarser grid is performed. Each processor stores the values of r_{h_k} at the grid points shown in Fig. 2a. On the coarsest grid, the solution is computed by an algorithm that can be parallelized by domain decomposition without overlap. Before a correction computed on the $(k+1)$ th-level grid is interpolated to the k th-level grid, each processor stores the correction values at the $(k+1)$ th-level subgrid points shown in Fig. 2b. The k th-level correction and the solution at the next time level are computed at the corresponding subgrid points. Before proceeding to the $(n+2)$ th time level, each processor stores the solution values at the $(n+1)$ th time level computed at the grid points inside the subdomain and at their nearest neighbors in other subdomains.

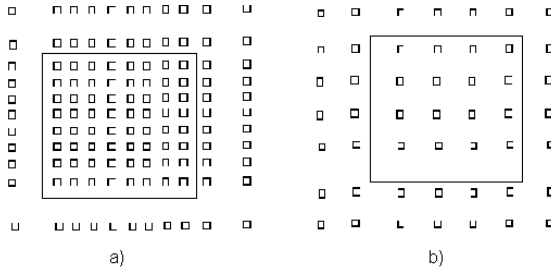


Figure 2: (a) Grid points where r_{h_k} must be known for computing $R_{h_{k+1}}$. (b) Grid points where $\Delta_{h_{k+1}}$ known for computing Δ_{h_k} . Squares delineate interior subdomains.

5 NUMERICAL RESULTS

The algorithm was tested by computing several model problems on a PC and 4-, 16-, and 64-processor of the MVS-100K supercomputer. Both coarse grid correction equations and implicit scheme on the fine grid were computed with MICCG(0) [5] or its parallelized version [6]. The model problems were solved on L grids with $L < k_0 = [0.5(2 - \beta) \log_2 N + 1]$. A single smoothing iteration was performed on each grid, with $\sigma = 0.5$, $h_x = h_y = h_z = h = 1/N$, and $0 < t \leq T = 0.2$. The resulting solution was compared with that obtained by using the fully implicit scheme on the fine grid.

Problem 1 (1) was computed on a unit square domain for $\kappa = 1$, $C_v\rho = 1$, $f = 0$, $g = 1$, and $T_0 = 1 + 32xy(1 - x)(1 - y)$. Tables 1 and 2 list the maximum relative errors $\alpha_1 = \max_n \frac{(\max_{i,j} |u_{ij}^n - (u_{ij}^{sm})^n|)}{\max_{i,j} |(u_{ij}^{sm})^n|}$ of the solutions obtained for two values of $K = \tau/h^2$, respectively. These

results demonstrate the stability and accuracy of the method as applied to Problem 1.

Computations of Problem 1 performed with $N = 4096$ and $K = 4000$ to $T = 0.04$ show that the ratio $c_{14} = t_1(p)/t_4(p)$ exceeds 30, where $t_1(p)$ and $t_4(p)$ are the time for computing Problem 1 with the implicit scheme and by the proposed method with $L = 4$ on p processors, respectively ($p = 1, 4, 16$). It can be shown that the algorithm with $N = 4096, K = 4000$, and $L = 4$ reduces the time for computing the problem by a factor of 400 to 500, as compared to the explicit scheme.

Table 1. Relative error α_1 in Problem 1 for $K = 4000$.

L	N=1024	N=2048	N=4096
L=2	0.123· 10-5	0.298· 10-6	
L=3	0.617· 10-5	0.149· 10-5	0.371· 10-6
L=4	0.234· 10-4	0.568· 10-5	0.141· 10-5
L=5	0.770· 10-4	0.187· 10-4	0.465· 10-5

Table 2. Relative error α_1 in Problem 1 for $K = 16000$.

L	N=2048	N=4096	N=8192
L=2	0.318· 10-6	0.772· 10-7	
L=3	0.163· 10-5	0.396· 10-6	0.982· 10-7
L=4	0.649· 10-5	0.158· 10-5	0.391· 10-6
L=5	0.237· 10-4	0.576· 10-5	0.143· 10-5
L=6	0.772· 10-4	0.188· 10-4	0.465· 10-5

We solved three-dimensional initial-boundary value problem (1) on a unit cube for $\kappa = 1$, $C_v\rho = 1$, $f = 0$, $g = 1$, and $T_0 = 1 + 128xyz(1 - x)(1 - y)(1 - z)$ (Problem 2). Table 3 lists $\alpha_2 = \max_n \frac{(\max_{i,j,l} |u_{ijl}^n - (u_{ijl}^{sm})^n|)}{\max_{ijl} |(u_{ijl}^{sm})^n|}$ for the resulting solutions. These results demonstrate the stability and accuracy of the method as applied to Problem 2.

Table 3. Relative error α_2 in Problem 2.

L	N=96,K=100	N=200,K=100	N=96,K=300	N=200,K=300
L=2	0.116· 10-3	0.241· 10-4	0.164· 10-3	0.296· 10-4
L=3	0.450· 10-3	0.942· 10-4	0.726· 10-3	0.133· 10-3
L=4			0.212· 10-2	0.396· 10-3

As Problem 3, we computed problem (1) on a unit square with $C_v\rho = 1$, $f = 0$, $g = 1$, $T_0 = 1 + 32xy(1-x)(1-y)$, and discontinuous thermal conductivity as a function of coordinates $\kappa = 100(1 + 0.3 \sin(10\pi x) \sin(10\pi y))$ if $(x - 0.5)^2 + (y - 0.5)^2 < 1/16$ and $\kappa = 1$ otherwise. Tables list the resulting errors α_1 . Computations of this other model problems demonstrate good accuracy of our method as applied to initial-boundary value problems for the heat equation with discontinuous parameters.

Table 4. Relative error α_1 in Problem 3 for $K = 100$.

L	N=512	N=1024	N=2048
L=2	9.167· 10-3	8.641· 10-3	5.977· 10-3
L=3	1.671· 10-2	1.559· 10-2	1.152· 10-2

Table 5. Relative error α_1 in Problem 3 for $K = 1000$.

L	N=512	N=1024	N=2048
L=2	5.092· 10-3	3.152· 10-3	2.285· 10-3
L=3	8.086· 10-3	6.391· 10-3	7.062· 10-3
L=4	1.700· 10-2	1.184· 10-2	1.301· 10-2

We have also solved a one-dimensional problem of nonlinear heat wave propagation, using the algorithm with $L = 3$ and three smoothing iterations. The computed results were almost identical to those obtained by using a fully implicit scheme.

Conclusions. A new numerical method is proposed for solving parabolic equations. Model initial-boundary value problems for the heat equation are used as examples to show theoretically and numerically that the method is similar to an implicit scheme in terms of stability and accuracy. The conservative property of the scheme of the method with $L = 2$ is demonstrated for a model problem. The method significantly reduces computational complexity as compared to implicit and explicit schemes on the fine grid.

References

1. R.P. Fedorenko, A relaxation method for solving elliptic difference equations, *Zh. Vychisl. Mat. Mat. Fiz.* **1**(5) (1961) 922-927 (in Russian).
2. W. Hackbusch, Parabolic multi-grid methods, in R. Glowinski and J.-L. Lions, eds., *Computing Methods in Applied Sciences and Engineering VI*, pp. 189-197, Amsterdam: North Holland, 1984.

3. M.E. Ladonkina, O.Yu. Milyukova, and V.F. Tishkin, Numerical algorithm for solving diffusion equations on the basis of multigrid methods, *Comp. Math. Math. Phys.* **49**(3) (2009) 502-524.
4. O.A. McBryan, P.O. Frederickson, J. Linden, A. Schüller, K. Solchenbach, K. Stüben, C.A. Thole, and U. Trottenberg, Multigrid methods on parallel computers—a survey of recent developments, *Impact Comput. Sci. Eng.* **3** (1991) 1-75.
5. I. Gustafsson, A Class of First Order Factorization Methods, *BIT* **18** (1978) 142-156.
6. O.Yu. Milyukova, Parallel approximate factorization method for solving discrete elliptic equations, *Parallel Comput.* **27** (2001) 1365-1379.

SOLUTION OF BVP FOR HYPERELASTIC MATERIAL BY MEANS OF RKPM

VRATISLAVA MOŠOVÁ

Institute of Exact Science, Moravian College
Jeremenkova 42, 772 00 Olomouc, Czech Republic.
vratislava.mosova@mvso.cz

Abstract. The numerical solution of the boundary value problem for the neo-Hookean material is presented in this contribution. The solution is realized by means of the Reproducing Kernel Particle Method (RKPM).

1 INTRODUCTION

The Reproducing kernel particle method (see [7]) belongs to the class of meshless methods. All meshless methods have, in contrast with the traditional simulation algorithms, one common feature: they need no explicitly given mesh in the beginning of computation. It is advantageous especially in 3D, because the construction of mesh in the beginning or remeshing during computation can be very time consuming process.

The initial idea of meshless methods can be found in the Smooth particle hydrodynamic method (SPHM). This method was originally used for solving problems in infinity domains (see [10]) but it gave worse results by solving problems concerning finite domains. The Reproducing kernel particle method and the Diffuse Element Method (DEM) (see [3]) are numerical algorithms that were published for solving problems from the area of solid mechanics a few years later. Possibility of application of meshless methods on parabolic problems is explored recently. For instance, a new numerical method based on the coupling between variational multiscale method and meshfree methods was developed for Burgers' equation (see [12]).

If we want roughly specify the RKPM, we can include it into the meshless methods that are based on the idea of reproducing of kernel. Note

M. Koleva and L. Vulkov (Eds.), Proceedings of the Fifth Conference on Finite Difference Methods: Theory and Applications (FDM: T&A 2010) 2011, pp. 138–146.

© Rousse University Press 2011

that the SPHM belongs also to this group. The first step in the RKPM is the construction of shape functions by means of the reproduction of kernel technique (see [8]). It is also possible to reach a formally analogical form of shape functions using the Moving least square method (see [9], [4]) or using the idea of Partition of unity (see [1]).

The theoretical foundation of RKPM are given in the article [1]. The generalization of the RKPM is Reproducing kernel hierachical partition of unity method (RKHPUM). That method was developed by Li (see [9]) in 1999 and gives possibility to work with shape functions of higher order.

Our attention will be focused on the numerical solution of problems from the finite elasticity in this contribution. Essentially we concentrate on deformations of hyperelastic neo-Hookean material. It is useful to study behaviour of such material, because it can represent, for instance, a simple model of rubber or myocardium (see [11]). The solution of such problem we want to solve by means of the RKPM.

The content of this contribution is divided into following parts: The mathematical model of hyperelastic materials is introduced in Section 2. The construction of the RKP shape functions is given in Section 3. Application of the RKPM to a boudary value problem for neo-Hookean material is built in Section 4.

2 HYPERELASTICITY

Let $\Omega \subset \mathbb{R}^3$ be a bounded open connected set that is occupied by elastic material, $\partial\Omega = \partial\Omega_0 \cup \partial\Omega_1$ be its Lipschitz continuous boundary. The set $\overline{\Omega}$ is named the reference configuration. When some forces act on $\overline{\Omega}$, it starts to change and the respective deformation is described by means of a mapping $\varphi : \overline{\Omega} \rightarrow \mathbb{R}^3$ that is smooth enough, injective (except boundary) and orientation preserving (to be physically acceptable as a deformation). New deformed configuration will be denoted by $\overline{\Omega}^\varphi$.

Next, the matrix

$$F = \nabla\varphi = \begin{pmatrix} \frac{\partial\varphi_1}{\partial x_1} & \frac{\partial\varphi_1}{\partial x_2} & \frac{\partial\varphi_1}{\partial x_3} \\ \frac{\partial\varphi_2}{\partial x_1} & \frac{\partial\varphi_2}{\partial x_2} & \frac{\partial\varphi_2}{\partial x_3} \\ \frac{\partial\varphi_3}{\partial x_1} & \frac{\partial\varphi_3}{\partial x_2} & \frac{\partial\varphi_3}{\partial x_3} \end{pmatrix}, \quad (1)$$

is named the deformation gradient. It is an important quantity in the mathematical theory of elasticity. It is associated with changes of volumes. With respect to the definition of deformation, it has to satisfy $\det\nabla\varphi > 0$.

Denote by f the body forces applied to the body Ω , g the surface forces that act on $\partial\Omega_1$ and φ_0 the deformation on $\partial\Omega_0$. Suppose that

the forces applied are conservative. Our task is to find the equilibrium position of an elastic body now. We can get it from the Cauchy theorem and the Piola transform¹. We receive the following equations (see [5])

$$-\operatorname{div} T(x, \nabla \varphi) = f(x, \varphi) \text{ in } \Omega, \quad (2)$$

$$T(x, \nabla \varphi)n = g(x, \nabla \varphi) \text{ on } \partial\Omega_1, \quad (3)$$

$$\varphi(x) = \varphi^0(x) \text{ on } \partial\Omega_0, \quad (4)$$

where $T(x, F)$ is the first Piola-Kirchhoff stress tensor and n is the unit outer normal vector.

The constitutive behaviour of hyperelastic materials is usually derived from a stored energy function W .

Definition 1. A material is hyperelastic if there exists a stored energy function $W = W(x, F)$ such that

$$T(x, F) = \frac{\partial W}{\partial F}(x, F). \quad (5)$$

Remark 1. For instance, the neo-Hookean material is used for modelling homogeneous, isotropic materials. The stored energy function has the following form in this case,

$$W = \frac{\mu}{2}(\operatorname{tr} F^T F - I) - \mu \ln(\det F^T F) + \frac{\lambda}{2} \ln(\det F^T F), \quad (6)$$

where μ, λ are the Lamé coefficients.

If we combine the relation (5) with equations (2), (3), (4), we receive that the deformation φ of a hyperelastic body satisfies the system of equations

$$-\operatorname{div} \frac{\partial W}{\partial F}(x, \nabla \varphi) = f(x, \varphi) \text{ in } \Omega, \quad (7)$$

$$\frac{\partial W}{\partial F}(x, \nabla \varphi) n = g(x, \nabla \varphi) \text{ on } \partial\Omega_1, \quad (8)$$

$$\varphi(x) = \varphi^0(x) \text{ on } \partial\Omega_0. \quad (9)$$

¹ The Cauchy theorem gives possibility to express relations between the tensor field of stress and the vector field of body and surface forces. These relations are expressed by means of a system of partial differential equations in Ω^φ and boundary conditions on $\partial\Omega^\varphi$. It is possible to bring over this system by means of the Piola transform from the deformed configuration to the reference configuration. (See [5].)

The "divergence" structure of these equations makes them amenable to a variational formulation. Since finding the minimum of the total energy functional is equivalent to a weak solution of the boundary value problem (7), (8), (9), our task is to find $\varphi \in V_0$, where

$$V_0 = \{\varphi \in W^{1,2}(\Omega) \mid \varphi = \varphi^0 \text{ on } \partial\Omega_0, \det \nabla \varphi > 0\}, \quad (10)$$

such that

$$\int_{\Omega} \frac{\partial W}{\partial F}(x, \nabla \varphi) : \nabla \psi \, dx = \int_{\Omega} f \cdot \psi \, dx + \int_{\partial\Omega_1} g \cdot \psi \, ds, \quad \forall \psi \in W_0^{1,2}(\Omega). \quad (11)$$

Remark 2. Existence of such a weak solution depends greatly on the form of the stored energy function W . In case of hyperelastic materials the question of existence of a solution can be solved on the basis of polyconvex functionals (see [2], [5]).

3 RKPM APPROXIMATION

The base for the RKPM is following integral transformation

$$u^R(x) = \int_{-\infty}^{\infty} K(x, y) u(y) \, dy. \quad (12)$$

If the kernel $K(x, y)$ is equal the Dirac function $\delta(x)$, the function $u(x)$ will be reproduced exactly. But it is difficult to deal with the Dirac function numerically. Hence we will consider the 1D approximation in form

$$\tilde{u}(x) = \int_{\Omega} \Phi(x - y) C(x, x - y) u(y) \, dy \quad (13)$$

where $\Phi(x - y)$ is some nonnegative weight function which has small support and $C(x, x - y) = \sum_{i=0}^s b_i(x)(x - y)^i$ is a correction function that allows us to achieve the desired consistency. If we expand the function $u(y)$ into a Taylor series we receive

$$\tilde{u}(x) = \int_{\Omega} \Phi(x - y) \sum_{i=0}^s b_i(x)(x - y)^i \sum_{n=0}^{\infty} \frac{(-1)^n (x - y)^n}{n!} u^{(n)}(y) \, dy. \quad (14)$$

If we multiply the expressions out, compare the coefficients of the terms and denote

$$p(x) = (1, x, x^2, \dots, x^s)^T,$$

$$\begin{aligned}
b(x) &= (b_0(x), b_1(x), \dots, b_s(x))^T, \\
m_k(x) &= \int_{\Omega} (x-y)^k \Phi(x-y) dy, \\
M(x) &= \begin{pmatrix} m_0(x) & m_1(x) & \dots & m_s(x) \\ m_1(x) & m_2(x) & \dots & m_{s+1}(x) \\ \dots & \dots & \dots & \dots \\ m_s(x) & m_{s+1}(x) & \dots & m_{2s}(x) \end{pmatrix},
\end{aligned} \tag{15}$$

we receive the following system of equations

$$M(x)b(x) = p(0).$$

Because M is non-singular it is possible to express

$$b(x) = M^{-1}(x)p(0).$$

Substitution into (13) and use of the trapezoidal quadrature for N particles lead to the RKP approximation

$$\tilde{u}(x) = \sum_{I=1}^N \Psi_I(x) u(x_I)$$

where

$$\Psi_I(x) = p^T(x_I - x) M^{-1}(x) p(0) \Phi(x_I - x) \Delta x_I$$

is the shape function.

Let us return to the problem (7), (8), (9) now. Its numerical solution we will construct in particles $x_1, \dots, x_N \in \Omega \subset \mathbb{R}^3$. At first we have to choose a monomial basis $p(x) = (p_1(x), \dots, p_l(x))$ of order s ² and some one-dimensional weight function³ Φ_1 . In \mathbb{R}^3 , the weight function can be

² For example $p(x) = (1, \xi_1, \xi_2, \xi_3, \xi_1\xi_2, \xi_1\xi_3, \xi_2\xi_3, (\xi_1)^2, (\xi_2)^2, (\xi_3)^2)$ is the monomial basis of the second order in \mathbb{R}^3 .

³ The most chosen weight functions are:

Gaussian function

$$\Phi_1(x) = \begin{cases} \frac{e^r(x^2-1)}{1-e^r} & \text{if } |x| \leq 1, \\ 0 & \text{if } |x| > 1, \end{cases}$$

where $r > 0$.

Cubic spline

$$\Phi_1(x) = \begin{cases} \frac{2}{3} - 4x^2 + 4|x|^3 & \text{if } |x| \leq \frac{1}{2}, \\ \frac{4}{3} - 4|x| + 4x^2 - \frac{4}{3}|x|^3 & \text{if } \frac{1}{2} \leq |x| \leq 1, \\ 0 & \text{if } |x| > 1. \end{cases}$$

constructed from a one-dimensional weight function in the following way

$$\Phi(x) = \prod_{i=1}^3 \Phi_1(\xi_i), \text{ where } x = (\xi_1, \xi_2, \xi_3).$$

Definition 2. Let the particles $x_1, \dots, x_N \in \Omega$, the monomial basis p of order s and the weight function Φ_1 be given. Interpolants constructed by means of the RKPM have the form

$$\tilde{\varphi}(x) = \sum_{I=1}^N \Psi_I(x) c_I. \quad (16)$$

The shape functions

$$\Psi_I(x) = p^T \left(\frac{x_I - x}{\rho} \right) b(x) \Phi \left(\frac{x_I - x}{\rho} \right) \Delta V_I, \quad (17)$$

where $\rho > 0$ is a dilatation parameter, ΔV_I is the quadrature weight and the function $b(x)$ is the solution of the system

$$M(x)b(x) = p(0). \quad (18)$$

Here, the moment matrix

$$M(x) = \sum_{I=1}^N p^T \left(\frac{x_I - x}{\rho} \right) p \left(\frac{x_I - x}{\rho} \right) \Phi \left(\frac{x_I - x}{\rho} \right) \Delta V_I. \quad (19)$$

Remark 3. The RKPM has serious limitations - it does not exactly reproduce essential (Dirichlet) boundary conditions since it uses shape functions that are not strictly interpolants. It means that there can be nodes x_J on the boundary where $\Psi_I(x_J) \neq \delta_{IJ}$. Consequently,

$$\tilde{\varphi}(x_J) = \sum_I \Psi_I(x_J) c_I \neq \varphi(x_J).$$

Several attempts have been made to solve this problem. For instance, it is possible to introduce a modified shape function that possesses Kronecker delta properties.

Conic function

$$\Phi_1(x) = \begin{cases} (1 - x^2)^k & \text{if } |x| \leq 1, \\ 0 & \text{if } |x| > 1, \end{cases}$$

where $k > 1$.

See [1], [6], [7].

Remark 4. The unique solvability of (18), (19) depends on the size of $\text{supp } \Phi$ and on the distribution of the particles x_I , $I = 1, \dots, N$. If we put

$$A(x) = \{x_I \mid x \in \text{supp } \Phi\left(\frac{x_I - x}{\rho}\right)\},$$

then a necessary condition for the unique solvability of (18), (19) is, that for $\forall x \in R^3$

$$\text{card } A(x) \geq \dim P^s.$$

(See [1].)

Remark 5. If the shape functions (17) reproduce polynomials up to order s and $h = x_I - x_{I-1}$, $I = 2, \dots, N$, then for a smooth function u the error $\|u - \tilde{u}\|$ has order $O(h^s)$. (See [1].)

4 BVP FOR NEO-HOOKEAN MATERIAL

In this section, we devote our attention to neo-Hookean material (6) that is homogeneous (i.e. $W(x, F) = W(F)$) and incompressible ($\det F = 1$). In this case, the stored energy function

$$W = \frac{\mu}{2} (\text{tr } F^T F - I). \quad (20)$$

Its derivative

$$\frac{\partial W}{\partial F} = \mu F \quad (21)$$

and the relation (11) has the form

$$\int_{\Omega} \mu F : \nabla \psi \, dx = \int_{\Omega} f \cdot \psi \, dx + \int_{\partial \Omega_1} g \cdot \psi \, ds, \quad \forall \psi \in W^{1,p}(\Omega). \quad (22)$$

We put the supposed form of the solution (16) into the weak formulation (22) now. We receive three systems of equations

$$A^j c^j = f^j + g^j, \quad j = 1, 2, 3, \quad (23)$$

where

$$A^j = \left(A_{IK}^j \right)_{I,K=1}^N, \quad A_{IK}^j = \mu \int_{\Omega} \left(\sum_{i=1}^3 \frac{\partial \Psi_I}{\partial \xi_i} \frac{\partial \Psi_K}{\partial \xi_i} \right) dx,$$

$$f^j = (f_1^j, \dots, f_N^j)^T, \quad f_K^j = \int_{\Omega} f^j \Psi_K dx, \quad K = 1, \dots, N$$

$$g^j = (g_1^j, \dots, g_N^j)^T, \quad g_K^j = \int_{\partial\Omega} g^j \Psi_K ds, \quad K = 1, \dots, N$$

and the unknown vector

$$c^j = (c_1^j, \dots, c_N^j)^T.$$

Approximation of the solution has then the form

$$\tilde{\varphi}^j(x) = \sum_{I=1}^N \Psi_I(x) c_I^j, \quad j = 1, 2, 3.$$

5 CONCLUSION

We focused our attention on hyperelastic materials and the RKPM. Hyperelastic materials serve for modelling of large deformations. The RKPM belongs to meshless methods. It means that no explicitly given mesh is required at the beginning of computation. This fact is suitable in case of large deformation of domains. The basic concept and implementation of the RKPM for solving problems of finite elasticity in case of neo-Hookean material have been presented in this contribution.

References

1. Babuška, I., Banerjee, U. , Osborn, J. E.: Survey of meshless and generalized finite element methods: An unified approach, *Acta Numer.* (2003) 1-125
2. Ball, J. M., Constitutive inequalities and existence theorems in nonlinear elasto-statics. In R. J. Knops, editor, *Nonlinear Analysis and Mechanics*, Heriot-Watt Symposium, Vol. 1. Pitman, (1977).
3. Belytschko, T., Lu, Y., Gu, I.: Element-Free Galerkin Methods, *Internat. J. Numer. Methods Engrg.* **37** (1994) 229-256.
4. Belytschko, T., Guo, Y., Liu, W.K.: A unified stability analysis of meshless particle methods, *Internat. J. Numer. Methods Engrg.* **48** (2000) 1359-1400.
5. Ciarlet, P. G.: *Mathematical Elasticity*. North-Holland Amsterodam (1988), 1-215
6. Fries, T. P., Matthies, H. G.: *Classification and Overview of Meshfree Methods*, Technical University Braunschweig, Germany, (2004)
7. Chen, J. S., Pan, C., Wu, C. T., Liu, W. K.: Reproducing kernel particle methods for large deformation analysis of non-linear structures, *Comput. Methods Appl. Mech. Engrg.* **139** (1996) 195-227.
8. Chen, J. S., Pan, C., Wu, C. T.: Large deformation analysisiss of rubber based on a reproducing kernel particle methods, *Comput. Mech.* **19** (1997) 211-227.
9. Li, S. , Liu, W. K.: Reproducing kernel hierarchical partition of unity, *Internat. J. Numer. Methods Engrg.* **45** (1999) 251 - 317.
10. Monaghan, J. J.: Why Particle Methods Work., *Sci. Stat. Comput.* **3**(4) (1982) 422-433.

11. Stypa, J.: *Existenz Einer Lösung für die Nichtlineare Elastizitätstheorie mit Anwendung in der Hertzmechanik*, Wesfälischen Wilhelms- Universität Münster (2000)
12. Zhang, L., Ouyang, J., Wang, X., Zhang, X.: Variational multiscale element-free Galerkin method for 2D Burgers equation, *Journal of Computational Physics* **229**(19) (2010) 7147-7161.

THE SOLUTIONS OF FRACTIONAL STURM-LIOUVILLE PROBLEMS WITH α - ORDINARY AND SINGULAR POINTS

A. NEAMATY¹ AND R. DARZI²

¹ Department of Mathematics, University of Mazandaran, Babolsar, Iran

Namaty@umz.ac.ir

² Islamic Azad University Neka Branch, Neka, Iran

R.Darzi@umz.ac.ir

Abstract. In this paper, is verified the solution around an α -ordinary point $x_0 \in [a, b]$ for fractional Sturm-Liouville equation

$$D^{2\alpha}y(x) + p(x)y(x) = \lambda q(x)y(x), \quad \frac{1}{2} < \alpha \leq 1. \quad (1)$$

Also, the solutions around an singular point $x_0 \in [a, b]$ for fractional differential equation

$$(x-x_0)^{2\alpha} D^{2\alpha}y(x) + p(x)y(x) = (x-x_0)^{2\alpha} \lambda q(x)y(x), \quad \frac{1}{2} < \alpha \leq 1, \quad (2)$$

is investigated. Here, $p(x)$ and $q(x)$ are α -analytic functions and $D^{2\alpha}y(x)$ represents sequential fractional derivative of order 2α of function $y(x)$. The fractional derivative are described in the Caputo sense.

1 INTRODUCTION

Fractional differential equation have become important tool for modeling the anomalous dynamics of numerous processes involving complex systems found in many diverse fields of science and engineering [2,3]. The linear sequential fractional differential equation of order $n\alpha$ with constant coefficients has been extensively studied, and there are methods to obtain explicitly the general solution for both equation, homogeneous and non-homogeneous, without using the integral transform. Here, we apply the series method, based on the expansion of the unknown solution $y(x)$ in a fractional power series [1,4] to obtain solutions of fractional Sturm-Liouville equation. In singular sense we present a generalization of the Frobenius theory.

M. Koleva and L. Vulkov (Eds.), Proceedings of the Fifth Conference on Finite Difference Methods: Theory and Applications (FDM: T&A 2010) 2011, pp. 147–153.

© Rousse University Press 2011

2 FRACTIONAL CALCULUS

Definition 1. A real function $f(x)$, $x > 0$, is said to be in the space C_μ , $\mu \in R$ if there exists a real number $n(> \mu)$, such that $f(x) = x^n f_1(x)$, where $f_1(x) \in C[0, \infty)$, and it is said to be in the space C_μ^k if and only if $f^{(k)} \in C_\mu$, $k \in N$.

Definition 2. The Riemann-Liouville fractional integral operator of order of $\nu > 0$, of a function $f \in C_\mu$, $\mu \geq -1$, is defined as [7]

$$I_a^\nu f(x) = \frac{1}{\Gamma(\nu)} \int_a^x (x-r)^{\nu-1} f(r) dr.$$

$$I^\nu f(x) = I_0^\nu f(x), \quad I^0 f(x) = f(x).$$

Definition 3. The fractional Caputo's derivative of f is given by

$$D^\nu f(x) = I^{k-\nu} D^k f(x) = \frac{1}{\Gamma(k-\nu)} \int_0^x (x-r)^{k-\nu-1} f^{(k)}(r) dr.$$

where, $f \in C_{-1}^k$, $k-1 < \nu \leq k$ for $k \in N$, $x > 0$.

Noting to above definitions, for $k-1 < \nu \leq k$, $k \in N$, and $f \in C_\mu^k$, $\mu \geq -1$ and also $x > 0$, we have

- i) $D_a^\nu I_a^\nu f(x) = f(x)$
- ii) $I_a^\nu D_a^\nu f(x) = f(x) - \sum_{j=0}^{k-1} f^{(j)}(0^+) \frac{(x-a)^j}{j!}$.

Definition 4. Fractional differential of order 2α of function $y(x)$ is defined as:

$$D_{a+}^{2\alpha} y(x) = D_{a+}^\alpha D_{a+}^\alpha y(x).$$

where D_{a+}^α denote the Caputo fractional derivative of order α .

Definition 5. Let $\alpha \in (0, 1]$, $f(x)$ be a real function defined on the interval $[a, b]$ and $x_0 \in [a, b]$. Then $f(x)$ is said to be α -analytic at x_0 , if there exists an interval $N(x_0)$ such that for $x \in N(x_0)$, $f(x)$ can be expressed as $\sum_{n=0}^{\infty} a_n (x-x_0)^{n\alpha}$ ($a_n \in R$), this series being absolutely convergent for $|x-x_0| < r$ ($r > 0$).

Definition 6. A point $x_0 \in [a, b]$ is said to be an α -ordinary point of the Eq.(1), if $p(x)$ and $q(x)$ are α -analytic in x_0 .

Definition 7. Let $\alpha \in (0, 1]$, $a \in R$ and $\beta \in R \setminus Z^-$. Then, the derivative of order 2α of $(x-a)^\beta$ is defined as: $D_{a+}^{2\alpha} (x-a)^\beta = \frac{\Gamma(\beta+1)}{\Gamma(\beta-2\alpha+1)} (x-a)^{\beta-2\alpha}$.

Definition 8. *The Mittag-Leffler function $E_\nu(z)$ for $\nu > 0$ and $z \in C$ is defined by the series representation:*

$$E_\nu(z) = \sum_{k=0}^{\infty} \frac{z^k}{\Gamma(k\nu + 1)}, \quad \nu > 0, \quad z \in C.$$

3 SOLUTIONS OF FRACTIONAL STURM-LIOUVILLE PROBLEM WITH α -ORDINARY AND SINGULAR POINTS

In first, we consider the solutions around α -ordinary point $x_0 > a$ to the Eq.(1).

Theorem 1. *Let $\alpha \in (\frac{1}{2}, 1]$, and $x_0 > a$ be a α -ordinary point of the Sturm-Liouville equation*

$$D^{2\alpha}y(x) + p(x)y(x) = \lambda q(x)y(x), \quad (3)$$

where $p(x) = \sum_{n=0}^{\infty} p_n(x-x_0)^{n\alpha}$ and $q(x) = \sum_{n=0}^{\infty} q_n(x-x_0)^{n\alpha}$ are power series expansion of the α -analytic function $p(x)$ and $q(x)$, respectively. Then, there exists function

$$y(x) = \sum_{n=0}^{\infty} a_n(x-x_0)^{n\alpha}, \quad (4)$$

which is the solution of Eq.(3) for $x \in (x_0, x_0 + r)$, ($r > 0$). Here, a_0 is a non-zero arbitrary constant, $a_1 = 0$ and the coefficients a_n , $n = 2, 3, \dots$, are given by

$$a_{n+2} = \frac{\Gamma(n\alpha + 1)(\lambda c_n - b_n)}{\Gamma((n+2)\alpha + 1)}, \quad n = 0, 1, 2, \dots,$$

where $b_n = \sum_{l=0}^n p_l a_{n-l}$ and $c_n = \sum_{l=0}^n q_l a_{n-l}$.

Proof. We shall seek a solution of Eq.(3) of the form $\sum_{n=0}^{\infty} a_n(x-x_0)^{n\alpha}$. Substituting (4) in (3) and definition (2.7), we get

$$\begin{aligned} & \sum_{n=1}^{\infty} \frac{\Gamma(n\alpha + 1)}{\Gamma((n-2)\alpha + 1)} a_n (x-x_0)^{(n-2)\alpha} \\ & + \sum_{n=0}^{\infty} \left(\sum_{l=0}^n a_l p_{n-l} - \lambda \sum_{l=0}^n a_l q_{n-l} \right) (x-x_0)^{n\alpha} = 0. \end{aligned}$$

To add the two series, it is necessary that both summation indices start with the same number and that the powers of x in each series be "in

phase" that is, if one series starts with a multiple of, say, x to the first power, then we want the other series to start with the same power. Here, the first series starts with $x^{-\alpha}$, whereas the second series starts with x^0 . By writing the first term of the first series outside the summation notation, we see that both series start with the same power of x - namely x^0

$$\begin{aligned} & a_1 \frac{\Gamma(\alpha+1)}{\Gamma(1-\alpha)} (x-x_0)^{-\alpha} + \sum_{n=2}^{\infty} \frac{\Gamma(n\alpha+1)}{\Gamma((n-2)\alpha+1)} a_n (x-x_0)^{(n-2)\alpha} \\ & + \sum_{n=0}^{\infty} \left(\sum_{l=0}^n a_l p_{n-l} - \lambda \sum_{l=0}^n a_l q_{n-l} \right) (x-x_0)^{n\alpha} = 0. \end{aligned}$$

Now, to get the same summation index, we are inspired by the exponents of x . Let us, replace n by $n+2$ in the first series. We are in a position to add the series in term by term

$$\begin{aligned} & a_1 \frac{\Gamma(\alpha+1)}{\Gamma(1-\alpha)} (x-x_0)^{-\alpha} + \sum_{n=0}^{\infty} \left\{ \frac{\Gamma((n+2)\alpha+1)}{\Gamma(n\alpha+1)} a_{n+2} \right. \\ & \left. + \left(\sum_{l=0}^n a_l p_{n-l} - \lambda \sum_{l=0}^n a_l q_{n-l} \right) \right\} (x-x_0)^{n\alpha} = 0. \end{aligned} \quad (5)$$

Since (5) is identically zero, it is necessary that the coefficient of each power of x be set equal to zero. So, we obtain $a_1 = 0$ and the following recurrence formula

$$a_{n+2} = \frac{\Gamma(n\alpha+1)(\lambda c_n - b_n)}{\Gamma((n+2)\alpha+1)}, \quad n = 0, 1, 2, \dots, \quad (6)$$

with

$$b_n = \sum_{l=0}^n p_l a_{n-l}, \quad c_n = \sum_{l=0}^n q_l a_{n-l}$$

which allows us to express a_n ($n \geq 2$), in terms of a_0 and a_1 . Now, we prove the convergence of the series (4). Let $0 < r_1 < r$, since $p(x)$ and $q(x)$ are convergent, there exist constants $M_1 > 0$ and $M_2 > 0$, such that $|p_{n-l}| \leq \frac{M_1 r^{l\alpha}}{r^{n\alpha}}$ and $|q_{n-l}| \leq \frac{M_2 r^{l\alpha}}{r^{n\alpha}}$. Consequently,

$$\left| \frac{\Gamma((n+2)\alpha+1)}{\Gamma(n\alpha+1)} \right| |a_{n+2}| \leq \frac{(M_1 + |\lambda|M_2) \left(\sum_{l=0}^n a_l r^{l\alpha} \right)}{r^{n\alpha}}.$$

Now, we define $d_0 = |a_0|$, $d_1 = 0$ and d_n ($n > 0$) as follows:

$$\left| \frac{\Gamma((n+2)\alpha+1)}{\Gamma(n\alpha+1)} \right| d_{n+2} = \frac{(M_1 + |\lambda|M_2) \left(\sum_{l=0}^n d_l r^{l\alpha} \right)}{r^{n\alpha}}. \quad (7)$$

Using the asymptotic representation

$$\frac{\Gamma(w+a)}{\Gamma(w+b)} = w^{a-b} \left[1 + O\left(\frac{1}{t}\right) \right], \quad |\arg(w+a)| < \pi, \quad |w| \rightarrow \infty, \quad (8)$$

we have that the series $\sum_{n=0}^{\infty} d_n (x - x_0)^{n\alpha}$, converges for all x , such that $|x - x_0| < r_1$, and from this we conclude that the series (4) converges for $x - x_0 < r$.

Example 1. Consider the regular fractional eigenvalue problem

$$D^{\frac{3}{2}}y(x) + \lambda y(x) = 0. \quad (9)$$

subject to

$$y'(0) = 0, \quad y(1) = 0.$$

We shall seek to this equation the solution around the α -ordinary point $x_0 = 0$. According with theorem (3.1) the general solution is $y(x) = \sum_{n=0}^{\infty} a_n x^{n\alpha}$, where a_0 is arbitrary constant, $a_1 = 0$ and $a_{n+2} = \frac{(-\lambda)^{\frac{n}{2}}}{\Gamma(\frac{3n}{4}+1)} a_0$, $n = 0, 1, 2, \dots$. Thus, general solution is

$$y(x) = a_0 \sum_{n=0}^{\infty} \frac{(-\lambda x^{\frac{3}{2}})^n}{\Gamma(\frac{3n}{2}+1)} = a_0 E_{\frac{3}{2}}(-\lambda x^{\frac{3}{2}}),$$

where $E_{\frac{3}{2}}$ denotes the Mittage-Leffler function.

The results are the same as ADM [5]. It is interesting that the obtained results are same as HAM [6], when we consider $h = -1$, in HAM. Now, by using boundary condition, we explore the first three eigenvalues ($\lambda_{1,i}$, $\lambda_{2,i}$ and $\lambda_{3,i}$) numerically in following table where represents the number of terms used in the following series, i.e.

$$y(t) \cong \sum_{n=0}^i y_n(t).$$

The numerical evidence in table suggests that the first three eigenvalue are

$$\lambda_1 = 2.11027708, \quad \lambda_2 = 13.76538223, \quad \lambda_3 = 24.24328676$$

Table 1.: The approximation to the first three eigenvalues

i	$\lambda_{1,i}$	$\lambda_{2,i}$	$\lambda_{3,i}$
17	2.11027708	13.76538387	24.10237991
18	2.11027708	13.76538208	24.26958889
19	2.11027708	13.76538224	24.23941883
20	2.11027708	13.76538223	24.24383027
21	2.11027708	13.76538223	24.24329538
22	2.11027708	13.76538223	24.24328578
23	2.11027708	13.76538223	24.24328687
24	2.11027708	13.76538223	24.24328675
25	2.11027708	13.76538223	24.24328676

Now, we consider the solutions around singular point $x_0 > a$ to the equation

$$(x-x_0)^{2\alpha} D^{2\alpha}y(x) + p(x)y(x) = (x-x_0)^{2\alpha} \lambda q(x)y(x), \quad \frac{1}{2} < \alpha \leq 1, \quad (10)$$

where $p(x) = \sum_{n=0}^{\infty} p_n (x-x_0)^{n\alpha}$ and $q(x) = \sum_{n=0}^{\infty} q_n (x-x_0)^{n\alpha}$ are power series expansion of the α -analytic function $p(x)$ and $q(x)$, respectively.

Theorem 2. Let $\alpha \in (\frac{1}{2}, 1]$, and $x_0 > 0$ be a singular point of the Eq.(10). Then, there exists a unique solution on semi interval (x_0, x_0+r) , for some $(r > 0)$ of Eq.(10) given by

$$y(x) = (x-x_0)^s \sum_{n=0}^{\infty} a_n (x-x_0)^{n\alpha}, \quad (11)$$

where $a_0 \neq 0$ and s being a number to be determined.

Proof. We shall seek a solution of Eq.(10) of the form (11). Substituting (11) in (10) and using (2.7), similar to theorem (3.1), we get

$$\begin{aligned} a_0 \left(\frac{\Gamma(s+1)}{\Gamma(s-2\alpha+1)} + p_0 \right) (x-x_0)^s + & \left(a_1 \frac{\Gamma(s+\alpha+1)}{\Gamma(s-\alpha+1)} + p_0 a_1 + p_1 a_0 \right) (x-x_0)^{s+\alpha} \\ & + \sum_{n=2}^{\infty} a_n \left(\frac{\Gamma(n\alpha+s+1)}{\Gamma((n-2)\alpha+s+1)} + b_n - \lambda c_{n-2} \right) (x-x_0)^{n\alpha+s} = 0 \end{aligned}$$

where

$$b_n = \sum_{l=0}^n p_l a_{n-l}, \quad c_n = \sum_{l=0}^n q_l a_{n-l}.$$

So, since $a_0 \neq 0$, we obtain

$$\frac{\Gamma(s+1)}{\Gamma(s-2\alpha+1)} + p_0 = 0, \quad a_1 = \frac{-p_1 a_0}{\frac{\Gamma(s+\alpha+1)}{\Gamma(s-\alpha+1)} + p_0},$$

$$a_n = \frac{\lambda c_{n-2} - b_{n-1}}{\frac{\Gamma(n\alpha+s+1)}{\Gamma((n-2)\alpha+s+1)} + p_0}, \quad n = 2, 3, \dots$$

The proof of convergence for $x - x_0 < r$ is analogous to that used for theorem (3.1), if we take into account the above mentioned asymptotic relation (7).

Example 2. Consider the following fractional equation

$$x^{\frac{3}{2}} D^{\frac{3}{2}} y(x) + y(x) = \lambda x^{\frac{3}{2}} y(x). \quad (12)$$

Let us find seek to equation (11), the solution around singular point $x = 0$. According with theorem (3.2), we obtain $s = -.25$. Since $a_0 \neq 0$ is arbitrary constant, we get

$$a_1 = 0, \quad a_2 = \frac{\lambda a_0}{\frac{\Gamma(\frac{9}{4})}{\Gamma(\frac{3}{4})} + 1} \quad a_3 = \frac{a_2}{\frac{\Gamma(3)}{\Gamma(\frac{3}{2})} + 1}, \quad \dots$$

Remark 1. For the case when the Caputo derivatives is replaced by the Riemann-Liouville derivative the results coincide exactly with those in the Caputo sense.

References

1. M.A. Al-Bassam, Some existence theorems on differential equations of generalized order, *J. Reine Angew. Math* **218** (1965) 70 - 78.
2. B. Bonilla, M. Rivero, J.J. Trujillo, *Theory of Sequential Linear Differential Equations. Application*, Departamento de Analysis Mathematico, Universidad de La Laguna, 2005.
3. A.A. Kilbas, H.M. Srivastava, J.J. Trujillo, *Theory and Application of Fractional Differential Equation*, Elsevier Amsterdam, 2006.
4. A.A. Kilbas, J.J. Trujillo, Differential equation of fractional order: Methods, results and problems, *Appl. Anal.* **78** (2001) 153 - 192.
5. Q. M. Al-Mdallal, An efficient method for solving fractional sturm-liouville problems, *Chaos Solitons and Fractals* **78** (2009) 183-189.
6. A. Neamaty, R. Darzi, A. Dabbaghian, Homotopy analysis method for solving fractional sturm-liouville problems, *Aus. J. Basic. Appl.Sci* (in press).
7. K. S. Miller, *An Introduction to the Fractional Calculus and Fractional Differential Equation*, JohnWiley and Sons, New York, (1993).

FINITE - DIFFERENCE METHOD FOR COMPUTATION OF THE 3-D GAS DYNAMICS EQUATION WITH ARTIFICIAL VISCOSITY

I.V. POPOV AND I.V. FRYAZINOV

4A Miusskaya square, 125047, Moscow, Russia, Institute for Mathematical Modeling,
Russian Academy of Sciences

Abstract. In this work a new numerical method for the solution of the gas dynamics problems for 3-D systems in Eulerian variables is presented. The proposed method uses the approximation $O(\tau^2 + h_x^2 + h_y^2 + h_z^2)$ in the areas of the solution's smoothness and beyond the compression waves, τ for the time step, h_x, h_y, h_z for the space variables steps. In the proposed difference scheme in addition to the Lax-Wendroff corrections, artificial viscosity μ monotonizing the scheme is introduced. The viscosity is obtained from the conditions of the maximum principle. Test calculations of contact breaks movement, shock waves and disintegration of breaks were performed.

1 INTRODUCTION

The presented work is devoted the further development of a method of adaptive artificial viscosity (AAV) in three-dimensional Cartesian system of co-ordinates. As well as earlier in works [1], method AAV was tested for problems of gas dynamics.

2 PROBLEM STATEMENT

Let's consider Euler's equations in the Cartesian three-dimensional system of co-ordinates:

$$\frac{\partial}{\partial t}(\mathbf{U}) + \frac{\partial}{\partial x}\mathbf{F}_1(\mathbf{U}) + \frac{\partial}{\partial y}\mathbf{F}_2(\mathbf{U}) + \frac{\partial}{\partial z}\mathbf{F}_3(\mathbf{U}) = 0, \quad (1)$$

M. Koleva and L. Vulkov (Eds.), Proceedings of the Fifth Conference on Finite Difference Methods: Theory and Applications (FDM: T&A 2010) 2011, pp. 154–165.

© Rousse University Press 2011

where $\mathbf{U} = (\rho, I_x, I_y, I_z, E)^T$, $\mathbf{F}_1(\mathbf{U}) = (\rho u, I_x u + p, I_y u, I_z u, (E + p)u)^T$, $\mathbf{F}_2(\mathbf{U}) = (\rho v, I_x v, I_y v + p, I_z v, (E + p)v)^T$, $\mathbf{F}_3(\mathbf{U}) = (\rho w, I_x w, I_y w, I_z w + p, (E + p)w)^T$, ρ is the density, $\mathbf{v} = (u, v, w)$ is the velocity, $\mathbf{I} = \mathbf{v}\rho$ is the momentum, $E = e + \rho \frac{u^2 + v^2 + w^2}{2}$ is the total energy of gas, $e = \rho\varepsilon$ is the internal energy of gas. These equations are solved in the region $0 < x < l_x$, $0 < y < l_y$, $0 < z < l_z$, $t > 0$. The system of equations is closed by the ideal gas equation $p = (\gamma - 1)e$, γ is an indicator of adiabatic curve Poisson.

At the ends of the interval and at the initial time the functions ρ , \mathbf{v} , and E (or p) are specified. On a hard wall, zero density and momentum flux are given and velocity is equal to zero.

3 APPROXIMATION OF THE EQUATION SYSTEM

For presentation simplicity, in the initial domain $0 < q < l_q$, $q = x, y, z$, a uniform grid will be introduced with the step $h_q = \frac{l_q}{N_q - 1}$, where N_q is the number of points of division on co-ordinate q .

Let us introduce the time step τ , whose value will be determined later.

Let's write out initial system of the equations taking into account amendments Lax-Wendroff in the form of difference-differential. We will consider the equation of continuity, we use decomposition:

$$\rho^{n+1} = \rho^n + \tau \frac{\partial \rho^n}{\partial t} + \frac{\tau^2}{2} \frac{\partial^2 \rho^n}{\partial t^2} + \dots$$

The first derivative on time we will express from of the continuity equation, replacing it on

$$\frac{\partial \rho^n}{\partial t} = - \left(\frac{\partial}{\partial x} (\rho u)^n + \frac{\partial}{\partial y} (\rho v)^n + \frac{\partial}{\partial z} (\rho w)^n \right).$$

To find the second derivative on time differentiate the equation of continuity on time and we use the equation for an impulse. We will receive for the third composed following representation:

$$\begin{aligned} \frac{\partial^2 \rho^n}{\partial t^2} &= - \frac{\partial}{\partial t} \left[\frac{\partial}{\partial x} (\rho u)^n + \frac{\partial}{\partial y} (\rho v)^n + \frac{\partial}{\partial z} (\rho w)^n \right] = \\ &= \frac{\partial^2}{\partial x^2} (\rho u^2 + p)^n + \frac{\partial^2}{\partial y^2} (\rho v^2 + p)^n + \frac{\partial^2}{\partial z^2} (\rho w^2 + p)^n + \end{aligned}$$

$$+2\frac{\partial^2}{\partial x\partial y}(\rho uv)^n+2\frac{\partial^2}{\partial x\partial z}(\rho uw)^n+2\frac{\partial^2}{\partial y\partial z}(\rho vw)^n=0.$$

As a result, we have following difference-differential the equation

$$\frac{\rho^{n+1}-\rho^n}{\tau}+\frac{\partial}{\partial x}\left(W_\rho^x\right)^n+\frac{\partial}{\partial y}\left(W_\rho^y\right)^n+\frac{\partial}{\partial z}\left(W_\rho^z\right)^n=0. \quad (2)$$

Where

$$\begin{aligned} W_\rho^x &= \rho u - \frac{\tau}{2} \left[\frac{\partial}{\partial x} (\rho u^2) + \frac{\partial}{\partial y} (\rho uv) + \frac{\partial}{\partial z} (\rho uw) + \frac{\partial p}{\partial x} \right], \\ W_\rho^y &= \rho v - \frac{\tau}{2} \left[\frac{\partial}{\partial x} (\rho uv) + \frac{\partial}{\partial y} (\rho v^2) + \frac{\partial}{\partial z} (\rho vw) + \frac{\partial p}{\partial y} \right], \\ W_\rho^z &= \rho w - \frac{\tau}{2} \left[\frac{\partial}{\partial x} (\rho uw) + \frac{\partial}{\partial y} (\rho vw) + \frac{\partial}{\partial z} (\rho w^2) + \frac{\partial p}{\partial z} \right], \end{aligned}$$

are components of density flux.

The derived equation (2) in the difference form will be as follows

$$\begin{aligned} \rho_{ikm}^{n+1} &= \rho_{ikm}^n - \tau \frac{\left(W_\rho^x\right)_{i+1/2km}^n - \left(W_\rho^x\right)_{i-1/2km}^n}{h_x} - \\ &- \tau \frac{\left(W_\rho^y\right)_{ik+1/2m}^n - \left(W_\rho^y\right)_{ik-1/2m}^n}{h_y} - \tau \frac{\left(W_\rho^z\right)_{ikm+1/2}^n - \left(W_\rho^z\right)_{ikm-1/2}^n}{h_z}, \end{aligned}$$

where

$$\begin{aligned} \left(W_\rho^x\right)_{i+1/2km}^n &= \frac{u_{i+1km}^n + u_{ikm}^n}{2} \frac{\rho_{i+1km}^n + \rho_{ikm}^n}{2} - \left(LW_\rho^x\right)_{i+1/2km}^n, \\ \left(W_\rho^y\right)_{ik+1/2m}^n &= \frac{v_{ik+1m}^n + v_{ikm}^n}{2} \frac{\rho_{ik+1m}^n + \rho_{ikm}^n}{2} - \left(LW_\rho^y\right)_{ik+1/2m}^n, \\ \left(W_\rho^z\right)_{ikm+1/2}^n &= \frac{w_{ikm+1}^n + w_{ikm}^n}{2} \frac{\rho_{ikm+1}^n + \rho_{ikm}^n}{2} - \left(LW_\rho^z\right)_{ikm+1/2}^n, \end{aligned}$$

are the Lax-Wendroff corrections.

$$\begin{aligned} \left(LW_\rho^x\right)_{i+1/2km}^n &= \frac{\tau}{2} \left[\frac{(\rho u^2 + p)_{i+1km}^n - (\rho u^2 + p)_{ikm}^n}{h_x} \right] + \\ &+ \frac{\tau}{8} \left[\frac{(\rho uv)_{i+1k+1m}^n - (\rho uv)_{i+1k-1m}^n}{h_y} + \frac{(\rho uv)_{ik+1m}^n - (\rho uv)_{ik-1m}^n}{h_y} \right] + \end{aligned}$$

$$\begin{aligned}
& \frac{\tau}{8} \left[\frac{(\rho uw)_{i+1km+1}^n - (\rho uw)_{i+1km-1}^n}{h_z} + \frac{(\rho uw)_{ikm+1}^n - (\rho uw)_{ikm-1}^n}{h_z} \right], \\
& \left(LW_\rho^y \right)_{ik+1/2m}^n = \frac{\tau}{2} \left[\frac{(\rho v^2 + p)_{ik+1m}^n - (\rho v^2 + p)_{ikm}^n}{h_y} \right] + \\
& \frac{\tau}{8} \left[\frac{(\rho uv)_{i+1k+1m}^n - (\rho uv)_{i-1k+1m}^n}{h_x} + \frac{(\rho uv)_{i+1km}^n - (\rho uv)_{i-1km}^n}{h_x} \right] + \\
& \frac{\tau}{8} \left[\frac{(\rho vw)_{ik+1m+1}^n - (\rho vw)_{ik+1m-1}^n}{h_z} + \frac{(\rho vw)_{ikm+1}^n - (\rho vw)_{ikm-1}^n}{h_z} \right], \\
& \left(LW_\rho^z \right)_{ik+1/2m}^n = \frac{\tau}{2} \left[\frac{(\rho w^2 + p)_{ikm+1}^n - (\rho w^2 + p)_{ikm}^n}{h_z} \right] + \\
& \frac{\tau}{8} \left[\frac{(\rho uw)_{i+1km+1}^n - (\rho uw)_{i-1km+1}^n}{h_x} + \frac{(\rho uw)_{i+1km}^n - (\rho uw)_{i-1km}^n}{h_x} \right] + \\
& \frac{\tau}{8} \left[\frac{(\rho vw)_{ik+1m+1}^n - (\rho vw)_{ik-1m+1}^n}{h_y} + \frac{(\rho vw)_{ik+1m}^n - (\rho vw)_{ik-1m}^n}{h_y} \right].
\end{aligned}$$

By analogy, equations for the momentum and energy will be written in the flux form. We have

$$\begin{aligned}
I_{ikm}^{n+1} &= I_{ikm}^n - \tau \frac{(W_I^x)_{i+1/2km}^n - (W_I^x)_{i-1/2km}^n}{h_x} - \\
&- \tau \frac{(W_I^y)_{ik+1/2m}^n - (W_I^y)_{ik-1/2m}^n}{h_y} - \tau \frac{(W_I^z)_{ikm+1/2}^n - (W_I^z)_{ikm-1/2}^n}{h_z}, \\
E_{ikm}^{n+1} &= E_{ikm}^n - \tau \frac{(W_E^x)_{i+1/2km}^n - (W_E^x)_{i-1/2km}^n}{h_x} - \\
&- \tau \frac{(W_E^y)_{ik+1/2m}^n - (W_E^y)_{ik-1/2m}^n}{h_y} - \tau \frac{(W_E^z)_{ikm+1/2}^n - (W_E^z)_{ikm-1/2}^n}{h_z}.
\end{aligned}$$

Lax-Wendroff corrections result in the approximation $O(\tau^2 + h_x^2 + h_y^2 + h_z^2)$. They are insufficient for the scheme's monotonicity. Additional dissipation must be introduced into the difference scheme (artificial viscosity).

4 ARTIFICIAL VISCOSITY

Let's enter artificial viscosity μ into considered grid equations. To the fluxes $(W_q^\alpha)^n$ (where $q = \rho, I, E$, $\alpha = x, y, z$) we will add the term

$$\begin{aligned}(W_{\mu q}^x)_{i+1/2km}^n &= \bar{\mu}_{i+1/2km}^n \frac{q_{i+1km}^n - q_{ikm}^n}{h_x}, \\ (W_{\mu q}^y)_{ik+1/2m}^n &= \bar{\mu}_{ik+1/2m}^n \frac{q_{ik+1m}^n - q_{ikm}^n}{h_y}, \\ (W_{\mu q}^z)_{ikm+1/2}^n &= \bar{\mu}_{ikm+1/2}^n \frac{q_{ikm+1}^n - q_{ikm}^n}{h_z}.\end{aligned}$$

Then, the equations can be written as

$$\begin{aligned}\frac{q^{n+1} - q^n}{\tau} + \frac{\partial (W_q^x)^n}{\partial x} + \frac{\partial (W_q^y)^n}{\partial y} + \frac{\partial (W_q^z)^n}{\partial z} &= \\ = \frac{\partial (W_{\mu q}^x)^n}{\partial x} + \frac{\partial (W_{\mu q}^y)^n}{\partial y} + \frac{\partial (W_{\mu q}^z)^n}{\partial z}.\end{aligned}$$

Let's receive now artificial viscosity μ . For this purpose we will consider a special case $\mathbf{v} = \mathbf{v}_0$, $p = p_0$, where \mathbf{v}_0 is the constant vector, p_0 is the constant. Then, the continuity equation can be written as

$$\frac{\partial \rho}{\partial t} + u_0 \frac{\partial \rho}{\partial x} + v_0 \frac{\partial \rho}{\partial y} + w_0 \frac{\partial \rho}{\partial z} = 0.$$

The equations for the impulse I_α ($\alpha = x, y, z$), and the energy E are obtained by multiplying the last equality at u_0, v_0, w_0 and $\frac{|\mathbf{v}_0|^2}{2}$, respectively. If in the equations for ρ, I_α , and E viscosity would be various, then there could be computational complexity. Therefore, we choose viscosities μ to be the same for all equations.

As in the one-dimensional case [1], we replace in the grid continuity equation $p_{x_\alpha \hat{x}_\alpha}$ at $(c^2 \rho_{x_\alpha})_{\hat{x}_\alpha} + (\alpha S_{x_\alpha})_{\hat{x}_\alpha}$, where S is the entropy, and freeze the coefficients c^2 , v_α and $\bar{\mu}_\alpha$ for ρ_{x_α} . We moved to the right side the Lax-Wendroff amendments, containing the differences through the point $\rho_{x_\beta}^\circ$, which slightly affects the monotony of the difference scheme in the flow W_ρ^α , as well as the terms containing entropy.

Let's consider the grid to be uniform in each direction with steps h_α . As a result, we have

$$\rho_{i_\alpha}^{n+1} = \rho_{i_\alpha}^n - \tau \sum_\alpha v_\alpha \rho_{x_\alpha, i_\alpha}^\circ + \frac{\tau^2}{2} \sum_\alpha (v_\alpha^2 + c^2) \rho_{x_\alpha \hat{x}_\alpha, i_\alpha}^n + \tau \sum_\alpha \bar{\mu}_\alpha \rho_{x_\alpha \hat{x}_\alpha, i_\alpha}^n + \tau F_{\rho, i_\alpha}^n.$$

This equation can be written as

$$\rho_{i_\alpha}^{n+1} = \sum_{\alpha} (A_{\alpha} \rho_{i_\alpha+1}^n + C_{\alpha} \rho_{i_\alpha-1}^n) + \rho_{i_\alpha}^n \left(1 - \sum_{\alpha} B_{\alpha} \right) + \tau F_{i_\alpha}^n,$$

where

$$\begin{aligned} A_{\alpha} &= -\frac{\tau}{2h_{\alpha}} v_{\alpha} + \frac{\tau^2}{2h_{\alpha}^2} (v_{\alpha}^2 + c^2) + \frac{\tau}{h_{\alpha}^2} \bar{\mu}_{\alpha}, \\ C_{\alpha} &= \frac{\tau}{2h_{\alpha}} v_{\alpha} + \frac{\tau^2}{2h_{\alpha}^2} (v_{\alpha}^2 + c^2) + \frac{\tau}{h_{\alpha}^2} \bar{\mu}_{\alpha}, \\ B_{\alpha} &= \frac{\tau^2}{h_{\alpha}^2} (v_{\alpha}^2 + c^2) + 2 \frac{\tau}{h_{\alpha}^2} \bar{\mu}_{\alpha} = A_{\alpha} + C_{\alpha}. \end{aligned}$$

The maximum principle and estimation

$$\max |\rho^{n+1}| \leq \max |\rho^n| + \tau \max |F^n|$$

will occur when $A_{\alpha} > 0$, $C_{\alpha} > 0$, and $\sum_{\alpha} B_{\alpha} < 1$. The requirements $A_{\alpha} > 0$, $C_{\alpha} > 0$ lead to the inequality

$$\bar{\mu}_{\alpha} > 0.5h_{\alpha}|v_{\alpha}| - 0.5\tau(v_{\alpha}^2 + c^2) = M_{\min \alpha}.$$

As $0.5\tau(v_{\alpha}^2 + c^2) > 0.5h_{\alpha}|v_{\alpha}| \left(\frac{\tau}{h_{\alpha}} \sqrt{v_{\alpha}^2 + c^2} \right)$, that it is possible to demand, that

$$\bar{\mu}_{\alpha} > \mu_{\min \alpha} 0.5h_{\alpha}|v_{\alpha}| \left(1 - \frac{\tau}{h_{\alpha}} \sqrt{v_{\alpha}^2 + c^2} \right) > M_{\min \alpha}.$$

And the requirement $\sum_{\alpha} B_{\alpha} < 1$, leads to an inequality

$$\bar{\mu}_{\alpha} < \mu_{\max \alpha} 0.5 \frac{h_{\alpha}^2}{\tau} \left(1 - \frac{\tau}{h_{\alpha}} \sqrt{v_{\alpha}^2 + c^2} \right) < M_{\max \alpha}.$$

Artificial viscosity $\bar{\mu}_{\alpha}$ should be positive, that $\frac{\tau}{h_{\alpha}} \sqrt{v_{\alpha}^2 + c^2} < 1$ and $\frac{\tau}{h_{\alpha}} > \sqrt{v_{\alpha}^2 + c^2}$. All conditions will be executed when

$$\mu_{\min \alpha} = 0.5h_{\alpha}|v_{\alpha}| \left(1 - \left(\frac{\tau}{h_{\alpha}} \sqrt{v_{\alpha}^2 + c^2} \right)^d \right) < \bar{\mu}_{\alpha} <$$

$$< 0.5h_\alpha \sqrt{v_\alpha^2 + c^2} \left(1 - \left(\frac{\tau}{h_\alpha} \sqrt{v_\alpha^2 + c^2} \right)^2 \right) = \mu_{\max \alpha}.$$

We return to the index record

$$\begin{aligned} & \bar{\mu}_{\alpha i_\alpha + 1/2} \\ &= 0.5h_{\alpha i_\alpha + 1/2} Q_{\alpha i_\alpha + 1/2} \left(1 - \left(\frac{\tau}{h_{\alpha i_\alpha + 1/2}} \sqrt{\left(v_{\alpha i_\alpha + 1/2}^{(\alpha)} \right)^2 + \left(c_{i_\alpha + 1/2}^{(\alpha)} \right)^2} \right)^d \right), \\ & \text{where } c_{i_\alpha + 1/2}^{(\alpha)} = \sqrt{\gamma \left| \frac{p_{i_\alpha + 1/2}^{(\alpha)}}{\rho_{i_\alpha + 1/2}^{(\alpha)}} \right|} \text{ and } d = 1, 2. \end{aligned}$$

The expressions for $\bar{\mu}_{\alpha i_\alpha + 1/2}$ obtained above will be used in constructing modified viscosity $\bar{\mu}_{\alpha i_\alpha + 1/2} = \xi_{\alpha i_\alpha + 1/2} \bar{\mu}_{\alpha i_\alpha + 1/2}$, where $0 \leq \xi_{\alpha i_\alpha + 1/2} \leq 1$. The factor $\xi_{\alpha i_\alpha + 1/2}$ will take into account the absence of artificial viscosity in cells belonging to the areas of the contact discontinuity (CD) and rarefaction waves (RW).

The time step by time τ_n will be determined from the ratio

$$Ku = \max_\alpha \max_{x_\alpha} \left(\frac{\tau_n}{h_{\alpha i_\alpha + 1/2}} \sqrt{\left(\left(v_{\alpha i_\alpha + 1/2}^{(\alpha)} \right)^n \right)^2 + \left(\left(c_{i_\alpha + 1/2}^{(\alpha)} \right)^n \right)^2} \right)$$

for a given Courant number (Ku).

Note also that rapid changes can occur in the gas. In this case, the step τ_n should be chosen in accordance with these changes and to be small. This leads to a decrease in the number of Ku for the respective time periods.

5 AREAS OF INTRODUCTION OF ARTIFICIAL VISCOSITY

The viscosity containing in amendments of Lax-Wendroff, leads to washing out of the CD and of the shock waves (SW). We will not enter the artificial viscosity in CD area not to increase here the washing out of solution.

In the CD area the value

$$\frac{\partial p}{\partial l} = (\gamma - 1) \left(\rho \frac{\partial \varepsilon}{\partial l} + \varepsilon \frac{\partial \rho}{\partial l} \right),$$

where $l = \frac{\nabla \rho}{|\nabla \rho|}$ is the unit vector in a direction of a gradient of density.

The derivative $\frac{\partial p}{\partial l}$ is small in comparison with derivatives $\frac{\partial \varepsilon}{\partial l}$ and $\frac{\partial \rho}{\partial l}$. Therefore, the values $\frac{\partial \varepsilon}{\partial l}$ and $\frac{\partial \rho}{\partial l} > 0$ have the opposite signs.

Thus, in the CD area

$$\frac{\partial}{\partial l} \left(\frac{p}{\rho} \right) < 0. \quad (\text{CD})$$

In the RW area also we will not enter artificial viscosity not to lower accuracy of the numerical decision. In the RW region inequality [2] will hold true

$$\frac{\partial v_l}{\partial l} > 0. \quad (\text{RW})$$

On a shock wave (SW) the condition is satisfied

$$\frac{\partial v_l}{\partial l} < 0. \quad (\text{SW})$$

In the SW area performance of condition, the minimum viscosity is entered $Q_{\alpha i_\alpha + 1/2} = |v_{\alpha i_\alpha + 1/2}^{(\alpha)}|$.

The artificial viscosity is also introduced in the vicinity of the solution's nonmonotonicity points where the density has local extremum:

$$(\rho_{q_\alpha+1} - \rho_{q_\alpha})(\rho_{q_\alpha} - \rho_{q_\alpha-1}) < 0, \quad q_\alpha = i, k, m.$$

At performance of last inequality the maximum artificial viscosity on the intervals adjoining the considered knot, with viscosity was introduce

$$Q_{\alpha i_\alpha + 1/2} = \sqrt{\left(v_{\alpha i_\alpha + 1/2}^{(\alpha)}\right)^2 + \left(c_{i_\alpha + 1/2}^{(\alpha)}\right)^2}.$$

On other intervals artificial viscosity is not introduced $\mu \equiv 0$.

Therefore, artificial viscosity is introduced on SW, in the regions of the oscillations of the grid's solution and is not introduced in RW and CD areas.

The artificial viscosity is calculated on the values of the decision obtained on the previous time layer. The fulfillment of conditions (CD), (RW), (SW) and local extremum of density is checked on values of the decision obtained at the "predictor" stage.

The scheme of computation of artificial viscosity is shown in Figure 1.

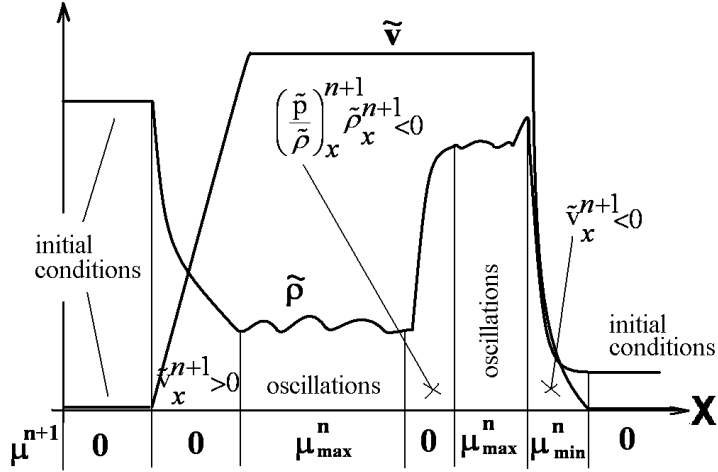


Figure 1. Distributions of density, velocity and artificial viscosity.

6 PROBLEM SOLUTION STAGES

At the first stage ("predictor") all the functions are obtained in the absence of the artificial viscosity $\mu \equiv 0$.

$$\begin{aligned} \tilde{q}_i^{n+1} = & q_i^n - \frac{\tau_n}{h_x} \left[(W_q)_{i+1/2km}^n - (W_q)_{i-1/2km}^n \right] - \\ & - \frac{\tau_n}{h_y} \left[(W_q)_{ik+1/2m}^n - (W_q)_{ik-1/2m}^n \right] - \frac{\tau_n}{h_z} \left[(W_q)_{ikm+1/2}^n - (W_q)_{ikm-1/2}^n \right], \end{aligned}$$

where $q = \rho, I, E$, $\tilde{q} = \tilde{\rho}, \tilde{I}, \tilde{E}$. Thus all the "predictor" values are obtained.

At the second stage ("corrector") from the obtained "predictor" values $\tilde{\rho}, \tilde{I}, \tilde{E}$ intervals are found, on which artificial viscosity should be introduced. Section 5 describes the determination of the region where the artificial viscosity is introduced and the viscosity value is considered in Section 4.

For the "corrector", we have the following finite-difference scheme:

$$\begin{aligned} q_i^{n+1} = & \tilde{q}_i^{n+1} - \frac{\tau_n}{h_x} \left[\left(W_{\mu q}^x \right)_{i+1/2km}^n - \left(W_{\mu q}^x \right)_{i-1/2km}^n \right] \\ & - \frac{\tau_n}{h_y} \left[\left(W_{\mu q}^y \right)_{ik+1/2m}^n - \left(W_{\mu q}^y \right)_{ik-1/2m}^n \right] \\ & - \frac{\tau_n}{h_z} \left[\left(W_{\mu q}^z \right)_{ikm+1/2}^n - \left(W_{\mu q}^z \right)_{ikm-1/2}^n \right]. \end{aligned}$$

The time step is found from the condition

$$\tau_n = \frac{Ku}{M_x/h_x + M_y/h_y + M_z/h_z}, \quad M_x = \max_{1 \leq i \leq N_x} \sqrt{(v^2 + c^2)_{i+1/2km}^n},$$

$$M_y = \max_{1 \leq k \leq N_y} \sqrt{(v^2 + c^2)_{ik+1/2m}^n}, \quad M_z = \max_{1 \leq m \leq N_z} \sqrt{(v^2 + c^2)_{ikm+1/2}^n}.$$

When the "predictor" and "corrector" equations are added, the "predictor" values vanish. They determine the region of the artificial viscosity's introduction. As the numerical calculations shown, the Courant number does not exceed 0.6. The best accuracy is realized when the Courant number accepts its maximum value.

The "predictor" decision on the layer t^{n+1} obtained under the condition $\mu \equiv 0$ has a weakly oscillations that makes it possible to determine accurately the CD, BW, and RW regions. The "corrector" stage makes it possible to suppress the arising oscillations of decision. The decisions obtained at the "predictor" and "corrector" stages are close. However to refuse a "corrector" stage it is impossible. If the "corrector" stage is rejected, the oscillations occur again.

7 NUMERICAL RESULTS

As the test of proposed method the 3D Riemann problem was taken. This problem was solved in the cube $[0, 1]^3$ divided on eight equal parts. In each part of cube the parameters density, speed and pressure were taken the same as well as in work [2] (see Table 1).

Table 1. Boundary values of gas-dynamic parameters

Octant	1	2	3	4	5	6	7	8
ρ	ρ_2	ρ_1	ρ_1	ρ_2	ρ_1	ρ_2	ρ_2	ρ_1
u	v_0	0	v_0	0	v_0	0	v_0	0
v	v_0	v_0	0	0	v_0	v_0	0	0
w	v_0	v_0	v_0	v_0	0	0	0	0
p	p_2	p_1	p_1	p_2	p_1	p_2	p_2	p_1

Where $\rho_1 = 0.5065$, $\rho_2 = 1.1$, $p_1 = 0.35$,
 $p_2 = 1.1$, $v_0 = 0.8939$ and $\gamma = 1.4$.

Boundary conditions in a test problem have been chosen by the following: normal derivatives of all variables are equal to zero. The problem decision was calculated up to the moment of time $t = 0.25$. The obtained

numerical decision was compared with results calculated with the help of program DSBS LF 4 [2]. The numerical decision in the work [2] was computed on the space grid 300^3 . The proposed AAV method was tested on the grid 202^3 .

The results obtained with the help of AAV method are presented on the Fig. 2-4 at the left. The results obtained with the help of DSBS LF 4 program are shown on the Fig. 2-4 at the right.

The Fig. 2 shows the isosurfaces of density at the moment of time $t = 0.25$ for value $\rho = 1.5$. The Fig. 3 demonstrates the isolines of density on a plane $z = 0$. The Fig. 4 presents the isolines of density on a plane $z = 0.612$. Results of calculations well coincide.

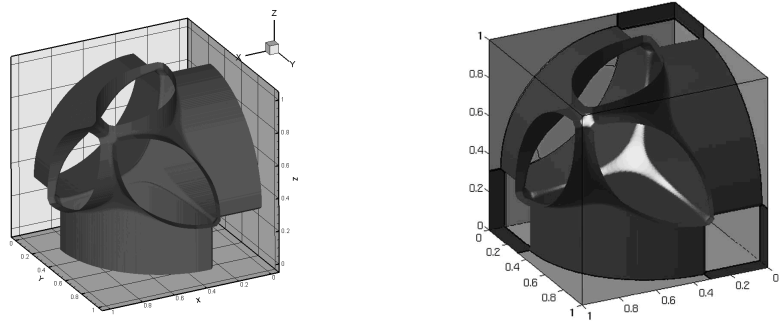


Figure 2. Isosurfaces of density.

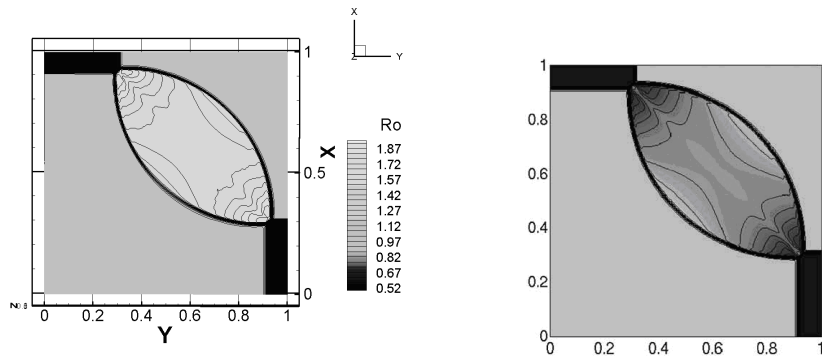


Figure 3. Isolines of density on a plane $z = 0$.

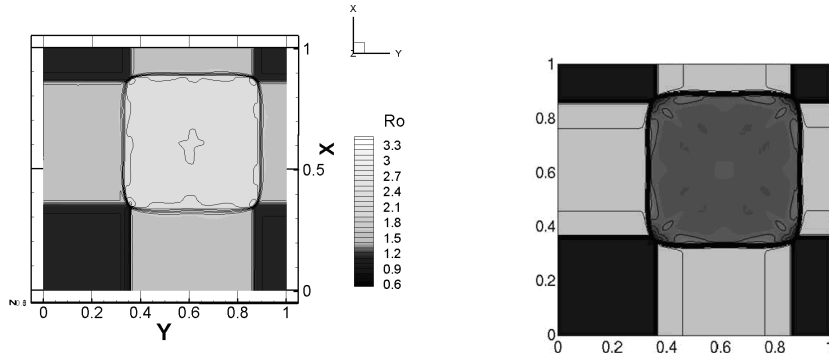


Figure 4. Isolines of density on a plane $z = 0.612$.

References

1. I.V. Popov and I.V. Fryazinov, Finite Difference Method for Solving the Gas Dynamics Equations by Introducing the Adaptive Artificial Viscosity, *Mat. Model.* **20**(8) (2008) 48-60 (in Russian).
2. Milan Kucharik, Richard Liska, Stanly Steinberg, Burton Wendroff, Optimally-stable second-order accurate difference schemes for non-linear conservation laws in 3D, *Appl. Numer. Math.* **56** (2006) 589-607.

ANALOGUE OF A CUBIC SPLINE FOR A FUNCTION WITH A BOUNDARY LAYER COMPONENT

A.I. ZADORIN AND M.V. GURYANOVA

Omsk filial of Sobolev Mathematics Institute SB RAS,
Pevtsova 13, Omsk, 644099, Russia
zadorin@ofim.oscsbras.ru

Abstract. Analogue of cubic spline-interpolation for a function with a boundary layer component is constructed. Proposed interpolant is exact on the boundary layer component. Results of numerical experiments indicated that constructed interpolant has the accuracy $O(h^3)$, when the cubic spline leads to large errors.

1 INTRODUCTION

Spline-interpolation methods for functions with bounded derivatives are well known, see for example [1], [2]. But when we apply polynomial interpolations for a function with a boundary layer component, it leads to significant errors [3]. So, it is an interesting problem to construct spline-interpolation formulas of the uniform accuracy for functions with boundary layer components.

Let a function $u(x)$ has a form:

$$u(x) = p(x) + \gamma\Phi(x), \quad x \in [0, 1], \quad (1)$$

where regular component $p(x)$ has some bounded derivatives,

$\Phi(x)$ is known boundary layer component, with rapid changes in some regions, constant γ is not given.

In particular, $u(x)$ may be the solution of a boundary value problem:

$$\varepsilon u''(x) + a(x)u'(x) - b(x)u(x) = f(x), \quad u(0) = A, \quad u(1) = B, \quad (2)$$

where

$$a(x) \geq \alpha > 0, \quad b(x) \geq 0, \quad \varepsilon > 0,$$

M. Koleva and L. Vulkov (Eds.), Proceedings of the Fifth Conference on Finite Difference Methods: Theory and Applications (FDM: T&A 2010) 2011, pp. 166–173.

© Rousse University Press 2011

functions a, b, f are smooth enough. According to [4] a solution of a problem (2) has a form (1) with

$$\Phi(x) = \exp(-a_0\varepsilon^{-1}x), |p^{(j)}(x)| \leq C_0 \left[\varepsilon^{1-j} \exp(-\alpha\varepsilon^{-1}x) + 1 \right], j \geq 0, \quad (3)$$

where $a_0 = a(0)$, $\gamma = -\varepsilon u'(0)/a_0$, $|\gamma| \leq C$. In this example the function $\Phi(x)$ has large derivatives for small values of ε in the neighbourhood of the point $x = 0$, C_0 does not depend on a parameter ε .

Let a function $u(x)$ of a form (1) is given at nodes of an uniform mesh Ω :

$$\Omega = \{x_n : x_n h, n = 0, 1, \dots, N, x_0 = 0, x_N = 1, \Delta_n = [x_{n-1}, x_n] \}.$$

Denote $u_n = u(x_n)$, $n = 0, 1, 2, \dots, N$.

In [5], [6] we constructed formulas of the spline-interpolation, fitted to the boundary layer component $\Phi(x)$. We proved that constructed interpolants have the property of the convergence, uniform in gradients of the interpolated function in the boundary layer. We constructed formulas of first and second order of the uniform accuracy. But this interpolants have not continuous derivative on whole interval $[0, 1]$, because constructed on separate mesh intervals.

Purpose of this article – to construct the analogue of the cubic spline, exact on the boundary layer component $\Phi(x)$. We shall achieve for constructed interpolant $g(x)$ the property $g(x) \in C^2[0, 1]$.

2 CONSTRUCTION OF THE INTERPOLANT

We take into account the condition $g(x) \in C^2[0, 1]$ and define:

$$g''(x) = M_{j-1} + \left(M_j - M_{j-1} \right) \frac{\Phi''(x) - \Phi''_{j-1}}{\Phi''_j - \Phi''_{j-1}}, \quad x \in \Delta_j, \quad (4)$$

where $M_j = g''(x_j)$, $\Phi''_j = \Phi''(x_j)$.

We integrate (4) twice and obtain:

$$\begin{aligned} g(x) = & \left(M_{j-1} - \frac{M_j - M_{j-1}}{\Phi''_j - \Phi''_{j-1}} \Phi''_{j-1} \right) \frac{(x - x_{j-1})^2}{2} + \frac{M_j - M_{j-1}}{\Phi''_j - \Phi''_{j-1}} \Phi(x) \\ & + K_1(x - x_{j-1}) + K_2. \end{aligned} \quad (5)$$

We seek constants K_1, K_2 from interpolation conditions $g(x_{j-1}) = u_{j-1}$, $g(x_j) = u_j$ for each interval Δ_j . Then we from (5) obtain:

$$\begin{aligned} g(x) &= \frac{M_j - M_{j-1}}{\Phi''_j - \Phi''_{j-1}} \left(\Phi(x) - \Phi_{j-1} - \frac{\Phi_j - \Phi_{j-1}}{h}(x - x_{j-1}) \right. \\ &\quad \left. - \frac{1}{2}\Phi''_{j-1}(x - x_{j-1})(x - x_j) \right) + \frac{1}{2}M_{j-1}(x - x_{j-1})(x - x_j) \quad (6) \\ &\quad + (u_j - u_{j-1})\frac{x - x_{j-1}}{h} + u_{j-1}, \quad x \in \Delta_j. \end{aligned}$$

By the construction $g(x) \in C^2[0, 1]$, therefore for $j = 1, 2, \dots, N-1$

$$g'(x_j - 0) = g'(x_j + 0).$$

In last relation we use $g(x)$ from (6), and obtain a three-point relation on $\{M_j\}$:

$$\begin{aligned} &\frac{1}{h^2(\Phi''_j - \Phi''_{j-1})} \left(\Phi_j - \Phi_{j-1} - h\Phi'_j + \frac{h^2}{2}\Phi''_j \right) M_{j-1} \\ &+ \left[1 - \frac{1}{h^2(\Phi''_j - \Phi''_{j-1})} \left(\Phi_j - \Phi_{j-1} - h\Phi'_j + \frac{h^2}{2}\Phi''_j \right) \right. \\ &\quad \left. - \frac{1}{h^2(\Phi''_{j+1} - \Phi''_j)} \left(\Phi_{j+1} - \Phi_j - h\Phi'_j - \frac{h^2}{2}\Phi''_j \right) \right] M_j \quad (7) \\ &+ \frac{1}{h^2(\Phi''_{j+1} - \Phi''_j)} \left(\Phi_{j+1} - \Phi_j - h\Phi'_j - \frac{h^2}{2}\Phi''_j \right) M_{j+1} \\ &= \frac{u_{j+1} - 2u_j + u_{j-1}}{h^2}, \quad 0 < j < N. \end{aligned}$$

Now we define boundary conditions for a system (7) and write a system on $\{M_j\}$, $1 < j < N$ in a form:

$$A_j M_{j-1} + (1 - A_j - C_j) M_j + C_j M_{j+1} = \frac{u_{j+1} - 2u_j + u_{j-1}}{h^2}, \quad (8)$$

$$M_0 = u''(0), \quad M_N = u''(1), \quad (9)$$

where

$$A_j = \frac{1}{h^2(\Phi''_j - \Phi''_{j-1})} \left(\Phi_j - \Phi_{j-1} - h\Phi'_j + \frac{h^2}{2}\Phi''_j \right),$$

$$C_j = \frac{1}{h^2(\Phi''_{j+1} - \Phi''_j)} \left(\Phi_{j+1} - \Phi_j - h\Phi'_j - \frac{h^2}{2}\Phi''_j \right).$$

So, we constructed the analogue of the cubic spline (6), with coefficients M_j , defined from three-point system (8)-(9).

By the construction $g(x) \in C^2[0, 1]$. Now we prove that constructed interpolant $g(x)$ exact on the component $\Phi(x)$. Let $u(x) = \Phi(x)$. One can verify that $M_j = \Phi''_j$, $j = 0, 1, \dots, N$ is the solution of the system (8), (9). Then from (6) we obtain $g(x) = \Phi(x)$.

Let the derivative $\Phi'''(x)$ keeps sign on each mesh interval (x_j, x_{j+1}) . Then

$$0 < A_j < 1/2, \quad 0 < C_j < 1/2. \quad (10)$$

Using Taylor series for function $\Phi(x)$ we obtain that for some $s_1, s_2 \in \Delta_{j+1}$

$$C_j = \frac{\Phi'''(s_1)}{6\Phi'''(s_2)} > 0.$$

Similarly for some $s_3, s_4 \in \Delta_j$

$$A_j = \frac{\Phi'''(s_3)}{6\Phi'''(s_4)} > 0.$$

Now we prove that $C_j < 1/2$. We have

$$C_j = \frac{1}{h^2(\Phi''_{j+1} - \Phi''_j)} \left(\frac{h^2}{2} \Phi''(s) - \frac{h^2}{2} \Phi''_j \right) = \frac{1}{2} \cdot \frac{\Phi''(s) - \Phi''_j}{\Phi''_{j+1} - \Phi''_j} < \frac{1}{2}.$$

We took into account that $s \in (x_j, x_{j+1})$ and the function $\Phi''(x)$ increases or decreases in the interval (x_j, x_{j+1}) . Similarly we have $A_j < 1/2$.

So, we proved the inequalities (10).

Let $\Phi(x)$ corresponds to the exponential boundary layer and $\Phi(x) = e^{-\frac{x}{\varepsilon}}$. Then

$$C_j = \left[\frac{h^2}{2} + \varepsilon^2 - \varepsilon^2 \exp(-\varepsilon^{-1}h) - \varepsilon h \right] / \left[h^2(1 - \varepsilon(-\varepsilon^{-1}h)) \right]. \quad (11)$$

It follows from (11) that

$$\lim_{\varepsilon \rightarrow 0} C_j(\varepsilon) = \frac{1}{2}.$$

Similarly,

$$\lim_{\varepsilon \rightarrow 0} A_j(\varepsilon) = \frac{1}{2}.$$

So, if we suppose only that $\Phi^{(3)}(x)$ keeps a sign in mesh intervals, the estimates (10) can not be improved.

We obtain the formula of the cubic spline-interpolation [7] from (6), (8), (9), if $\Phi(x) = x^3$:

$$\begin{aligned} g_3(x) &= \frac{M_j - M_{j-1}}{6h}(x - x_{j-1})(x - x_j)(x + x_j - 2x_{j-1}) \\ &\quad + \frac{M_{j-1}}{2}(x - x_{j-1})(x - x_j) + \frac{u_j - u_{j-1}}{h}(x - x_{j-1}) + u_{j-1}, \end{aligned} \quad (12)$$

where coefficients $M_j = g_3''(x_j)$ can be found from a system:

$$\frac{1}{6}M_{j-1} + \frac{2}{3}M_j + \frac{1}{6}M_{j+1} = \frac{u_{j+1} - 2u_j + u_{j-1}}{h^2}, \quad 1 < j < N, \quad (13)$$

$$M_0 = u''(0), \quad M_N = u''(1). \quad (14)$$

According to ([2], p. 116) the next estimate is true:

$$|g_3(x) - u(x)| \leq \frac{5}{384} \max_s |u^{(4)}(s)| h^4, \quad s, x \in [0, 1]. \quad (15)$$

Note that we can consider $g_3(x)$ as the cubic spline for the function $g(x)$, therefore similarly to (15)

$$|g_3(x) - g(x)| \leq \frac{5}{384} \max_s |g^{(4)}(s)| h^4, \quad s, x \in [0, 1]. \quad (16)$$

Using (15) and (16), we obtain

$$|g(x) - u(x)| \leq \frac{5}{384} [\max_s |u^{(4)}(s)| + \max_s |g^{(4)}(s)|] h^4, \quad s, x \in [0, 1]. \quad (17)$$

So, if functions $u(x), g(x)$ have not large gradients, nonpolynomial interpolant (6) has the accuracy of the order $O(h^4)$ as the cubic interpolant. But when a function $u(x)$ has regions of large gradients, the interpolant $g(x)$ is more accurate thanks to the fitting to the boundary layer component.

Usually we know only values $\{u_n\}$, but for the constructed interpolant we need $u''(0), u''(1)$. In a case of large gradients we can not use polynomial interpolations to find this derivatives. On the interval $[x_{j-1}, x_{j+2}]$ we construct the interpolant

$$g_\Phi(x) = K_1 + K_2(x - x_{j-1}) + K_3(x - x_{j-1})^2 + K_4\Phi(x). \quad (18)$$

We use interpolation conditions at nodes $\{x_{j-1}, x_j, x_{j+1}, x_{j+2}\}$ and find all $\{K_j\}$. Then we obtain

$$\begin{aligned} g_\Phi''(x) &= \frac{u_{j+1} - 2u_j + u_{j-1}}{h^2} + \frac{u_{j+2} - 3u_{j+1} + 3u_j - u_{j-1}}{\Phi_{j+2} - 3\Phi_{j+1} + 3\Phi_j - \Phi_{j-1}} \times \\ &\quad \times \left[\Phi''(x) - \frac{\Phi_{j+1} - 2\Phi_j + \Phi_{j-1}}{h^2} \right], \quad x \in [x_{j-1}, x_{j+2}]. \end{aligned} \quad (19)$$

It is easy to see that the difference formula (19) is exact in a case $u(x) = \Phi(x)$ and we can use this formula in regions of large gradients.

Consider a case, when a function $\Phi(x)$ corresponds to the boundary layer near the point $x = 0$. Then we use (19) and replace boundary conditions (9) by the next:

$$\begin{aligned} M_0 &= \frac{u_2 - 2u_1 + u_0}{h^2} + \frac{u_3 - 3u_2 + 3u_1 - u_0}{\Phi_3 - 3\Phi_2 + 3\Phi_1 - \Phi_0} \left[\Phi''(0) - \frac{\Phi_2 - 2\Phi_1 + \Phi_0}{h^2} \right], \\ M_N &= \frac{2u_N - 5u_{N-1} + 4u_{N-2} - u_{N-3}}{h^2}. \end{aligned} \quad (20)$$

Conditions (20) have second order of an accuracy, for example

$$|u''(1) - M_N| \leq \frac{11}{12} \max |u^{(4)}(s)|h^2, \quad 1 - 3h < s < l.$$

So, we constructed the interpolant (6), (8), (20). It is the analogue of the cubic spline, fitted to the boundary layer component $\Phi(x)$.

3 NUMERICAL RESULTS

Consider a function

$$u(x) = e^{-\frac{x}{\varepsilon}} + \cos(x), \quad x \in [0, 1], \quad \varepsilon \in (0, 1].$$

Define the interpolation error for given ε and h

$$\Delta_h = \max_j |g(\tilde{x}_j) - u(\tilde{x}_j)|, \quad \tilde{x}_j = \frac{x_{j-1} + x_j}{2}, \quad j = 1, 2, \dots, N.$$

In Table 1 the error Δ_h of the interpolant (6), (8)-(9) is presented for different values of ε and h .

Define the convergence rate

$$CR_h = \log_2 \left(\Delta_h / \Delta_{h/2} \right).$$

In Table 2 the convergence rate CR_h of the interpolant (6), (8)-(9) is presented for different values of ε and h . We see that $CR_h \approx 4$ for $\varepsilon = 1$ and $CR_h \approx 3$ for small values of a parameter ε .

In Table 3 the error Δ_h of the cubic interpolant (12)-(14) is presented for different values of ε and h . We see that the interpolation error is essential for small values of ε . In all tables $ae \pm m$ means $a \times 10^{\pm m}$.

Now we replace exact boundary conditions (9) by finite differences, using (20). In Table 4 the error Δ_h of the interpolant (6), (8), (20) is presented for different values of ε and h . We see that approximate conditions (20) don't decrease the accuracy of the constructed interpolant (6), (8)-(9).

Table 1. The interpolation error of spline (6), (8), (9)

ε	h				
	2^{-4}	2^{-5}	2^{-6}	2^{-7}	2^{-8}
1	1.37e-007	8.51e-009	5.30e-010	3.31e-011	2.07e-012
2^{-1}	2.22e-007	1.37e-008	8.54e-010	5.33e-011	3.33e-012
2^{-2}	3.96e-007	2.43e-008	1.51e-009	9.38e-011	5.85e-012
2^{-3}	7.62e-007	4.61e-008	2.83e-009	1.75e-010	1.09e-011
2^{-4}	1.56e-006	9.19e-008	5.56e-009	3.41e-010	2.11e-011
2^{-5}	3.30e-006	1.91e-007	1.13e-008	6.82e-010	4.18e-011
2^{-6}	6.61e-006	4.10e-007	2.37e-008	1.40e-009	8.44e-011
2^{-7}	1.02e-005	8.27e-007	5.12e-008	2.96e-009	1.74e-010
2^{-8}	1.20e-005	1.29e-006	1.03e-007	6.39e-009	3.69e-010
2^{-9}	1.25e-005	1.51e-006	1.61e-007	1.29e-008	7.98e-010

Table 2. The convergence rate of spline (6), (8), (9)

ε	h			
	2^{-4}	2^{-5}	2^{-6}	2^{-7}
1	4.01e+000	4.00e+000	4.00e+000	4.00e+000
2^{-1}	4.01e+000	4.01e+000	4.00e+000	4.00e+000
2^{-2}	4.02e+000	4.01e+000	4.01e+000	4.00e+000
2^{-3}	4.05e+000	4.02e+000	4.01e+000	4.01e+000
2^{-4}	4.11e+000	4.08e+000	4.05e+000	4.03e+000
2^{-5}	4.01e+000	4.11e+000	4.09e+000	4.05e+000
2^{-6}	3.22e+000	3.64e+000	4.02e+000	4.11e+000
2^{-7}	3.05e+000	3.23e+000	3.64e+000	4.02e+000

Table 3. The interpolation error of cubic spline (12)-(14)

ε	h				
	2^{-4}	2^{-5}	2^{-6}	2^{-7}	2^{-8}
1	1.95e-007	1.22e-008	7.64e-010	4.78e-011	2.99e-012
2^{-1}	1.62e-006	1.03e-007	6.46e-009	4.05e-010	2.54e-011
2^{-2}	2.38e-005	1.53e-006	9.70e-008	6.10e-009	3.83e-010
2^{-3}	3.55e-004	2.37e-005	1.53e-006	9.67e-008	6.08e-009
2^{-4}	4.89e-003	3.55e-004	2.37e-005	1.53e-006	9.66e-008
2^{-5}	5.57e-002	4.89e-003	3.55e-004	2.37e-005	1.53e-006
2^{-6}	4.55e-001	5.57e-002	4.89e-003	3.55e-004	2.37e-005
2^{-7}	2.55e+000	4.55e-001	5.57e-002	4.89e-003	3.55e-004
2^{-8}	1.13e+001	2.55e+000	4.55e-001	5.57e-002	4.89e-003
2^{-9}	4.65e+001	1.13e+001	2.55e+000	4.55e-001	5.57e-002

Table 4. The interpolation error of the spline (6), (8), (20)

ε	h				
	2^{-4}	2^{-5}	2^{-6}	2^{-7}	2^{-8}
1	8.45e-007	5.07e-008	3.10e-009	1.92e-010	1.19e-011
2^{-1}	1.82e-006	1.04e-007	6.19e-009	3.78e-010	2.34e-011
2^{-2}	4.26e-006	2.22e-007	1.27e-008	7.57e-010	4.63e-011
2^{-3}	1.46e-006	6.71e-008	3.60e-009	2.07e-010	1.24e-011
2^{-4}	2.16e-006	8.79e-008	4.20e-009	2.51e-010	1.56e-011
2^{-5}	3.97e-006	1.62e-007	9.71e-009	5.90e-010	3.63e-011
2^{-6}	7.56e-006	3.75e-007	2.20e-008	1.30e-009	7.87e-011
2^{-7}	1.08e-005	7.81e-007	4.90e-008	2.85e-009	1.68e-010
2^{-8}	1.18e-005	1.23e-006	1.01e-007	6.26e-009	3.62e-010
2^{-9}	1.34e-005	1.45e-006	1.58e-007	1.28e-008	7.90e-010

ACKNOWLEDGEMENT

Supported by Russian Foundation for Basic Research under Grant 11-01-00875.

References

1. J.H. Ahlberg, E.N. Nilson, J.L. Walsh, *The Theory of Splines and their Applications*, Academic Press, New York (1967)
2. Yu. S. Zavyalov, B.I.Kvasov and V. L. Miroshnichenko, *Methods of Spline Functions*, Nauka, Moscow, 1980 (in Russian).
3. A.I.Zadorin, Method of interpolation for a boundary layer problem, *Sib. J. of Numer Math.* **10**(3) (2007) 267-275 (in Russian).
4. J.J.H. Miller, E. O'Riordan, G.I. Shishkin, *Fitted Numerical Methods for Singular Perturbation Problems*, World Scientific, Singapore (1996)
5. A.I. Zadorin, Interpolation Method for a Function with a Singular Component. *LNCS* **5434** (2009) 612-619.
6. A.I. Zadorin, N.A. Zadorin, Spline interpolation on a uniform grid for functions with a boundary-layer component, *Comp. Math. and Math. Physics* **50**(2) (2010) 211-223.
7. N.S. Bakhvalov, N.P. Zidkov and G.M. Kobel'kov, *Numerical Methods*, Nauka, Moscow, 1987 (in Russian).

NUMERICAL INVESTIGATION OF TIME-PERIODIC SOLUTIONS

E. V. ZEMLYANAYA¹ and N.V.ALEXEEVA²

¹ Laboratory of Information Technologies, Joint Institute for Nuclear Research,
Dubna 141980, Russia, elena@jinr.ru

² Department of Mathematics, University of Cape Town, Rondebosch 7701,
South Africa, Nora.Alexeeva@uct.ac.za

Abstract. We study localised attractors of the parametrically driven, damped nonlinear Schrödinger equation. Time-periodic solitons of this equation are obtained as solutions of the boundary-value problem on a two-dimensional domain. Stability and bifurcations of periodic solitons and their complexes is classified. We show that the bifurcation diagram can be reproduced a three-mode approximation.

1 INTRODUCTION

This paper deals with the parametrically driven damped nonlinear Schrödinger equation,

$$i\psi_t + \psi_{xx} + 2|\psi|^2\psi - \psi = h\psi^* - i\gamma\psi. \quad (1)$$

Here $\gamma > 0$ is the damping coefficient, and $h > 0$ the amplitude of the parametric driver. Equation (1) describes the nonlinear Faraday resonance in a vertically oscillating water trough [1],[2] and the effect of phase-sensitive amplifiers on solitons in optical fibers [3],[4]. The same equation controls the magnetization waves in an easy-plane ferromagnet placed in a combination of a static and microwave field [5] and the amplitude of synchronized oscillations in vertically vibrated pendula lattices [6],[7].

Localised stationary or periodic solutions of Eq.(1) exist only if $h > \gamma$. When $h > h_c$, where

$$h_c = \sqrt{1 + \gamma^2}, \quad (2)$$

M. Koleva and L. Vulkov (Eds.), Proceedings of the Fifth Conference on Finite Difference Methods: Theory and Applications (FDM: T&A 2010) 2011, pp. 174–182.

© Rousse University Press 2011

any localised solution is unstable to spatially-extended perturbations. The evolution of this instability leads to the spatiotemporal chaos. Two stationary soliton solutions of Eq. (1) are well known [5]:

$$\psi_{\pm}(x) = A_{\pm} e^{-i\theta_{\pm}} \operatorname{sech}(A_{\pm}x), \quad (3)$$

where

$$A_{\pm} = \sqrt{1 \pm \sqrt{h^2 - \gamma^2}}, \quad \theta_+ = \frac{1}{2} \arcsin \frac{\gamma}{h}, \quad \theta_- = \frac{\pi}{2} - \theta_+.$$

The soliton $\psi_{-}(x)$ is unstable for all h and γ . The soliton $\psi_{+}(x)$ exists for all $h \geq \gamma$; its stability properties depend on γ and h .

When $\gamma > 0.356$, the ψ_{+} soliton is stable for all h in the range $\gamma < h < h_c(\gamma)$. When $\gamma < 0.356$, on the other hand, the soliton (3) is only stable for $\gamma < h < h_{\text{Hopf}}(\gamma)$, where the value $h_{\text{Hopf}}(\gamma)$ lies between γ and $h_c(\gamma)$ (dashed curve in Fig. 1). As we increase h past $h_{\text{Hopf}}(\gamma)$ keeping $\gamma < 0.356$ fixed, the stationary soliton loses its stability to a time-periodic soliton [5, 8]. The transformation scenario arising as h is increased further, depends on the value of γ . According to the numerical simulations of [9], for γ smaller than approximately 0.26 the periodic soliton follows a period-doubling route to temporal chaos. In a wide region of h values above the chaotic domain, the equation does not support any stable spatially-localised solutions. In this “desert” region, the only attractor determined in direct numerical simulations was the trivial one, $\psi = 0$. Finally, for even larger values of h , the unstable soliton seeds the spatio-temporal chaos [9]. As h is increased for the fixed γ larger than 0.275 (but smaller than 0.365), the soliton follows a different transformation scenario. Here, the period-doubling cascade does not arise and the soliton death does not occur. The periodic soliton remains stable until it yields directly to a spatio-temporal chaotic state [9].

In a short intermediate range of γ -values, $0.26 < \gamma < 0.275$, we have a combination of the above two scenarios. The increase of h for the fixed γ results in the period-doubling of the soliton, followed by the temporal-chaotic and “desert” regions. However, as we continue to raise h , an inverse sequence of bifurcations is observed which brings the stable single-periodic soliton back. On further increase of h , it loses its stability to a spatio-temporal chaotic state [9].

In the region $\gamma > 0.356$, where the stationary soliton ψ_{+} is stable for all h in the range $\gamma < h < h_c(\gamma)$ [5], no periodic solutions can detach from this stationary branch. However, the stationary *two*-soliton solutions do undergo Hopf bifurcations here [10]. The stability domain for the two-soliton complex (denoted $\psi_{(++)}$) on the (γ, h) -plane is shown in Fig. 1.

It is bounded by the curve $h_c(\gamma)$ from above. The second solid curve shown in Fig. 1 demarcates the Hopf bifurcation points of the two-soliton complex [11].

The purpose of our work is to follow the transformations of temporally periodic solutions of Eq. (1) as its parameters are varied, identify the arising bifurcations and eventually explain the attractor chart for this equation which was compiled using direct numerical simulations in Ref. [9]. We will also add missing details to this chart (such as coexisting attractors in cases of bistability) and attempt interpreting it using a simple three-mode approximation.

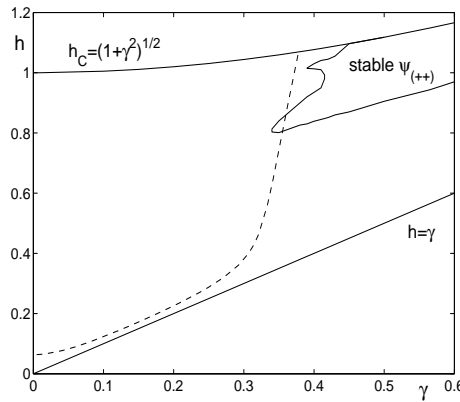


Figure 1. The existence and stability chart of the stationary two-soliton complexes. For each γ , the region of existence of the complexes extends in the direction of larger h , beyond the value h_c .

2 NUMERICAL APPROACH

So far, the direct numerical simulation has been the only way to obtain periodic solutions and study their stability. The shortcoming of this method is that simulations capture only *stable* solutions. This means that the actual mechanisms and details of the transformations (which are bifurcations involving both stable and unstable solutions) remain unaccessible. Neither can simulations be used to identify alternative attractors in cases of bi- or multi-stability.

We use a new approach to the analysis of these hidden mechanisms. Instead of determining attractors of Eq. (1) through numerical simulations over a sufficiently long time, we will be looking for periodic solutions by solving Eq. (1) as a boundary-value problem on a two-dimensional domain

$(-\infty, \infty) \times (0, T)$. The boundary conditions will be set as

$$\psi(x, t) = 0 \quad \text{as } x \rightarrow \pm\infty, \quad \text{and} \quad \psi(x, t + T) = \psi(x, t). \quad (4)$$

The period T is regarded as an unknown, along with the solution $\psi(x, t)$. Letting $\tilde{t} = t/T$ ($0 < \tilde{t} < 1$) and defining $\tilde{\psi}(x, \tilde{t}) = \psi(x, t)$, the boundary-value problem (1),(4) can be reformulated on the rectangle $(-L, L) \times (0, 1)$ (where L is chosen to be sufficiently large):

$$i\tilde{\psi}_{\tilde{t}}(x, \tilde{t}) + T\Phi(\tilde{\psi}(x, \tilde{t}), h, \gamma) = 0, \quad \tilde{\psi}(\pm L, \tilde{t}) = 0, \quad \tilde{\psi}(x, 0) = \tilde{\psi}(x, 1). \quad (5)$$

Here,

$$\Phi(\tilde{\psi}(x, \tilde{t}), h, \gamma) = \tilde{\psi}_{xx} + 2|\tilde{\psi}|^2\tilde{\psi} - \tilde{\psi} - h\tilde{\psi}^* + i\gamma\tilde{\psi}.$$

Eq. (5) is supplemented with an additional equation (phase condition):

$$\Phi(\tilde{\psi}(x^*, \tilde{t}^*), h, \gamma) = 0, \quad x^* = t^* = 0. \quad (6)$$

Solutions $(T, \tilde{\psi})$ of the 2D boundary-value problem (5),(6) were path-followed in h for the fixed γ , with the Hopf bifurcation points of the static solution (Fig.1) used as starting points in the continuation process. We employ a predictor-corrector algorithm [13] with Newtonian iteration at each h . Most calculations were performed on the domain $(-L, L) = (-50, 50)$, with the stepsizes of the fourth-order finite-difference approximation being $\Delta x = 0.05$ and $\Delta \tilde{t} = 0.01$.

Stability of solutions is classified by examining the Floquet multipliers of the corresponding linearised equation. Details are in [11].

3 RESULTS OF NUMERICAL STUDY

In [11, 12], we applied the above numerical approach to periodic solitons with $\gamma = 0.3$, 0.265, and 0.565 as representative sections of various parts of the attractor chart. Here, we focus on the case $\gamma = 0.35$ for which the periodic one- and two-soliton solutons coexist (see Fig.1).

We start with one-soliton solutions. Our numerical continuation shows that in the case $\gamma = 0.35$, the transformation of the solution is similar to the one in the case $\gamma = 0.30$; see Fig. 2. The left endpoint of each of the two curves in that figure corresponds to the stationary single-soliton solution ψ_+ . The corresponding value of h equals $h = 0.385$ for $\gamma = 0.30$ and $h = 0.7500$ for $\gamma = 0.35$. At this value of h the stationary ψ_+ soliton undergoes the Hopf bifurcation and a stable *periodic* soliton is born. At the turning point h_{sn} , the periodic solution loses its stability. Numerically,

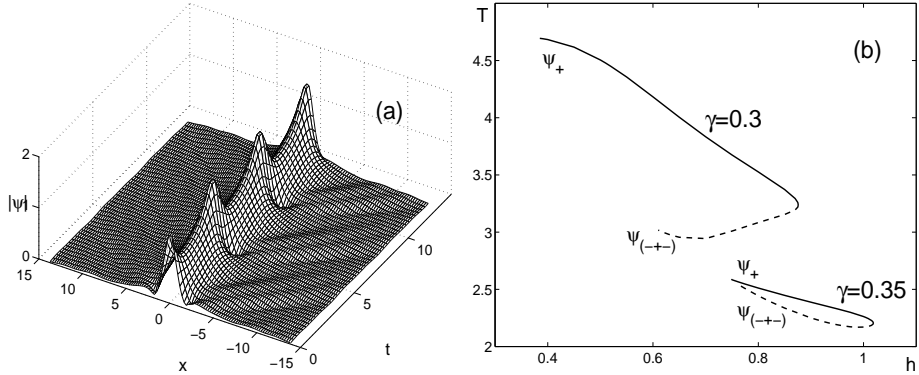


Figure 2. (a) The absolute value of the stable periodic solution with $\gamma = 0.30$, $h = 0.55$. Here $T = 4.356$; (b) The period of the periodic solutions with $\gamma = 0.30$ and $\gamma = 0.35$. The solid curves show the stable and the dashed ones unstable branches.

the turning-point value is $h_{\text{sn}} = 0.8761$ for $\gamma = 0.30$ and $h_{\text{sn}} = 1.0186$ for $\gamma = 0.35$. The end point of the unstable branch ($h = 0.61$ for $\gamma = 0.30$ and $h = 0.760$ for $\gamma = 0.35$) corresponds to a stationary three-soliton complex $\psi_{(-+-)}$.

Near the leftmost point of the ($\gamma = 0.3$)-curve in Fig. 2, the periodic solution looks like a single soliton with a periodically oscillating amplitude and width. As we continue along the curve, the oscillating solution evolves into a three-hump structure which may be interpreted as a triplet of solitons. Near the end point of the curve, the amplitude of oscillations decreases and we arrive at the stationary three-soliton complex.

We now turn to the two-soliton complexes. For γ in the range $0.34 < \gamma < 0.40$ the stability domain of the stationary two-soliton complex is bounded by *two* Hopf bifurcations (see Fig. 1). Each Hopf bifurcation gives rise to a temporally periodic two-soliton solution. Let, for instance, $\gamma = 0.35$. Here, the “lower” Hopf bifurcation occurs at $h_{H1} = 0.806$. This bifurcation is supercritical; for $h < h_{H1}$, the unstable stationary two-soliton solution is replaced by a stable periodic two-soliton complex. As we continue the periodic complex in the direction of smaller h , at some point ($h = 0.79$) it loses its stability to a double-periodic complex of two solitons. As we continue the unstable branch, it makes a number of turns (Fig. 3a), the spatiotemporal complexity of the solution increases (Fig. 4a) but it never regains its stability. The “upper” Hopf bifurcation occurs at $h_{H2} = 0.832$. This bifurcation is subcritical: the emerging periodic branch is unstable and coexists with the stable stationary branch (i.e. the periodic branch continues in the direction of *lower* h , see Fig. 3b).

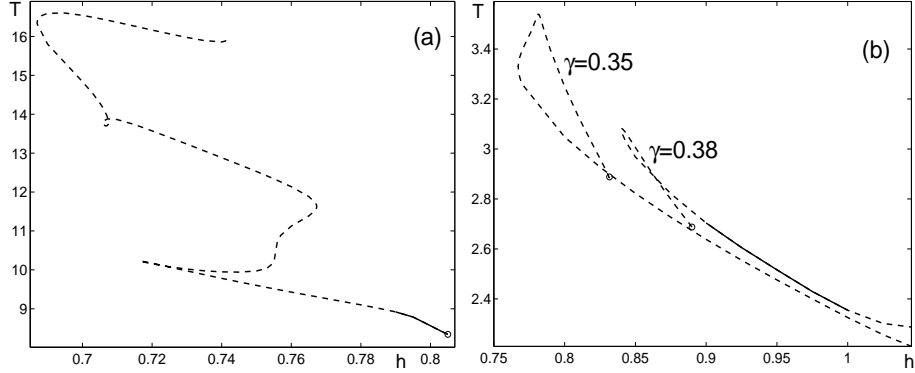


Figure 3. (a) The period of the first branch of the two-soliton periodic solution for $\gamma = 0.35$. (b) The second branch of the periodic two-soliton solution with $\gamma = 0.35$ and $\gamma = 0.38$. The solid curve marks the stable and the dashed one unstable branch. The circles indicate the starting point of the continuation (the point where the stationary two-soliton complex undergoes the Hopf bifurcation).

The entire branch is unstable in the case $\gamma = 0.35$. However, the increase of γ results in the stabilization of the periodic two-soliton solution. This is exemplified by $\gamma = 0.38$ — see the second branch in Fig.3b which features a stable interval $h_1 < h < h_2$, with $h_1 = 0.9415$ and $h_2 = 1.015$. At the bifurcation points $h_{1,2}$ the periodic two-soliton solution loses stability to a quasi-periodic two-soliton complex.

4 THREE-MODE APPROXIMATION

We decompose ψ as

$$\psi = A_+ [U(\bar{x}, \bar{t}) + iV(\bar{x}, \bar{t})] e^{-i\theta_+},$$

where A_+ and θ_+ are as in Eq.(3), and $\bar{t} = A_+^2 t$, $\bar{x} = A_+ x$. This casts Eq.(1) in the following form:

$$\begin{aligned} -V_t - 2FV &= -U_{xx} + U - 2(U^2 + V^2)U, \\ +U_t + 2HV &= -V_{xx} + V - 2(U^2 + V^2)V \end{aligned} \quad (7)$$

(where we have omitted bars above x and t .)

We assume that only three modes are significant for the time evolution of ψ , namely modes with frequencies zero, one and minus one Ω . Other modes are assumed to have negligible amplitudes. Hence we expand $\psi(x, t)$ as

$$\begin{aligned} U(x, t) &= u(x) + \mathcal{A}(x)e^{i\Omega t} + \mathcal{A}^*(x)e^{-i\Omega t}, \\ V(x, t) &= v(x) + \mathcal{B}(x)e^{i\Omega t} + \mathcal{B}^*(x)e^{-i\Omega t}, \end{aligned} \quad (8)$$

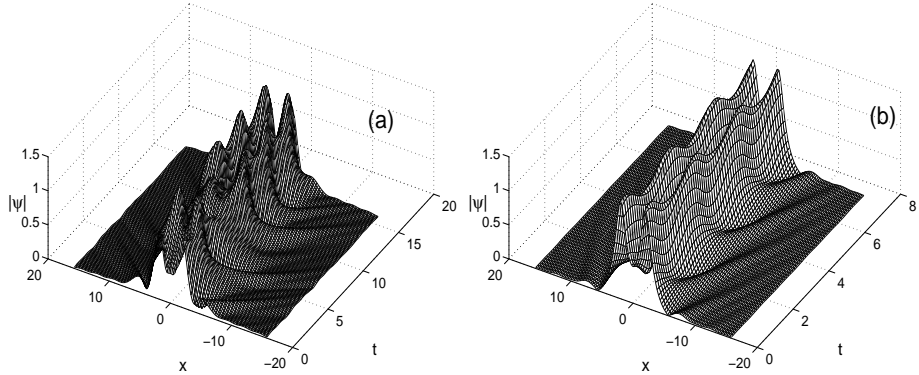


Figure 4. (a) A two-soliton periodic solution with complex temporal behaviour arising at the end point of the curve presented in Fig. 3. Here $h = 0.741$, $T = 15.9$; figure shows the solution over one period. (b) The two-soliton periodic solution on the stable branch shown in Fig. 3. Here $\gamma = 0.38$, $h = 0.95$, $T = 2.476$. Several periods of oscillation are shown.

where u and v are real and \mathcal{A} and \mathcal{B} complex coefficient functions, decaying to zero as $|x| \rightarrow \infty$. Substituting in the equations (7) and equating coefficients of like harmonics, we get

$$\begin{aligned} u_{xx} - u + 2(u^2 + v^2)u + 4(3|\mathcal{A}|^2 + |\mathcal{B}|^2)u + 4(\mathcal{A}\mathcal{B}^* + \mathcal{A}^*\mathcal{B})v - 2\Gamma v &= 0 \\ v_{xx} - v + 2(u^2 + v^2)v + 4(|\mathcal{A}|^2 + 3|\mathcal{B}|^2)v + 4(\mathcal{A}\mathcal{B}^* + \mathcal{A}^*\mathcal{B})u + 2Hv &= 0, \\ \mathcal{A}_{xx} - \mathcal{A} + 2(3u^2 + v^2)\mathcal{A} \\ &\quad + 2(3|\mathcal{A}|^2 + 2|\mathcal{B}|^2)\mathcal{A} + 2(2uv + \mathcal{A}^*\mathcal{B})\mathcal{B} - 2\Gamma\mathcal{B} - i\Omega\mathcal{B} &= 0, \\ \mathcal{B}_{xx} - \mathcal{B} + 2(u^2 + 3v^2)\mathcal{B} \\ &\quad + 2(2|\mathcal{A}|^2 + 3|\mathcal{B}|^2)\mathcal{B} + 2(2uv + \mathcal{B}^*\mathcal{A})\mathcal{A} + 2H\mathcal{B} + i\Omega\mathcal{A} &= 0. \end{aligned} \tag{9}$$

Here we have introduced $\Gamma = \gamma/A_+^2$ and $H = \sqrt{h^2 - \gamma^2}/A_+^2$.

One homoclinic solution of the system (9) exists for all H and Γ ; it is $u = \operatorname{sech} x$, $v = \mathcal{A} = \mathcal{B} = 0$. This solution corresponds to the stationary soliton $\psi_+(x)$ of equation (1). A nontrivial homoclinic solution (corresponding to a periodically oscillating soliton of Eq.(1)) bifurcates from it as H is increased for the fixed Γ . The bifurcation point corresponds to the point of the Hopf bifurcation of the stationary soliton within Eq.(1).

The system (9) was solved, numerically, for the case $\gamma = 0.3$. We continued in h starting from the Hopf bifurcation point. At each step of continuation the Newtonian iteration with the Numerov's fourth-order approximation was employed. Solutions of the two-dimensional boundary-value problem (1),(4) and the three-mode system (9) are compared in Fig. 5. It is seen that the three-mode approximation can reproduce, qualita-

tively, the transformation of periodic solitons as h is varied. However, in order to make the approximation better, we have to increase number of modes.

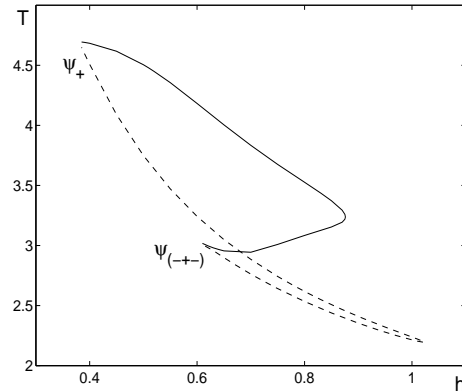


Figure 5. The function $T(h)$ for the full system (solid curve) and three-mode approximation (dashed). Here $\gamma = 0.3$

5 CONCLUSIONS

Our numerical approach allows to answer a number of questions raised by the one-soliton attractor chart of Ref.[9]. One such question is of the existence of periodic solutions with higher periods for γ in the interval $0.275 < \gamma < 0.365$. According to Fig. 2, the periodic one-soliton solution with γ in that region does not undergo any period-doubling bifurcations; hence there cannot be any $2T$, $4T$ etc solutions here, neither stable nor unstable. The absence of higher-periodic solutions should not be considered as a signature of “reduced soliton complexity” though. We have discovered a number of stable periodic two-soliton complexes in the region of large damping coefficients. These do undergo period-doubling bifurcations, as a result of which there is a wealth of stable higher-periodic multisoliton solutions. The complete classification of periodic solitons and their complexes will be addressed in future publications.

EVZ was supported by the DST grant in the frame of JINR/RSA Research Collaboration Programme and partially supported by RFBR (grant No.09-01-00770).

References

1. C. Elphick, E. Meron , Localized structures in surface waves, *Phys. Rev. A* **40** (1989) 3226-3229.
2. X.N. Chen, R.J. Wei, Dynamic behaviour of a nonpropagating soliton under a periodically modulated oscillation, *J. Fluid Mech.* **259** (1994) 291-303.
3. S. Longhi, Ultrashort-pulse generation in degenerate optical parametric oscillators. *Opt. Lett.* **20** (1995) 695-697.
4. V.J. Sánchez-Morcillo, et al., Vectorial Kerr-cavity solitons. *Opt. Lett.* **25** (2000) 957-959.
5. I.V. Barashenkov, M.M. Bogdan, V.I.Korobov, Stability Diagram of the Phase-Locked Solitons in the Parametrically Driven, Damped Non- Linear Schrödinger Equation. *Europhys. Lett.* **15** (1991) 113-118.
6. B. Denardo et al., Observations of localized structures in nonlinear lattices – domain walls and kinks. *Phys. Rev. Lett.* **68** (1992) 1730-1733.
7. N.V. Alexeeva, I.V. Barashenkov, G.P. Tsironis, Impurity-induced stabilisation of solitons in arrays of parametrically driven nonlinear oscillators. *Phys. Rev. Lett.* **84** (2000) 3053-3056.
8. N.V. Alexeeva, I.V. Barashenkov, D.E. Pelinovsky, Dynamics of the parametrically driven NLS solitons beyond the onset of the oscillatory instability, *Nonlinearity* **12** (1999) 103-140.
9. M. Bondila,I.V. Barashenkov, M.M. Bogdan, Topography of attractors of the parametrically driven damped nonlinear Schrödinger equation, *Physica D* **87** (1995) 314-320.
10. I.V. Barashenkov, E.V. Zemlyanaya, Stable complexes of parametrically driven, damped Nonlinear Schrödinger solitons, *Phys. Rev. Lett.* **83** (1999) 2568-2571.
11. E.V. Zemlyanaya, I.V. Barashenkov, N.V. Alexeeva, Temporally-Periodic Solitons of Parametrically Driven Damped NLS, *LNCS* **5434** (2009) 139-150.
12. E.V. Zemlyanaya, N.V. Alexeeva, Oscillating solitons of the damped-driven NLS equation, *Theor. and Math. Physics* **159** (2009) 536-544.
13. E.V. Zemlyanaya, I.V. Barashenkov, Numerical study of the multisoliton complexes in the damped-driven NLS, *Math. Modelling* **16**(3) (2004) 3-14 (Russian).

Author Index

- Alexeeva, N., 174
Atanasova, P., 1
- Boglaev, I., 9
Boyadjiev, T., 1
- Chernogorova, T., 22
- Darzi, R., 37, 147
Dementyeva, E., 88
- Franz, S., 44
Fryazinov, I., 154
- Geiser, J., 58
Gospodinov, P., 68
Guryanova, M., 166
- Havasi, A., 78
Horváth, R., 78
- Karepova, E., 88
Kolev, M., 97, 108
Koleva, M., 119
Kopteva, N., 44
- Ladonkina, M., 129
- Malyshев, A., 88
Milyukova, O., 129
Mošová, V., 138
- Neamaty, A., 37, 147
Nemes, A., 78
- Popov, I. , 154
- Roussinov, V., 68
- Shukrinov, Yu., 1
Stefanov, S., 68
Szabó, T., 78
- Tanoğlu, G., 58
Tishkin, V., 129
Todorov, V., 22
- Zadorin, A., 166
Zemlyanaya, E., 1, 174
Zubik-Kowal, B., 108

Proceedings of the Fifth International Conference **Finite Difference Method: Theory and Applications**, June 28 - July 2, 2010, Lozenetz, Bulgaria

Volume Editors:

Miglena Koleva
Lubin Vulkov

© Cover design:
Lusina Terziyan

ISBN: 978-954-8467-44-5

First edition
Format: B5
Pages: 190
Publisher: MEDIATEH

© Rousse University Press, Rousse, 2011.